Identification and Evaluation of Unique Chemicals for Optimum Membrane Compatibility and Improved Cleaning Efficiency

Kenneth P. Ishida, Richard M. Bold and Donald W. Phipps, Jr.
Orange County Water District
Fountain Valley, CA

Contract No.
41812

Amount of Contract
$145,000

Submitted to
California Department of Water Resources
Sacramento, CA

April 2005

Acknowledgments

This work was conducted under the auspices of the Desalination Research and Innovation Partnership (DRIP) with funding graciously provided by the California Department of Water Resources via State Proposition 13 and the Orange County Water District (OCWD).

The authors wish to express their appreciation to the Metropolitan Water District of Southern California, La Verne for coordinating all the research projects associated with the DRIP members.

The authors wish to thank the following people for their contributions to this study: Professor Amy Childress at University of Nevada, Reno for performing the streaming potential measurements and Dr. Harry Ridgway of AquaMem Associates for computing the QSAR molecular descriptors. A special thank you goes to Tom Knoell for coordinating the three DWRP13 projects at OCWD and for handling all the logistics of our reverse osmosis field operations.

Table of Contents

Executive Summary

Introduction

Despite advancements made in reverse osmosis (RO) and nanofiltration (NF) membrane separation processes, the occurrence of biotic and abiotic fouling limits the efficient operation of these processes. Accumulation of foulants on the membrane surface often leads to a rapid decline in membrane performance in terms of decreased water flux and increased salt passage. Reduction in the rate of biological and colloidal accumulation on the membrane surface is paramount to the efficient operation of separation processes. Proprietary advancements have resulted in a wide variety of RO membranes with distinct surface chemistries, some of which slow biofouling.

The application of cleaning agents, however, continues to be a critical factor in reducing the effects and economic impact of membrane fouling. Cleaning practices are now dictated to a significant extent by the type of RO membrane in operation. Chemicals once known to compromise the performance of traditional polyamide (PA) membranes (one classification of RO membranes) may now show promise given the recent alterations made to the polymer membrane surfaces. Understanding the molecular interactions between chemical cleaning agents and the RO membranes with different surface chemistries and their influence on membrane performance is vital to the development and implementation of cost-effective treatment processes. Still lacking is a basic understanding of how chemicals interact or associate with the membrane surface and how these chemicals affect membrane performance. This research project has helped lay some of the groundwork for understanding the complex interaction of chemical agents with the polymer RO membranes. This knowledge will help in the development of more effective membrane cleaning chemicals while minimizing the compromising effect they might have on membrane performance.

Objectives

There were four major objectives: (1) determine the effect a select group of cleaning agents have on membrane performance, (2) determine the chemical compounds that strongly interact with the membrane surface, (3) correlate the molecular properties of the compounds with membrane chemistry and performance and develop a predictive model for membrane chemical compatibility and performance, and (4) test select cleaning agents on fouled RO membranes to determine their efficacy in restoring membrane performance.

Approach

Seven commercial reverse osmosis membranes and one experimental membrane were studied. These included thin-film composite PA membranes from FilmTec (BW-30), Hydranautics (ESPA2 and LFC3), Koch Membranes (TFC-HR and TFC-ULP), a thin-film composite polyamide-urea (PA-U) membrane from Trisep Corporation (X-201), a cellulose acetate (CA) membrane from GE Osmonics / Desal and an experimental

thin-film composite polyamide (TMC/MPD) membrane manufactured by Separation Systems Technology (SST) in San Diego, Calif. Each membrane was characterized by contact angle (hydrophobicity), streaming potential (zeta potential/surface charge), atomic force microscopy (AFM) (surface roughness) and Fourier transform infrared (FT-IR) spectrometry (molecular structure). Each membrane was then exposed to 37 chemical compounds with various chemistries. This select group of compounds included nonionic, cationic, anionic, zwitterionic (i.e., an overall neutral compound with localized positive and negative charges), chelating and oxidizing chemical cleaners. A number of commercial enzymatic and oxidizing cleaners were also included in the study. The effect of these cleaning compounds on RO membrane performance (e.g., water flux and solute flux) was measured using a 1 x 3 in. flat sheet block test system. The strength of molecular association between the chemical compound and the membrane surface was measured by attenuated total reflection FT-IR spectrometry and principal components analysis (PCA). Quantitative structure activity relationship (QSAR) descriptors of each cleaning compound were calculated with computer software. Membrane performance data were used to generate artificial neural network (ANN) models to predict performance based on molecular QSAR descriptors, i.e., the ANN models identified molecular properties of the cleaning agents that affect membrane compatibility.

Outcome

Characterization of RO Membranes

Surface and molecular properties of each of the eight membranes were measured. All of the membranes had a negative surface charge. Contact angle was measured by the inverted air bubble method. The CA membrane had the highest contact angle, indicating that it had the most hydrophilic surface character of the eight membranes. The Hydranautics ESPA2 membrane had the lowest contact angle and thus was the most hydrophobic in relative terms. The CA and TMC/MPD membrane had the smoothest surface. The TMC/MPD membrane was coated with polyvinyl alcohol after it was manufactured, which helped to smooth out the characteristically rough PA surface. The FilmTec BW-30 had the greatest relative carboxylate content, based on the carboxylate (COO^-)-to-amide (N-H) band intensity ratio, and the greatest hydroxyl content (OH / amide I ratio). These IR band intensity ratios are a measure of the bulk properties of the PA as opposed to the surface properties measured by contact angle and AFM. The Koch TFC-HR membrane had the thinnest PA film (amide / 874 cm^{-1} ratios), and the Hydranautics LFC3 and ESPA2 had the thickest layer of the PA membranes.

Membrane Performance After Exposure to Cleaning Agent

Water flux and solute rejection (conductivity) were measured after the membranes were stabilized on a sodium chloride feed overnight. The membranes were exposed to the chemical cleaning compound for 1 hr, after which the water flux and solute rejection were remeasured. Most of the compounds caused the water flux and solute rejection to drop. A given compound did not always affect all the PA membranes the same, i.e., the relative trends were not necessarily similar. For example, dodecylbenzenesulfonic acid

(DBSA) caused the water flux of the Hydranautics ESPA2 and LFC3 membranes to increase but caused the flux of the other five PA membranes to go down. One general trend stood out with respect to individual cleaning compounds. The cationic compounds benzalkonium chloride and cetylpyridinium chloride and the nonionic compounds polyethylene glycol dodecyl ether (Genapol X-80), polyethylene glycol lauryl ether (Genapol C-100), polyoxyethylene (20) sorbitan monolaurate (Tween 20) and polyoxyethylene (20) sorbitan monostearate (Tween 80) caused the greatest flux decline on average for all five of the PA membranes. These compounds consistently caused the greatest decline in water and solute flux and fell to the bottom of the compound lists related to membrane performance. In effect they caused the membranes to "tighten up" regardless of the manufacturer of the PA membrane.

The performance data, i.e., change in water flux and change in solute rejection following exposure to cleaning compound, were compiled and averaged based the general type or class of cleaning agent for each of the individual membranes. These averages are displayed for the PA and PA-U membranes in Table ES.1 and Table ES.2 (below). With the exception of the effect of the enzymatic compounds on the FilmTec BW-30 membrane, the average change in water flux for all the PA membranes was minimal. As a general class, the cationic and nonionic compounds caused a significant reduction in the solute flux (see Table ES.2). The Hydranautics LFC3 appeared to be the most susceptible to the cleaning compounds as, on average, all classes of compounds caused the solute flux to increase. As expected the oxidizing compounds caused the solute flux to increase, with the exception Hydranautics ESPA2.

Table ES.1
Average Change in Water Flux (L/m^2·day) Based on Class of Cleaning Agent

Cleaning Agent	SST	Hydranautics	Trisep	Koch	Koch	Hydranautics	FilmTec	**Average Change**
Type / Class (#)	TMC/MPD	LFC3	X-201	TFC-ULP	TFC-HR	ESPA2	BW-30	**Water Flux**
Anionic (7)	-0.17	0.16	-0.33	-0.66	-0.88	-0.12	-0.37	**-0.34**
Anionic-chelating (1)	0.28	1.11	-0.21	1.84	0.34	1.49	-0.41	**0.63**
Cationic (6)	-1.18	-1.57	-1.22	-2.85	-2.30	-1.44	-0.79	**-1.62**
Chelating (3)	0.07	0.07	-0.22	-0.78	-1.39	0.25	-0.10	**-0.30**
Enzymatic (3)	-0.28	-0.18	-0.29	-1.46	-0.97	0.06	-48.4	**-7.35**
Nonionic (9)	-0.85	-0.77	-0.91	-2.54	-1.86	-0.76	-1.98	**-1.38**
Oxidizing (4)	-0.09	0.27	-0.16	-0.44	-0.36	-0.89	-0.15	**-0.26**
Oxidizing/BFT (1)	-	1.33	0.61	4.46	2.14	1.71	0.22	**1.74**
Zwitterionic (4)	-0.63	-0.60	-0.99	-2.00	-1.04	-0.34	0.04	**-0.79**

Table ES.2
Average Change in Solute Flux (moles/m^2·day) by Chemical Class of Cleaning Agent

Cleaning Agent	SST	Hydranautics	Trisep	Koch	Koch	Hydranautics	FilmTec	**Average Change**
Type / Class (#)	TMC/MPD	LFC3	X-201	TFC-ULP	TFC-HR	ESPA2	BW-30	**Solute Flux**
Anionic (7)	28	50	9.4	106	-28	5.8	-51	**17.1**
Anionic-chelating (1)	42	57	14	34	-6.3	351	-290	**29**
Cationic (6)	-38	8.0	-59	-24	-30	-2.0	-133	**-39.7**
Chelating (3)	8.1	25	1.26	24	-34	1.7	-35	**16.5**
Enzymatic (3)	-1.1	45	-102	37	23	41	-48	**-0.58**
Nonionic (9)	15	16	-96	-3.2	-24	5.0	-141	**-32.6**
Oxidizing (4)	13	88	70.3	56	7.2	-138	4.0	**14.4**
Oxidizing/BFT (1)	---	1540	1602	510	321	266	---	**848**
Zwitterionic (4)	-14	24	-95	202	-9.2	11	-45	**10.4**

Average changes in performance of the CA membrane are displayed in Table ES.3. The cleaning compounds had a minimal effect on the water flux, with the exception of the commercial Diamite BFT oxidizing agent. This was expected, as strong oxidizing agents are not compatible with CA membranes. Anionic and zwitterionic cleaning agents caused the solute flux to decrease, while the remaining classes of compounds caused the solute flux to increase.

Table ES.3
Average Change in Performance of Cellulose Acetate Membrane

Chemical Agent Type / Class (#)	Average Change Water Flux (L/m^2·day/psi)	Average Change Solute Flux (moles/m^2·day)
Anionic (7)	-0.003	-78
Anionic-chelating (1)	-0.061	45
Cationic (6)	-0.196	96
Chelating (3)	0.071	37
Enzymatic (3)	0.191	136
Nonionic (9)	-0.117	45
Oxidizing (4)	0.021	72
Oxidizing / BFT (1)	5.117	20048
Zwitterionic (4)	-0.605	-17

Chemical Interaction with Membrane Surface / PCA

Twenty-one of the 37 cleaning compounds were selected for PCA. Infrared spectra of the membrane exposed to the cleaning chemical were compared to the spectra of the unexposed control membranes. The results of the PCA were tabulated by assigning a numerical value to each compound that related to its adsorption or interaction with the membrane surface. If the test spectra and control spectra did not separate based on plots of their principal components, the compound was assigned a value of 1, indicating a weak interaction or no lasting interaction with the membrane surface. If the test and control spectra partially separated from each other, the compound was assigned a value of 1.5, indicating moderate association or adsorption on the membrane surface. Finally, if the test and control spectra completely separated from each other, the compound was assigned a value of 2, indicating a strong association with the membrane surface. These values or "separation indices" are displayed in Table ES.4 (see below).

Of the 21 compounds analyzed by PCA, the nonionic surfactant deconoyl-N-methylglucamide (Mega 10) was the least adsorptive. It had the lowest average separation index, which meant that in the majority of cases the test spectra looked similar to the control spectra, indicating no adsorption on the surface or no alteration of the membrane molecular structure. Other compounds that did not closely associate with the membrane surface were n-dodecyl-N,N-dimethylglycine (Empigen BB), sodium dodecylsulfate (SDS), zosteric acid and the combination of dodecylbenzenesulfonic acid (DBSA) and sodium tripolyphosphate (STP). The Hydranautics LFC3 and FilmTec BW-30 were the most resistant to the chemical exposure as only minor changes to the IR spectra of these membranes were observed, and thus their average separation index was low. Compounds that partially separated from the control spectra (representing moderate adsorption) were grouped with the compounds that strongly associated with the membrane. This represented 17 of the 21 compounds and revealed that 82% of the chemical compounds analyzed by PCA demonstrated strong to moderate adsorption or interaction with the surface of the membranes (see Table ES.5 below).

It is important to note that the PCA results that indicated no chemical interaction did not always equate to no loss or little change in membrane performance. For example, in two cases (FilmTec BW-30 and Hydranautics LFC3), benzalkonium chloride did not appear to interact (or associate) strongly with the membrane and yet caused a significant decrease in water flux and solute flux. Therefore, infrared spectroscopic analysis of chemical-exposed membranes (by means of a simple soak test) should not be the only determining factor when assessing chemical compatibility. Actual measurements of water flux and solute rejection should be made following any exposure of the membrane to the cleaning agent.

Table ES.4
Molecular Interactions with Membrane Surface / Separation Index

		CA	TMC/MPD	BW-30	LFC3	HR	ULP	ESPA2	X-201	**Ave**
Benzalkonium chloride	cationic	2	2	1	1	2	2	2	2	**1.8**
Benzensulfonic acid	cationic	2	2	1	1	2	1.5	2	2	**1.7**
Biz	anionic	2	1	1.5	1.5	2	2	2	2	**1.8**
Cetylpyridinium chloride	anionic	1.5	1.5	1.5	2	2	2	2	2	**1.8**
Citric acid	chelator	1.5	2	1	1.5	2	2	2	1.5	**1.7**
DBSA	anionic	2	2	1.5	1.5	1.5	1.5	2	2	**1.8**
DBSA and STP	anionic	2	1.5	1	1	2	2	2	1.5	**1.6**
Diamite BFT	oxidizing	2	NA	2	1.5	2	1.5	2	2	**1.9**
Empigen BB	zwittergent	2	1.5	2	1	2	1	1	2	**1.6**
Endozime	enzymatic	2	2	2	1.5	2	1.5	1.5	2	**1.8**
Genapol C-100	nonionic	2	2	2	1	2	2	2	1.5	**1.8**
Mega-10	nonionic	1	2	1.5	2	1	1.5	1	1	**1.4**
Minncare	oxidizing	2	NA	2	1.5	2	1	2	1.5	**1.7**
Nonylglucopyranoside	nonionic	1.5	2	1	1.5	2	2	2	1.5	**1.7**
Protease	enzymatic	1.5	1	2	2	2	2	2	1.5	**1.8**
SDS	anionic	2	2	1	1	2	1	2	1.5	**1.6**
STP	chelator	2	2	1.5	1.5	2	1.5	2	1.5	**1.8**
Triton X-100	nonionic	2	2	1	1	2	1.5	2	2	**1.7**
Tween 20	nonionic	2	2	2	1	2	1.5	2	2	**1.8**
Zosteric Acid	anionic	2	1.5	1.5	1	2	1	1.5	2	**1.6**
Zwittergent 1.5-16	zwittergent	2	2	1	1	2	2	2	2	**1.8**
Sum		39	34	31	28	40.5	34	39	37	
Average		**1.9**	**1.2**	**1.5**	**1.3**	**1.9**	**1.6**	**1.9**	**1.8**	

1 – No separation
1.5 – Partial separation
2 – Separation

Artificial Neural Network Models

QSAR molecular descriptors were calculated by computer for each of the chemical cleaning agents. These descriptors were used in combination with membrane physical and chemical properties and membrane performance data to construct ANN models for a PA, CA, and PA-U membrane. Sensitivity indices are displayed in Table ES.6. Of the more than 300 potential molecular descriptors, these were the ones determined to be most important in predicting membrane performance following exposure to a given chemical compound. The greater the magnitude of the sensitivity index the greater is its significance on membrane performance. These indices may have positive or negative

Table ES.5
Summary of Molecular Interactions with Membrane Surface

Membrane Type	Separation Index 2 Complete Separation (Strong Association)	1.5 Partial Separation (Partial Association)	1 No Separation (No Association)
All membranes	57.8%	24.7%	17.5%
CA	76.2%	19.0%	4.8%
TMC/MPD*	68.4%	21.1%	10.5%
BW-30	33.3%	28.6%	38.1%
LFC3	14.3%	38.1%	47.6%
TFC-HR	90.5%	4.75%	4.75%
TFC-ULP	42.9%	38.1%	19.0%
ESPA2	81.0%	9.5%	9.5%
X-201	57.1%	38.1%	4.8%

*-Based on exposure to 19 of 21 chemical cleaning compounds excluding Diamite BFT and Minncare.

values. For example, a positive correlation of water flux with polarity implies that the water flux of the membrane will increase upon exposure to chemical compounds with a high dipole moment. If a homologous series of compounds were tested with increasing dipole moment, the magnitude of the increase in water flux should increase across the series.

Polyamide-Urea ANN Model

Four molecular descriptors were determined to be important for predicting water flux of the PA-U membrane. These descriptors were related to charge and the molecular complexity of the chemical compounds. As the negative charge on the test compounds increased, the water flux decreased with increasing magnitude, indicating a negative relationship between charge and water flux. The water flux was also inversely related to the molecular complexity of the cleaning compound the membrane was exposed to. Therefore, the greater the magnitude of the molecular complexity, the greater was the decrease in water flux following chemical exposure.

Six molecular descriptors were determined to be important in predicting solute flux. Four were associated with the chemical compound's dipole and ability to form hydrogen bonds and were positively correlated with solute flux. Thus, compounds with a large dipole moment (e.g. DBSA) and an enhanced ability to form hydrogen bonds (e.g. alcohols and carboxylic acids) typically caused the solute flux of the membrane to increase following

Table ES.6
Sensitivity Indices of Molecular Descriptors

	Change in Water Flux			Change in Solute Flux		
	PA	**CA**	**PA-Urea**	**PA**	**CA**	**PA-Urea**
Charge / Polarity						
Zeta potential slope	0.4718					
Dipole	0.1445					
MaxNeg			-0.4795	-0.6646		
Py		0.0024				
Pz		29.0442				
Dx		-10.2415			-12.4020	
Dz						-5.4917
Qxx						-12.7533
Qyy		-0.9572				-1.2787
Sumdel1				-2.8423		
Tets2				-0.4554		
ssCH3	0.2961					
SdssC					21.4926	
SHother	-4.2971					
Hmax						1.2612
Hmin					-11.0764	
Gmin	-0.5802					
Molecular Complexity						
COO^-/AMII	0.0017	NA	NA		NA	NA
AMII/874	0.2643	NA	NA	0.2997	NA	NA
Projected Area				0.6818		
xpc4						-0.6113
xvpc4						0.2355
xvc3		-0.4530				
nxc3					-1.6797	
LD50			-0.1138			
phia		0.4327				
IC			-2.4014			
numHBa					1.6945	
SHHBd					12.4138	
nelem			0.4392		-0.1215	
HBP (Hydrophobicity)						
LogP					2.5910	

exposure. Two of the descriptors were associated with molecular complexity. One was negatively correlated with solute flux and the other was positively correlated with solute flux.

Cellulose Acetate ANN Model

Six molecular descriptors were determined to be important in predicting a compound's effect on the water flux of a CA membrane. The molecular dipole was a significant factor affecting water flux. However, two of the descriptors associated with the dipole were positively correlated with water flux and two were negatively correlated with water flux. Two were very low in magnitude and offset each other. The other two, Pz (29.0442) and Dx (-10.2415), differed 4-fold in magnitude. A positive correlation of the dipole with water flux indicates that compounds with a large dipole moment will cause a large increase in water flux. Two other descriptors were associated with molecular complexity. Both were equal and oppositely correlated to water flux.

Eight molecular descriptors were determined to be important in predicting solute flux of the CA membrane. Three were associated with the compound's charge. One was positively correlated and two were negatively correlated with solute flux. Four of the descriptors were associated with molecular complexity. Two were positively correlated and two were negatively correlated with solute rejection.

The influence of molecular properties of the chemical compounds on the CA membrane's performance was less clear cut. However, an ANN model capable of predicting a compound's effect on membrane performance was generated from the measurements made in the field (see below).

Polyamide ANN Model

There were a total of seven molecular descriptor inputs of significance to the PA ANN model. Four QSAR descriptors associated with the charge and polarity of the compound had an influence on the water flux. These descriptors related to the compound's ability to form a dipole and form intermolecular interactions with methyl groups. Chemical compounds with these properties caused the water flux of the membrane to increase, i.e., compounds with large dipole moments (e.g. DBSA and SDS), large aliphatic (methylene and methyl) content caused the water flux to increase following exposure to the membrane. Compounds with an increased ability to form hydrogen bonds (e.g. alcohols and carboxylic acids) and certain types of intermolecular interactions caused the water flux to decrease following exposure.

The ANN model of the PA membrane also identified membrane properties as being influential in affecting water flux. Membranes with a thicker PA layer and a lower crosslink density performed better as compared to those membranes with a thinner PA film and lower crosslink density. In general these membranes with the thicker PA layer (e.g. Hydranautics ESPA2, LFC3 and FilmTec BW-30) demonstrated increased water flux and decreased salt passage following chemical exposure, i.e., they performed better

than the other membranes in the study. PA membranes with a low crosslink density have a greater density of free carboxylate groups and greater negative charge spread throughout the membrane. This PA negativity seemed to equate to an improvement in water flux following chemical exposure.

Five molecular descriptors were determined to be relevant in determining solute rejection. One was related to negative charge on the compound and the other was related to structural complexity. Both negatively correlated with solute flux. Therefore, exposure to compounds with high negative charge and high molecular complexity would cause the membrane to "tighten up" and result in a reduction in solute passage. Finally, the PA thickness positively correlated with solute flux indicating that membrane with a thicker PA layer allowed greater solute passage.

ANN Model Summary

All of the molecular descriptors described above were determined to be influential in predicting how a chemical compound will affect the water flux and salt rejection of a RO membrane. The magnitude of the sensitivity index and the direction of the correlation varied widely. However, distinct relationships between a compound's molecular properties, the physical properties of the membrane, and their influence on the membrane's performance were revealed and these relationships were used to predict a compound's effect on membrane performance.

Prediction of Chemical Compound Effect on Membrane Performance

The ANN models were designed to predict changes in membrane water flux and solute passage following exposure to any compound for which the pertinent molecular descriptors are known. Of the hundreds of molecular descriptors that were calculated for each compound, only 10 were determined to be important to predict compound performance (compatibility) for the PA-U membrane, 13 descriptors for the CA membrane and 8 descriptors, along with 3 membrane properties, for the PA membrane (see Table ES.6). QSAR molecular descriptors were calculated for all 74 compounds in the master list of potential cleaning agents. Only 27 of these were tested on RO membranes and used to generate the ANN models to predict a compound's effect on membrane performance. Using the models constructed from the membrane performance data and the pertinent molecular descriptors, the change in water flux (Table ES.7) and change in solute flux (Table ES.8) were predicted for the remaining 66 compounds. The data from compounds in bold font represent real field measurements of membrane performance.

A number of compounds of homologous series were tested during this study and some treads in membrane performance were apparent. For example in the Tween (20-80) series, the short (C_{12}) aliphatic chain length Tween 20 caused more reduction in water flux than the Tween 80 with the longer (C_{18}) chain. However, unexplainably, there was no difference in the magnitude of the decrease in solute rejection across the homologous series. The water flux of the Hydranautics LFC3 and ESPA2 membranes were actually

Table ES.7
Predicted Change in Specific Water Flux ($L/m^2 \cdot day/psi$) by ANN Models

Compound[a]	**Membrane**					
	BW-30	**ESPA-2**	**TFC-HR**	**TFC-ULP**	**X-201**	**CA**
Formic acid	-0.63	-0.53	-1.72	-0.12	-0.21	-0.13
Propionic acid	-0.83	-0.41	-1.90	0.70	-0.23	-0.15
Acetic acid	-0.81	-0.67	-2.29	0.49	-0.24	-0.12
Butyric acid	-0.90	-0.50	-1.91	0.68	-0.21	-0.19
Capric acid	-1.02	-0.92	-2.29	-2.46	-0.43	-0.02
Caproic acid	-0.92	-0.51	-1.90	0.58	-0.26	-0.23
Lauric acid	-1.02	-0.90	-2.18	-2.60	-0.52	0.07
Hexadecanoic acid	-1.28	-1.31	-1.82	-1.57	-0.47	0.25
Octadecanoic acid	-1.44	-1.33	-2.17	-2.10	-0.35	0.24
Benzalkonium chloride	-2.44	-4.45	-4.02	-4.21	-1.86	-0.26
Cetylpyridinium chloride	-2.90	-1.46	-3.43	-4.19	-1.44	-0.03
Zosteric acid	-1.24	-0.58	-1.23	-0.66	-0.30	-0.38
Benzenesulfonic acid	-1.08	-0.40	-0.72	-1.94	-0.18	-0.13
p-toluenesulfonic acid	0.03	0.12	-0.13	0.24	-0.03	-0.10
Ethylbenzenesulfonic acid	0.06	0.09	-0.15	0.10	-0.11	-0.11
Octylbenzenesulfonic acid	0.03	-0.12	-0.38	0.00	-0.37	-0.17
DBSA	0.04	-0.09	-1.00	0.02	-0.43	-0.15
Butanesulfonic acid	-0.48	-1.17	-2.37	-2.72	-0.44	0.01
Pentanesulfonic acid	-0.16	-1.53	-2.79	-3.11	-0.32	0.02
Heptanesulfonic acid	0.18	-1.18	-1.28	-3.21	-0.19	0.01
Hexanesulfonic acid	0.01	-1.39	-2.49	-3.15	-0.54	0.01
Octanesulfonic acid	0.23	-0.62	-0.46	-2.77	-0.10	-0.01
Nonanesulfonic acid	0.23	-0.11	-0.35	-0.46	-0.14	-0.02
Decanesulfonic acid	0.20	0.07	-0.37	-0.07	-0.19	-0.04
Dodecanesulfonic acid	0.10	0.06	-0.43	-0.33	-0.29	-0.11
Hexadecanesulfonic acid	-0.12	-0.69	-0.52	-0.88	-0.55	-0.40
SDS	0.41	-0.16	-0.76	-0.34	-0.42	0.28
HEXglucopyranoside	-1.64	-1.46	-1.88	-2.33	-1.14	0.08
HEPglucopyranoside	-1.67	-1.46	-2.01	-2.36	-1.26	0.01
OCTglucopyranoside	-1.78	-1.73	-2.10	-2.50	-1.29	-0.09
NONglucopyranoside	-1.81	-1.74	-2.20	-2.52	-0.56	-0.08
DECglucopyranoside	-1.85	-1.78	-2.28	-2.55	-0.42	-0.08
DODglucopyranoside	-1.92	-1.82	-2.43	-2.59	-0.37	-0.07
EDTA	-0.84	-0.18	-0.79	-1.66	-0.60	-0.04
Citric acid	-0.33	-0.34	-0.89	-1.24	-0.49	-0.18
Genapol C-100	-2.84	-2.03	-3.39	-2.80	-1.34	-0.12
Genapol X-80	-2.01	-0.57	-3.06	-2.81	-1.30	-0.25

[a]-Compounds in bold were actually tested on RO membranes and the change in water flux and solute rejection measured.

Table ES.7 (continued)
Predicted Change in Specific Water Flux (L/m^2·day/psi) by ANN Models

Compound	Membrane					
	BW-30	**ESPA2**	**TFC-HR**	**TFC-ULP**	**X-201**	**CA**
Mega 8	-0.27	-1.25	-2.92	-2.54	-0.61	-0.05
Mega 9	-0.53	-1.07	-2.90	-2.40	-0.37	0.00
Mega 10	-0.32	-1.13	-3.01	-2.58	-0.35	0.08
Nonyltrimethylammonium Br	-0.57	-0.56	-3.27	-3.30	-0.77	-0.15
Decyltrimethylammonium Br	-0.70	-0.53	-3.43	-3.28	-0.85	-0.14
DTAB	-0.95	-0.52	-3.68	-3.25	-1.04	-0.11
Tetradecyltrimethylamm Br	-1.16	-0.56	-3.87	-3.25	-1.28	-0.09
CTAB	-1.36	-0.63	-4.01	-3.27	-1.52	-0.07
Octadecyltrimethylamm Br	-1.53	-0.71	-4.11	-3.29	-1.73	-0.05
Tetrabutylammonium bromide	-1.67	-0.75	-4.00	-3.68	-0.68	0.11
TEA	-0.62	-0.54	-2.38	-1.78	-0.49	0.05
Tetrapentylammonium bromide	-1.99	-1.03	-4.28	-3.66	-0.90	0.16
Tetraheptylammonium bromide	-2.41	-1.47	-4.51	-3.61	-1.09	0.21
Tetrahexylammonium bromide	-2.23	-1.27	-4.42	-3.64	-0.54	0.18
Tetraoctylammonium bromide	-2.57	-1.63	-4.57	-3.59	-1.67	0.22
Tetradecylammonium bromide	-2.97	-1.82	-4.64	-3.54	-1.51	0.27
Tetrahexyldecylammonium Br	-2.07	-1.78	-4.73	-3.36	-1.27	0.24
Triton X-45	-0.57	-0.47	-1.91	-2.30	-0.42	-0.63
Triton X-100	-1.12	0.06	-2.42	-2.38	-1.22	-0.09
Tween 20	-3.51	-0.34	-3.44	-2.71	-1.13	0.24
Tween 40	-3.38	-0.64	-3.62	-2.97	-1.10	0.04
Tween 60	-3.47	-0.27	-3.38	-2.61	-1.06	-1.34
Tween 80	-3.46	-0.14	-3.29	-2.47	-1.04	0.00
Zwit 3-8	0.59	-0.13	-1.96	-0.98	-0.71	-0.19
Zwit 3-10	0.69	-0.20	-1.54	-0.97	-0.80	-0.14
Zwit 3-12	0.59	-0.31	-1.29	-0.95	-0.89	-0.14
Zwit 3-14	0.49	-0.46	-1.32	-1.05	-0.97	-0.25
Zwit 3-16	0.42	-0.66	-1.70	-1.24	-1.04	-0.33
Empigen BB	-0.26	-1.99	-2.60	-3.29	-0.44	-1.33

[a]-Compounds in bold were actually tested on RO membranes and the change in water flux and solute rejection measured.

Table ES.8
Predicted Change in Solute Flux (moles/m^2·day) by ANN Models

Compound	Membrane						
	BW-30	**ESPA2**	**LFC3**	**TFC-HR**	**TFC-ULP**	**X-201**	**CA**
Formic acid	91.2	81.4	3.0	5.4	54.0	115	1270
Propionic acid	94.3	90.6	9.7	41.3	58.1	-3.1	1270
Acetic acid	96.8	89.2	7.2	35.9	58.9	-1.9	1270
Butyric acid	90.8	90.7	10.8	42.9	57.1	-8.5	1270
Capric acid	71.1	87.7	-12.4	15.0	57.3	3.8	647
Caproic acid	84.9	90.3	11.9	43.8	55.8	-4.5	1270
Lauric acid	67.4	84.3	-29.4	-10.0	57.9	9.6	847
Hexadecanoic acid	76.7	17.7	98.8	11.7	0.0	23.5	1270
Octadecanoic acid	36.8	18.7	91.7	0.1	38.3	27.5	1270
Benzalkonium chloride	-430	-416	56.6	-282	-370	-109	-87.1
Cetylpyridinium chloride	-356	-305	35.5	-37.1	-77.3	-45.7	63.4
Zosteric acid	-133	-91.7	-6.1	-56.3	-99.6	-13.1	-44.8
Benzenesulfonic acid	-58.8	23.1	-10.8	9.7	-25.3	-37.8	26.8
p-toluenesulfonic acid	-26.6	-77.7	48.9	14.1	-27.4	-19.7	1270
Ethylbenzenesulfonic acid	-27.4	-65.0	70.0	-19.3	-68.8	-2.6	768
Octylbenzenesulfonic acid	-75.0	-2.4	51.0	-43.5	-67.6	-45.7	564
DBSA	-168	24.0	54.7	-30.6	-77.1	-52.4	19.7
Butanesulfonic acid	-80.8	60.2	14.6	-61.8	-18.5	-69.0	39.2
Pentanesulfonic acid	-93.4	49.8	6.5	-73.3	-14.1	-79.4	3.2
Heptanesulfonic acid	-91.2	30.5	-31.6	-61.4	-0.3	-55.7	8.8
Hexanesulfonic acid	-96.9	39.2	-12.4	-75.2	-7.4	-48.9	-16.8
Octanesulfonic acid	-77.4	24.8	-37.4	-33.1	4.7	-28.3	48.6
Nonanesulfonic acid	-59.7	22.4	-24.5	-2.2	-0.6	-33.8	69.8
Decanesulfonic acid	-42.1	22.7	1.9	18.9	-32.3	-10.8	71.7
Dodecanesulfonic acid	-13.1	25.5	13.5	8.2	-159	3.9	39.4
Hexadecanesulfonic acid	-131	19.4	36.9	-45.6	-183	26.4	-59.3
SDS	-93.3	-6.0	54.5	-44.2	-99.6	98.3	61.9
HEXglucopyranoside	-115	-115	-31.0	-59.2	-110	-64.3	706
HEPglucopyranoside	-118	-157	-29.1	-51.7	-110	-77.1	495
OCTglucopyranoside	-122	-197	-25.4	-45.3	-111	-86.3	270
NONglucopyranoside	-127	-241	-20.8	-39.9	-113	-73.3	157
DECglucopyranoside	-134	-274	-16.1	-35.5	-115	-69.1	76.6
DODglucopyranoside	-146	-263	-7.2	-28.8	-122	-55.7	-24.9

[a]-Compounds in bold were actually tested on RO membranes and the change in water flux and solute rejection measured.

Table ES.8 (continued)
Predicted Change in Solute Flux (moles/m^2·day) by ANN Models

Compound	Membrane						
	BW-30	**ESPA2**	**LFC3**	**TFC-HR**	**TFC-ULP**	**X-201**	**CA**
EDTA	-67.3	34.5	7.7	-3.3	-118	-14.8	75.0
Citric acid	-68.0	-48.1	-16.5	-85.3	-165	-91.1	-1.1
Genapol C-100	-162	61.1	-32.9	-27.2	-216	-99.5	88.7
Genapol X-80	-171	49.9	-5.1	-23.6	-182	-87.0	-9.1
Mega 8	-29.1	-88.7	14.4	-24.2	-17.9	-127	143
Mega 9	-30.8	-95.9	24.1	-31.4	-37.8	-130	78.4
Mega 10	-39.5	-102	35.2	-34.2	-35.8	83.7	30.0
Nonyltrimethylamm Br	21.8	88.8	9.4	19.1	-34.4	13.9	-119
Decyltrimethylamm Br	16.8	91.0	27.2	16.2	-18.2	2.0	53.5
Dodecyltrimethylamm Br	7.5	83.1	47.1	2.7	-205	-28.5	594
Tetradecyltrimethylamm Br	-5.5	73.1	10.4	-16.7	-344	-58.4	333
Hexadecyltrimethylamm Br	-70.8	26.2	-56.4	-38.7	-332	-86.3	74.8
Octadecyltrimethylamm Br	-318	-112	-3.4	-66.3	-321	-111	-80.2
Tetrabutylammonium Br	-10.3	67.0	-44.1	-21.4	-347	51.8	-286
Tetraethylamm Br	-2.3	54.9	17.0	-10.1	-50.9	-74.0	55.3
Tetrapentylamm Br	-397	-215	38.0	-88.7	-324	29.2	-287
Tetraheptylamm Br	-444	-432	44.6	-347	-399	77.4	-325
Tetrahexylamm Br	-430	-404	55.8	-212	-355	28.1	-314
Tetraoctylamm Br	-451	-436	28.6	-421	-431	51.4	-330
Tetradecylamm Br	-460	-435	-5.5	-461	-463	-132	-231
Tetrahexyldecylamm Br	-470	-358	-82.6	-472	-482	-191	87.1
Triton X-45	-147	-80.3	17.1	-31.0	-50.1	-109	-53.5
Triton X-100	-169	64.4	-24.1	-25.2	-217	-152	10.1
Tween 20	-196	8.4	12.4	-27.3	-58.1	-237	27.1
Tween 40	-196	8.7	12.6	-27.3	-58.3	-223	-81.9
Tween 60	-197	8.5	12.6	-26.2	-56.6	-51.8	-82.0
Tween 80	-197	8.6	12.7	-26.2	-56.7	-38.2	69.5
Zwit 3-8	-54.0	38.7	38.9	-42.5	-213	-169	22.3
Zwit 3-10	-148	45.2	42.6	-50.9	-217	-188	62.5
Zwit 3-12	-130	24.7	43.3	-48.9	-215	-87.5	62.7
Zwit 3-14	-23.9	-13.3	46.6	-45.2	-217	-71.7	18.3
Zwit 3-16	7.5	-12.6	51.4	-41.5	-224	-49.9	-21.0
Empigen BB	50.7	-26.0	81.6	20.3	-6.8	28.1	-178

[a]-Compounds in bold were actually tested on RO membranes and the change in water flux and solute rejection measured.

observed and predicted to increase following exposure to the Tween series, while the other PA and PA-U membrane all tightened up. The observed trends in the sulfonic acid series included a decrease in water flux with increasing aliphatic chain length, but less solute passage after exposure to the low chain length butanesulfonic acid as compared to the hexadecanesulfonic acid. The models predicted that exposure to the Zwittergents would cause the water flux of the Hydranautics ESPA2 and LFC3 membranes to increase. However, the water flux for the remaining PA and PA-U membranes would be

expected to decrease following chemical exposure. The model for the Koch TFC-ULP membrane, predicted a drop in water flux independent of the type of Zwittergent detergent.

In general the model predicted increasing or decreasing water flux and solute rejection with increasing or decreasing methylene (CH_2) chain length within a homologous series of compounds. When two or more test data were available for compounds within a given series, the predicted performance did not always transition smoothly, although the general trend in a positive or negative direction was maintained. Testing the accuracy of the predictions or validation of these models through real measurements of performance of these compounds was outside the scope of this study. The ANN models are available upon request through the OCWD website at www.ocwd.com or by phone at (714) 378-3200.

Application of Cleaning Agents on Fouled RO Membranes

Four RO membranes—FilmTec BW-30, Hydranautics ESPA2, Hydranautics LFC3 and Koch TFC-HR—were operated on secondary-treated wastewater in order to rapidly foul the surface. Due to logistical problems associated with plant shutdowns and equipment failure, only four cleaning agents were tested to determine their ability to remove the foulant layer and restore membrane water flux and solute rejection (see Table ES.9).

The surfactant Genapol C-100 (polyethylene glycol laurel ether) produced very poor results on all four PA membranes. The solute flux increased 10 to 20% and the water flux dropped 15 to 30%. Though very poor, these results were actually consistent with what was observed in the chemical compatibility studies.

Protease was one of the most chemically compatible enzymatic-cleaning compounds, having a minimal effect on membrane water flux and solute flux. However, when applied to the fouled PA membranes, a significant increase (~10 to 30%) in solute flux was observed, while the water flux was unaffected. This treatment did not produce desirable results, as there was no improvement in water flux and the solute passage actually increased.

Zwittergent 3-16 (n-hexyldecyl-N,N-dimethyl-3-ammonio-1-propanesulfonate) was another surfactant that performed well in the initial compatibility study. The results from the cleaning study were mixed. Application of Zwittergent 3-16 to the fouled Hydranautics ESPA2 membrane caused the water flux to decrease by ~18% and the solute flux to decrease by ~28%. Thus, the surfactant had a tightening effect on the ESPA2 membrane. The water flux of the other membranes improved slightly, but the solute flux increased significantly (25 to 38%).

DBSA (dodecylbenzenesulfonic acid), a common cleaning agent for PA membranes, did not fare much better. Water flux dropped by as much as 13% with the Hydranautics ESPA2 membrane but improved by ~10% when applied to the fouled Hydranautics LFC3 membrane. The solute flux of the Hydranautics ESPA2 membrane dropped 49% while

Table ES.9
Chemical Cleaning of Fouled RO Membranes

Membrane	DBSA		Genapol C-100		Zwittergent 3-16		Protease	
	%Δ Solute Flux	%Δ Water Flux	%Δ Solute Flux	%Δ Water Flux	%Δ Solute Flux	%Δ Water Flux	%Δ Solute Flux	%Δ Water Flux
FilmTec BW-30	-1.7	-5.6	12.1	-25.6	25.1	6.6	9.0	1.3
Hydranautics ESPA2	-49.1	-13.1	20.6	-17.6	-27.5	-17.7	16.9	-.07
Hydranautics LFC3	-29.1	9.8	2.27	-15.1	29.7	2.1	32.0	1.4
Koch TFC-HR	-2.0	-9.5	10	-32.2	37.6	4	23.9	-0.9

increasing 29% for the LFC3 membrane. The FilmTec BW-30 and Koch TFC-HR were only moderately affected by cleaning with DBSA. The FilmTec BW-30 water flux dropped ~6% and the solute flux dropped about 2%. The Koch TFC-HR water flux dropped ~10% and the solute flux dropped about 2%.

The secondary-treated wastewater feed used to form the fouling layer on the RO membrane in this study can be considered to be quite aggressive and heavily laden with foulants. However, this study did produce data on cleaning efficiency under the most extreme conditions.

Conclusions

Defining and understanding how molecular properties of chemical compounds influence changes in membrane performance is very difficult. The ANN models of the PA, CA and PA-U membranes provided an abundant amount of detailed information on how specific molecular properties influence membrane performance. Membrane water flux and solute passage were affected by numerous molecular properties associated with the cleaning agents. Many of the descriptors were obscure in nature. However, very useful generalizations could be drawn from them. Charge, polarity and molecular complexity properties appeared to be the most influential factors in determining a compound's effect on water flux and solute rejection. Generally speaking chemical compounds with high polarity or dipole moment were more likely to cause membrane water flux to increase and solute flux to decrease, while compounds with increasing aliphatic (CH_2) character caused the water flux to decrease. Finally, compounds with increased geometric complexity and increased electronegativity led to a reduction of solute passage. These molecular properties were determined to be the most influential in predicting or determining the compound's influence on membrane performance.

Three independent ANN models were generated for a PA-U, CA and PA RO membrane. While hundreds of molecular descriptors of can be calculated for a given cleaning compound, only 8 to 12 descriptors were determined to be important for the prediction of the compound's effect on membrane performance. Knowing the value of these molecular descriptors, one can calculate or predict the change in water flux and change in solute flux following exposure to the chemical compound. The ANN models are available on request through the OCWD website at www.ocwd.com or by phone at (714) 378-3200.

The ability to detect a chemical compound's association with the membrane surface was demonstrated using FT-IR spectrometry. However, conclusions about a compound's chemical compatibility with a membrane with respect to performance should not be drawn solely from infrared spectroscopic analysis. A compound may adsorb to the membrane surface at very low concentrations and remain undetected by IR analysis and yet still cause significant loss of membrane performance. Therefore, a decision on whether a compound can be used in the field should not be based entirely on a benchscale soak test and analysis of molecular adsorption by infrared spectrometry. Assessing a compound's compatibility with a given membrane is more adequately addressed using a combination of laboratory and field analysis, that being an assessment of molecular properties, measure of molecular adsorption and ANN modeling to predict the compound's influence on performance. RO fouling and chemical cleaning is a very complex process that still is not well understood.

Recommendations

The addition of more membrane performance data and molecular descriptors from other cleaning compounds will improve the ANN models. The selection and testing of compounds that actually perform poorly will help to strengthen these models by spreading out the input data with respect to performance, as a majority of the test compounds were clustered fairly close together. Future studies should be directed toward quantitation of these chemical cleaning agents on the surface of the membranes following cleaning and the correlation of the quantity adsorbed with the magnitude of change in membrane performance. These studies should also focus on the chemical characterization or identification of the foulants that are removed by individual cleaning agents, as well as focus on the macromolecular components that remain adsorbed on the membrane surface.

Benefit to California

In conclusion, this study has provided greater insight into how specific chemical properties of cleaning compounds influence membrane water flux and solute rejection. The hope is that enough knowledge and understanding of the fundamental interactions between chemical agents and polymer membranes will be gained through further studies such that cleaning compounds can be tailored specifically to the membrane and the foulants to achieve the greatest compatibility and cleaning efficiency.

Abstract

In an effort to gain a better understanding of the molecular interactions between chemical cleaning agents and reverse osmosis membranes, a group of potential chemical cleaning agents was exposed to eight different reverse osmosis membranes. These membranes included five thin-film composite polyamides (PA), a polyamide-urea (PA-U), a cellulose acetate (CA) and an experimental PA. Each membrane was exposed to 37 individual compounds that included nonionic, cationic, anionic, zwitterionic (neutral compound with both positive and negative charges), chelating and oxidizing chemical compounds. Following exposure to the cleaning agents it was determined that 82% of the compounds strongly associated with the membrane surface. The nonionic surfactant Mega 10 was the least reactive. The Hydranautics LFC3 and FilmTec BW-30 were the most resistant to the chemical exposure in that little chemical changes to these membranes were observed. Poor membrane performance often conflicted with the infrared spectroscopic analysis that indicated no adsorbed compounds on the surface. Limited applications of cleaning chemicals to fouled membranes produced mixed results, affecting water flux and solute flux inconsistently. Quantitative structure activity relationship (QSAR) molecular descriptors were generated by computer for each of the potential chemical-cleaning agents. Artificial neural network models were constructed and the correlation of molecular properties with membrane performance were determined. Three models were constructed (a PA, a CA and a PA-U) that were used to predict a chemical compound's effect on water flux and solute flux. Charge, polarity and hydrogen bonding properties appeared to be the most influential factors in determining a compound's effect on water flux and solute rejection.

1. Introduction

1.1 Background

Despite advancements made in reverse osmosis (RO) and nanofiltration (NF) membrane separation processes, the occurrence of biotic and abiotic fouling limits the efficient operation of these processes. Accumulation of foulants on the membrane surface often leads to a rapid decline in performance in terms of decreased water flux and increased salt passage (Ridgway and Safarik, 1991). While effective methods of controlling particulate and mineral scaling have been developed, membrane fouling by microorganisms is less well understood (Ridgway and Flemming, 1993). Reduction in the rate of biological and colloidal accumulation on the membrane surface is paramount to the efficient operation of separation processes (Flemming, 1993; Seidel and Elimelech, 2002). Proprietary advancements have resulted in a wide variety of RO membranes with distinct surface chemistries, some of which slow biofouling. Polyvinyl alcohol has been applied to NF and RO membranes to reduce surface roughness and reduce negative surface charge, two properties that are believed to promote fouling (Kim, et al., 2004). This post-manufacturing modification is also commonly employed to make the surface more hydrophilic, as hydrophobic surfaces are more prone to certain types of microbial fouling (Campbell, et al., 1999). Other forms of surface modification, such as polymer grafting, have also been applied to reduce membrane fouling (Tanaguchi, et al., 2002; Kilduff, et al., 2000). Despite any new developments in surface modification to reduce membrane fouling, chemical cleaning is a necessary process to ensure prolonged operation of membrane systems (Ebrahim, 1994; Madaeni, et al., 2001) and to reduce the economic impact of membrane fouling.

Issues related to chemical compatibility will continue to be a concern. Cleaning practices are now dictated to a significant extent by the type of RO membrane in operation. Chemicals once known to compromise the performance of traditional polyamide (PA) membranes (one classification of RO membranes) may now show promise given the recent alterations made to the polymer membrane surfaces. Understanding the molecular interactions between chemical cleaning agents and RO membranes with different surface chemistries and how these interactions influence membrane performance is vital to the development and implementation of cost-effective treatment processes.

1.2 Overview

Newly designed polymer membranes are being developed at a rapid pace. These membranes now possess different surface chemistries, which influence chemical adsorption and how chemical cleaning agents interact with the macromolecular fouling layer. The Cadotte (1981) trimesoyl chloride and *m*-phenylenediamine thin-film composite PA RO membrane has distinct advantages and disadvantages its earlier predecessor the cellulose acetate (CA) membrane. The major advantage of the thin-film composite membrane is its ability to produce high water flux at much lower pressures while maintaining high solute rejection. The disadvantage is the virtual lack of tolerance to exposure to free chlorine (Glater, et al., 1994, Avlonitis, et al., 1992;

Glater, et al., 1983), which is effective in controlling microbial fouling. The rough surface properties may also make the thin-film composite membrane more susceptible to fouling (Elimelech, et al., 1997; Hoek, et al., 2003). As a result many manufacturers have developed new membranes that claim to more fouling resistant. However, it is often not known beforehand whether a particular chemical treatment will damage the polymer membrane.

Continuous chloramination of the feedwater has been shown to be effective at controlling biofilm growth, i.e., fouling, on PA membranes in current use, but can still lead to a significant loss of membrane performance (Lozier, 2005). Studies with chemical preservatives have demonstrated the need to use caution when exposing membranes to chemical agents. Exposure to chemical biocides for potential use as membrane preservatives has revealed that the selection of the wrong chemical agents or combination of chemical agents can result in irreversible loss of performance (Ishida, et al., 1995). When surfactants are applied to a fouled surface, the foulants are displaced. However, the potential exists for the cleaning agent to adsorb to the polymer surface and affect membrane performance. Previous studies at OCWD demonstrated that dodecylbenzene-sulfonic acid (DBSA) could rapidly displace protein and polysaccharide from a thin film of CA and adsorb to the surface (Ishida, et al. 1998). The DBSA remained adsorbed to the CA surface following a rinse.

Chemical cleaning efficiency of biofilms on RO membranes has been studied in the past (Whittaker, et al., 1984). However, this study did not address the effects these chemicals have on membrane performance. In a more recent study, Liikanen, et al. (2002) evaluated chemical cleaners and their effects on a NF membrane. The findings of Bartlet, et al. (1995) suggest that there is a specific chemical concentration and temperature for optimum cleaning. Use of the wrong chemical additives can irreversibly damage the membrane, with significant financial loss and downtime. A better understanding of how cleaning agents interact with the membrane surface and the fouling layer is needed. It is critically important that we understand the molecular interactions that take place at the membrane surface as well as the interactions that occur between membranes and foulants and chemical cleaners and foulants. Knowledge of this type will lead to the development of more efficient and cost-effective chemical treatments for use in the field of membrane separations.

It has been widely reported that electrostatic and hydrophobic/hydrophilic interactions between the membrane and the foulants have a significant influence on cleaning efficiency and membrane compatibility (Vrijenhoek, E.M., et al., 2001; Braghetta, et al., 1998; Cho, et al., 2000). Results from previous investigations suggest it is theoretically possible to predict a compound's effect on water flux and salt rejection based on the knowledge of its fundamental molecular properties (see below). Since more than one molecular attribute may influence a compound's interaction with the membrane and affect water flux and salt rejection, multivariate statistical procedures such as multiple linear regression analysis are required to accurately model the phenomenon. A multivariate statistical approach that seeks to correlate a minimum set of independent molecular descriptors with molecular activity of function, e.g., water flux and solute

rejection, is referred to as quantitative structure-activity relationship (QSAR) analysis. The predictive statistical model developed from this analytical approach is referred to as a QSAR model.

In recent years, QSAR models have been successfully developed for a variety of experimental systems involving complex bio-organic and bio-polymer interactions. Campbell, et al. (1999) at OCWD developed regression-based QSAR models to predict the effectiveness of charged and neutral surfactants for inhibiting the attachment of fouling bacteria to PA and CA membranes. In another study, radiolabeled surrogate compounds were used to construct a series of QSAR-based empirical multivariate models describing the interactions of organic molecules (Rodriguez, et al., 2004) and pharmaceuticals (Rodriguez, et al., 2004) with several commercial PA and CA RO membranes. Models were constructed using artificial neural networks (ANN) based on data obtained from calculated QSAR molecular descriptors and direct measurements of compound-membrane associations. Penetration, adsorption/absorption, and rejection of molecules at the membrane interface were shown to be associated with molecular properties that included charge/polarity, structural complexity, hydrogen bonding and hydrophobicity.

ANNs have been applied to predict fouling of flat sheet ultrafilters (Bowen, et al., 1998; Bowen, et al., 1998) and tubular RO membranes (Niemi, et al., 1995). ANNs have also been considered for use in the prediction of membrane fouling during drinking water treatment (Delgrange, et al., 1998; Delgrange, et al., 1998). Most recently ANNs have been constructed to predict membrane fouling during nanofiltration of ground and surface water (Shetty and Chellam, 2003), utilizing inputs such as pH , total dissolved solids, UV_{254}, flow rate and permeate flux.

The current study looked at a number of potential cleaning compounds from seven general classes—anionic, cationic, nonionic, zwitterionic (neutral compound with both positive and negative charges), chelating, enzymatic and oxidizing agents—with a broad range of molecular properties. Multivariate ANN-based techniques were applied to create QSAR models that could accurately predict a compound's effect on membrane performance in terms of water flux and solute rejection.

1.3 Project Objectives

1.3.1 Test Chemical Compounds

Select several broad classes of chemical compounds (anionic, cationic, chelating agents, etc.) that could potentially serve as cleaning agents. Determine the effect these test compounds have on performance by measuring the change in water flux and solute rejection following exposure to each chemical agent.

1.3.2 Determine Binding Strength and Membrane Effects

Determine how strongly these chemical compounds adsorb to membranes with different surface chemistries.

1.3.3 Construct Artificial Neural Network (ANN) Model Describing Association of Cleaning Chemicals with Reverse Osmosis Membranes

Correlate chemical structures of the cleaning agents with membrane surface chemistries and develop a predictive model for chemical compatibility with membrane type.

1.3.4 Test Select Chemicals on Fouled Membranes

Perform field investigations to determine the effectiveness of select cleaning agents on membranes fouled with different sources of feedwater.

1.4 Report Organization

This report contains a detailed explanation of how the experiments were set up and implemented (Section 2.0). It includes a list of chemical cleaning agents, commercial membranes and methods used to characterize the membranes and cleaning chemicals and outlines how ANN models were built to describe the interaction of chemical agents with the surface of the polymer membranes. In the following section (Section 3.0), the results from individual experiments are presented with critical analysis of the findings. In the final section (Section 4.0), conclusions are drawn from the results obtained by the studies and recommendations are made for what should be done in the future.

2 Project Approach

The major focus of this study was to determine the affect a select group of chemical cleaning agents had on performance of RO membranes and relate the molecular properties of these compounds with the chemical and physical properties of the membranes. The membranes were characterized by numerous techniques to determine properties such as surface roughness, hydrophobicity, charge, polymer structure or ultrastructure, and chemical composition. Performance was based on the membrane water flux and solute rejection. Detailed molecular descriptors were generated by computer for each of the test compounds. A neural network model relating the membrane performance with cleaning chemical properties (defined by the molecular descriptors) was generated.

In the second phase of the study, cleaning compound-membrane interactions were investigated by infrared spectrometry and principal components analysis (PCA). Cleaning agents that demonstrated good membrane compatibility were tested on fouled membranes operated on a real feedwater source and their cleaning efficiency assessed and correlated with molecular properties of the compound.

2.1 Chemical Cleaning Agents

A master list of 67 compounds was initially generated (Table 1). From this list a total of 36 individual compounds and commercial solution and one chemical combination were selected for the study. There were seven general classes of chemical compounds that included (1) anionic, (2) cationic, (3) zwitterionic, (4) nonionic polar surfactants, (5) chelating compounds, (6) enzymatic compounds, and (7) oxidizing agents. The complete list of test compounds is displayed in Table 2. Molecular structures of these compounds are displayed in Appendix I. Many of the cationic quaternary amines were only sparingly soluble in water and thus were dropped from the study.

2.2 Reverse Osmosis Membranes

A total of eight RO membranes were selected for this study. Five of the membranes were commercially available thin-film composite PA, one was a commercially available polyamide-urea (PA-U), and one was an experimental thin-film composite RO membrane manufactured by Separation Systems Technology (SST), San Diego, Calif. This membrane was similar in composite to the commercial membranes made of trimesoyl chloride (TMC) and *m*-phenylenediamine (MPD) patented by Cadotte (1981). However, the support membrane was made of polyetherimide instead of polysulfone (PS). The last of the eight membranes was a commercial cellulose [tri-]acetate (CA). A list of the RO membranes including the manufacturer and model number is shown in Table 3.

Samples of the FilmTec BW-30 and Desal CA were cut from large rolls of flat sheet maintained at OCWD. Trisep X-201 and Hydranautics LFC3 membranes were obtained from full elements (40 x 2.5 in.) purchased through a local distributor (Applied Membranes, Inc. Vista, Calif.). Membrane sheets (10 x 10 in.) were cut from the element, rinsed in distilled water, dried and stored in ultraviolet-protective plastic bags. Flat sheet samples of TFC-ULP and TFC-HR were obtained directly from Koch Membrane Systems (San Diego, Calif.).

2.3 RO Test Protocol

Test swatches were cut slightly greater than 1 x 3 in. from flat sheets of membrane. Swatches were loaded into polyvinyl chloride RO test cells (Figure 1). Three of the block pressure cells were run in series. Four groups of three test cells were run in parallel (Figure 2) so that four membranes could be tested in triplicate during each experimental run. Feedwater consisted of 100 L of 1,000-ppm sodium chloride retained in a 120 L holding tank at 25° C and pH 5.5. The transmembrane pressure to each set of three test cells was adjusted independently to 200 psi. The test membranes were operated at a tangential crossflow of 1.6 gpm and the flux and rejection were allowed to stabilize overnight. In the morning, prior to the addition of cleaning agent, the water flux, feed and permeate conductivity (TDS) and temperature of the feedwater were measured. A volume of 4 L of cleaning solution was prepared in 1,000-ppm sodium chloride feedwater and the pH adjusted with hydrochloric acid or sodium hydroxide. With the RO system turned off, the cleaning solution was heated to 40°C and recirculated over the surface of

the RO membranes (Figure 3). After 1 hr the cleaning solution was flushed from the test cells with 4 L (~ 8 volumes) of 1,000-ppm sodium chloride feedwater. Test membranes were operated in RO for 15 min at 200 psi and 1.6 gpm to stabilize the membranes before water flux, conductivity and water temperature were measured. Membrane controls were run separately under the same conditions over the same period of time less any exposure to the cleaning agents. Membrane swatches were removed, dip rinsed three times in distilled water and placed in plastic petri dishes for transport back to the lab.

2.4 Characterization of Reverse Osmosis Membranes

2.4.1 Attenuated Total Reflection Fourier Transform Infrared Spectrometry

Mid-infrared internal reflection spectrometry or attenuated total reflection Fourier transform infrared (ATR/FTIR) spectrometry was used to assess changes in chemical structure of the polymer membranes and to determine if the chemical compounds remained adsorbed on the membrane surface (Ridgway, et al., 1999). ATR/FTIR spectrometry works by focusing infrared light on the end of an IR transparent internal reflection element (IRE) of high refractive index. At each internal reflection IR radiation penetrates a short distance (~1 μm) from the interface. IR active samples, such as polymer membranes, placed in contact with IRE surface absorb some the light producing a vibrational spectrum unique to the membrane or chemical compound. The resulting vibrational spectrum can be used to determine chemical structure and changes in chemical structure associated with damage to the membrane surface or adsorption of chemical species.

The sample swatches removed from the test system were placed in a glove box purged with compressed air passed through a Balston drier (Parker Hannifin, Haverhill, MA). The swatches were stored in the glove box until the infrared analysis was performed. Each swatch was cut into six equally sized pieces, in half across the width and then in thirds down the length. The center pieces were pressed against the surface of a 45º single-reflection germanium (Ge) ThunderDome internal reflection element (Thermo Spectra-Tech, Madison, WI). Sample spectra consisted of 256 coadded scans collected at 4-cm^{-1} resolution with a Magna 550 Fourier transform infrared (FTIR) spectrometer (Thermo Electron Corp., Madison, WI). Spectra of the control membranes were obtained in the same manner. The sample area of each spectrum collected with the Ge single reflection IRE was a circle 2 mm in diameter. A total of 30 control spectra and 18 sample spectra were collected for each membrane. The single-beam spectra of the samples were (1) ratioed against the single beam of the bare internal reflection element, (2) converted to absorbance, (3) truncated at 650 cm^{-1}, (4) corrected for the wavelength dependence of internal reflection and (5) baseline corrected utilizing GRAMS/AI (Version 7.02) software (Thermo Galactic, Salem, NH). Principal components analysis (PCA) was performed with PLSplus IQ (Thermo Galactic, version 5.20) software. Twenty-five (25) control membrane spectra and 15 cleaning agent-exposed membrane spectra were retained for the PCA. The full spectral range between 4000 cm^{-1} and 650 cm^{-1} was used in the analysis. The data were mean centered and cross-validated.

2.4.2 Atomic Force Microscopy

Microscale surface features can influence performance of the separations membrane. AFM can be used to map microscale topography and pore geometries of air-dried as well as fully hydrated polymer membranes (Ridgway, et al., 1999). Images were acquired utilizing silicon ultralevers, which were gold-coated cantilevers with integrated high-aspect ratio silicon nitride conical tips. These cantilevers are designed for maximum penetration into pores and other surface irregularities that are frequently encountered on the surface of polymer membranes. Tapping-mode AFM was employed to minimize translational forces between the AFM tip and the membrane surface.

Prior to analysis the membrane samples were sonicated for 1 hr in 18 Mohm-cm deionized water (Barnstead/Thermolyne, Dubuque, IA) and dried in a glove box purged with compressed air passed through a Balston dryer. The sonication was applied to the samples to remove preservatives that are often applied to the membranes at part of the manufacturing process.

The surface morphologies of the membranes were characterized by tapping mode AFM using Park Scientific Instruments model CP Auto Probe (Digital Instruments/Veeco Metrology, Santa Barbara, CA), equipped with a non-contact/contact head and a 100-µm scanner, operated in a constant force mode. Small membrane pieces were attached to a stainless steel sample holder using 12-mm carbon conductive tabs and mounted on the piezo scanner of the AFM. Images were acquired utilizing silicon "ultralevers" (force constant = 0.24 N/m). AFM images were acquired at a scan rate of 1.0-1.5 kHz with an information density of 256 x 256 pixels. The RMS roughness and mean surface height were calculated for each membrane using Park Scientific software provided with the CP AutoProbe. For a transect containing N data points, the RMS roughness is given by the standard deviation of the individual height measurements. The mean height is given by the average of the individual height determinations within the selected height profile.

2.4.3 Transmission Electron Microscopy

Transmission electron microscopy (TEM) was used to obtain high-resolution images of the cross section of the membranes. TEM provides information about the thickness and internal structure of the thin polymer layer of membrane that was not provided by AFM measurements. The TEM analysis was performed at the Central Facility for Advanced Microscopy and Microanalysis (http://micron.ucr.edu) on the campus of University of California Riverside.

Membrane samples were stained with 1% aqueous OsO_4 for 1 hr. The samples were then dehydrated in a graded ethanol series of 30%, 50%, 70%, 90% and 100% for 10 min each, followed by 3 changes of 100% ethanol for 10 min each. Samples were placed in 1/3 Spurr resin and 2/3 ethanol for 2 hr, 2/3 Spurr and 1/3 ethanol for 2 hr and 2 treatments of 100% Spurr 2 hr each. Samples were placed in flat embedding molds in fresh resin and polymerized overnight at 70°C. Sections were taken on an RMC-MT-X ultramicrotome and then viewed on a Philips CM 300 transmission electron microscope.

2.4.4 Captive Air Bubble Contact Angle

Contact angle provides information about the relative hydrophobicity of the surface of separations membranes (Ridgway, et al., 1999). The hydrophobicity of the substrata influences the strength and kinetics of molecular interactions. Contact angle describes an important surface parameter in studies of the molecular interactions of cleaning agents with the polymer membrane surface. Since the membranes are normally operated in a fully hydrated state, captive bubble determinations on wet membranes are more relevant for actual operating conditions. Contact angle, reported in degrees, is compared with select standard materials. An air bubble released from a syringe travels upward onto the surface of a hydrated membrane where it becomes trapped, or "captive." The degree of hydrophobicity can be determined from the height/width ratio of the bubble. A hydrophobic membrane causes the bubble to spread over the membrane surface since water is excluded from the bubble-membrane interface. This "flattening" corresponds to a smaller ratio, while a hydrophilic surface would result in a larger ratio. The contact angle is derived algorithmically from the height/width ratio and is inversely related. Thus, the smaller the height/width ratio, the larger is the contact angle and the greater the hydrophobicity of the membrane surface. The following formulas are used to convert the bubble aspect ratio values to contact angles.

$$\text{contact angle} = 2 \arctan (2h/w) \qquad \text{For angles ,} < 90°$$

where h = the bubble height and w = the bubble diameter.

The relative surface hydrophobicities of the membranes were compared by captive (air) bubble contact angle measurements. The determinations were made by introducing an air bubble under the surface of the membrane submerged in 18 Mohm-cm deionized water with the active membrane surface facing down. The bubble trapped under the surface of the membrane was imaged with a CCD camera. The digitized image was analyzed using ImagePro (MediaCybernetics, Version 3.0, Silver Spring, MD) software to measure the bubble height and width and the tangent contact angle. The dimensions are automatically transferred to an Excel spreadsheet (Microsoft Corporation, Redmond, WA) and the contact angle calculated. The contact angle of five bubbles were measured for each of 3 swatches for a total of 15 measurements. The mean and standard deviation were reported.

2.4.5 Streaming Potential / Zeta Potential

The surface charge on each membrane was determined using methods developed by Childress and Elimelech (1996). Zeta potential measurements were performed using a streaming potential analyzer (ZetaCAD, CAD Instrumentation, Les Essarts Le Roi, France). This instrument includes an analyzer, measuring cell, electrodes, and a data control system. The feed solution was driven through the measuring cell using pressurized nitrogen. Sensors for measuring the temperature and electrical conductivity of the measuring solution were located internally and pH was measured externally.

The cell for measurements of membrane surface charge was designed to create a parallel channel that is 30 x 80 x 0.25 mm high. Two membrane coupons (40 x 80 mm) were used for each measurement. One piece, with its active layer facing up, was placed in the bottom of the cell and the other piece, with its active layer facing down, placed on top. Two polytetrafluoroethylene (PTFE) spacers were used to separate the two membranes to create the flow channel. The cell cover was fitted with a rubber seal and fixed to the bottom cell assemblage with screws.

The Ag/AgCl electrodes that measure the induced streaming potential were mounted at each end of the channel. To prevent polarization of the electrodes, the direction of flow through the cell was alternated for each run. Additionally, the electrodes were stored in 0.01 M NaCl solution overnight to prevent build-up of charge.

Streaming potential measurements for all membranes were performed at an ionic strength of 0.017 M NaCl (1000 ppm) and over a pH range of 3 to 9. Membranes were supplied as dry sheets and were stored in deionized water at 5° C. Solution pH was adjusted using hydrochloric acid and sodium hydroxide. Electrolyte solution was circulated through the system for 30 minutes to equilibrate the ionic strength and pH of the feed solution in the measuring cell. Furthermore, this allows equilibration of the membrane in the test solution as recommended by Childress and Elimelech (1996). All streaming potential measurements were performed at room temperature (~23˚C). The results for each pH value were an average of 6 measurements taken at that pH. Following each test the system was rinsed with two liters of deionized water.

Zeta potential was calculated from the streaming potential using the Helmoltz-Smoluchowski equation:

$$\zeta = \frac{\Delta U_s}{\Delta P} \frac{\mu}{\varepsilon \varepsilon_0} \frac{L}{A} \frac{1}{R}$$

where ζ is the zeta potential; U_s is the streaming potential; P is the applied pressure, $\Delta U_s/\Delta P$ is the slope of the streaming potential versus applied pressure curve; μ is the dynamic viscosity of the solution; ε is the permittivity of the test solution; ε_0 is the permittivity of free space; L is the channel length; A is the channel cross-sectional area; and R is the channel resistance.

Besides the actual zeta potential at pH 5.5, the change in zeta potential as a function of pH was calculated and used as a means of characterizing the membranes. The slope was calculated by fitting a regression line between the three zeta potential measurements at pH ~4.5, 5.5 and ~7. This membrane property was reported as zeta potential slope.

2.4.6 Chemical Cleaning Protocol of Fouled Membranes

Test swatches slightly greater than 1 x 3 in. were cut from flat sheets of membrane. Swatches were loaded into polyvinyl chloride RO test cells as described above. The membrane swatches were fed secondary-treated wastewater (Q1) and allowed to stabilize

over 15 min. The pressure was then adjusted on each bank until an average water flux of 15 to 20 gfd was achieved. The applied pressure and permeate flux were measured and constituted the "Q1 initial" flux and "Q1 initial" pressure. Feed TDS and pH were also measured. Flux was measured frequently using the middle cell and pressure was adjusted to maintain constant Q1 permeate flux. The permeate TDS was measured periodically to assess salt rejection. The membrane was considered "fouled" when the increase in pressure required to maintain "Q1 initial" flux (~15 gfd) on the bank was ~15-20%. At this point, the permeate TDS and flux of the three test cells were measured. The pressure was adjusted to return the average flux to "Q1 initial" flux. The new pressure, which constituted the "fouled" pressure, was recorded. Likewise, the permeate flux and TDS were regarded as the "fouled" TDS and flux.

Two (2) liters of chemical cleaning agent were prepared in deionized water containing 1,000-ppm NaCl and adjust to the desired pH with HCl or NaOH. The cleaning solution (40˚C) was recirculated through the cells containing the fouled membranes for 30 min at a low flow (~0.5 gpd). The solution was allowed to soak in contact with membranes for 2 hr then flushed from the test cells with tap water for 15-20 min. A total volume of 5-10 L was flushed through then a volume of 4 L was recirculated for 20-30 min.

The Q1 feed to RO test cells was reopened and after 15 min flux and rejection were measured. The pressure was adjusted to return the flux to the initial ~15 gfd. The pressure and flows were then recorded.

Flux data was converted to specific flux ($L/m^2 \cdot day/psi$) and the values of percent rejection were converted to specific solute flux ($moles/m^2/day$) for the purposes of reporting and normalization. The final pressure and TDS were compared with the "fouled readings," and percent change in water flux and solute flux were reported.

2.4.7 Construction of Artificial Neural Network (ANN) Models Describing the Affect of Chemical Compounds on Membrane Performance

Multivariate analysis methods based on standard statistical approaches are capable of predicting the behavior of reasonably complex systems provided the systems are well behaved and that the input functions describing the system are statistically independent of each other. In the case of organic compound interactions with RO membranes, there may be reasonably smooth relationships within the scope of the interactions that could model well by traditional techniques. However, the molecular descriptors are by nature not entirely independent of one another. For example, it is difficult to design a molecule in which the molecular weight increases very much with out a concomitant increase in molecular complexity. Thus, existence of Interco relations between molecular descriptor inputs makes modeling compound-membrane interaction more difficult. However, neural network computing is less susceptible to these issues than are more traditional modeling methods. Moreover, neural computing methods are capable of describing the behavior of highly complex, nonlinear systems in which the exclusive rules of the interaction are either unknown or difficult to quantify. As with genetic algorithms, the

details regarding how ANNs are designed and constructed is outside the scope of this report. Bharath and Drosen (1994) provide a good review.

An ANN is composed of a network of virtual neurons ("perceptrons"). Information enters each perceptron via "synapses"; each feeding a simple function with a weighting factor that can emphasize or de-emphasize the overall influence of the function. The effects of all the input functions are summed in the perceptron, then fed to an output function (often sigmoidal) by which the perceptron passes information to units further down in the network. The neural net is constructed by interconnecting layers of these perceptrons. Although highly complex multilayered networks are possible, the design adopted for this study was a three-layered network consisting of an input layer, a "hidden" processing layer and an output layer (a single output perceptron in this case). The relationship between inputs and the outputs of a complex system are embossed upon the network by "training" it using concrete exemplars from the real world. During the training process, perceptrons are added and the values of the weighting factors are adjusted until the behavior of the network converges on the behavior of the real system as determined by one or more correlative comparisons. At this point, the network has "learned" to recognize patterns in the input data that predict the output data. As with any empirical mathematical modeling method, challenging the network with a "validation" set of exemplars evaluates the predictive ability of the network. Test data typically consist of 10% to 20% of the exemplars that were not present during training. A well-trained network will predict behavior of the test exemplars as well as it did the training exemplars.

2.4.8 Membranes and Membrane Dependent Performance Parameters

Two membrane performance parameters (water flux and salt rejection) were modeled for each of the eight membranes in this study. The data were pooled for the five thin-film composite polyamide membranes (FilmTec BW-30, Hydranautics LFC3 and ESPA2, and Koch TFC-HR and TFC-ULP) and used to construct a "universal" PA model describing the chemical properties that affect membrane water flux and salt rejection. The Trisep X-201 (PA-U) and the Desal CA membranes were modeled separately.

2.4.9 Membrane Descriptors

The RO membranes were characterized by numerous techniques (see above) including TEM, AFM, contact angle, streaming potential and infrared spectrometry. The surface and chemical properties of the membranes were tabulated for use in developing the ANN models.

2.4.10 Generation of Cleaning Compound QSAR Descriptors

Each cleaning compound was constructed using molecular modeling computer software (QSARis, SciVision, Inc., Lexington, MA) and initially more than 363 molecular descriptors were calculated for each of the compounds and placed in a master list. The

descriptors were organized into 17 major categories, each of which contained numerous sub-categories, as indicated below:

- Atom-type-e-state (80 categories)
- Atom-type-e-state-acnt (80 categories)
- Connect-valence (34 categories)
- Connect-subgraph-counts (19 categories)
- HE-state-acnt (8 categories)
- Internal-H-bonds-e-state (18 categories)
- Info-content (7 categories)
- HE-state-for-groups (5 categories)
- HE-state-catagories (14 categories)
- Kappa-shape-index (8 categories)
- Log-LD50 (2 categories)
- Molecular properties (19 categories)
- Total-topological-properties (11 categories)
- 3d-general (11 categories)
- 3d-molecular-moment (13 categories)
- simple-connectivities (33 categories)

From this group the number of descriptors was quickly reduced to 192 as many had values of zero.

2.4.11 Selection of Best QSAR Descriptors for Correlation with Chemical Properties and Membrane Performance

Due to software limitations that restricted the total number of independent-variable (descriptor) inputs that could be used for the development of QSAR models, the total number of descriptors was reduced further. A list of 73 molecular descriptors was selected from the group of 192 based on previous studies at OCWD (Rodriguez and Phipps, 2004, Rodriguez, et. al., 2004). These 73 molecular descriptors where determined to be most relevant to the characterization of chemical interactions with polymer separations membranes. The descriptors were reclassified into five major groups of chemical properties consisting of (1) charge/polarity, (2) molecular complexity, (3) hydrogen bonding, (4) hydrophobicity, and (5) other (see Table 4).

2.4.11.1 Training and Validation Descriptors and Randomization of Order

In constructing the ANN models, not all of the data were utilized in the building phases. The data on the cleaning compounds were divided into a "training" set and a "validation" set. Training set consisted of 25 compounds from the list of 37 compounds that were tested in RO (Table 5). The list was limited to 25 because some of the test compounds were proprietary mixtures and others were enzymes. Three other compounds were held back for the validation set. These compounds, Zwittergent 3-12, octanesulfonic acid and dodecyltrimethylammonium bromide, were each the middle compound in a homologous

series of test compounds. For all individual membrane models, data spreadsheets were created containing a line of data for each compound. Exemplars were constructed for each of the 24 training compounds by combining the 73 molecular descriptors (independent variables) with the measured membrane water flux and salt rejection (dependent variables). The original field replicates were used in the process rather than the average flux and rejection. Each of the 24 cleaning compounds in the training set was represented by 3 replicates, raising the total number of exemplars to 72 for each membrane. This was done to capture the full range of statistical variation present in the field measurements and because there was a small number of test compounds in the training set.

For the PA model that included the five PA membranes the numerical membrane properties or descriptors (Table 6) were included as input parameters, the assumption being that one or more of these membrane properties could be as influential on compound-membrane performance as the QSAR molecular descriptors.

In all cases, the order of the compounds was randomized prior to any input elimination or modeling efforts. This was achieved by first creating random numbers using the Excel randomization function and assigning these numbers to each line of exemplar data, then sorting the exemplars using these random numbers. This resulted in a complete randomization of the order of the cleaning compounds in the data spreadsheet. Randomization of the order of the exemplars was performed before each input selection or modeling effort as an additional precaution to insure that the order in which data were presented did not influence the final results.

2.4.11.2 Identification of Subsets of Influential Descriptors Using a Genetic Algorithm (GA)

Selection of input parameters (descriptors) for this study was achieved using a genetic algorithm provided as part of the Neural Works Predict package (Neural Works Predict, Neuralware, Carnegie, PA). The program utilized a logistic multiple linear regression fitness evaluation. In addition to the normal GA selection criteria, an additional "Cascaded Variable Selection" was employed to rapidly eliminate inputs with a low probability of inclusion in the optimum input set (a function especially useful with large input arrays). Inclusion of inputs by the GA was detected by construction of a single neural network and performing a sensitivity analysis to detect influential inputs (methods described below). The GA eliminated descriptors that did not predict compound-membrane interactions and typically reduced the 73 descriptor set down to subsets from 6 to 10 descriptors.

2.4.11.3 Identification of Most Common Influential Descriptors

The GA converges on an optimum fit between the input parameters and the output parameter, but it does not necessarily predict a globally optimum input set. More than one combination of inputs may lead to an acceptable solution, especially if the inputs are partially intercorrelated, as are many of the molecular descriptors. Even though efforts

were taken to reduce intercorrelation, some still persisted. Therefore, some randomness exists in the selection of inputs (descriptors) by the GA. From a statistical basis the GA should choose the most highly influential inputs most frequently. Thus, a histogram constructed from multiple, independent GA selections should reveal the most influential input parameters for subsequent modeling. A histogram was constructed for each model by operating the GA on each data set for 10 interations. For each interation, the order of descriptors in the data spreadsheet was re-randomized, ensuring that the GA started with a completely different and randomized seed population each time. Inputs selected by the GA were detected as described above and recorded to produce a histogram. Influential descriptors were retained using a simple filter based on inclusion of the descriptor in ≥ 50% of the descriptor sets by the GA. This method typically resulted in selection of 6 to 10 of the inputs per spreadsheet for inclusion in the ANN model.

2.4.11.4 Construction of Artificial Neural Network Models

As before, the order of exemplars was randomized prior to GA selection and ANN model construction. This ensured that any ordering of the exemplars would not influence selection of inputs by the GA or training of the ANN. ANN models were constructed from the surviving input (descriptors) parameters using NeuralWorks Predict v2.41 (Neuralware, Carnegie, PA). Although the input data were theoretically "clean", the output data were considered to be "moderately noisy". The software settings were was adjusted accordingly to help prevent model over fitting (modeling variations caused by noise). Input data entering and leaving the network had to be transformed from real world values to the relative input values required by the ANN. This was accomplished by use of one or more transformation functions. Whereas during selection of salient inputs the choice of transforms was limited to one, in this case up to three transforms could be assigned per input (thus, there could be up to three input perceptrons per descriptor in the ANN). Transformation functions could either be linear (scaling only), or nonlinear (log, ln, exponential, power, inverse, inverse power or hyperbolic tangent) expressions. The software automatically optimized the choice of functions by regression analysis.

2.4.11.5 Selection of Model Inputs Using the Genetic Algorithm

The method used was more extensive than that for identification of salient input parameters described above in an attempt to further reduce the number of input parameters per ANN model. Once again a multiple logistic linear regression routine was employed with the cascade variable selection activated.

2.4.11.6 Training and Selecting the Best ANN Model

Three networks were constructed using the training data. Construction and training the networks proceeded using an adaptive gradient learning rule in which back-propagated gradient information was used to guide an iterative search algorithm. Back-propagation involves determining the difference between the desired output (the actual laboratory result) and the network prediction, then adjusting the output layer (perceptron) weighting

factors in proportion to the difference. The calculations involved in this correction are then used as a basis for making correction to weights in the hidden layer and finally in the input layer (Bharath and Drosen, 1994). Performance of the networks was evaluated by comparison of the linear correlation (R) between the predicted outputs and the actual laboratory flux data, and the best of the three ANNs chosen. Correlation values were found to be in excess of 0.95 in most cases for these models.

2.4.11.7 Validation of the Selected Neural Network

The test exemplar set previously described was used to determine the ability of the network to model behavior of the surrogates. Comparison of the correlation coefficient was used as a measure of overall performance. Close matches between training and validation data sets were taken as an indication of a good model. Typically, training and test R values were within 0.05 - 0.07 for these models. Additional measures of good model behavior included tight predicted 95% confidence limits. The number of molecular descriptors per model at this point was 4 to 10.

2.4.11.8 Using Sensitivity Analysis to Eliminate Non-Influential ANN Inputs

Due to the more stringent GA settings and the ability to employ more than one transformation function during ANN model construction, the possibility existed that not all of the descriptors provided to the model would be chosen for inclusion in the model. In order to eliminate inputs that had been rejected by the ANN, a sensitivity analysis was performed on the entire data set. This analysis generally indicates the degree and direction of influence that each input in the ANN model has on the model output. If the sensitivity analysis is zero, the input likely has no significant effect on the model and may be eliminated without a significant change in model fitness.

Inputs discovered with null sensitivity indices were eliminated from the input data set and a new ANN model was then constructed using the above methods. This process was continued until all inputs demonstrated influence in the model. It typically took 2 to 3 iterations to achieve this. This served to simplify each flux model by eliminating one or two inputs without significantly sacrificing model predictability. The final ANN models contained from 4 to 10 input descriptors.

2.4.11.9 Characterization and Validation of ANN Models

For each ANN model, the predicted output was graphically compared with the actual measured flux data, the correlation coefficients between predicted and actual flux data were determined, and the 95% confidence intervals were calculated. A final sensitivity analysis was performed to evaluate the influence of each molecular descriptor included in the model on membrane water flux and solute passage. The predicted affect of membrane flux and rejection were calculated for the entire list of 67 compounds for which QSAR descriptors were available.

3 Project Outcomes

3.1 Characterization of Reverse Osmosis Membranes

3.1.1 Surface Structure by AFM

The two-dimensional AFM images (100 μm^2) of the eight RO membranes are displayed in Figure 4. The surface of the membranes was characterized in terms of RMS roughness, average roughness, mean height, peak height, volume, and surface area. These data are tabulated for the eight membranes in Table 7. Plots of these surface properties were generated and are displayed for RMS roughness and average roughness in Figure 5, mean height, median height and peak height in Figure 6, volume in Figure 7 and surface area in Figure 8. Of the eight membranes, the SST TMC/MPD polyamide membrane was the smoothest while the Hydranautics ESPA2 was the roughest. However, it should be noted that the SST TMC/MPD polyamide membrane was coated with a polyvinyl alcohol that was not removed by the 1 hr sonication in deionized water. The polyvinyl alcohol effectively filled in the depressions or valleys and had a smoothing effect on the membrane surface.

3.1.2 Membrane Ultrastructure by TEM

TEM images of the eight membranes are displayed in Figures 9 through 16. Images are displayed at 8,000X for the Desal CA and Trisep X-201 in Figure 9, FilmTec BW-30 and SST TMC/MPD in Figure 10, Hydranautics ESPA2 and LFC3 in Figure 11, Koch TFC-HR and TFC-ULP in Figure 12. Images are displayed at 42,000X for the Desal CA and at 60,000X for the Trisep X-201 in Figure 13, FilmTec BW-30 and SST TMC/MPD in Figure 14, Hydranautics ESPA2 and LFC3 in Figure 15, Koch TFC-HR and TFC-ULP in Figure 16.

The CA membrane is not a thin-film composite; therefore, a discrete separations layer is not visible in the TEM images. The more densely colored material toward the top of the image in Figure 9 is CA. The lighter material is the TEM embedding resin. The thin-film composite membrane is composed of three independent layers, two of which are visible in the TEM images. The thin polyamide or polyamide-urea (Trisep X-201) separations layer is on the order of 0.3 to 0.5 μm. The bulk of the material in the images is attributed to the 20- to 25-μm PS support that has a "Swiss cheese" or bubble-like appearance. The polyetherimide support of the TMC/MPD membrane made by SST is more granular in composition (see Figure 10).

The PA (or PA-U) layer is not a homogenous discrete layer as seen with the CA membrane. This polymer separations layer varies in appearance from lacy in texture to appearing as a collection of thin-walled bubble-like structures at the surface and extends 0.3 to 0.5 μm from the surface of the PS support. All of the thin-film composite membranes appear to have a continuous rather dense granular base structure at the interface between the PS support and the PA or PA-U layer. However, it is the upper layers that contribute to the surface roughness. It is not known whether the actual

separation, i.e., desalination occurs within the bubble structures or at the dense base layer of the membrane.

The Hydranautics LFC3 membrane appears to be coated with a material that excluded the TEM preparatory resin and appears to slightly reduce the roughness of the surface of the membrane relative to the ESPA2 membrane (see Figure 11 and Figure 15). The Hydranautics LFC3 is believed to be a polymer-coated Hydranautics ESPA3 membrane. The identity of the polymer coating is not known although it is believed to be polyvinyl alcohol.

3.1.3 Surface Hydrophobicity by Captive Air Bubble Contact Angle

Captive air bubble contact angle measurements are displayed in Figure 17 and Figure 18. The contact angles for the thin-film composite membranes were normalized to the "standard" PA, i.e., FilmTec BW-30, to account for day-to-day variations. The CA membrane had the highest contact angle indicating greater hydrophobicity relative to the seven thin-film composite membranes. The SST TMC/MPD membrane had the highest contact angle (61.64º) of the thin-film composite membranes. Hydranautics ESPA2 had the lowest contact angle (60.63º) indicating that it was the least hydrophobic of all the membranes.

3.1.4 Surface Charge / Zeta Potential by Streaming Potential

The zeta potential at the surface of the membranes was determined over a range of pH from 3 to 9. The data are compiled in Table 8. A plot of the zeta potential as a function of pH is displayed in Figure 19. The SST TMC/MPD membrane was not determined as in sufficient membrane was available for analysis. As the pH was increased from ~3 to 9 the zeta potential decreased, i.e., the surface became more negatively charged. The membranes have an isoelectric point between 3.5 and 4.0 except for the Koch TFC-ULP, which still had a significant negative charge (-6.43 mV) at pH 3.5. The TFC-ULP membrane was not tested below pH 3.5. Above pH 4.5 all seven RO membranes had a negative zeta potential. The negative charge on the PA membranes is believed to be associated with carboxylate (COO^-) functional groups on the membrane. These carboxylic acid / carboxylate groups form during the manufacturing process when unreacted acid chloride (OCl) groups on TMC undergo hydrolysis. The source of negative charge on the CA membrane is believed to orginate from carboxylate groups (Demisch and Pusch, 1979). However, some of the negative charge may be associated with proprietary post-treatments. The zeta potential of the membranes appeared to stabilize as the pH rose above pH 7, except for the Hydranautics LFC3, which dropped from –20.81 mV at pH 7 to –23.19 mV at pH 9. At pH 5.6, near the test conditions of the feedwater, the FilmTec BW-30 was the least negative (-9.08 mV) and the Desal CA membrane was the most negative (-21.45 mV).

The change in zeta potential between pH 4.5 and 7 was calculated as another means of characterizing surface charge of the membranes. A linear regression line was fit to the

zeta potential measured within this range. The zeta potential slope provides information on how assessable the charged groups are at membrane surface (see Table 9).

3.1.5 Structural Characterization of RO Membranes by ATR/FTIR Spectrometry

The molecular structures of the three different membranes (CA, PA, and PA-U) are shown in Figure 20. The CA membrane is actually a cellulose triacetate membrane. Each of the hydroxyl groups is substituted with an acetate group. The Trisep X-201 membrane is a crosslinked PA-U membrane and it is very similar in structure to the PA membrane. Approximately one third of the bonds between the benzene rings are composed of a carbonyl (C=O) situated between two amide (N-H) groups as opposed to the single amide and single carbonyl group on the PA membranes. Representative ATR/FTIR spectra of the eight RO membranes are displayed in Figure 21 and Figure 22. These spectra were obtained from membranes that were operated on the 1,000-ppm NaCl feedwater for approximately 14 hr.

Infrared light that penetrates into the membrane during the sampling process passes through the thin (~0.3 um) PA layer and into the PS support layer at the point of internal reflection on the surface of the Ge IRE. Thus, the ATR spectra of the thin-film composite membranes are composed of a combination of PA (or PA-U) and PS infrared vibrational bands. The majority of vibrational bands in the IR spectra are associated with the PS support membrane. Spectra of PA and PS are displayed in Figure 23 along with a spectrum of the PA membrane. Vibrational bands of the PA and PS layers that are relevant to this study are labeled in Figure 23 and Figure 24.

Unused membranes were characterized using various band intensity ratios associated with pertinent functional groups. The amide I / 874 cm^{-1} and amide II / 874 cm^{-1} band intensity ratios were used to assess the relative polyamide film thickness (Figure 25). The 874 cm^{-1} band is associated with the PS support membrane. The thicker the polyamide film the greater the polyamide band intensities become relative to the absorption bands of the PS support. Therefore, the thicker the PA film the greater are the amide I / 874 cm^{-1} and amide II / 874 cm^{-1} band intensity ratios. The amide I / amide II (C=O/N-H) band intensity ratio was used as measure of PA secondary structure. Variations in this band intensity ratio may also be associated with differences in hydrogen bonding between the carbonyl and amide groups of adjoining polymer chains. Previous studies at OCWD have revealed differences in the relative band intensities of the amide I (C=O) and the amide II (N-H) of the PA membranes. The COO^- / amide I and COO^- / amide II band intensity ratios are displayed in Figure 26. These ratios are used to assess the relative crosslink density and relative carboxylate (COO^-) density of the polyamide membranes. In theory highly crosslinked polyamide membranes should also carry less negative charge. As more acid chlorides on TMC react to form amide (NH-C=O) bonds more crosslinking occurs and less acid chloride groups are left to undergo hydrolysis to form carboxylic acids or carboxylate groups. Finally, the OH / amide II band intensity ratio was used to measure relative polymer hydrophobicity. Membranes with a high hydroxyl (OH) content per unit of polymer membrane should be more polar and thus more hydrophilic in nature.

It is important to note that the ATR/FTIR spectroscopic analysis provides information on the bulk polymer membrane properties, as infrared radiation passes through the entire PA [PA-U] layer into the PS at the point of internal reflection. Other characterization methods such as AFM, contact angle and zeta potential address surface properties of the polymer membranes. The bulk PA properties and the surface PA properties may vary significantly.

Of the five PA membranes the Hydranautics LFC3 and ESPA2 membrane had the thickest PA layer, while the Koch TFC-HR and TFC-ULP had a significantly thinner polyamide layer. It is not valid to compare the amide II / 874 cm^{-1} ratio of the Trisep X-201 membrane with the PA membranes since this membrane contains a urethane bond (NH-[C=O]-NH). Therefore, the N-H contribution to the spectrum is much greater. If one assumes that the Trisep X-201 carbonyl (C=O) is similar to the amide I carbonyl and then compares the amide I / 874 cm^{-1} band intensity ratios, the thickness of the separations layer of the Trisep X-201 appears to lie between the Hydranautics and Koch membranes. Analysis of the TEM images seems to support this conclusion (see Figure **13**, Figure 15 and Figure 16).

The amide I / amide II band intensity ratio is typically a near 1 for the PA membranes. All five polyamide membranes had a similar amide I / amide II ratio (Figure 25). In the case of the Trisep X-201 membrane this ratio dropped to ~0.6 as the polyamide-urea membrane contains approximately one third more N-H groups per repeating unit of polymer membrane.

Analysis of the carboxylate / amide I and carboxylate / amide II band intensity ratios suggest that the FilmTec BW-30 and Hydranautics LFC3 membranes are less crosslinked and have greater negative charge (Figure 26). The ratios for the Koch TFC-HR and TFC-ULP suggest a greater degree of crosslinking occurs in these two membranes relative to the BW-30 and LFC3 membranes. The TFC-HR and TFC-ULP membranes should also be less negative in charge. However, the zeta potential data did not support this conclusion as the FilmTec BW-30 had the least negative surface charge, followed by the Koch TFC-HR and TFC-ULP membranes. The Hydranautics LFC3 was the most negative of the four membranes. Again it should be noted that streaming potential measures the zeta potential or negative charge at the surface of the membrane and the FilmTec BW-30 and Hydranautics LFC3 are both post-treated membranes. These treatments undoubtedly affect the properties of the polymer membranes and may shield surface from electrostatic charge. More studies need to be done to resolve the differences between these measurements of negative charge.

The OH stretch / amide II band intensity ratio of the FilmTec BW-30 and Hydranautics LFC3 membranes were the greatest (Figure 26). Membranes with a high hydroxyl (OH) content should be more hydrophilic. However, contact angle measurements of the membrane point to just the opposite conclusion (see Figure 17). The BW-30 and LFC3 membranes had the highest contact angle, the greatest hydrophobicity, relative to the TFC-ULP, TFC-HR and X-201 membranes. Again, the ATR/FTIR band intensity ratios

relate to the bulk membrane properties. AFM, zeta potential and contact angle relate specifically to the membrane surface. The fact that a membrane has high OH content does not mean that this functionality is located entirely at the surface. However, if the increased OH content is specifically associated with the post-treatment then one would expect the hydrophobicity to decrease, i.e., the contact angle to decrease. Surface roughness may factor into the contact angle measurements. However, at this time the results are contradictory and inconclusive.

Individual spectra of the RO membranes that were exposed to chemical cleaning agents are not displayed in the report due large number of IR spectra that were collected. A total of 37 chemical agents were screened on 8 different membranes. For each compound on each membrane, a minimum of 18 ATR/FTIR spectra was collected and 30 spectra were collected for each control membrane. Therefore, over 5568 infrared spectra were collected over the course of this study.

3.1.6 Summary of Reverse Osmosis Membrane Descriptors

Seventeen (17) membrane descriptors were compiled for the eight RO membranes. The Desal CA and SST TMC/MPD were not completely characterized by the infrared band intensity ratios of the other polyamide membranes. The SST TMC/MPD membrane as manufactured on a polyetherimide support membrane that interfered with the measurement of the PA band intensity ratios. A list of these descriptors and the values for each membrane are included in Table 10.

3.2 Membrane Performance Before Exposure to Cleaning Agent

Before the membranes were even exposed to the chemical-cleaning agents, each membrane was stabilized on a feedwater of 1,000-ppm NaCl for 14 hr. Since this was done for every membrane before the start of the experiment a large volume of data for water flux and salt rejection was available for tabulation. This data is displayed for the eight membranes in Figure 27 and Figure 28. The flux and rejection of each membrane represents the average of 90 to 100 independent measurements collected over the 1.5-year period. The data were arranged from lowest to highest water flux and from lowest to highest salt rejection. Membranes with the highest water flux did not necessarily have the highest salt rejection. An explanation of the box-and-whiskers plots can be found in Appendix II.. Of the eight membranes used in the study, Hydranautics ESPA2 had the highest water flux at 28 gfd and the Desal CA had the lowest water flux at 7 gfd. In terms of salt rejection, Koch TFC-HR had the highest salt rejection at 99.8% and the Trisep X-201 membrane the lowest at 95%.

3.3 Membrane Performance After Treatment with Chemical Cleaning Agent

The effect of chemical cleaning agents on membrane performance was assessed in terms of the change in specific water flux and change in solute flux of a 1,000-ppm NaCl feedwater following 1 hr of exposure. The data are plotted for each membrane and for each of the 37 cleaning compounds as a function of change in specific water flux and

change in solute flux (see Figure 119 through Figure 126). These plots can be broken up into four quadrants as there are four different scenarios in which water flux and solute rejection undergo change (1) water flux and solute rejection can both go up, i.e., the ideal situation, (2) water flux can go down and solute rejection can go up, (3) water flux can go up and solute rejection go down, and the worst case scenario (4) water flux and solute rejection can both go down, following exposure to the chemical cleaning agent.

The data for these performance plots are displayed in Table 11 through Table 26. Each table contains either the change in specific water flux or the change in solute flux caused by 1-hr exposure to the cleaning agents. The change water flux or solute flux were sorted from most positive to most negative. The membrane performance data from these plots were used to generate a predictive model for chemical-membrane compatibility.

The Hydranautics LFC3 membrane (Table 12) was the least susceptible to a water flux decline of the six TFC membranes that were exposed to the 37 chemical cleaning agents. Twenty-three of 37 or 62% of the chemicals caused the water flux to decline. This was followed by the Hydranautics ESPA2 (Table 13) with 30 of 37 or 81% of the cleaning compounds causing a flux decline. For the remaining membranes (BW-30, TFC-HR, TFC-ULP, and X-201) 89 to 92% of the compounds caused the water flux to decline after 1 hr of exposure and a retest. The data for the PA membranes were combined and the average change in water flux (Table 25) and solute flux (Table 26) calculated. The cationic surfactants benzalkonium chloride and cetylpyridinium chloride caused the greatest flux decline on average at –3.90 $L/m^2 \cdot day/psi$. The four nonionic surfactants Genapol C-100 and X-80 and Tween 80 and 20 all caused significant water flux decline averaging between –1.65 and –2.65 $L/m^2 \cdot day/psi$.

Protease, Diamite BFT, DBSA + STP, STP and Minncare consistently appeared at the top of the lists causing the water flux to increase. Diamite BFT and Minncare both contain strong oxidizing agents that increased the porosity of the membrane causing water flux and solute flux to increase. The degree to which the water flux increased varied from membrane to membrane. The water flux of the FilmTec BW-30 (Table 11) and Trisep X-201 (Table 16) membranes were affected marginally at 0.22 and 0.61 $L/m^2 \cdot day/psi$, while the water flux of the TFC-HR (Table 14) and TFC-ULP (Table **15**) increased 4.46 and 2.14 $L/m^2 \cdot day/psi$.

The FilmTec BW-30 (Table 18) and Hydranautics LFC3 (Table 19) membranes responded quite differently to the cleaning compounds with respect to change in solute flux. The BW-30 membrane experienced severe flux declines following exposure to the chemical cleaning agents, many on the order of –100 to –407 $moles/m^2/day$ as compared to a maximum of -77 $moles/m^2/day$ for all the compounds associated with the LFC3 membrane. On average the BW-30 solute flux dropped -117 $moles/m^2/day$ as compared to a +81 $moles/m^2/day$ increase for the LFC3 membrane. On average the water flux of both membranes dropped slightly, but the BW-30 “tightened” up and the LFC3 membrane “opened” up allowing more solute passage on average.

The Koch TFC-HR (Table 14 and Table 21) and TFC-ULP (Table 15 and Table 22) and Trisep X-201 (Table 16 and Table 23) membranes followed similar trends to the BW-30

membrane. A vast majority of the compounds caused the water flux and solute flux to decrease. Typically the compounds that caused the water flux to go up also caused the solute flux to increase. However, there were quite a few cases with the Trisep X-201 membrane where the water flux decreased slightly and yet the solute flux increase, e.g., SDS, Mega 10, decyltrimethylammonium bromide, dodecanesulfonic acid and Empigen BB.

Seventy percent of the cleaning compounds caused the water flux of the Desal CA membrane (Table 17) to decline, although most of the flux decline was less than 0.3 $L/m^2 \cdot day/psi$. Cationic, anionic, nonionic and zwitterionic compounds were all represented at the bottom of the tables listing change in water flux. There wasn't one class of compounds that stood out consistently that caused the water flux to drop following chemical exposure. The same could be said for the top end of the lists in these tables. As expected Diamite BFT caused the greatest increase in water flux (5.12 $L/m^2 \cdot day/psi$) for the CA membrane. The CA membrane was deacetylated by the oxidizing agents in the commercial cleaning solution. The rest of the compounds were also a mixture of enzymatic, anionic, nonionic, chelating and cationic. Again, one class of compounds did group toward the top of the list of compounds representing change in water flux. The six compounds that caused significant water flux decline in the PA and PA-U membranes did not cause the same concerted effect on water flux of the CA membrane. Benzalkonium chloride (-0.32 $L/m^2 \cdot day/psi$) and Genapol X-80 (-0.33 $L/m^2 \cdot day/psi$) ranked 33rd and 34th worst compounds in reducing the water flux of the CA membrane. Cetylpyridinium chloride (-0.05 $L/m^2 \cdot day/psi$) and Genapol C-100 (-0.13 $L/m^2 \cdot day/psi$) fell in the middle at 16th and 24th. Tween 20 (0.21 $L/m^2 \cdot day/psi$) and Tween 80 (no change) fell near the top of the list at 5th and 11th.

Empigen BB caused the greatest reduction in water flux and the greatest reduction in solute flux of the Desal CA membrane (Table 17 and Table 24). This was the general case for all the cleaning compounds in that compounds that caused the water flux to decline caused the solute flux to decline. The cleaning compounds caused the membrane to "tighten" up. Benzalkonium chloride and Genapol X-80 that fell to the bottom of the flux decline list were positioned at the top of the solute flux list causing the greatest decrease in solute passage. The standard deviation of benzalkonium chloride and Genapol X-80 were both high at ±89 and ±88 $moles/m^2 \cdot day$, respectively.

Data from the five PA and PA-U membranes representing change in water flux (Table **27**) and change in solute flux (Table 28) were combined and averaged for the different classes of compound. The oxidizing and chelating compounds on average caused the least amount of water flux decline. The nonionic and cationic compounds caused the greatest decline in water flux. The solute flux was most affected by the cationic and nonionic compounds. The enzymatic and zwitterionic compounds caused the least amount of flux decline.

The data were also averaged based on the general class of compounds for the CA membrane (Table 29). The oxidizing, enzymatic, and chelating agents all caused the water flux to increase on average, while the zwitterionic, cationic, and nonionic agents

generally caused the water flux to decline. The Diamite BFT oxidizing agent as could be expected significantly increased the solute flux of the CA membrane. Other than the Diamite BFT, the enzymatic and cationic cleaning compounds caused the greatest increase in solute flux. The anionic and zwitterionic compounds caused the solute flux to decline on average.

3.4 Cleaning Chemical Interaction with Membrane Surface / Principal Components Analysis (PCA)

Of the 37 chemical compounds tested for membrane compatibility and analyzed by ATR/FTIR spectrometry, 21 were selected for PCA. Compounds from five of the six general classes of cleaning agents were selected. Fifteen (15) of the chemical-treated membrane spectra and 25 spectra of the feedwater control membranes were used in each analysis. Due to the time constraints of the project and the large number of PCA that needed to be completed, a small set of spectra were not held back to be run as a validation test. All 15 spectra of the test compounds were compared to the control spectra in a single analysis. The PCA scores plots are displayed for each of the 21 compounds for each of the eight RO membranes in Figure 35 through Figure 118 in Appendix III. Data for two compounds, Minncare and Diamite BFT, were not available for the SST TMC/MPD as the supply of membrane ran out.

There are many variations that make up the IR spectra of the chemically treated membranes. Including any chemicals on the membrane surface, there may be changes to the polymer structure. Instrument variations such as detector noise, environmental variations such as water vapor, carbon dioxide or temperature (causing baseline differences), and experimental variations such as sample handling also contribute to the variability in the sample spectra. The assumption, however, is that the majority of the variations between the test set and control set of membrane spectra are dependent on the exposure to the chemical cleaning agent. PCA focuses specifically on these spectral variations. PCA is a method of representing an m-dimensional multivariate dataset in a smaller number of dimensions that are assumed to retain chemically relevant information about the clustering of the original data (Brereton, 2003 and Kramer, 1998). PCA breaks apart the spectral data into variations (factors, eigenvectors, or loadings) and the corresponding scaling coefficients (scores). The dataset is fit by a least-squares methodology to a new set of orthogonal axes called principal components. The principal components describe the directions of greatest orthogonal variation in the original data set. The variation spectra are often called factors and the scaling constants used to reconstruct the spectra are known as scores. The variation spectrum represents the changes in absorbance at all the wavelengths in the spectrum, while the scores represent the scaling factors used to reconstruct the spectrum. By plotting the scores of the factors or principal components, one can predict or determine how closely a set of test spectra resembles the control spectra.

PCA was applied to the ATR/FTIR spectra to determine whether the chemical cleaning agents interacted with or adsorbed strongly to the surface of the RO membranes. When molecules such as the cleaning agents come in contact with the membrane surface a

number interactions can occur that affect the vibrational spectrum in different ways (1) chemical compounds may adsorb on the membrane and change the vibrational structure, but later desorb and the membrane reverts back to its original state, (2) chemical compounds may adsorb onto the membrane surface, remain bound to the surface, add to the vibrational spectrum of the membrane and potentially change the vibrational spectrum of the membrane through molecular interactions, e.g., hydrogen bonding, or (3) the chemical compounds may react with the membrane, change the molecular structure, and may be consumed or washed away during the rinse or retest step. In this case, the compound permanently alters the molecular structure of the membrane, e.g., deacetylation of a CA membrane by oxidizing agents. The chemical agents actually wash away leaving a "path" of destruction behind. This type of destructive interaction leads to permanent changes in the membrane vibrational structure that are easily noted. Other spectroscopic changes may not be as easy to discern and take the form of small shifts in frequency or changes in the intensity of the vibrational bands of the membrane.

In the case of this study where low concentrations of chemical cleaning agents were involved, the amount of adsorbed material was often small and the amount of change or damage to the membrane was minor. This made it difficult to visually discern whether the chemically treated membrane spectrum was any different from the untreated spectrum. Difference spectroscopy is often applied, where a control or reference membrane spectrum is digitally subtracted from the spectrum of the treated sample. Residual bands in the spectrum associated with the chemical additive are delineated and changes in vibrational structure of the polymer membrane are assessed. However, this methodology is not without difficulties. Differences in relative intensities of vibrational bands in the test sample and control can leave residual or negative bands in the spectrum. Shifts in frequency between the test spectrum and the control result in derivative-shaped bands and make interpretation difficult; however, they do indicate a change in molecular interactions. Difference spectra are often difficult to interpret when chemical constitutes are present at low concentrations just above the noise. Therefore, a more sensitive and more statistically stringent method was warranted. PCA was utilized to aid in the determination of whether spectra of membranes treated with cleaning agents were any different from the untreated control spectra of the membranes.

For this study individual sample spectra were not analyzed to determine whether the chemicals agents were still adsorbed on the membrane surface based on difference spectrometry. The data from the PCA scores plots were tabulated based on whether the set of chemically treated membrane spectra were different from the set of control membrane spectra. Spectra of the treated membranes that completely separated from the control membrane spectra did so based on one of two conclusions (1) the chemical agent was still adsorbed on the surface and added to the vibrational signature of the membrane or (2) the chemicals caused a change in the polymer structure and then desorbed. A weighting system was applied to each chemical entry. If the chemical-exposed membrane spectra completely separated from the control membrane spectra, the cleaning agent was assigned a value of 2. If there was a partial separation of the test and control membrane spectra with a few spectra lying across either side of the plane separating the data, the cleaning agent was assigned a value of 1.5. Finally, if there was no separation

between the test and control data the cleaning agent was assigned a value of 1. The data were tabulated and are displayed in Table 30. Generalizations of the nature of chemical interactions of these compounds with the membrane surface are discussed in the two sections below.

3.4.1 Cleaning Compound Interactions Based on Membrane Type

The data for all eight RO membranes were pooled and treated as a whole. In most of the cases, the separation between the chemically treated membrane and control spectra based on the scores plots of the principal components was very clear. Complete separation of the two data sets occurred in 57.8% of the cases, indicating a strong molecular interaction had occurred between the cleaning compounds and membrane surface (Table 31). In many cases a majority of the chemically treated spectra separated from the control spectra with only a few scattered data points lying on either side of the line or plane of separation. This occurred 24.7% of the time but still strongly suggests that a molecular interaction had occurred between the cleaning and the membrane surface. If these compounds (24.7%) are grouped with the compounds that strongly interacted with the membrane surface (57.8%) then 82.5% of the cleaning compounds could be considered to have associated with the membrane in some way either strongly or weakly and altered the vibrational spectrum of the membrane. No separation or no difference in the test and control membrane spectra was observed in only 17.5% of the cases, meaning no close association, no strong interaction of the cleaning compound with the membrane surface was observed in only 17.5% of all cases studied.

The SST TMC/MPD membrane was least affected by the 21 test compounds with an average "separation index" of 1.2 (Table 30). However, two cleaning agents Diamite BFT and Minncare were not tested on the TMC/MPD membrane. Both compounds typically interacted strongly with the membrane surface and imparted changes. Therefore, the separation index for TMC/MPD would likely be higher if these two compounds had been tested. In actuality the Hydranautics LFC3 and FilmTec BW-30 membranes were least affected by exposure to the 21 cleaning compounds. In 47.6% of the cases, the test spectra of the Hydranautics LFC3 membrane were determined not to be different from the control spectra, i.e., no separation of the test and control spectra. In only 14.3% of the cases was complete separation the test and control spectra observed indicating the chemical agent strongly interacted with the membrane. This left 38.1% of the cases where there was partial separation of the test and control spectra of the Hydranautics LFC3 membrane. With respect to the FilmTec BW-30 membrane, in 38.1% of the cases no lasting interaction was observed and therefore no separation or difference between the chemically treated membrane spectra and control spectra were detected. Partial separation of the test and control spectra occurred 28.6% of the time and in 33.3% of the cases the chemically treated spectra completely separated from the control spectra of the FilmTec BW-30 membrane. Both the Hydranautics LFC3 and FilmTec BW-30 membranes are reportedly coated or post-treated. These coatings are believed to be polyvinyl alcohols that make the membrane surface more resistant to chemical adsorption, retention and alteration.

The Desal CA, Koch TFC-HR and Trisep X-201 membranes were affected the most by exposure to the 21 cleaning compounds. These membranes had the highest average separation indices indicating a strong lasting interaction with the test compounds. However, as stated above, the effect the 37 chemical cleaning compounds have on membrane performance is of greater importance. Compounds may adsorb strongly to the membrane surface but not significantly affect membrane water flux and salt rejection.

The FilmTec BW-30 and the Hydranautics LFC3 membranes were determined to be the most "Teflon-like" with respect to surface adsorption of cleaning compounds based on the PCA of the IR spectra. However, the two PA membranes were at opposite ends of the list when it came to the chemical agents influence on water flux. The BW-30 recorded the most water flux declines and the LFC the least number of flux declines associated with exposure of the cleaning compounds. The LFC3 has a lower water flux to start with ~15 gfd as compared to ~20 gfd for the BW-30 membrane. The membranes were not cleaned under pressure. Therefore, increased mass transport to the surface of the BW-30 membrane is not a determining factor. The difference in chemistry of the coating may actually be the major determining factor in how the LFC3 responds to exposure to the 37 cleaning compounds. The coating applied to these membranes is believed to be a polyvinyl alcohol, but the exact polymer type is not known. Differences in the molecular weights between the two polyvinyl alcohols could contribute to the differences in the change in water flux.

3.4.2 Cleaning Compounds Association with RO Membranes

With respect to the chemical cleaning agents, Mega 10 was the most benign compound, seeming to associate or strongly adsorb on the membranes the least. Of the 21 compounds that were analyzed by PCA, Mega 10 had the lowest average at 1.4 for the weighted results of the PCA (Table 30). Mega 10 is a nonionic polar hydroxyl (OH) containing detergent with an aliphatic tail. Other compounds affecting the membrane spectra, or imparting a change to a lesser extent included the combination of DBSA and STP, Empigen BB, SDS and zosteric acid, all with a separation index of 1.6. Most of these compounds are anionic surfactants. Empigen BB is zwitterionic surfactant with a tertiary amine and carboxylic acid. All the membranes in the study had a net negative surface charge at pH 5.5. Therefore, repulsive electrostatic interactions may be a contributing factor to the lack of a lasting adsorptive interaction with the membrane surface.

The data were sorted by class of cleaning compound and the average separation index was calculated. The nonionic and zwitterionic compounds demonstrated the lowest amount of interaction with the polymer membranes. The enzymatic and oxidizing agents exhibited the greatest amount of chemical interaction with the membranes. These could be expected as these solutions contain enzymes that are proteins that are known to interact strongly with most surfaces including membranes. Protein or enzymes adsorbed on the membrane surface are easily detected by infrared spectrometry. Oxidizing agents have a destructive effect on the membranes. They are capable of breaking covalent bonds between atoms of the polymer matrix, thereby altering the vibrational structure of

the membrane. This is especially evident in the spectra of the CA membrane that was exposed to Diamite BFT, an oxidizing cleaning agent (Figure 63). The CA membrane was deacetylated by this oxidizing agent. Thus, when PCA was applied to this data set there was a very distinct separation between the control and test set of membrane spectra.

3.4.3 Summary of PCA of Chemical-Exposed RO Membranes

While the PCA of the IR spectra tells us how strongly the chemical agent associates with the membrane surface, the PCA results do not tell us whether any changes (or how any changes) in the vibrational structure affect membrane performance in terms of a change in water flux or a change in solute passage. As revealed in the performance data, these RO membranes may adsorb the chemical agent yet still perform adequately in the field. Therefore, IR spectroscopic analysis of membranes exposed to cleaning compounds is not a reliable means of predicting of chemical compatibility. Analysis of the performance data, membrane properties and molecular properties of the compounds via construction of a neural network model may provide more detailed information on how molecular properties of the compounds and membrane directly influence membrane performance.

3.5 Artificial Neural Networks for the Modeling of Cleaning Agent Compatibility with RO Membranes

3.5.1 ANN Models: Polyamide, Cellulose Acetate and Polyamide-Urea

Three ANN models were constructed from the computer generated QSAR descriptors of the chemical cleaning compounds, the membrane properties that were measured and the change in membrane performance following exposure to the chemical cleaning compounds. Theses three models were a “universal” PA membrane that included data from the FilmTec BW-30, Hydranautics ESPA2 and LFC3 and Koch TFC-HR and TFC-ULP membranes (Figure 29 and Figure 30), a CA membrane from the GE Osmonics Desal CA membrane data (Figure 31 and Figure 32) and a PA-U from the Trisep X-201 membrane data (Figure 33 and Figure 34). (Plots of the change in water flux and change solute flux for the eight RO membranes, i.e., the performance data that were used to construct the ANN models are displayed in Appendix IV and ANN models for each individual RO membrane is displayed in Appendix V.)

The scatter plots for each of the ANN models compare the actual change in water flux and change in solute flux with the predicted value and serve as a visual indication of the model performance. The diagonal line drawn through each plot represents perfect agreement between the values predicted by the model and those measured in the field. The error bars represent one standard deviation about the mean for the actual behavior data (n = 3 to 6). The ANN model statistics are presented beneath the scatter plots and include (1) the linear correlation coefficient (R) between the predicted and measured values, (2) the average absolute error values between the predicted and measured values, (3) the root mean squared (RMS) error between the predicted and measured values, (4) accuracy indicates the fraction of data points that fall within a 20% noise band or

tolerance, (5) the 95% confidence interval for the model, and (6) the number of descriptor records used to create the model. The identity of the QSAR molecular descriptors used in the construction of the model is displayed below the statistical information. For each of the molecular descriptors, sensitivity index was calculated. The value represents the direction and the degree of influence each input parameter had on the model.

Performance of the ANN models was evaluated by comparing the linear correlation (R) coefficients between the predicted model outputs and the actual measurements made in the field. The PA and CA models for change water flux had an R value slightly above 0.94. The correlation coefficient for change of water flux for the PA-U model was lower at 0.9269. The solute flux did not model as well for the PA and PA-U membranes. The correlation coefficient dropped to 0.8016 and 0.8330, respectively. The model likely predicted change in solute flux poorly because the individual measurements contained more variation.

The cleaning solutions were inadvertently dissolved in 1,000-ppm sodium chloride instead of deionized water. However, the salt concentration was not high enough to osmotically shock the thin-film composite membranes. Osmotic shock is not an issue until the solute concentration reaches near 3.5% (or an osmotic pressure near 400 psi). Therefore, the level of noise in the solute flux measurements was likely attributed to the use of small (1 x 3 in.) membrane swatches. The PA and PA-U separations layer are very rugose and nonuniform in thickness. This structural property may contribute to the noise in the measurements of solute flux for the PA and PA-U models. The solute flux of the CA membrane modeled well with an R of 0.9438. The high correlation coefficient for the solute flux may be a reflection of the fact that the CA membrane is a uniformly dense polymer membrane. Therefore, membrane performance is likely to be more consistent from swatch to swatch.

3.5.2 Relationship of QSAR Molecular Descriptors with Membrane Performance

Knowing that the QSAR molecular descriptors are linked to the fundamental properties of the cleaning compounds, it was hoped that the nature of the individual descriptors and the degree to which the descriptors influence the predicted behavior of the cleaning compounds would provide insight in to how chemical structure affects membrane performance. Originally 73 molecular descriptors were considered as inputs to the model. Application of the GA reduced this number down to 6-10 per model. This provided an insight as to which descriptors proved to be influential in determining a compound's effect on membrane performance. However, the direction and magnitude of that influence was not revealed. In the case of multivariate linear models, it is possible to gain this insight by analysis of the magnitude and direction of the slopes of the individual linear equations from which the model was assembled. In the case of the ANN models, this is not possible. However, it is possible with the ANN models to compute at "sensitivity index" for each of the input descriptors. The sensitivity index is a measure of the overall magnitude and direction of influence that each of the model input descriptors has on the model output, i.e., water flux and solute rejection. If this index is calculated over the entire range of the input data set (for all the cleaning agents), then it tends to

represent the overall strength and direction the descriptors have on model flux and rejection. However, it may not represent long-range output response. If the real function contains local minima or maxima, the sensitivity index could be large because of a short-range influence, but would not indicate the long-range relationships in the function well.

A summary of the sensitivity indices for the PA, CA and PA-U membranes with regard to the effect chemical agents have on membrane performance is presented for change in water flux and change in solute flux in Table 32. The relevant molecular descriptors were grouped into three broad categories related to charge and polarity, molecular complexity and hydrophobicity. Of the original 73 molecular descriptors and 17 membrane descriptors a total of 21 survived as inputs used in the three ANN models relating to water flux and solute flux; 17 were related to charge and polarity, 13 were related to molecular complexity and 1 was related to hydrophobicity. Of the 17 charge and polarity-related inputs, one was related to the surface charge on the membrane—the zeta potential slope. Of the 13 inputs related to molecular complexity two were related to membrane properties, the relative carboxylate density (COO^-/AMII) and the relative PA thickness (AMII/874).

3.5.2.1 Polyamide Model

There were a total of seven inputs of significance to the PA ANN model. Four QSAR compound descriptors related to the charge and polarity of the compound had an influence on the water flux (see Table 32). These included the dipole (0.1445), ssCH3 (0.2961), SHother (-4.2971), and Gmin (-0.5802). As the dipole of the compounds increased the water flux would be expected to increase. The greater the magnitude of the dipole, the greater the expected the increase in water flux following exposure chemical compound. Compounds that had a greater ability of form intermolecular interactions with methyl groups (ssCH3) had a greater tendency to cause the membrane water flux to increase following chemical exposure. Compounds with the ability to form hydrogen bonds (SHother) and form certain types of intermolecular interactions (Gmin) caused the water flux to decrease.

Three membrane properties also had a significant influence on the water flux of the PA membranes. Two descriptors, COO^-/AMII (0.0017) and AMII/874 (0.2643), were related to chemical structure of the membrane. COO^-/AMII (0.0017) is a membrane descriptor that indicated that membranes with a high crosslink density performed better in terms of water flux when exposed the 37 compounds as a whole. Amide bonds of a PA membrane are formed when the acid chloride (COCl) group on TMC reacts with an amine (NH_2) group on MPD. Unreacted acid chloride quickly becomes hydrolyzed to form a carboxylic acid that exists primarily as an unprotonated carboxylate (COO^-) at pH 5.5. TMC can react to form a maximum of three amide bonds undergoing a crosslinking reaction when that third acid chloride is consumed. As more acid chloride groups react to form amide bonds less carboxylate groups are formed. Therefore, the ratio of the intensity of the carboxylate band to the amide II band (COO^-/AMII) provides information on the relative crosslink density. Again, membranes with a higher crosslink density had a higher water flux, i.e., performed better when tested with the cleaning agents in the study.

AMII/874 (0.2643) is a membrane descriptor that indicated that membranes with a thicker polyamide layer maintained a high water flux when tested with the cleaning agents. Relative thickness (AMII/874) of the PA film is measure by the ratio of the ~1550 cm^{-1} amide II band and 874 cm^{-1} PS band. As the PA film increases in thickness less infrared light penetrates into the underlying PS layer when sampled by ATR/FTIR spectrometry. Therefore, as the PA increases in thickness, the PA bands will increase in intensity relative to the PS bands. Membranes that had a thicker PA layer tended to maintain a higher water flux when exposed to the group of cleaning compounds. Intuitively, this makes sense because the RO membranes with a thinner PA layer typically had a higher flux. The mass transport to the surface is much greater and foulants or chemicals reach the surface at a greater rate. Therefore, membranes with a thicker PA layer are slower to concentrate chemicals at the surface and the flux may drop at slower rate.

The final descriptor was related to the surface charge on the membrane, the zeta potential slope. PA membranes capable of undergoing a high rate of protonization or deprotonization, i.e., the gain or loss of H^+, at the surface maintained a high level of water flux when exposed to the chemical compounds.

Five molecular descriptors MaxNeg, Sumdel1, Tets2, AMII/874 and projected area were determined to be relevant to the prediction of solute rejection. MaxNeg (-0.6646) is charge related and Sumdel1 (-2.8423), and Tets2 (-0.4554) are related to molecular complexity. All three were inversely related to solute rejection. Therefore, as the negative charge (MaxNeg) on the compound exposed to the membrane increased the solute passage of the membrane decreased. Sumdel1 (-2.8423) and Tets2 (-0.4554) are geometry complexity descriptors with negative sensitivity indices indicating as the structural complexity of the compounds increased the solute passage decreased.

The AMII/874 (0.2997) membrane thickness positively correlated with solute flux indicating thicker membranes allowed greater salt passage. The projected area (0.6818) is related to the AFM image. The projected area is actually not a relevant descriptor for this study and was inadvertently included with the input data to the ANN model. It represents the area over which the AFM was scanned. The computer was programmed to scan a 10 x 10 μm area and then download the area of 100 μm^2 to a spreadsheet. In a few instances, the projected area was reported to be slightly (~1-2%) less than 100 μm^2; however, this number has no bearing on the properties of the membrane.

3.5.2.2 Cellulose Acetate Model

Six molecular descriptors were determined to be important in predicting a compound's effect on the water flux of a CA membrane (see Table 32). Py, Pz, Dx and Qyy were associated with molecular polarity of the chemical compounds. Py (0.0024) and Pz (29.0442) are related to the dipole and were positively correlated with the change in water flux. Therefore, compounds with high dipole moments had a greater tendency to cause the water flux of the membrane to increase following chemical exposure.

Dx (-10.2415) and Qyy (-0.9572) were also related to the dipole of the compounds but were inversely related to water flux. Compounds with a large molecular dipole with these molecular properties would be expected to cause a decrease in water flux following exposure to the membrane. The magnitude of the Pz (29.0442) descriptor is 4 fold greater in the positive direction than Dx (-10.2415).

The two other descriptors were associated with molecular complexity. Xvc3 (-0.4530) was negatively correlated and phia (0.4327) was positively correlated to the change in water flux. Xvc3 is a chi index of molecular complexity. The magnitude of this descriptor increased from compound to compound, the water flux would be expected to decreased following chemical exposure. Phia is a descriptor that is defined as being inversely related to molecular complexity and related to length of alkyl chains of the molecule. The magnitude of phia increases with increasing homolgation and decreases with branching or cyclicity. It was positively correlated with water flux. Thus, if the compound's alkyl chain length increased or there was less branching or cyclicity (decreasing complexity), the water flux should increase.

Eight molecular descriptors were determined to be important in predicting solute flux of the CA membrane. Three are associated with compound charge. SdssC (21.4926) was positively correlated and Dx (-12.4020) and Hmin (-11.0764) were negatively correlated with solute flux. Four are associated with molecular complexity. SHHBd (12.4138) and numHBa (1.6945) were both positively correlated and nxc3 (-1.6797) and nelem (-0.1215) were negatively correlated solute rejection.

Dx (-12.4020) is associated with the dipole moment, the center of mass of the compound and the distance between them. Compounds with a large distance between the dipole caused the solute flux to decrease. Hmin (-11.0764) is the smallest atom hydrogen E-state and is related to a compound's ability to hydrogen bond. As the compounds hydrogen-bonding ability increased, the solute flux decreased, i.e., the greater the ability of a given compound to for hydrogen bonds, the greater the expected decrease in solute flux following exposure to the compound. SdssC (21.4926) is related to compounds with >C= moieties (such as aldehydes and ketones) that participate in intermolecular interactions. Compounds with a high >C= content tended to cause the water flux to increase following chemical exposure.

SHHBd (12.4138) is related to the number of hydrogen bond donors and numHBa (1.6945) is related to the number of hydrogen bond acceptors. Both positively correlated with solute flux, especially SHHBd, and cause the solute flux to increase. These two hydrogen-bonding descriptors contradict the Hmin descriptor. SHHBd (12.4138) and Hmin (-11.0764) are almost equal and opposite in magnitude. It is not known what the net effect of these descriptors have on membrane performance.

Nxc3 (-1.6797) is related to a compound's ability to cluster. Nelem (-0.1215) is the number of different elements in the molecule. As the magnitude of these descriptors increase in the compounds, the greater the magnitude of the decrease in membrane solute flux.

3.5.2.3 Polyamide-Urea Model

Four molecular descriptors were determined to be important in predicting change in water flux of the PA-U membrane (see Table 32). MaxNeg (-0.4795) is associated with compound charge and polarity and inversely related to water flux. Therefore, as the negative charge on the compounds increased, the water flux decreased with increasing magnitude. LD50 (-0.1138), IC (-2.4014) and nelem (0.4392) are associated with molecular complexity. LD50 and IC were inversely related to membrane water flux.

Six of the molecular descriptors were determined to be important in predicting solute flux. Four were associated with compound charge. Dz (-5.4917), Qxx (-12.7533), and Qyy (-1.2787) are related to the dipole of the compounds and were negatively correlated with solute flux. Hmax (1.2612) is related to the compound's ability to form hydrogen bonds and was positively correlated with solute flux Two of the descriptors were associated molecular complexity. Xpc4 (-0.6113) was negatively correlated and Xvpc4 (0.2355) was positively correlated with solute flux.

All the molecular descriptors described above were influential in predicting how a chemical compound will affect the water flux and salt rejection of a RO membrane. The magnitude of the sensitivity index and the direction of the correlation varied widely. However, distinct relationships between a compound's molecular properties, the physical properties of the membrane and a membranes performance were revealed.

3.5.3 Prediction of Cleaning Compound Effect on Membrane Performance

The ANN models were designed to predict the change in water flux and solute rejection following exposure to a compound for which the molecular descriptors are known. Only 27 compounds were used to generate the predictive ANN models. QSAR molecular descriptors were calculated for the 74 compounds in the master list of potential cleaning agents. Using the models constructed from the membrane performance data, the change in water flux (Table 33) and change in solute flux (Table 34) were predicted for the remaining 66 compounds utilizing the pertinent molecular descriptors. The performance data from compounds in bold font represent measurements made in the field.

A number of homologous series of compounds were tested during this study and some treads in membrane performance were apparent. For example in the Tween series, the short (C_{12}) aliphatic chain length Tween 20 caused more reduction in water flux than the Tween 80 with the long (C_{20}) chain. However, unexplainably, there was no difference in the magnitude of the drop in solute rejection across the homologous series. The water flux of the Hydranautics LFC3 and ESPA2 membranes were actually observed and predicted to increase following exposure to Tween series, while the other PA and PA-U membrane all "tightened" up.

The observed trends in sulfonic acid series included a decrease in water flux with increasing aliphatic chain length, but less solute passage after exposure to the low chainlength butanesulfonic acid as compared to the hexadecanesulfonic acid. The models

predicted that exposure to the Zwittergent series would cause the water flux of the Hydranautics ESPA2 and LFC3 membranes to increase. However, the water flux for the remaining PA and PA-U membranes are expected to decrease following exposure. The model for the TFC-ULP membrane, predicted a drop in water flux independent of the type of Zwittergent.

The models basically predicted an increasing or decreasing trend over the series when data for only one compound was available. This was evident with the Mega 8, 9, 10 detergent series and glucopyranoside homologous series. Based on data from one compound in the series, the models predicted that the water flux would go down following exposure to the glucopyranosides. The magnitude of the flux decline was less for the short chain hexaglucopyranoside than for the long chain dodecylglucopyranoside. The change in solute passage followed the same trend. The solute flux was predicted to decrease following exposure and more tightening up of the membrane would be expected to occur following exposure to the longer chain dodecylglucopyranoside surfactant. Two of the membranes, Hydranautics LFC3 and Koch TFC-HR were reversed in terms of the change in solute flux. More tightening or a greater reduction in solute flux was predicted for shorter chain length hexaglucopyranoside than the longer dodecylglucopyranoside.

The opposite trend was predicted for the Mega surfactant series. The model predicted an increasing reduction in solute passage of the thin-film composite PA and PA-U membranes with increasing aliphatic chain length. There was no well-defined trend associated with the change in water flux. The predicted change in water flux varied slightly from compound to compound but did not increase or decrease with increasing or decreasing surfactant aliphatic chain length.

Further validation of these models with more independent studies is needed. The compounds in the master list need to be tested with RO membranes. Acquisition of this data will determine the strength of these ANN models. In general the model predicted increasing or decreasing water flux and solute rejection with increasing or decreasing aliphatic (CH_2) chain length within a homologous series of surfactants. When two or more test data were available for compounds within a given series, the predicted performance did not always transition smoothly, although the general trend in a positive or negative direction was maintained. Testing the accuracy of the predictions through real measurements of performance of these compounds was outside the scope of this study.

3.5.4 Application of Chemical Cleaning Agents on Fouled RO Membranes

Four RO membranes, FilmTec BW-30, Hydranautics ESPA2, Hydranautics LFC3 and Koch TFC-HR, were operated on secondary-treated wastewater. Four cleaning agents were tested to determine their ability to remove the fouling layer and restore membrane water flux and solute rejection. Water flux, salt rejection and transmembrane pressure were measured up to the point where the membranes where determined to be fouled. A sufficient fouling layer and pressure drop (~15%) occurred after 24 hr of operation. The membranes were cleaned in place with one of four cleaning agents, DBSA,

Genapol C-100, Zwittergent 3-16 or protease. Feedwater was reapplied and the water flux, solute rejection, and transmembrane pressure remeasured. The percent change in water flux and solute rejection were calculated from the time at which the membranes were fouled (see Table 35). The surfactant Genapol C-100 produced very poor results on all four polyamide membranes. The solute flux increase 10 to 20% and the water flux actually dropped 15 to 30%. While these results were very poor, they were actually consistent with what was observed in the chemical compatibility studies. Genapol C-100 did not perform well on the polyamide membranes (Table 35).

Protease was one of the better performing enzymatic cleaning agents. However, when applied to the fouled polyamide membranes a significant increase (~10 to 30%) in solute flux was observed, while the water flux was unaffected. This treatment defeated the purpose of membrane cleaning, as there was no improvement in water flux and the solute passage actually increased.

Zwittergent 3-16 was another surfactant that performed well in the initial performance studies. The results from the cleaning study were mixed. Application of Zwittergent 3-16 to the fouled Hydranautics ESPA2 membrane caused the water flux to decrease by ~18% and the solute flux to decrease by ~28%. Thus, the surfactant had a "tightening" effect on the ESPA2 membrane. The water flux of the other membranes improved slightly, but the solute flux increased significantly (25 to 38%).

DBSA the industry standard cleaning agent for PA membranes did not fair much better. Water flux dropped as much as 13% with the Hydranautics ESPA2 membrane but improved by ~10% with the Hydranautics LFC3 membrane. The solute flux of the Hydranautics ESPA2 membrane dropped 49% while increasing 29% for the LFC3 membrane. The FilmTec BW-30 and Koch TFC-HR were only moderately affected by cleaning with DBSA. The FilmTec BW-30 water flux dropped ~6% and the solute flux dropped about 2%. The Koch TFC-HR water flux dropped ~10% and the solute flux dropped about 2%.

4 Project Conclusions and Recommendations

It is not always known beforehand whether a chemical cleaning agent will adversely affect the performance of a RO membrane. Application of the wrong chemical compound can impart permanent damage to the membrane necessitating costly replacement. While the basic composition of today's RO membranes are known, much less is known about the details by which chemical cleaning agents interact with the membrane surface (and the foulants on the surface). Understanding what molecular properties of cleaning compounds actively influence membrane performance is critical to the development of cleaning agents that effectively remove foulants to restore membrane performance and yet have no damaging effects on the membrane. The current study addressed the issue of compound-membrane interactions and attempted to identify molecular properties that were important in defining chemical compatibility with the polymer membranes and to develop a model to predict a cleaning compound's effect on membrane performance.

A list of potential cleaning agents was compiled that contained broad classes of compounds with varying molecular properties including cationic, anionic, zwitterionic, nonionic chelating and oxidizing compounds. In the first phase of the study, eight commercially available RO membranes and one experimental membrane were challenged with 37 chemical compounds. Changes in water flux and salt passage were measured for each membrane and served as inputs to a QSAR-based ANN model.

Most compounds had a "tightening" effect on the PA and PA-U membranes causing the water flux and salt passage to decrease. In general the chelating, enzymatic, and oxidizing compounds caused the water flux to drop the least for the PA membranes. The cationic, nonionic and anionic compounds caused the greatest drop in water flux. As a general class of compounds, the cationic and nonionic cleaning agents caused the greatest reduction in solute flux.

The CA membrane responded quite differently than the PA membranes. As a whole the enzymatic and chelating compounds caused the water flux to increase, while the zwitterionic, cationic and nonionic compounds caused the water flux to decrease. The anionic and zwitterionic compounds caused the solute flux to decrease, while the remaining classes of cleaning compounds (cationic, chelating, enzymatic, oxidizing and nonionic) caused the solute flux to increase.

A select group of 21 chemically treated membranes were analyzed by IR spectrometry and PCA to determine the extent of interaction of the compound with the membrane surface. In over 80% of the cases, the cleaning agents associated with the membrane altering the vibrational spectrum. Meaning in a vast majority of the cases, the chemical agents physically adsorbed to the surface and imparted a molecular change in the polymer membrane. However, a compound does not have to remain firmly adsorbed to the surface of the membrane to impart a lasting effect on performance. As expected the oxidizing agents exhibited the greatest amount of interaction with the membranes and alteration of the vibrational spectrum of the membrane, while the nonionic and zwitterionic compounds demonstrated the lowest amount of association with the polymer membranes.

The mechanism by which these compounds affect transport of the water molecules and solute molecules through the membrane are not well understood. There was no direct relationship or correlation between the PCA data indicating strong chemical association with the membrane surface and loss of water flux or solute rejection. While a noticeable change in performance may not be evident after a single cleaning, with multiple cleaning cycles over the lifetime of the membrane these chemical compounds may accumulate at the surface and slowly contribute to the decline in performance.

The testing of cleaning agents on fouled membranes was not as extensive as planned. Plant shutdowns and equipment failures limited the number of studies that were done. Application of a number of cleaning agents to the fouled RO membranes produced mixed results. Compounds that caused the water flux and solute rejection of the membrane to increase when applied to a clean membrane caused the flux and rejection of the fouled

membrane to decrease. The opposite scenario was also observed. These limited studies revealed how complex and difficult these processes, i.e., fouling and cleaning, are to study. The addition of a fouling layer adds another variable to the system to study. The chemical composition of the fouling layer was not determined, and compounds that were removed and compounds that remained were not identified.

Future studies should be directed toward quantitation of the chemical cleaning agents on the surface of the membranes following cleaning and the determination of their accumulation at the surface over time. These studies should also focus on the chemical characterization or identification of the foulants that are removed by individual cleaning compounds. The macromolecular foulants that remain at the membrane surface should also be characterized and a structure function relationship developed for cleaning agents and molecular foulants.

In the second phase of the study, ANN models were constructed to identify what QSAR molecular descriptors or chemical features influence membrane performance. QSAR analysis that uses molecular descriptors that define basic molecular structural and electronic features formed the basis from which the predictive modeling was achieved. The fundamental nature of these numerical factors (QSAR descriptors) tends to reflect the simpler molecular issues. Physicochemical properties of molecules (solubility, vapor pressure, melting point, etc.) are based on combinations of these more basic descriptors. Models using descriptors of the molecular structure as a basis for predicting RO membrane performance provided a means of analyzing the compound-membrane interactions in terms of the fundamental molecular interactions.

Defining and understanding how molecular properties of chemical compounds influential changes in membrane performance is very difficult. The ANN models of the PA, CA and PA-U membranes provided an abundant amount of detailed information on how specific molecular properties influence membrane performance. Membrane water flux and solute passage were affected by numerous molecular properties associated with the cleaning agents. Many of the descriptors were obscure in nature. However, very useful generalizations could be drawn from them. Charge, polarity and hydrogen-bonding properties appeared to be the most influential factors in determining a compound's influence on water flux and solute rejection.

The ANN model of the PA-U membrane identified electronegativity and nonpolar hydrogen / hydride as influential molecular properties. When exposed to compounds with high electronegativity or polarity the water flux could be expected to increase, while exposure to compounds with low structural complexity and increased aliphatic (CH_2) character will cause the water flux to decrease. As the dipole on the compounds increases the effect on the solute passage is in the opposite direction. And finally, as the hydrogen-bonding capabilities of the molecule increase the solute flux increases.

The ANN model of the CA membrane identified the molecular dipole as an influential molecular property having a significant positive influence on water flux and a "tightening" effect on the solute passage. However, compounds with an increased ability

to form hydrogen bonds (e.g., hydroxyl and carbonyl containing compounds) and compounds that contain a high concentration of >C= moieties (e.g., aldehydes and ketones) caused an increase in solute flux.

Finally the ANN model of the PA membrane identified both molecular and membrane properties as being influential to membrane performance. The RO membranes with a thicker PA layer and a lower crosslink density performed better when exposed the set of test compounds. Membranes with a thicker PA layer demonstrated increased water flux and decreased salt passage. Lower crosslink density equates to greater free carboxylate groups and greater negativity throughout the membrane. The chemical properties of note were charge, polarity, degree of aliphatic CH_2 content, and molecular complexity. Compounds with increased negativity seemed to improve water flux. Polar compounds with low aliphatic CH_2 content also had a positive influence on water flux, causing the water flux to increase following exposure. Finally, increasing the geometric complexity of the compound and increasing the electronegativity of the compounds resulted in a reduction of solute passage.

Three ANN models were constructed from the molecular descriptors of the cleaning agents and the performance data measured from the eight RO membranes discussed above. Data from the PA membranes were combined to create a "universal" PA model. ANN models of the CA and PA-U membrane were constructed separately. The ANN models constructed in the study to describe changes in water flux and salt passage associated with compound molecular descriptors held up well. The models did a better job of predicting the change in water flux than the change in solute passage, as there was greater noise associated with the field measurements of salt rejection.

The ANN models determined which molecular descriptors of the cleaning compounds were important in predicting membrane performance following chemical exposure. In summary, the PA model reduced to three membrane properties (COO^-/AMII, AMII/874, and zeta potential slope) and four compound descriptors (Dip, SsCH3, SHother, and Gmin) that could be used to predict the change in water flux. One membrane property (AMII/874) and three compound descriptors (MaxNeg, sumdilI, and tets2) were needed to predict the change in solute flux. The CA model reduced to six molecular descriptors (xvc3, Py, Pz, Dx, Qyy and phia) that predicted change in water flux. Nine molecular descriptors (nxc3, Dx, LogP, SdsCH, SdssC, Hmin, nelem, numHBa, and SHHBd) were needed to predict change in solute rejection. The PA-U model reduced to four molecular descriptors (MaxNeg, LD50, IC, and nelem) that determined the change in water flux and six molecular descriptors (xpc4, xvpc4, Dz, Qxx, Qyy, and Hmax) that were needed to predict change in solute rejection.

It is now possible to predict a given compound's effect on membrane water flux and solute passage by computing a number of well-defined molecular QSAR descriptors and entering them onto the appropriate ANN model. The three ANN models for the polyamide, polyamide-urea and cellulose acetate membranes are available upon request through the OCWD website at www.ocwd.com or by phone at (714) 378-3200.

The understanding how molecules and membranes interact is an incredibly complex issue to address. However, through a combination of testing in the field and experimentation in the laboratory, it is possible to make small steps toward understanding the complex interactions between chemical compounds and the membrane surface and the resulting effects on performance. Further studies should be directed toward validation of the three ANN models. Compounds from the master list should be tested in the field and the membrane performance compared to the values predicted by the model.

In conclusion, this study has provided greater insight into how specific molecular properties of cleaning compounds influence membrane water flux and solute rejection. The hope is that enough knowledge and understanding of the fundamental interactions between cleaning compounds and polymer membranes will be gained through further studies such that cleaning agents can be tailored specifically for the membrane and the foulant to achieve the greatest compatibility and cleaning efficiency.

References

Avlonitis, S., W.T. Hanbury, and T. Hodgkiess. 1992. Chlorine degradation of aromatic polyamides. Desalination 85:321-334.

Bartlett, M., M.R. Bird, and J.A. Howell. 1995. An experimental study for the development of a qualitative membrane cleaning model. J. Membr. Sci. 105:147-157.

Bharath, R. and J. Drosen. 1994. Neural Network Computing. McGraw-Hill, NY.

Bowen, W.R., M.G. Jones, and H.N.S. Yousef. 1998. Dynamic ultrafiltration of proteins—a neural network approach. J. Membr. Sci. 146:225-235.

Bowen, W. R., M.G. Jones, and H.N.S. Yousef. 1998. Prediction of the rate of crossflow membrane ultrafiltration of colloids: a neural network approach. Chem. Eng. Sci. 53:3793-3802.

Braghetta, A., F.A. DiGiano, and W.P. Ball. 1989. NOM accumulation at NF membrane surface: impact of chemistry and shear. J. Environ. Eng. ASCE 124:1087-1098.

Brereton, R.G. 2003. Chemometrics Data analysis for the laboratory and chemical plant. John Wiley & Sons, Ltd. pp. 489.

Cadotte, J. 1981. Interfacially synthesized reverse osmosis membrane. U.S. Patent No. 4,277,344.

Campbell, P., R. Srinivasan, T. Knoell, D. Phipps, K. Ishida, J. Safarik, T. Cormack, and H. Ridgway. 1999. Quantitative structure-activity relationship (QSAR) analysis of surfactants influencing attachment of a Mycobacterium Sp. to cellulose acetate and aromatic polyamide reverse osmosis membranes. Biotechnol. Bioengineering 64, 527-544.

Childress, A.E. and M. Elimelech. 1996. Effect of solution chemistry on the surface charge of polymeric reverse osmosis and nanofiltration membranes. J. Membrane Sci., 119:253.

Cho, J.W., G. Amy, and J. Pellegrino. 2000 Membrane filtration of natural organic matter: factors and mechanisms affecting rejection and flux decline with charged ultrafiltration (UF) membrane. J. Membr. Sci. 164:89-110.

Delgrange, C., C. Cabassud, M. Cabassud, L. Durand-Bourlier, and J.M. Laine. 1998. Neural networks for prediction of ultrafiltration transmembrane pressure—application to drinking water production. J. Membr. Sci. 150:111-123.

Delgrange, C., C. Cabassud, M. Cabassud, L. Durand-Bourlier, and J.M. Laine. 1998. Modeling of ultrafiltration fouling by neural network. Desalination 118:213-227.

Demisch, H.-U. and W. Pusch. 1979. Ion exchange capacity of cellulose acetate membranes. J. Electrochem. Soc., 123, 370.

Demisch, H.-U. and W. Pusch. 1979. Electric and electrokinetic transport properties of homogeneous weak ion exchange membranes. J. Colloid Interface Sci. 69, 247.

Ebrahim, S. 1994. Cleaning and regeneration of membranes in desalination and wastewater applications: state-of-the-art. Desalination 96:225-238.

Fairbrother, F. and H. Mastin. 1924. Studies in electro-endosmosis. J. Chem. Soc. 125, 2319.

Elimelech, M., X. Zhu, A.E. Childress, and S. Hong. 1997. Role of membrane surface morphology in colloidal fouling of cellulose acetate and composite aromatic polyamide reverse osmosis membranes. J. Membr. Sci. 127:101-109.

Flemming, H.-C. 1993. Mechanistic aspects of reverse osmosis membrane fouling and prevention. In Reverse Osmosis Membrane Technology, Water Chemistry and Industrial Applications. Z. Amjad, Ed. Van Hostrand Reinhod, NY. pp. 163-209.

Freger, V. 2003. Nanoscale heterogeneity of polyamide membranes formed by interfacial polymerization. Langmuir 19:4791-4797.

Glater, J., S.-K. Hong, and M. Elimelech. 1994. The search for a chlorine-resistant reverse osmosis membrane. Desalination 95:325-345.

Glater, J., M.R. Zachariah, S.B. McCray and J.W. McCutchan. 1983. Reverse osmosis membrane sensitivity to ozone and halogen disinfectants. Desalination 48:1-16.

Hoek, E.M.V., S. Bhattacharjee, and M. Elimelich. 2003. Effect of surface roughness on colloid-membrane DLVO interactions. Langmuir 19:4836-4847.

Ishida, K., C.E. Milstead, H.F. Ridgway, and R.L. Riley. 1995. Identification and evaluation of biocides for ROWPU systems. USA Tank and Automotive Command Mobility Technology Center—Belvoir. Fort Belvoir, VA.

Ishida, K., R.M. Bold, and H.F. Ridgway. 1998. Influence of molecular conditioning films on microbial colonization of synthetic membranes determined by internal reflection spectrometry. Final Report. NWRI Project No. MRDP 699-508-95. National Water Research Institute, Fountain Valley, CA.

Kilduff, J.E., S. Mattaraj, J. Sensibaugh, J.P. Pieracci, and G. Belfort 2000. Photochemical modification of poly(ether sulfone) and sulfonated poly(sulfone) nanofiltration membranes for control of fouling by natural organic matter. Desalination 10:115-121.

Kim, I.-C., Y.-H. Ka, J.-Y. Park, and K.-H. Lee. 2004. Preparation of fouling resistant nanofiltration and reverse osmosis membrane

Kramer, R. 1998. Chemometric techniques for quantitative analysis. Marcel Dekker, NY. pp. 203.

Liikanen, R., J. Yli-Kuivila, and R. Laukkanen. 2002. Efficiency of various chemical cleanings for nanofiltration membrane fouled by conventionally-treated surface water. J. Membr. Sci. 195:265-275.

Lozier, J.C. 2005. Evaluating chloramines fro control of RO membrane biofouling with ground and surface water supplies. In Proceedings of the AWWA Membrane Technology Conference, Phoenix, AZ, 6 March – 9 March 2005.

Madaeni, S.S., T. Mohamamdi, and M.K. Moghadam. 2001. Chemical cleaning of reverse osmosis membranes. Desalination 134:77-82.

Nauman, D., C. Schultz, and D. Helm. 1996. "What can infrared spectroscopy tell us about the structure and composition of intact bacterial cells?", In Infrared Spectroscopy of Biomolecules, H. H. Mantsch and D. Chapman, Eds. Wiley-Liss, NY, p. 279.

Niemi, H., A. Bulsari, and S. Palosaari. 1995. Simulation of membrane separation by neural networks. J. Membr. Sci. 102:185-191.

Ridgway, H., K. Ishida, G. Rodriguez, J. Safarik, T. Knoell, and R. Bold. 1999. Biofouling of membranes: Membrane preparation, characterization, and analysis of bacterial adhesion. In Methods in Enzymology, Vol. 310. Ed. Ron J. Doyle. Academic Press, NY. pp. 463-494.

Ridgway, H.R. and J. Safarik. 1991. Biofouling of reverse osmosis membranes, In Biofouling and Biocorrosion in Industrial Water Systems, H.-C. Flemming and G.G. Geesey, Eds. Springer-Verlag, Berlin, pp. 81-111.

Ridgway, H.R. and H.-C. Flemming. 1996. Membrane biofouling. In Water Treatment Membrane Processes. J. Mallevialle, P.E. Odendaal, and M.R. Wiesner, Eds. McGraw-Hill, NY Pp. 6.1-6.61.

Rodriguez, G. and D. Phipps, Jr. 2004. Prediction of organics removal by reverse osmosis membranes. U.S. Environmental Protection Agency. Contract No. XP-98973001-0.

Rodriguez, G., Buonora, S., Knoell, T., Phipps, D., Jr., and H. Ridgway. 2004. Rejection of pharmaceuticals by reverse osmosis membranes: quantitative structure activity relationship (QSAR) analysis. National Water Research Institute. Fountain Valley, CA. NWRI Project No. 01-EC-002.

Seidel, A. and M. Elimelech. 2002. Coupling between chemical and physical interactioins in natural organic matter (NOM) fouling of nanofiltration membranes: implications for fouling control. J. Membr. Sci. 203:245-255.

Shetty, G.R. and S. Chellam. 2003. Predicting membrane fouling during municipal drinking water nanofiltration using artificial neural networks. J. Membr. Sci. 217:69-86.

Taniguchi, M., J.E. Kilduff, and G. Belfort. 2002. Low NOM fouling synthetic membranes by UV-assisted graft polymerization. J. Membr. Sci. 22:59-70.

Vrijenhoek, E.M., S.K. Hong, and M. Elimelech. 2001. Influence of membrane surface properties on initial rate of colloidal fouling of reverse osmosis and nanofiltration membranes. J. Membr. Sci. 188:115-128.

Whittaker, C., H. Ridgway, and B.H. Olson. 1984. Evaluation of cleaning strategies for removal of biofilms from reverse osmosis membranes. Applied Environ. Microbiol. 48:395-403.

Glossary of Terms

AFM	atomic force microscopy
ATR	attenuated total reflection
CA	cellulose acetate
DBSA	dodecylbenzenesulfonic acid
DWRP13	Department of Water Resources Proposition 13
FTIR	Fourier transform infrared
Ge	germanium
gfd	gallons per square foot per day
gpm	gallons per min
IRE	internal reflection element
L	liter
mL	milliliter
Mohm-cm	megaohms-centimeter
N	number
NF	nanofiltration
NWRI	National Water Research Institute
OCWD	Orange County Water District
PA	polyamide
PA-U	polyamide-urea
PCA	principal components analysis
PS	polysulfone
Psi	pounds per square inch
PTFE	polytetrafluoroethylene
RMS	root mean square
RO	reverse osmosis
SDS	sodium dodecylsulfate
SST	Separation Systems Technology
STP	sodium tripolyphosphate
TDS	total dissolved solids

TEM	transmission electron microscopy
TFC	thin-film composite
TMC/MPD	trimesoyl chloride / *m*-phenylenediamine
ZnSe	zinc selenide
TEA	tetraethylammonium bromide
DMAB	decyltrimethylammonium bromide
DTAB	dodecyltrimethylammonium bromide
CTAB	hexadecyltrimethylammonium bromide

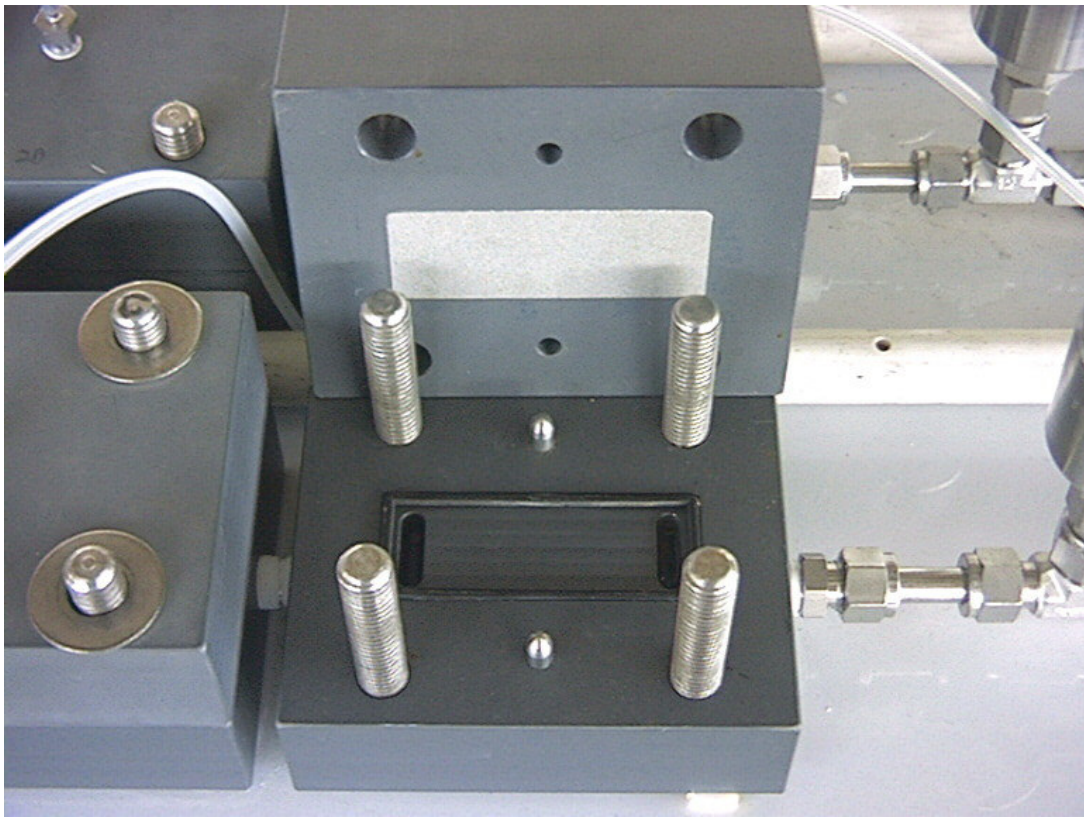

Figure 1. Polyvinyl chloride RO test cell. Porous stainless steel support on product-water side (top plate) and 1 x 3 in. membrane surface area with O-ring seal (bottom plate).

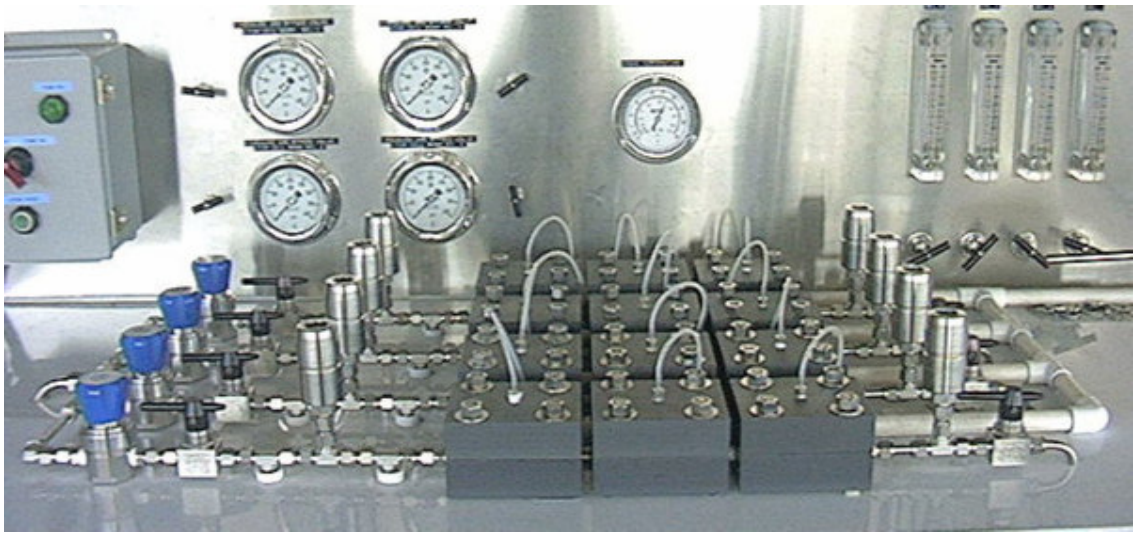

Figure 2. RO block test cell system. Three test cells run in series with four parallel groups of three test cells.

Figure 3. RO cleaning cycle bypass with cleaning agent recirculated over the surface of the membranes. Note detergent heating coil is missing from this picture.

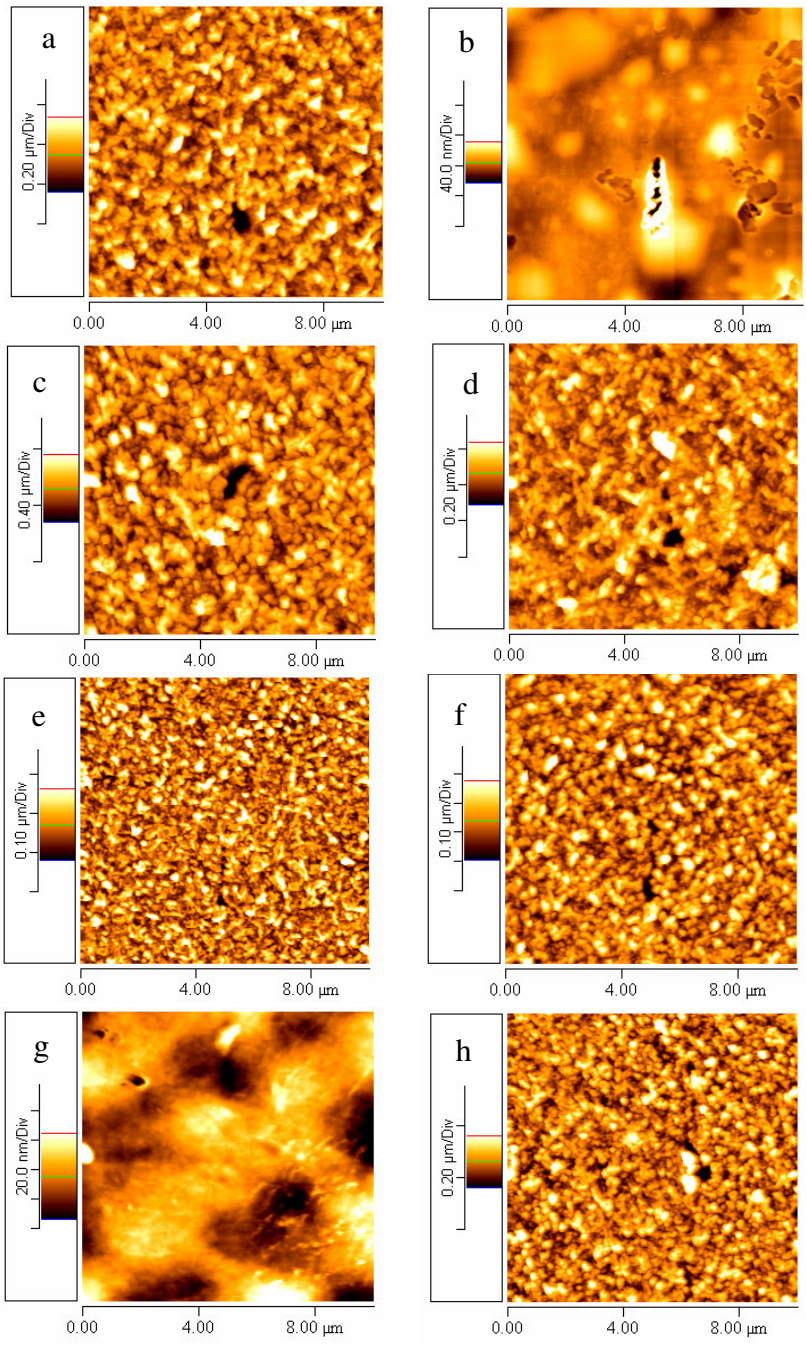

Figure 4. AFM images of (a) FilmTec BW-30, (b) SST TMC/MPD, (c) Hydranautics ESPA2, (d) Hydranautics LFC3, (e) Koch TFC-HR, (f) Koch TFC-ULP, (g) GE Osmonics / Desal CA, and (h) Trisep X-201 RO membranes.

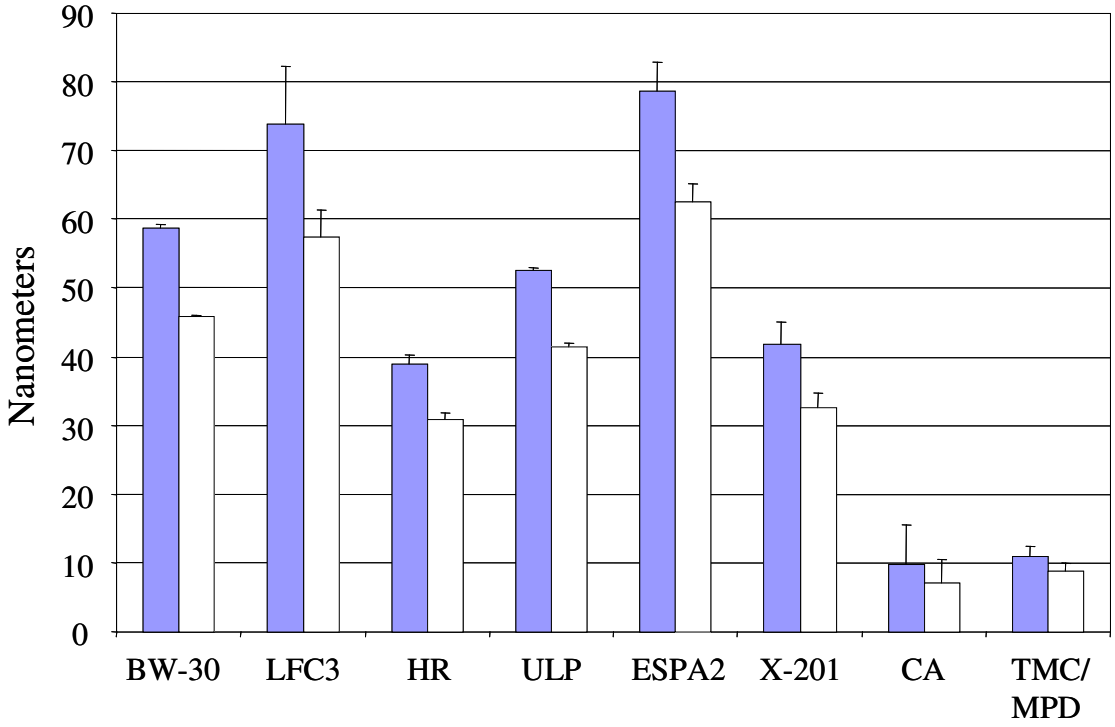

Figure 5. RMS roughness (left, solid) and average roughness (right, open) for FilmTec BW-30, Hydranautics LFC3, Koch TFC-HR, Koch TFC-ULP, Hydranautics ESPA2, Trisep X-201, Desal CA, and SST TMC/MPD RO membranes.

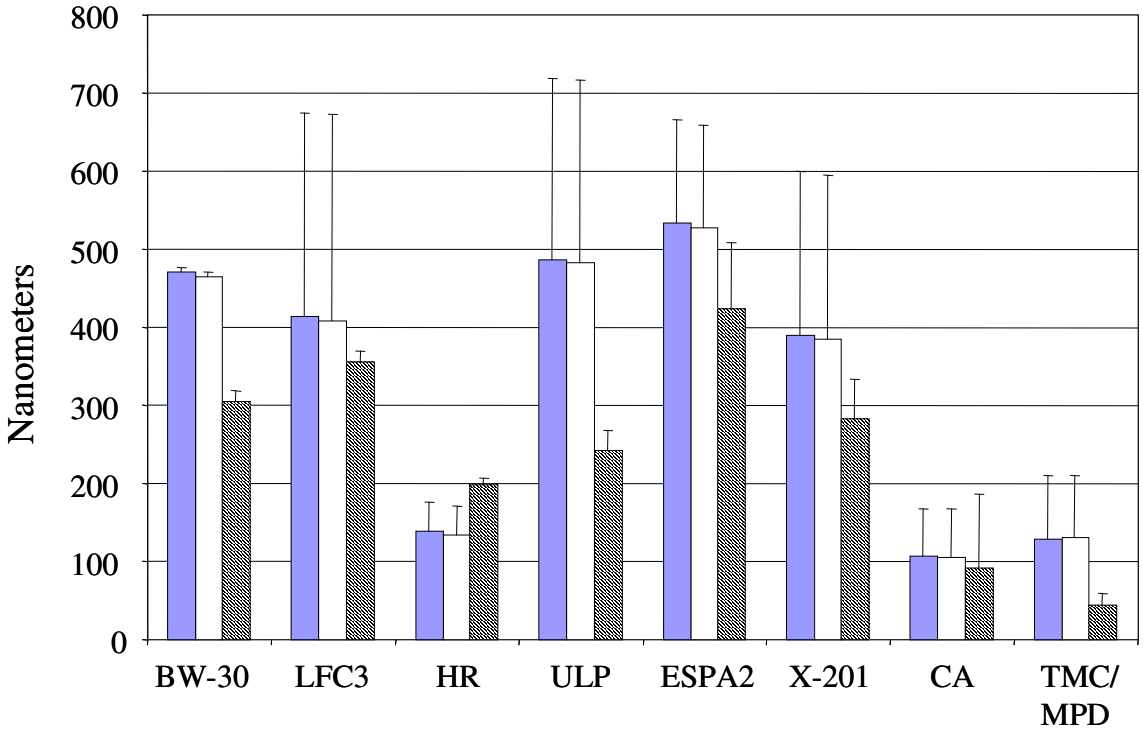

Figure 6. Mean height (left, solid), median height (middle, open) and peak (right, striped)for FilmTec BW-30, Hydranautics LFC3, Koch TFC-HR, Koch TFC-ULP, Hydranautics ESPA2, Trisep X-201, Desal CA and SST TMC/MPD RO membranes.

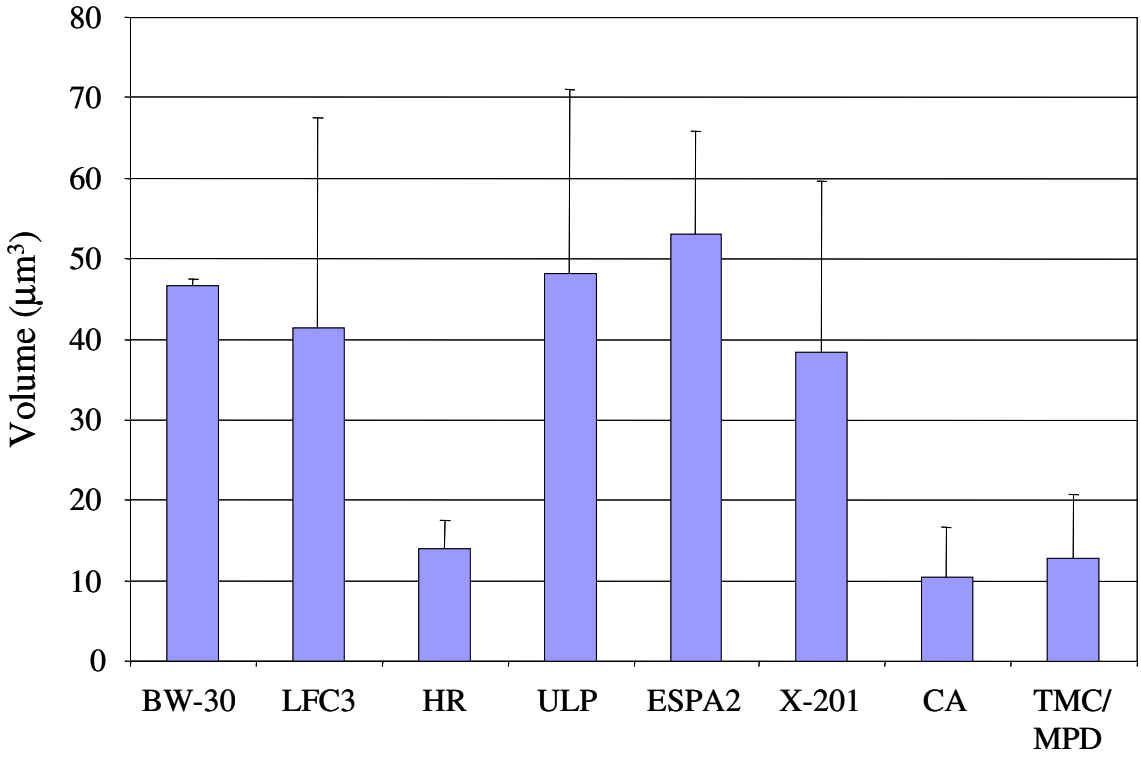

Figure 7. Volume (μm^3) for FilmTec BW-30, Hydranautics LFCS, Koch TFC-HR, Koch TFC-ULP, Hydranautics ESPA2, Trisep X-201, Desal CA , and SST TMC/MPD RO membranes.

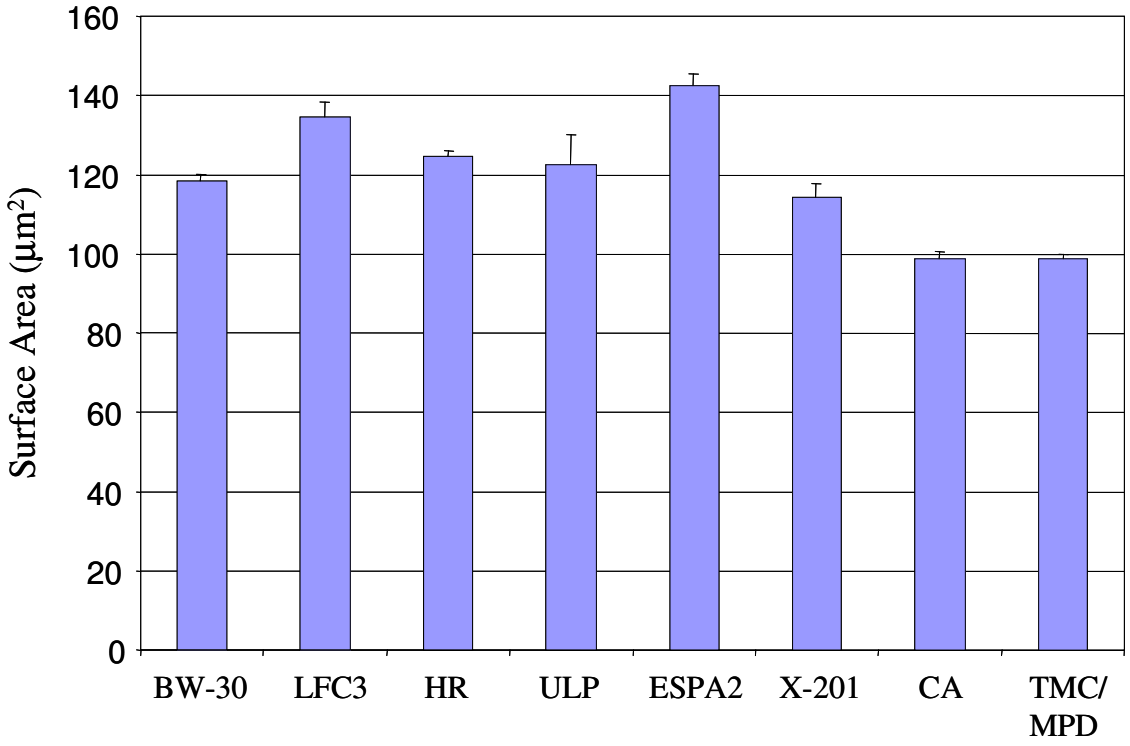

Figure 8. Surface area (μm^2) for FilmTec BW-30, Hydranautics LFCS, Koch TFC-HR, Koch TFC-ULP, Hydranautics ESPA2, Trisep X-201, Desal CA and SST TMC/MPD RO membranes.

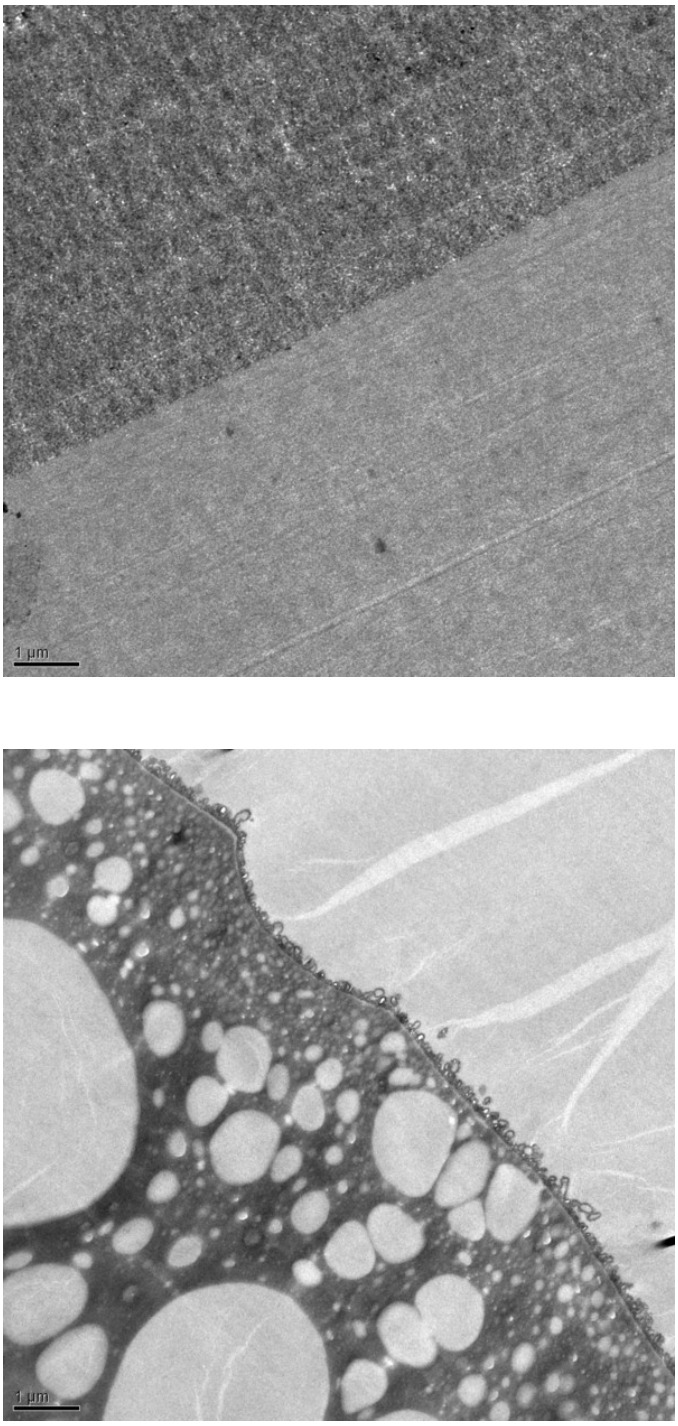

Figure 9. Transmission electron micrographs of Desal CA (top) and Trisep X-201 (bottom) RO membrane.

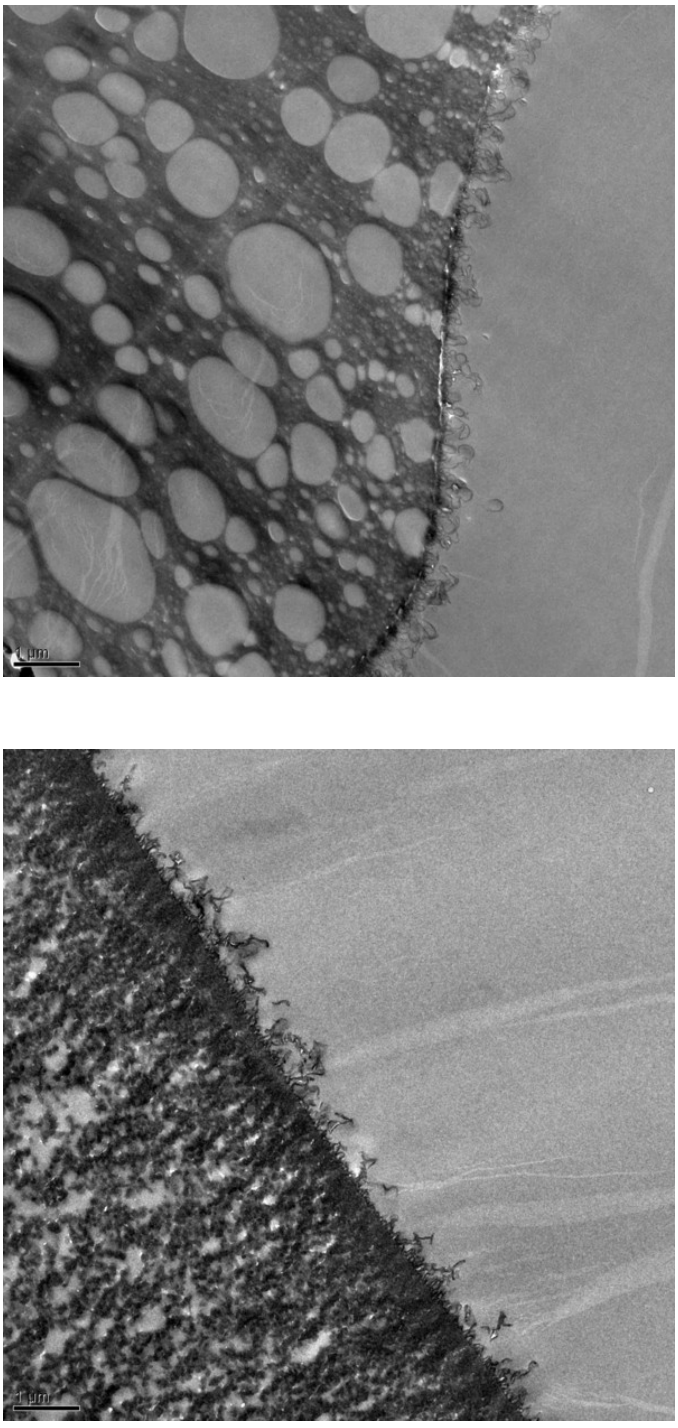

Figure 10. Transmission electron micrographs of FilmTec BW-30 (top) and SST TMC/MPD (bottom) RO membranes.

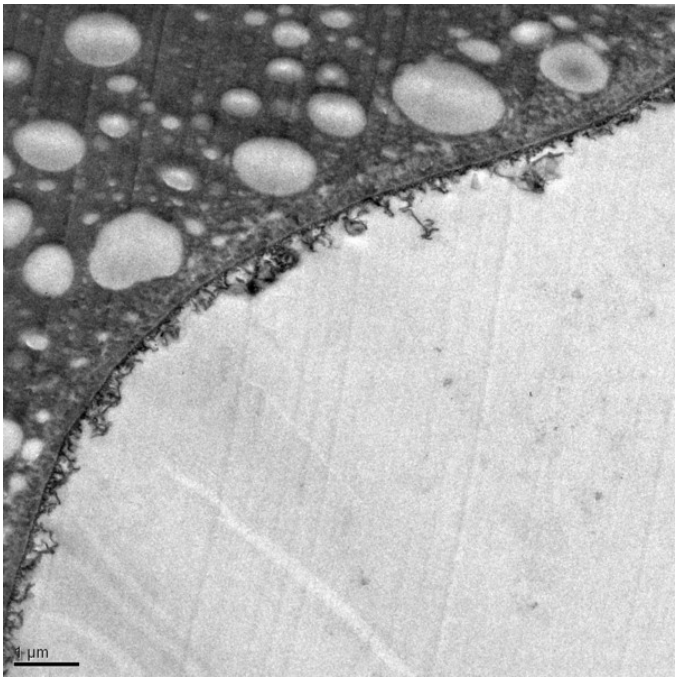

Figure 11. Transmission electron micrographs of Hydranautics ESPA2 (top) and LFC3 (bottom) RO membranes.

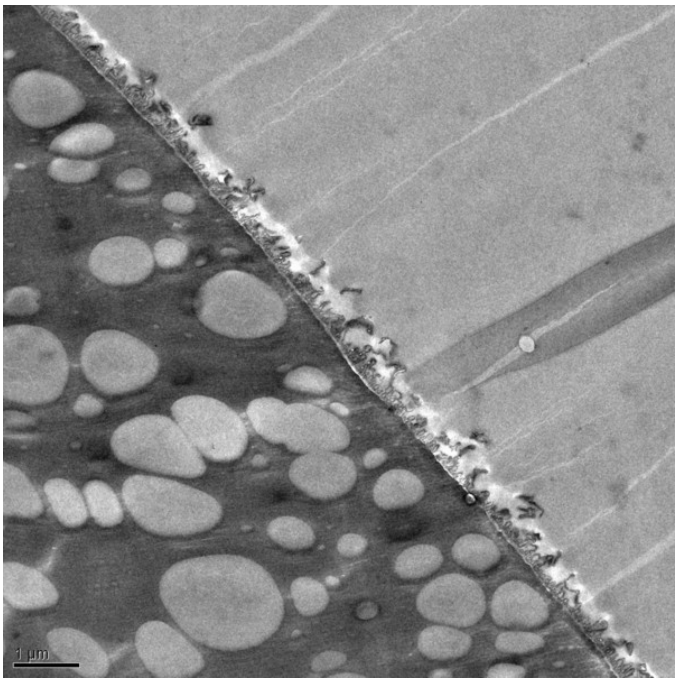

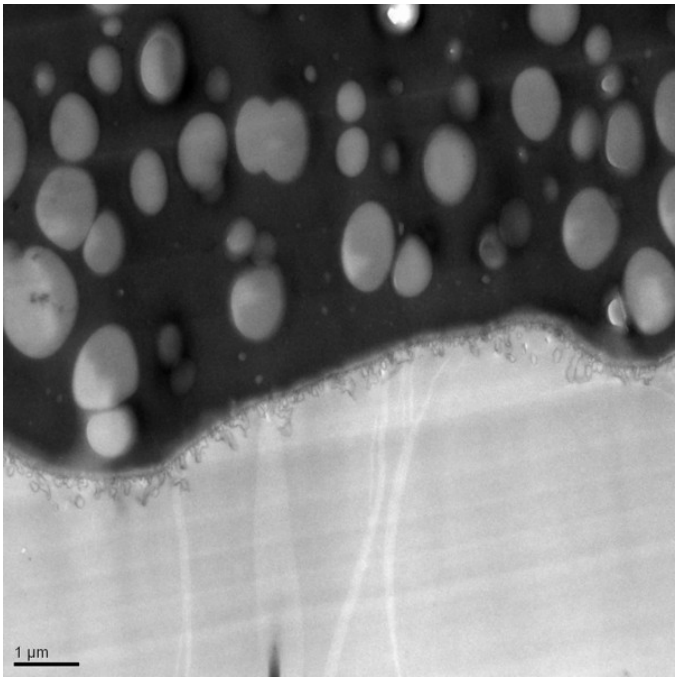

Figure 12. Transmission electron micrographs of Koch TFC-HR (top) and TFC-ULP (bottom) RO membranes.

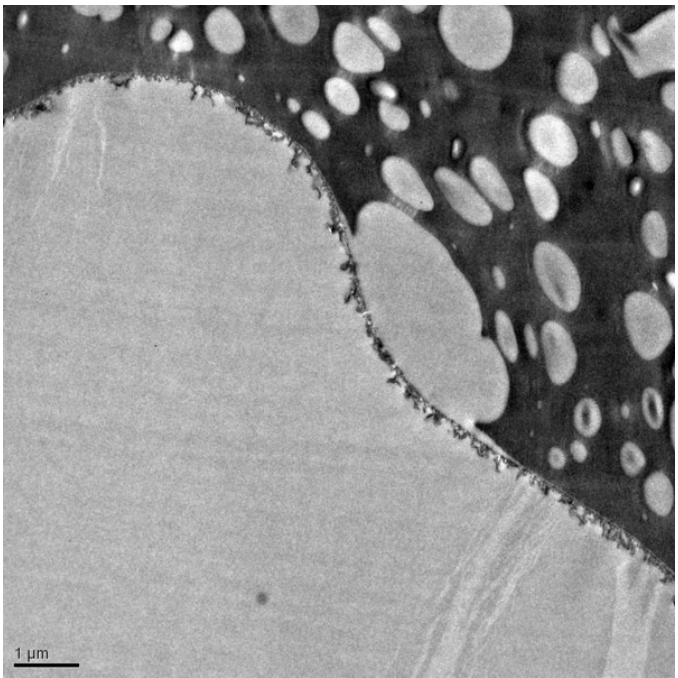

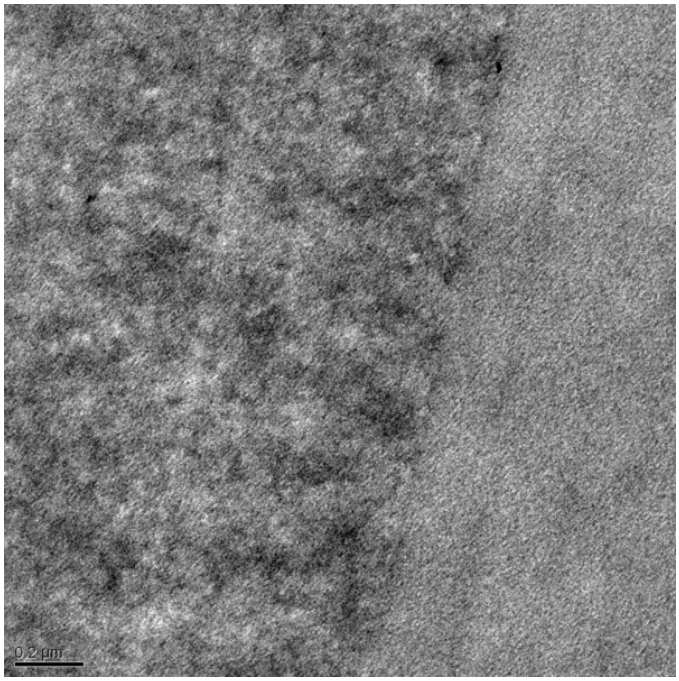

Figure 13. Transmission electron micrographs of Desal CA (top) and Trisep X-201 (bottom) RO membranes.

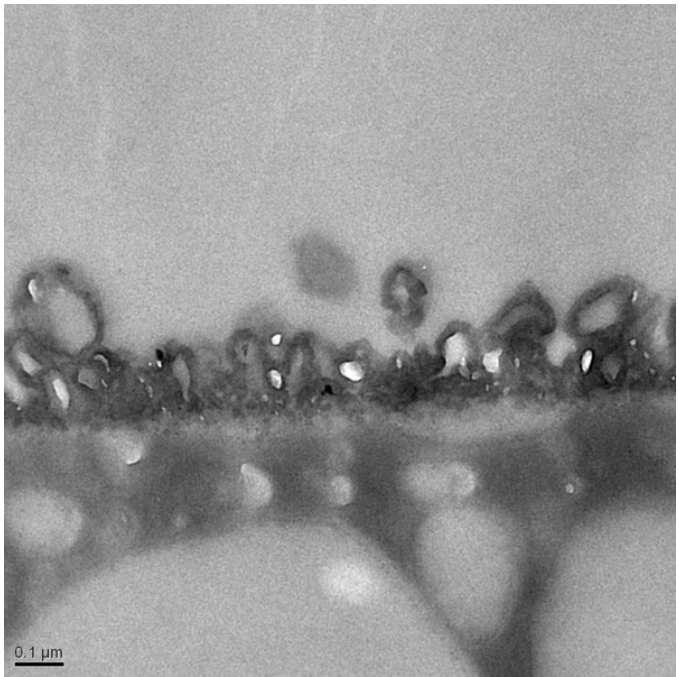

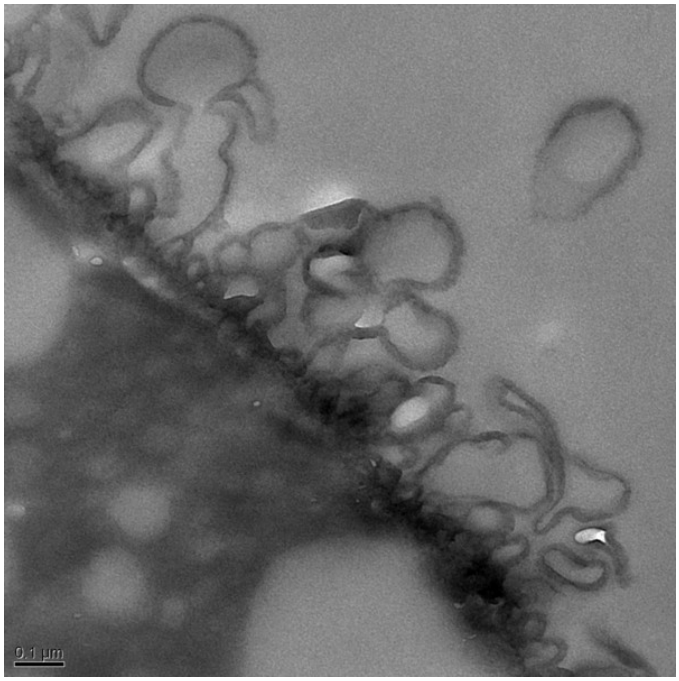

Figure 14. Transmission electron micrographs of FilmTec BW-30 (top) and SST TMC/MPD (bottom) RO membranes.

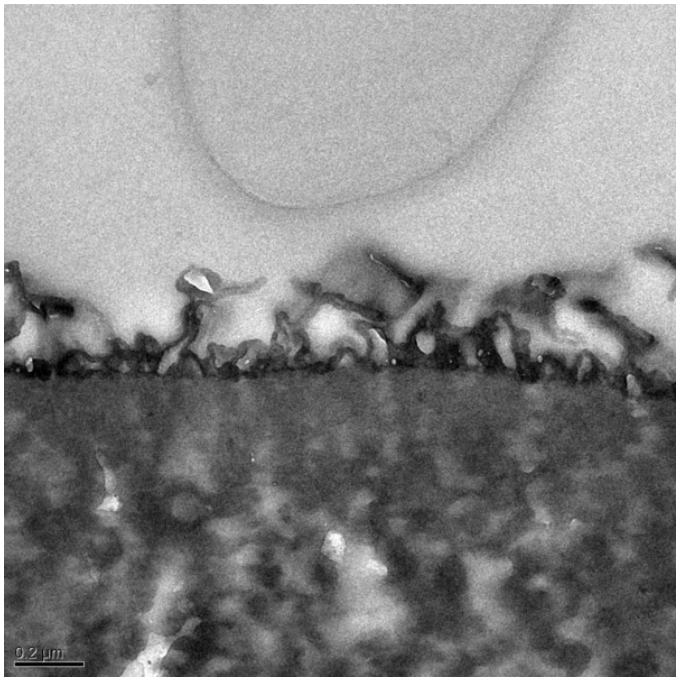

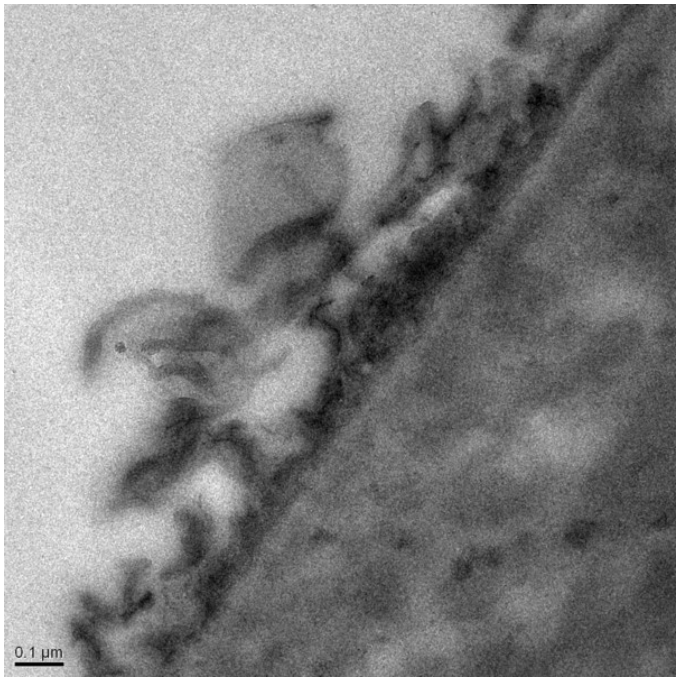

Figure 15. Transmission electron micrographs of Hydranautics ESPA2 (top) and LFC3 (bottom) RO membranes.

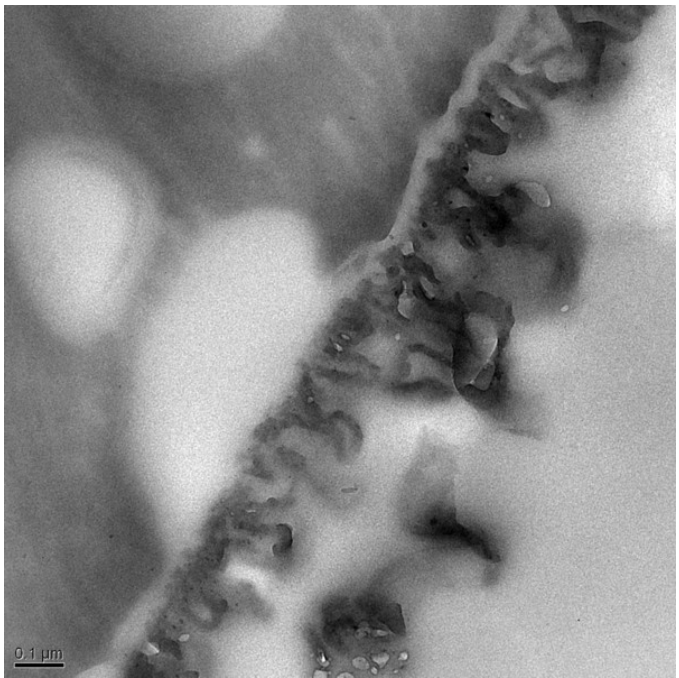

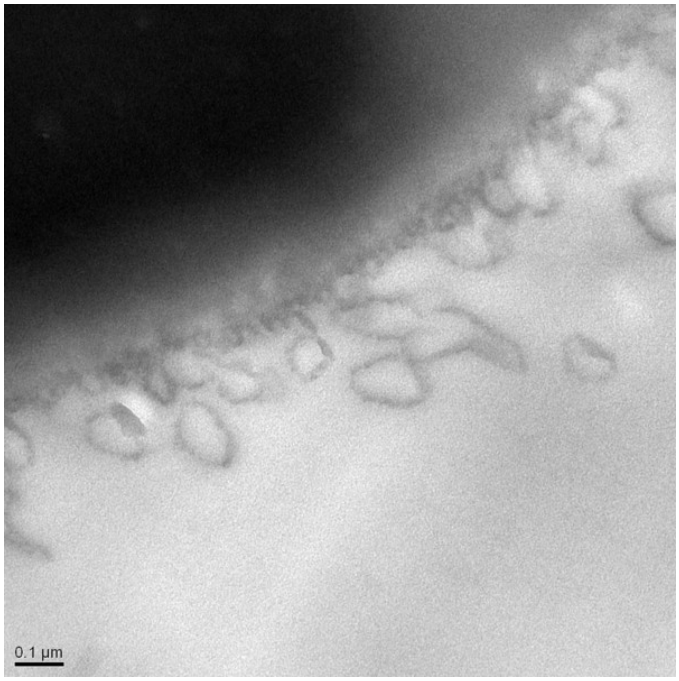

Figure 16. Transmission electron micrographs of Koch TFC-HR (top) and TFC-ULP (bottom) RO membranes.

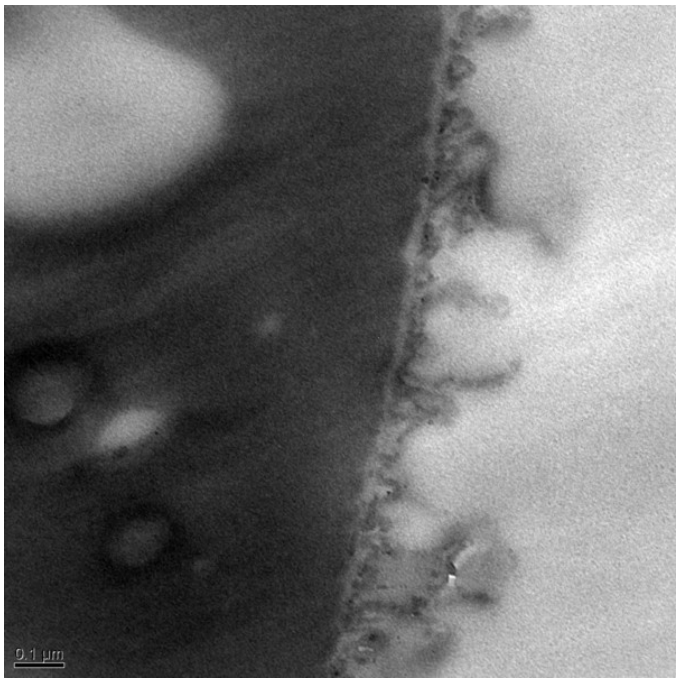

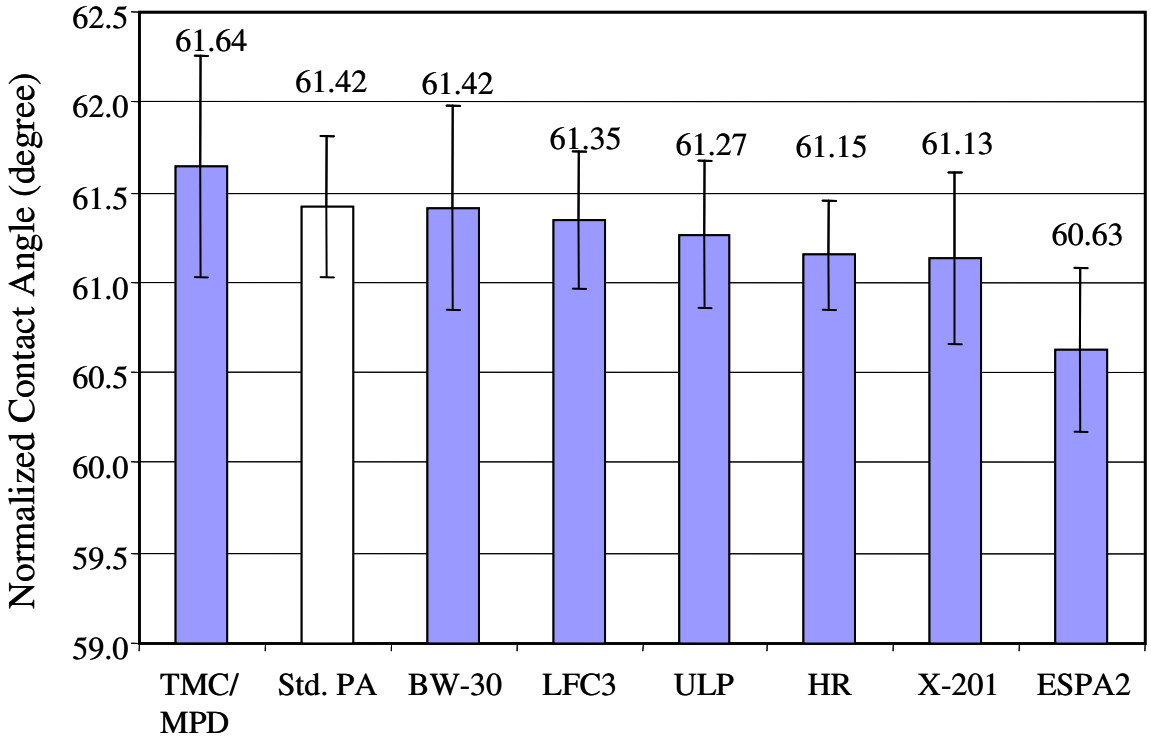

Figure 17. Normalized captive air bubble contact angle for FilmTec BW-30, Hydranautics LFC3 and ESPA2, Koch TFC-HR and TFC-ULP, Trisep X-201 and SST TMC/MPD RO membranes.

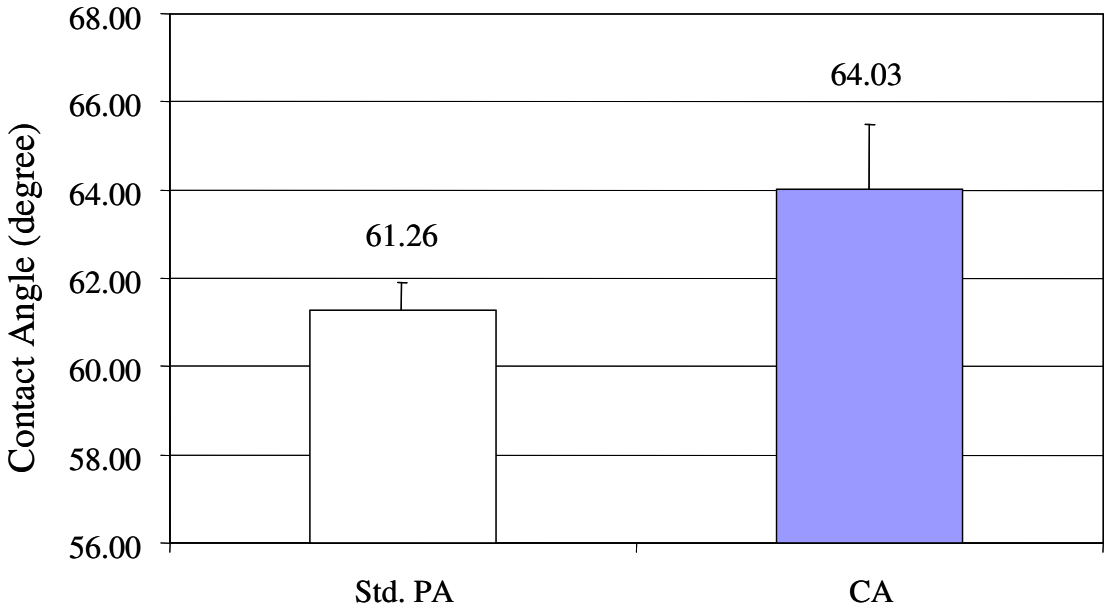

Figure 18. Normalized captive air bubble contact angle for FilmTec BW-30, Hydranautics LFC3 and ESPA2, Koch TFC-HR and TFC-ULP, Trisep X-201 and SST TMC/MPD RO membranes.

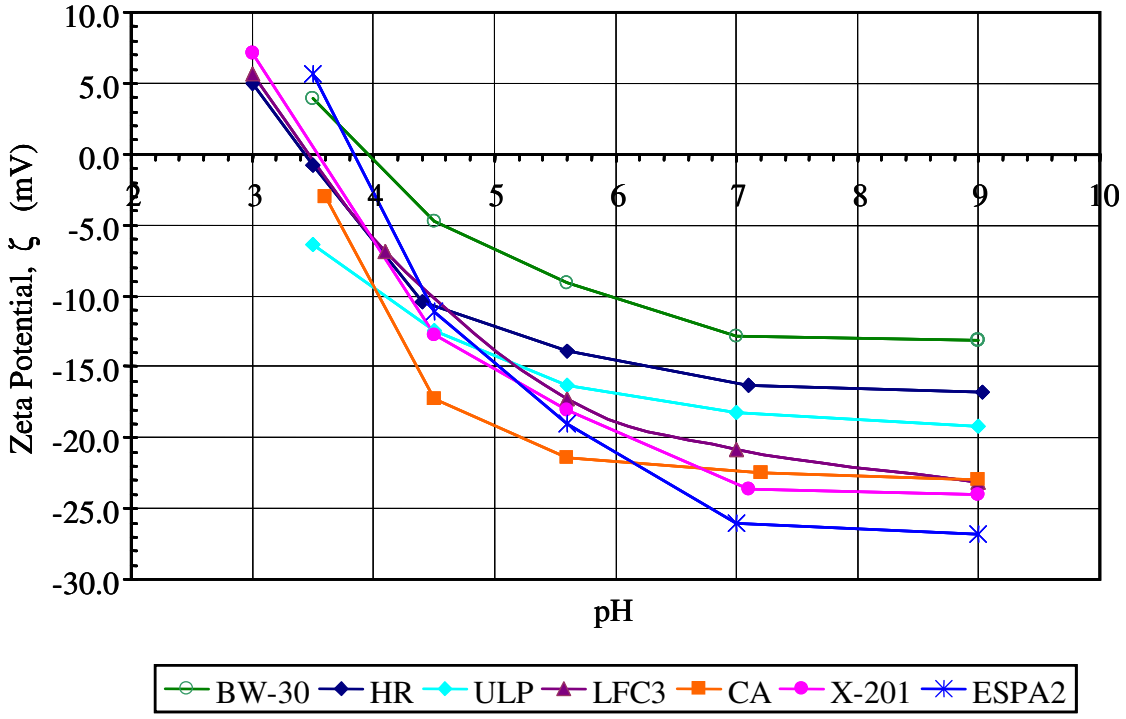

Figure 19. Zeta potential of FilmTec BW-30, Koch TFC-HR and TFC-ULP, Hydranautics LFC3, Desal CA, Trisep X-201, and Hydranautics ESPA2 RO membranes.

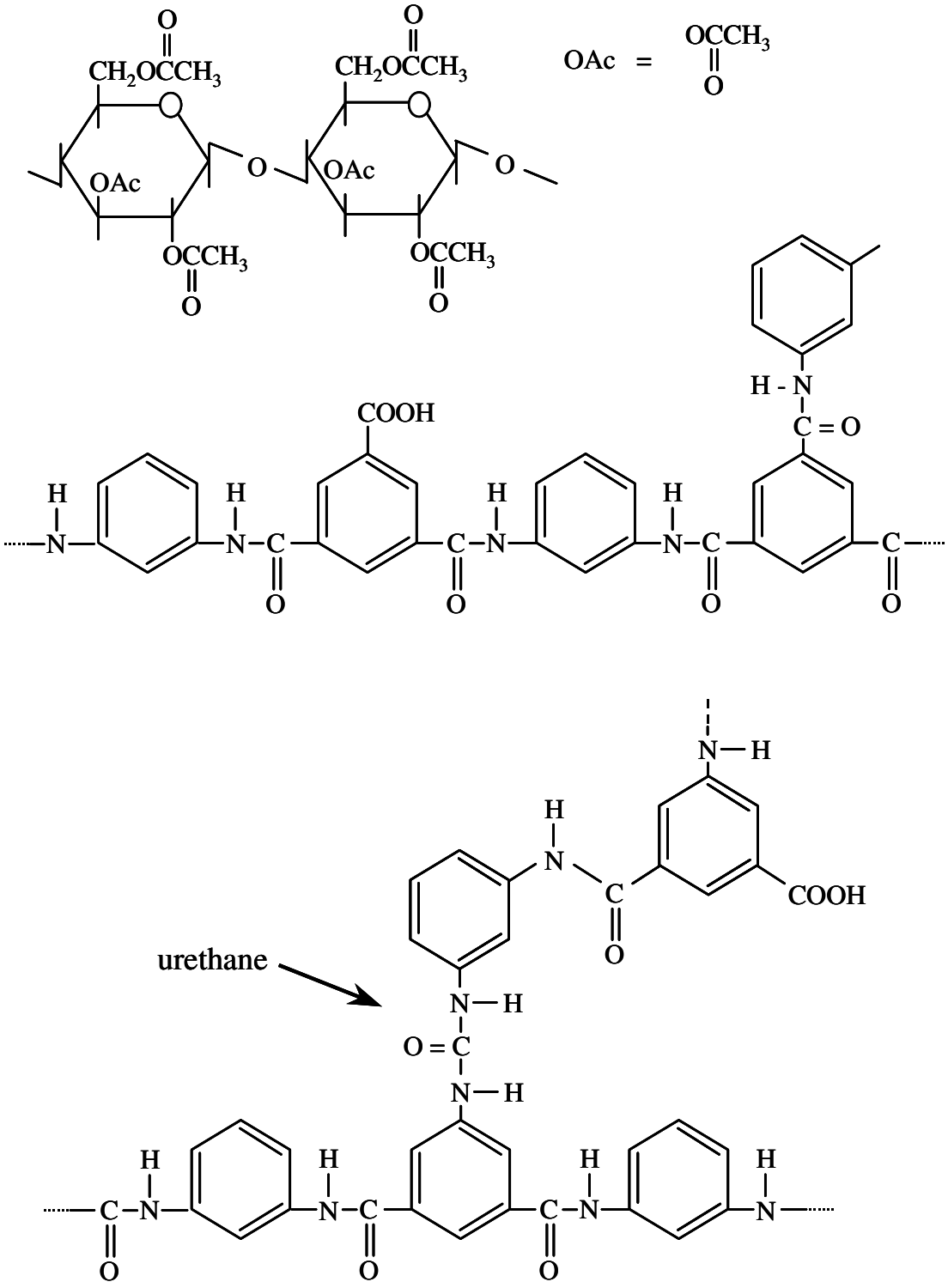

Figure 20. Chemical structure of cellulose [tri-] acetate (top), crosslinked polyamide (middle), and crosslinked polyamide-urea (bottom) RO membranes.

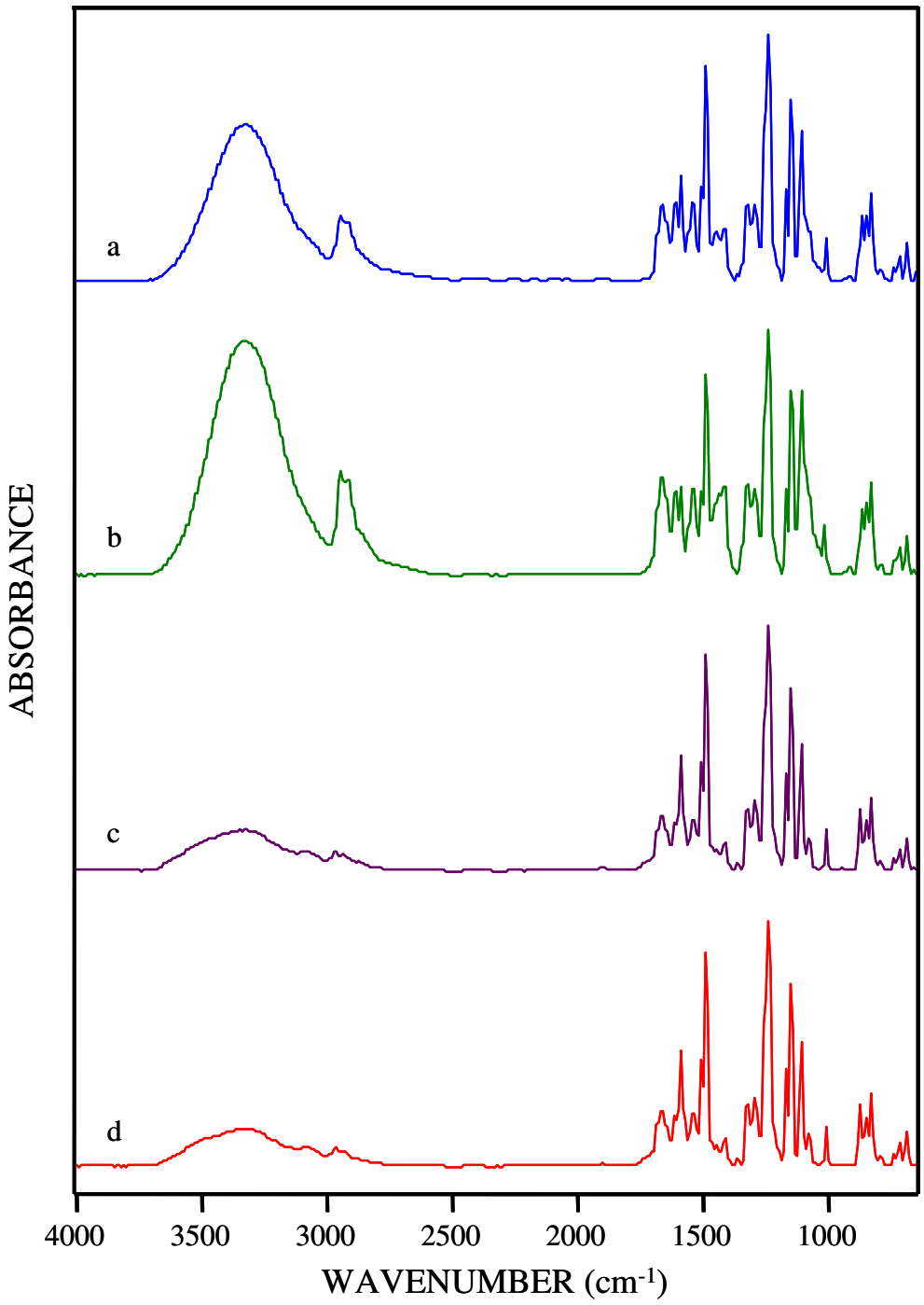

Figure 21. ATR/FTIR spectra of (a) FilmTec BW-30, (b) Hydranautics LFC3, (c) Koch TFC-HR and (d) Koch TFC-ULP RO membranes.

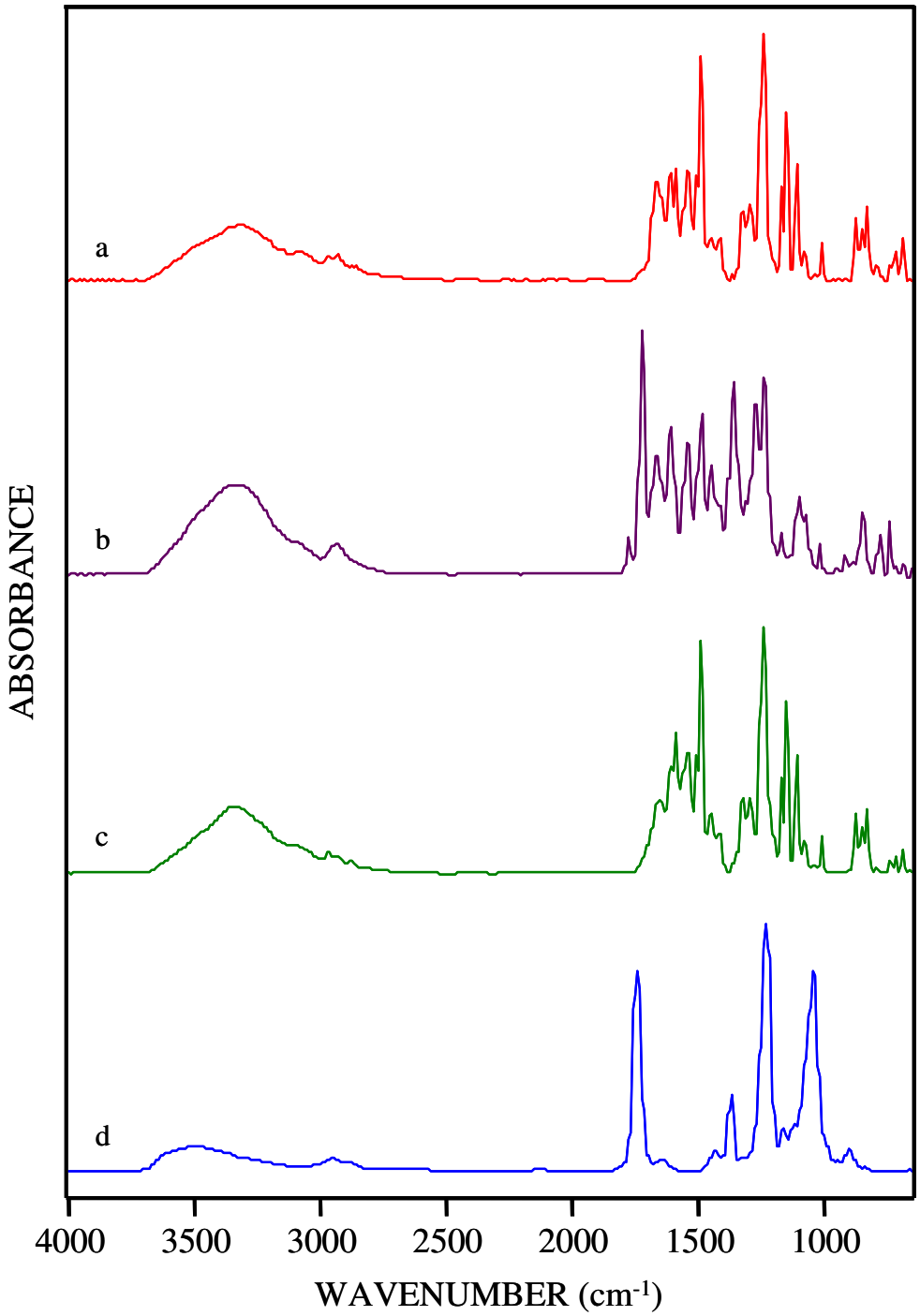

Figure 22. ATR/FTIR spectra of (a) Hydranautics ESPA2, (b) SST TMC/MPD, (c) Trisep X-201, and Desal CA RO membranes.

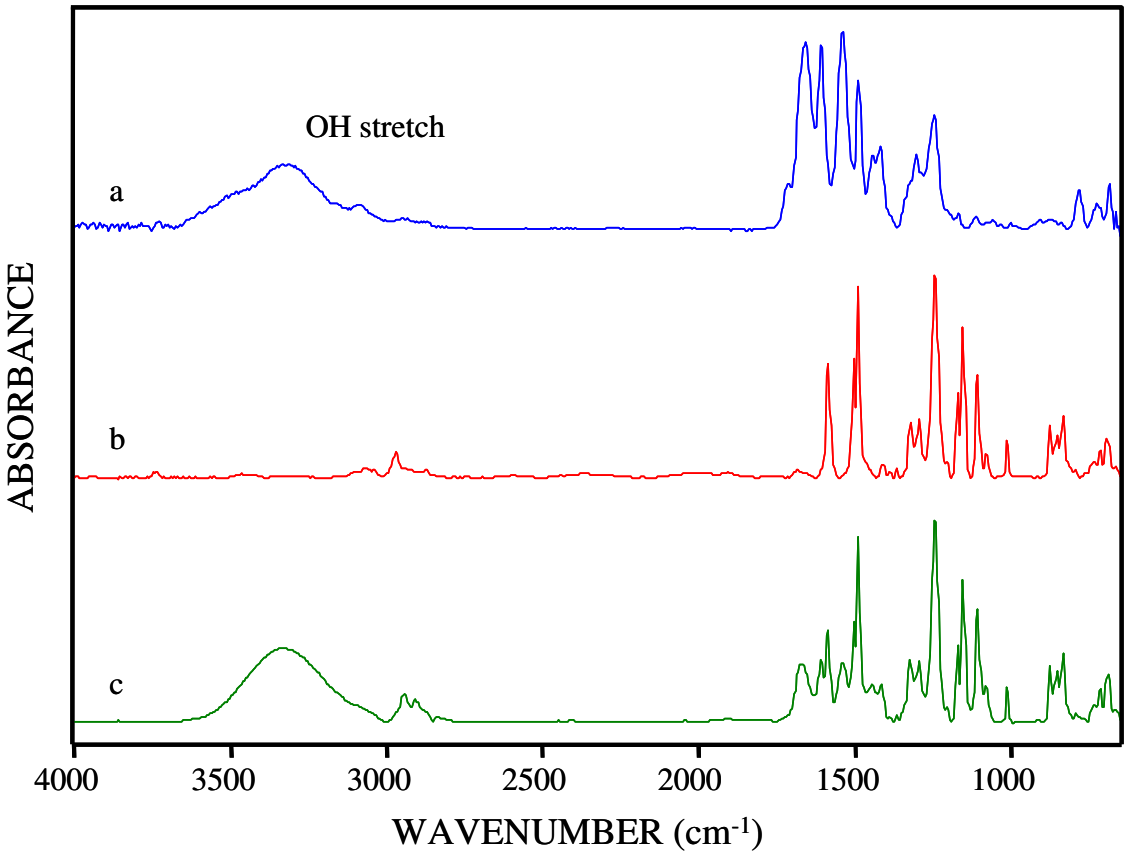

Figure 23. ATR/FTIR spectra of (a) polyamide, (b) polysulfone, and (c) thin-film composite RO membranes.

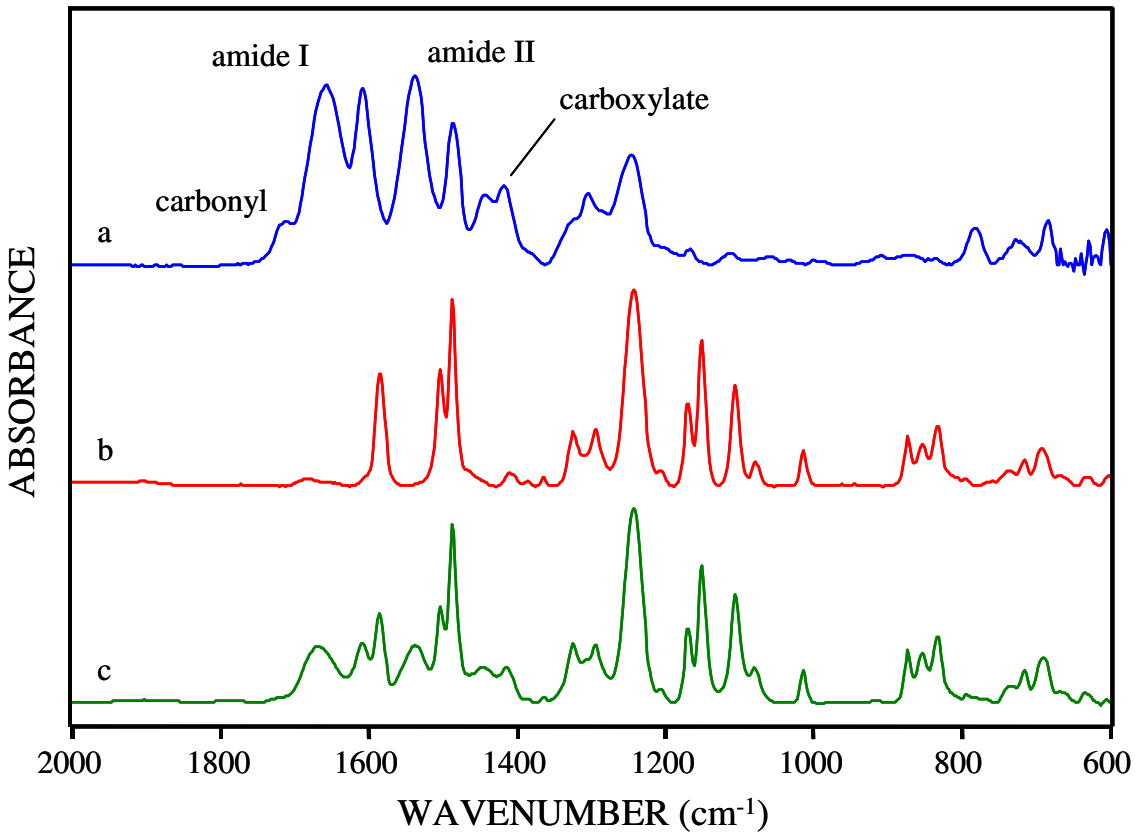

Figure 24. ATR/FTIR spectra of (a) polyamide, (b) polysulfone, and (c) thin-film composite RO membranes.

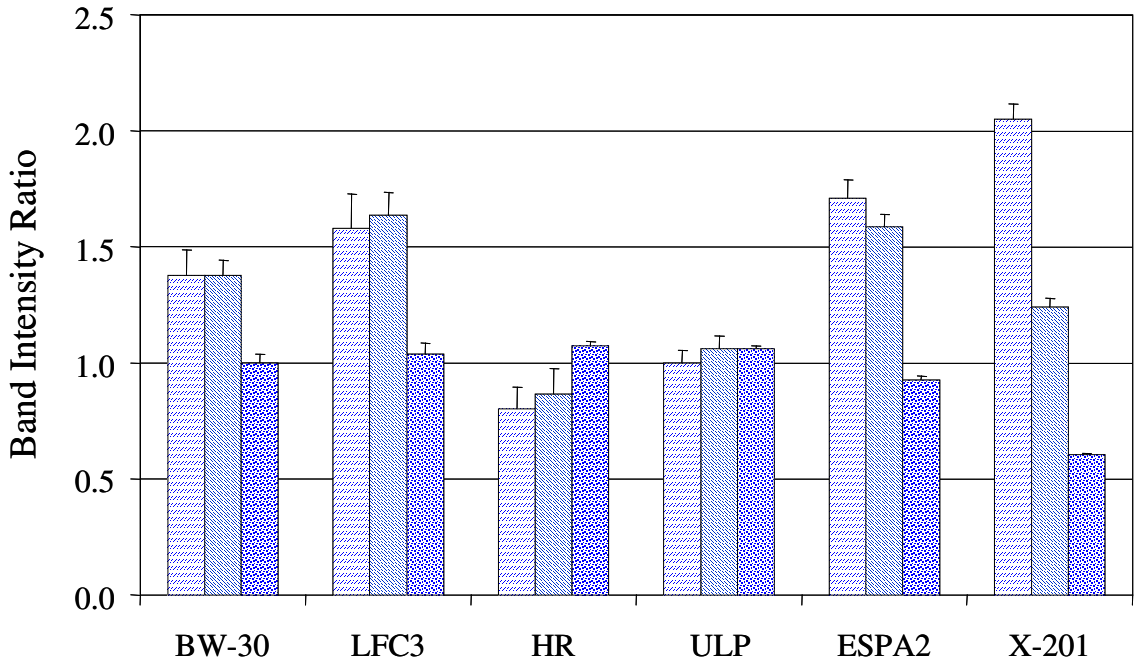

Figure 25. Characterization of thin-film composite RO membranes based on IR band intensity ratios represented by (left) amide II / 874 cm^{-1}, (middle) amide I / 874 cm^{-1} and (right) amide I / amide II.

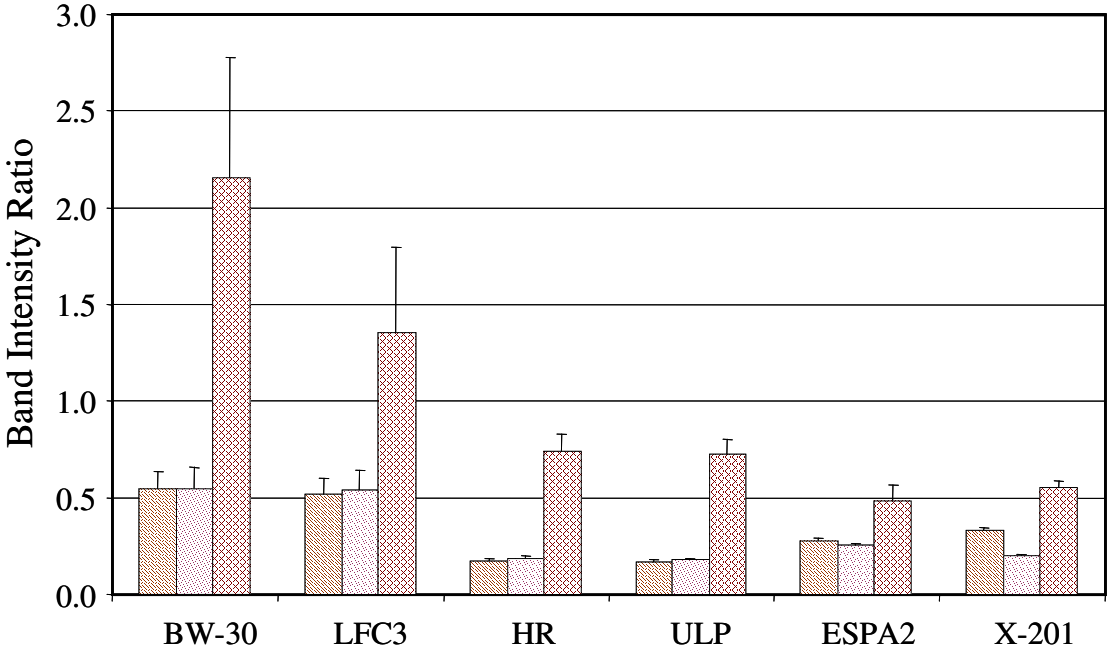

Figure 26. Characterization of thin-film composite RO membranes based on IR band intensity ratios represented by (left) carboxylate / amide I, (middle) carboxylate / amide II and (right) OH stretch / amide II.

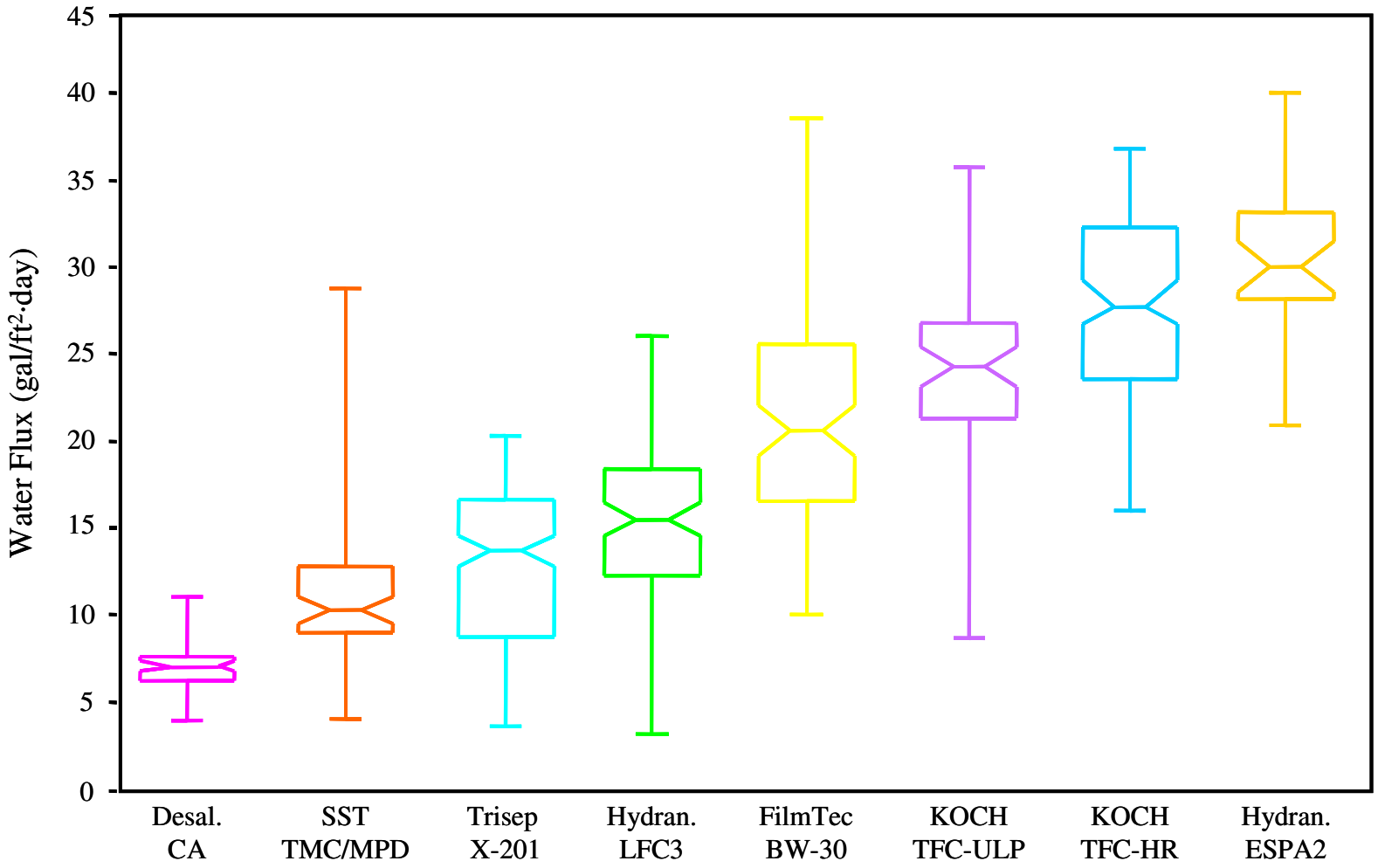

Figure 27. Water flux prior to chemical exposure. Test conditions: 1,000 ppm sodium chloride, pH 5.5, 200-210 psi, 24-26°C, and 14 hr.

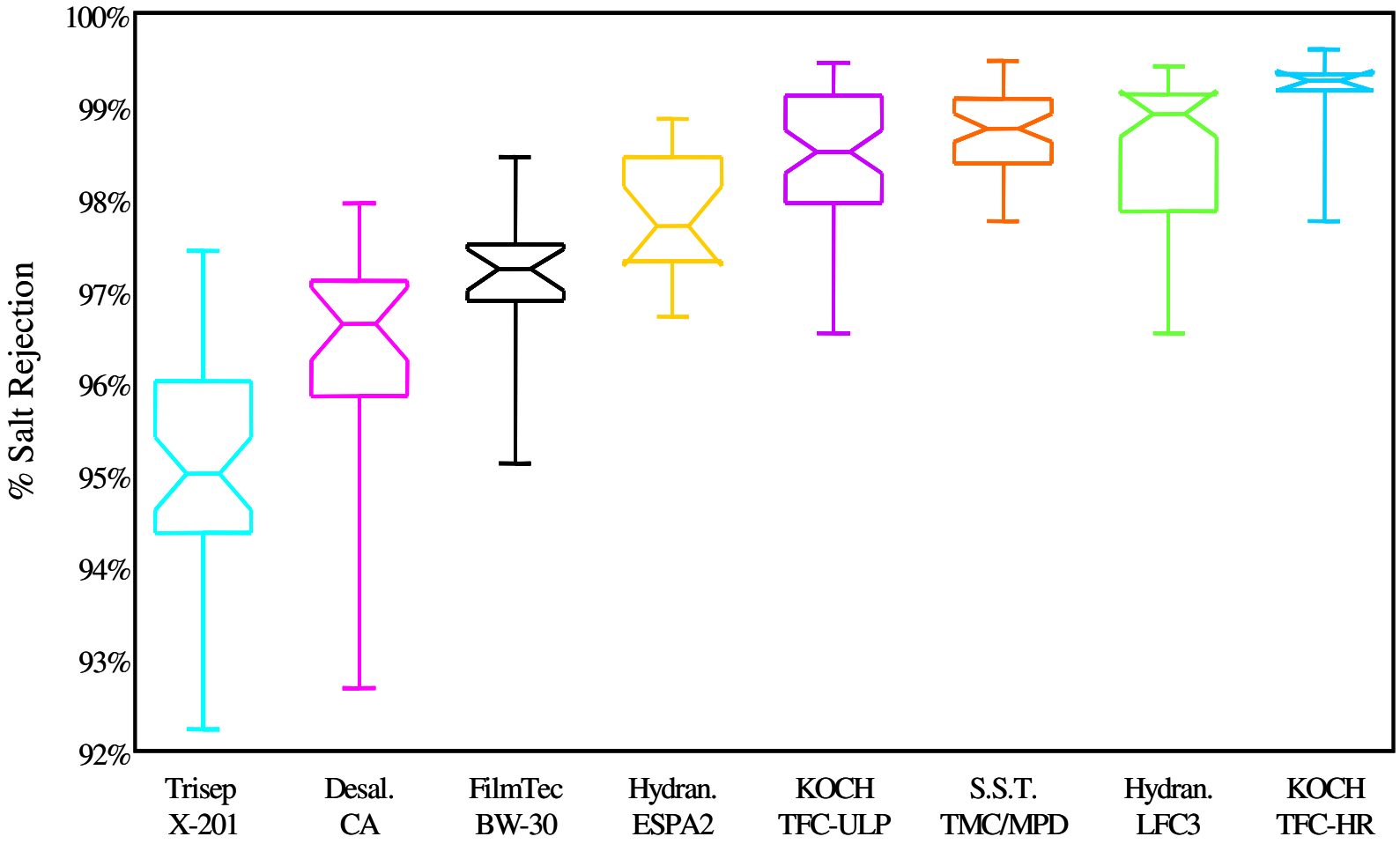

Figure 28. Solute flux prior to chemical exposure. Test conditions: 1,000 ppm sodium chloride, pH 5.5, 200-210 psi, 24-26°C, and 14 h

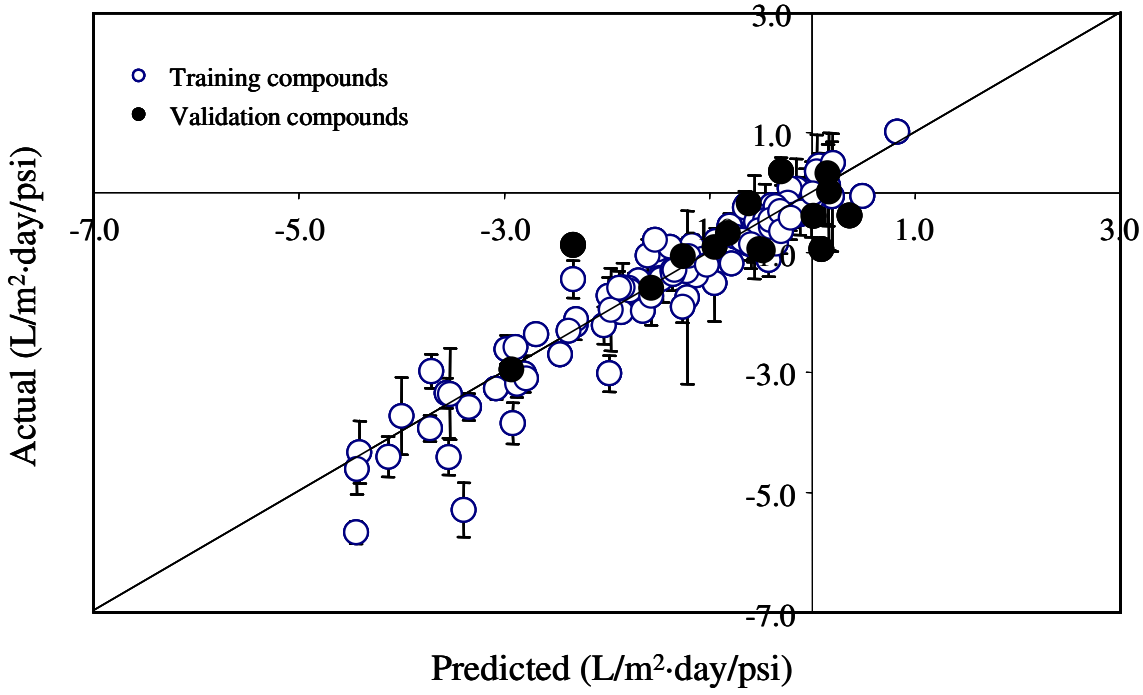

Model Statistics

	R	Avg. Abs.	RMS	Accuracy (20%)	Confidence Interval (95%)	Records
All	0.940	0.332	0.459	0.988	0.895	406
Train	0.939	0.331	0.461	0.989	0.900	284
Test	0.945	0.335	0.455	0.984	0.895	122

Sensitivity Index

COO-/ AMII	AMII / 874	Zeta Potential slope	Dip	SsCH3	SHother	Gmin
0.001691	0.264306	0.471789	0.144463	0.296114	4.2971	0.58016

Figure 29. ANN model results for change in specific water flux for the PA membrane after treatment with cleaning compounds.

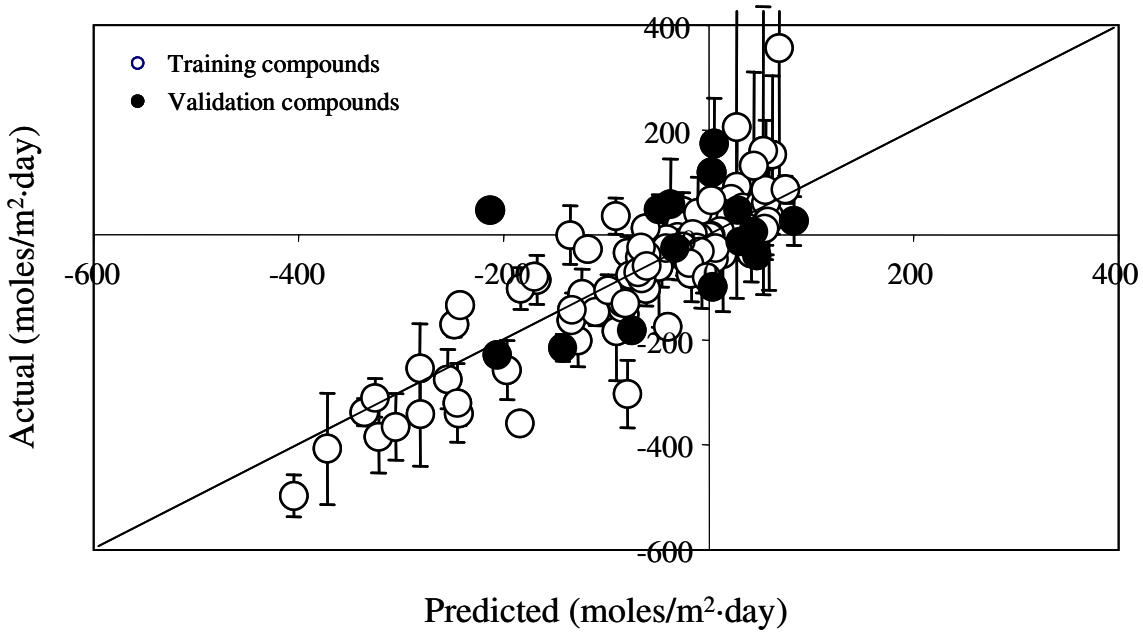

Model Statistics

	R	Avg. Abs.	RMS	Accuracy (20%)	Confidence Interval (95%)	Records
All	0.811	50.06	81.73	0.98	159	406
Train	0.821	48.56	80.33	0.98	157	324
Test	0.770	55.98	87.03	0.99	172	82

Sensitivity Index

AMII/874	MaxNeg	sumdelI	tets2
0.6140	-0.2740	-0.6850	-1.0104

Figure 30. ANN model results for change in solute flux for the PA membrane after treatment with cleaning compounds.

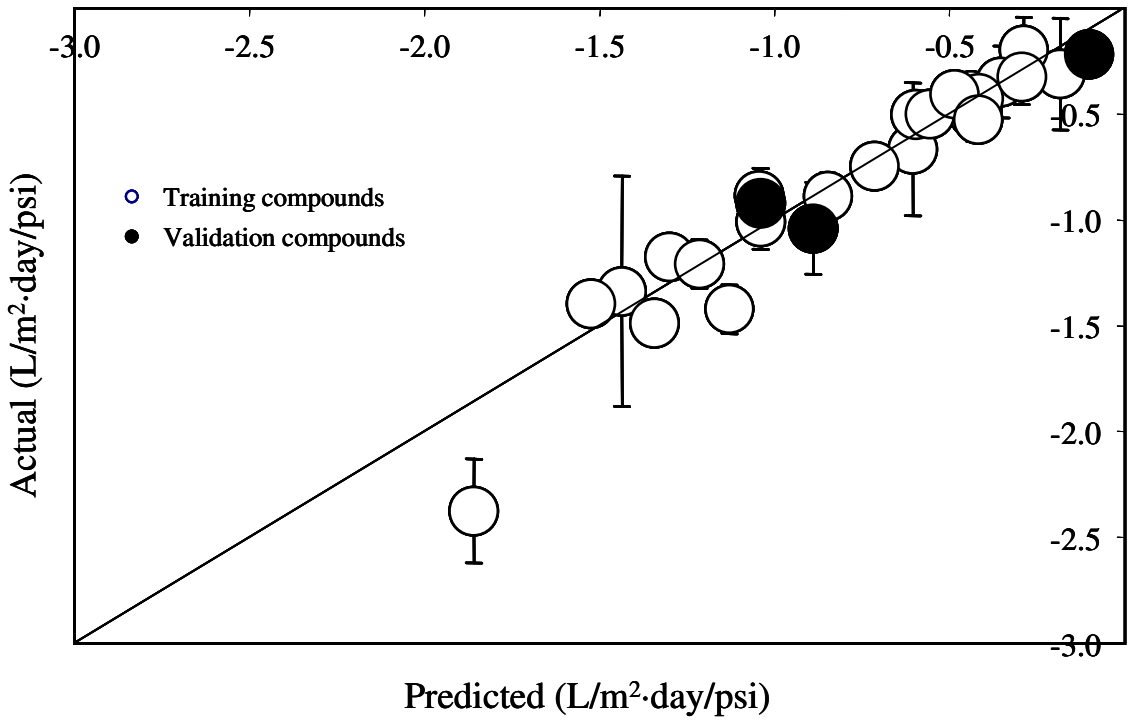

Model Statistics

	R	Avg. Abs.	RMS	Accuracy (20%)	Confidence Interval (95%)	Records
All	0.93	0.14	0.20	0.96	0.40	74
Train	0.93	0.13	0.19	0.96	0.38	51
Test	0.91	0.17	0.22	0.96	0.46	23

Sensitivity Index

MaxNeg	LD50	IC	nelem
-0.4795	-0.1138	-2.4014	0.4392

Figure 31. ANN Model results for change in specific water flux for PA-U (Trisep X-201) membrane after treatment with cleaning compounds

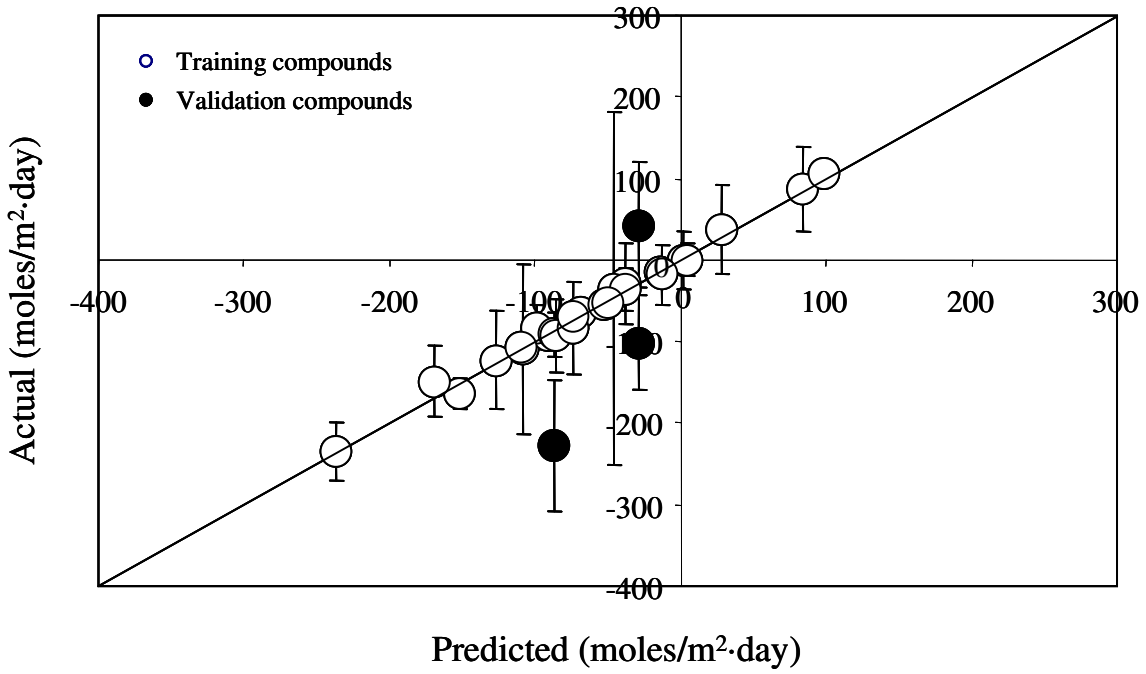

Model Statistics

	R	Avg. Abs.	RMS	Accuracy (20%)	Confidence Interval (95%)	Records
All	0.83	30.28	48.30	0.96	96	75
Train	0.80	31.48	52.09	0.95	104	60
Test	0.83	30.28	48.30	0.96	96	75

Sensitivity Index

xpc4	xvpc4	Dz	Qxx	Qyy	Hmax
-0.33	0.07	19.74	-14.12	-0.90	-0.27

Figure 32. ANN Model results for change in solute flux for PA-U (Trisep X-201) membrane after treatment with cleaning compounds

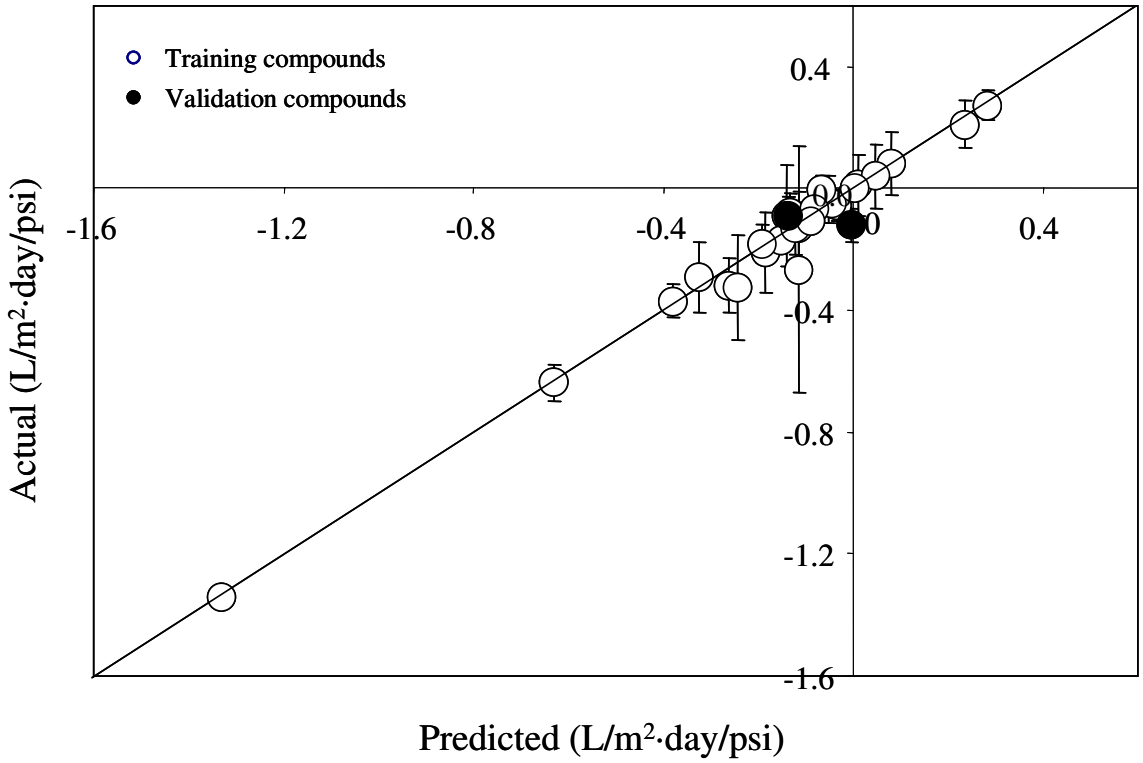

Model Statistics

	R	Avg. Abs.	RMS	Accuracy (20%)	Confidence Interval (95%)	Records
All	0.94	0.07	0.10	0.99	0.21	81
Train	0.94	0.06	0.11	0.98	0.21	64
Test	0.94	0.07	0.10	0.99	0.21	81

Sensitivity Index

xvc3	Py	Pz	Dx	Qyy	phia
-0.4530	0.0024	29.0442	-10.2415	-0.9572	0.4327

Figure 33. ANN Model results for change in specific water flux for a CA (GE Osmonics Desal CA) membrane after treatment with cleaning compounds

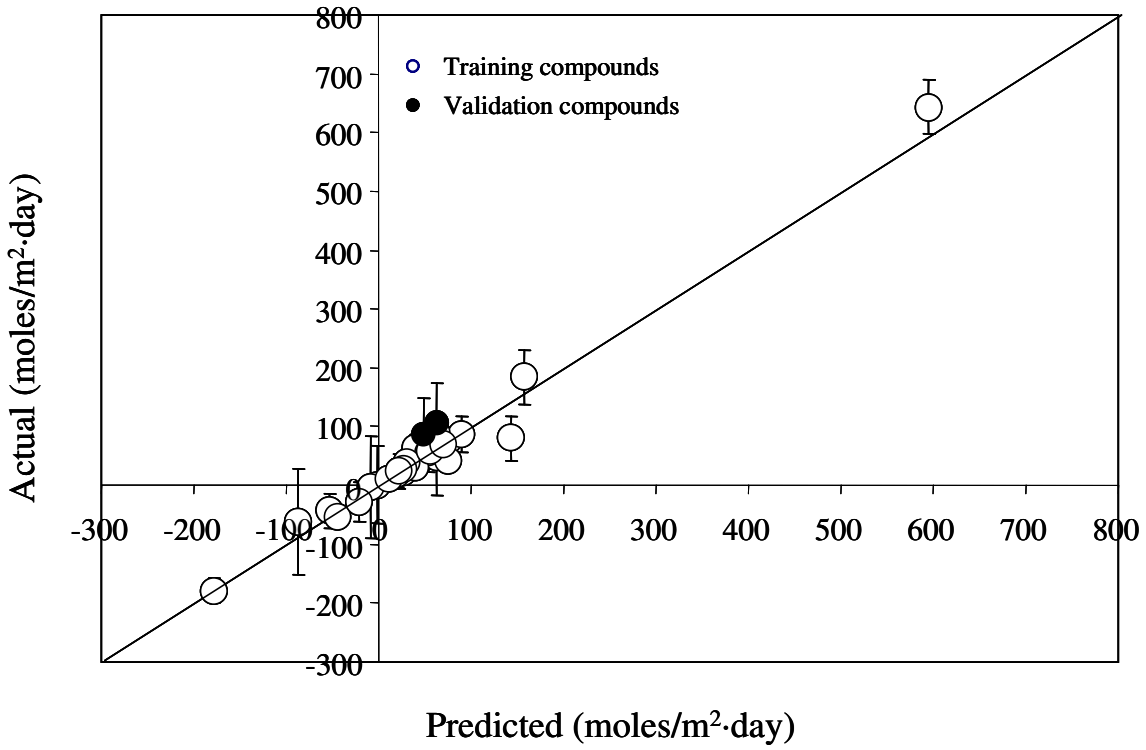

Model Statistics

	R	Avg. Abs.	RMS	Accuracy (20%)	Confidence Interval (95%)	Records
All	0.94	29.74	40.73	1.00	80.63	80
Train	0.96	26.17	36.77	1.00	73.14	64
Test	0.94	29.74	40.73	1.00	80.63	80

Sensitivity Index

nxc3	Dx	LogP	SdsCH	SdssC	Hmin	nelem	numHBa	SHHBd
-1.6797	-12.4020	2.5910	0.1291	21.4926	-11.0764	-0.1215	1.6945	12.4138

Figure 34. ANN Model results for change in solute flux for a CA (GE Osmonics Desal CA) membrane after treatment with cleaning compounds

Table 1. Master List of Chemical Cleaning Agents

Chemical Cleaning Agent	Chemical Cleaning Agent
Acetic acid	Nonyltrimethylammonium bromide
Benzalkonium chloride	Octadecanoic acid
Benzenesulfonic acid	Octadecyltrimethylammonium bromide
Biz Detergent	Octanesulfonic acid (Na+)
Butanesulfonic acid (Na+)	OCTglucopyranoside
Butyric acid	Octylbenzenesulfonic acid
Capric acid	Pentanesulfonic acid
Caproic acid	Peracetic acid
Cetylpyridinium chloride	Polyethyleneglycol (10) laurylether Genapol C-100
Citric acid	Polyethyleneglycol (8) dodecylether Genapol X-80
Decanesulfonic acid	Propionic acid
DECglucopyranoside	Protease
Decyltrimethylammonium bromide	Ptoluenesulfonic acid
Diamite BFT	Sodium Dodecylsulfate (SDS)
Dodecanesulfonic acid	STP
Dodecylbenzenesulfonic acid (DBSA)	STP + DBSA (2% STP, 0.2% DBSA)
Dodecyldimethylglycine (Empigen BB)	Tetrabutylammonium bromide
Dodecyltrimethylammonium bromide (DTAB)	Tetradecylammonium bromide
DODglucopyranoside	Tetradecyltrimethylammonium bromide
Endozime	Tetraethylammonium bromide (TEA)
Ethylenediaminetetraacetic acid (EDTA)	Tetraheptylammonium bromide
Formic acid	Tetrahexyldecylammonium bromide
Heptaglucopyranoside	Tetrahexylammonium bromide
Heptanesulfonic acid	Tetraoctylammonium bromide
Hexadecanesulfonic acid	Tetrapentylammonium bromide
Hexadecanoic acid	Triton X-100
Hexadecyltrimethylammonium bromide (CTAB)	Triton X-45
Hexanesulfonic acid	Tween 20
Hexaglucopyranoside	Tween 40
Hydrogen peroxide	Tween 60
Lauric acid	Tween 80
MEGA 8 Octanoyl-N-methylglucamide	Zosteric acid (Na+)
MEGA 9 Nonoyl-N-methylglucamide	Zwittergent 3-08
MEGA 10 Deconoyl-N-methylglucamide	Zwittergent 3-10
Minncare	Zwittergent 3-12
Nonanesulfonicacid	Zwittergent 3-14
Nonylglucopyranoside	Zwittergent 3-16

Table 2. Chemical Cleaning Agents[a]

Cationic Compounds (6)	**Chelating Compounds (3)**
Benzalkonium chloride	Citric acid
Cetylpyridinium chloride	Ethylenediaminetetraacetic acid (EDTA)
Tetraethylammonium bromide (TEA)	Sodium tripolyphosphate (STP)
Decyltrimethylammonium bromide (DMAB)	
Dodecyltrimethylammonium bromide (DTAB)	
Hexadecyltrimethylammonium bromide (CTAB)	
Anionic Compounds (7)	**Enzymatic Compounds (3)**
Benzenesulfonic acid	Endozime AW Triple Plus
Dodecylbenzenesulfonic acid (DBSA)	Biz Detergent
Butanesulfonic acid	Protease
Octanesulfonic acid	
Dodecanesulfonic acid	
Sodium Dodecylsulfate (SDS)	
Zosteric acid	
Zwitterionic Compounds (4)	**Oxidizing Compounds (4)**
Zwittergent 3-08	Diamite BFT (King Lee)
Zwittergent 3-12	Minncare (Minntech)
Zwittergent 3-16	Peracetic acid
Dodecyldimethylglycine (Empigen BB)	Hydrogen peroxide
Neutral / Polar Compounds (9)	**Combinations (1)**
Octanoyl-N-methylglucamide (Mega-8)	DBSA + STP (0.2% DBSA, 2% STP)
Deconoyl-N-methylglucamide (Mega-10)	
Triton X-45	
Triton X-100	
Tween 20	
Tween 80	
Nonylglucopyranoside	
Polyethyleneglycol (10) laurylether (Genapol C-100)	
Polyethyleneglycol (8) dodecylether (Genapol X-80)	

[a]-37 chemical cleaning agents

Table 3. Reverse Osmosis Membranes

Manufacturer	Model	Type
Dow FilmTec	BW-30	polyamide
Hydranautics	LFC3	polyamide
Hydranautics	ESPA2	polyamide
Koch Membrane Systems	TFC-HR	polyamide
Koch Membrane Systems	TFC-ULP	polyamide
Trisep Corporation	X-201	Polyamide-urea
Separation Systems Technology	TMC/MPD	polyamide
GE Osmonics	Desal	cellulose acetate

Table 4. Compound Molecular Descriptors

Charge/Polarity
3D Descriptors of Entire Molecule
ABS
Dipole
MaxHp
MaxNeg
MaxQp
Polarizability
3D Descriptors for CoMMA
P
Pz
P
Q
Dx
Dy
Dz
Qxx
Qyy
Atom Type E-State Descriptors
SsCH
SssCH
SaaCH
Sdss
Sd
SsC
Hydrogen Atom Type E-State Descriptors
SssO
Shother
Hmax
Gmax
Hmi
Gmi
Molecular Properties
Q
Qs

Hydrogen Bonding
Molecular Properties
numHBa
SHHb

Hydrophobicity
Log

Othe
LD50

Molecular Complexity
3D Descriptors of Entire Molecule
Ovality
Surfa
Chi Indices
x1
xp4
xc3
xpc4
xv1
xvp4
xvp7
xvp10
xvc3
xvpc4
xvch6
Subgraph Count Indices
nxp5
nxc3
nxch6
3D Descriptors for CoMMA
Ix
Iy
Total Topological Descriptors
W
P
sumdell
tets2
toto
Wt
nclass
Traditional Kappa Shape Indices
k0
k1
k2
k3
Information Indices
s
IC
R
idc
idcbar
Molecular Properties
fw
nelem
nrings
ncirc
phia
knot

Table 5. Chemical Cleaning Compounds for ANN Modeling

Chemical Cleaning Compounds
benzalkonium chloride
benzenesulfonic acid
butanesulfonic acid
cetylpyridiunium chloride
citric acid
deconoyl-N-methylglucamide (Mega 10)
decyltrimethylammonium bromide
dodecanesulfonic acid
dodecylbenzenesulfonic acid
dodecyldimethylglycine (Empigen BB)
dodecyltrimethylammonium bromide
EDTA
Genapol C-100
Genapol X-80
hexadecyltrimethylammonium bromide
nonylglucopyranoside
octanesulfonic acid
octanoyl-N-methylglucamide (Mega 8)
sodium dodecylsulfate
tetraethylammonium bromide
Triton X-100
Triton X-45
Tween 20
Tween 80
zosteric Acid
Zwittergent 3-08
Zwittergent 3-12
Zwittergent 3-16

[a]-Validation compounds in bold font.

Table 6. Thin-Film Composite PA Membrane Descriptors

Molecular Properties of TFD Polyamide RO Membranes
Hydrophobicity
Contact angle
Surface Topography
RMS roughness
Average roughness
Mean height
Median height
Peak height
Volume
Surface area
Projected area
Surface Charge
Zeta potential
Zeta potential slope
Chemical Structure
Carboxylate / amide I ratio
Carboxylate / amide II ratio
Amide II / 874 cm^{-1} ratio
Amide I / 874 cm^{-1} ratio
Hydroxyl / amide II ratio
Amide I / Amide II ratio

Table 7. RO Membrane Surface Topography as Determined by AFM

Membrane	RMS Roughness	Average Roughness	Mean Height	Median Height	Peak Height	Volume	Surface Area
BW-30	58.75 ± 0.64	45.9 ± 0.18	470 ± 6.2	464.4 ± 6.1	304.3 ± 14.9	46.66 ± 0.89	118.4 ± 1.7
LFC3	73.95 ± 8.31	57.33±4.11	413.6 ± 260.9	409.1 ± 263.4	355.4 ± 14.8	41.4 ± 26.1	134.7 ± 3.6
ESPA2	78.75 ± 4.15	62.6 ± 2.7	533.7 ± 132.2	527.8 ± 132	423.1 ± 85.8	53 ± 12.8	142.6 ± 3.1
HR	38.96 ± 1.29	30.9 ± 1.01	139.4 ± 36.4	134 ± 36.7	197.9 ± 9.5	13.94 ± 3.64	124.7 ± 1.31
ULP	52.57 ± 0.35	41.48 ± 0.56	486.8 ± 232.2	482.9 ± 234.6	243.1 ± 24.7	48.25 ± 22.7	122.7 ± 7.3
X-201	41.75 ± 3.31	32.53 ± 2.2	390 ± 210.4	385.1 ± 209.4	283.2 ± 51.2	38.4 ± 21.2	114.4 ± 3.4
TMC/MPD	9.87 ± 5.69	7.08 ± 3.51	106.2 ± 61.9	105.5 ± 61.6	90.97 ± 96.07	10.51 ± 6.19	99.05 ± 1.68
CA	11.0 ± 1.39	8.78 ± 1.26	129.3 ± 81.5	129.7 ± 81	43.45 ± 16.47	12.72 ± 7.97	98.9 ± 1.04

Mean ± standard deviation, n=2, 3

Table 8. Membrane Surface Charge as Determined by Streaming Potential

CA		FilmTec		ESPA2		LFC1		LFC3		HR		ULP		X-201	
pH	ζ (mV)	pH	ζ (mV)	pH	ζ (mV)	pH	ζ (mV)	pH	ζ (mV)	pH	ζ (mV)	pH	ζ (mV)	pH	ζ (mV)
3.60	-3.05	3.50	3.93	3.50	5.63	3.00	-4.91	3.70	5.65	3.00	4.98	3.50	-6.43	3.00	7.08
4.50	-17.23	4.50	-4.71	4.50	-11.12	4.10	-12.72	4.50	-6.86	3.50	-0.77	4.50	-12.48	4.50	-12.70
5.60	-21.45	5.60	-9.08	5.60	-19.03	5.60	-15.89	5.90	-17.31	4.40	-10.42	5.60	-16.27	5.60	-18.06
7.20	-22.44	7.00	-12.82	7.00	-26.03	7.00	-17.33	7.30	-20.81	5.60	-13.86	7.00	-18.26	7.10	-23.67
9.00	-22.95	9.00	-13.16	9.00	-26.83	9.00	-18.05	9.00	-23.19	7.10	-16.27	9.00	-19.18	9.00	-24.06
										9.03	-16.78				

Table 9. Zeta Potential Slope[a]

Membrane	Zeta Potential Slope
Hydranautics ESPA2	-5.9210
Hydranuatics LFC3	-4.8360
Trisep X-201	-4.1911
FilmTec BW-30	-3.2185
Koch TFC-ULP	-2.2723
Koch TFC-HR	-2.1437
GE Osmonics / Desal CA	-1.8348

[a]-Slope measured between pH 4.5 and ~7

Table 10. Summary of Membrane Properties Used for ANN Models

Membrane Properties	CA	TMC/MPD	BW-30	LFC3	TFC-HR	TFC-ULP	ESPA2	X-201
Contact Angle (degrees)	64.03	61.64	61.42	61.35	61.15	61.27	60.63	61.13
Zeta Potential (mV)[a]	-21.45	NA	-9.08	-17.31	-13.86	-16.27	-19.03	-18.06
Zeta Potential Slope[b]	-1.83	NA	-3.22	-4.84	-2.14	-2.27	-5.92	-4.19
RMS Roughness	11.0	9.87	58.75	73.95	38.96	52.57	78.75	41.75
Ave Roughness	8.78	7.08	45.9	57.33	30.9	41.48	62.6	32.53
Mean Height	129.3	106.2	470	413.6	139.4	486.8	533.7	390
Median Height	129.7	105.5	464.4	109.1	134	482.9	527.8	385.1
Peak Height	43.45	90.97	304.3	355.4	197.9	243.1	355.4	283.2
Volume	12.72	10.51	46.66	41.4	13.94	48.25	53	38.25
Surface Area	98.9	99.05	118.4	134.7	124.7	122.7	142.6	114.4
Projected Area	---	---	---	---	---	---	---	---
COO/Amide I Ratio	NA	NA	0.545	.515	.173	0.168	0.274	0.330
COO/Amide II Ratio	NA	NA	0.547	.538	.186	0.177	0.254	0.199
Amide I/Amide II Ratio	NA	NA	1.0	1.039	1.073	1.059	0.927	0.605
OH/Amide I Ratio	NA	NA	2.156	1.357	.737	0.724	0.487	0.551
Amide I / 874 cm^{-1} Ratio[a]	NA	NA	1.375	1.638	.864	1.059	1.584	1.241
Amide II / 874 cm^{-1} Ratio[a]	NA	NA	1.379	1.582	.804	1.0	1.710	2.052

[a]-pH 5.6
[b]-slope between pH 4.5 and ~7

Table 11. Average Change in Specific Water Flux (L/m^2·day/psi) for FilmTec BW-30 RO Membrane After 1 Hr Exposure to Cleaning Agent.

					Ranking by solute flux	
Cleaning Agent	Class	Avg	SDEV	N	Water	Solute
Empigen BB	zwit	1.02	0.08	3	1	3
Diamite BFT	oxidizing	0.22	0.05	3	2	1
Protease	enzymatic	0.09	0.10	3	3	5
CTAB	cationic	0.01	0.55	3	4	13
Triton X-100	nonionic	-0.02	0.09	3	5	19
DecyltrimethylammBr	cationic	-0.05	0.05	2	6	6
Citric acid	chelating	-0.06	0.92	3	7	15
Tween 80	nonionic	-0.07	0.09	3	8	25
STP	chelating	-0.12	0.54	6	9	27
Hydrogen Peroxide	oxidizing	-0.13	0.11	3	10	21
Minncare	oxidizing	-0.15	0.46	3	11	29
Zwittergent 3-8	zwit	-0.16	0.09	3	12	9
Peracetic acid	oxidizing	-0.17	0.08	3	13	26
Mega 8	nonionic	-0.21	0.15	3	14	11
EDTA	enzymatic	-0.21	0.17	3	15	20
Zwittergent 3-16	zwit	-0.24	0.27	3	16	4
Biz detergent	enzymatic	-0.25	0.11	3	17	8
Mega 10	nonionic	-0.28	0.22	3	18	14
Butanesulfonic acid	anionic	-0.35	0.08	3	19	17
DBSA	anionic	-0.36	0.34	6	20	31
Dodecanesulfonic acid	anionic	-0.36	0.02	2	21	10
SDS	anionic	-0.36	0.06	3	22	23
Benzenesulfonic acid	anionic	-0.37	0.12	5	23	12
DTAB	cationic	-0.38	0.13	6	24	2
Octanesulfonic acid	anionic	-0.38	0.04	3	25	28
DBSA + STP	anion-chelatg	-0.41	0.18	3	26	34
Endozime	enzymatic	-0.50	0.11	3	27	16
Triton X-45	nonionic	-0.51	0.09	3	28	24
Tween 20	nonionic	-0.53	0.20	3	29	33
Nonylglucopyranoside	nonionic	-0.65	0.17	3	30	22
TEA	cationic	-0.67	0.19	3	31	7
Zosteric acid	anionic	-0.71	0.44	3	32	30
Zwittergent 3-12	zwit	-0.94	0.08	3	33	32
Benzalkonium Cl	cationic	-1.50	0.65	3	34	37
Cetylpyridinium Cl	cationic	-2.69	0.08	3	35	35
Genapol X80	nonionic	-3.26	0.18	3	36	36
Genapol C-100	nonionic	-3.34	0.25	3	37	18
Avg of all 37 Cleaning Agents:		**-0.51**				

Table 12. Average Change in Specific Water Flux (L/m^2·day/psi) for Hyrdanautics LFC3 RO Membrane After 1 Hr Exposure to Cleaning Agent.

					Ranking by flux change	
Cleaning Agent	Class	Avg	SDEV	N	Water	Solute
Diamite BFT	oxidizing	1.33	0.16	3	1	1
DBSA + STP	anion-chelatg	1.11	0.27	3	2	14
SDS	anionic	0.50	0.49	3	3	10
Hydrogen Peroxide	oxidizing	0.43	0.85	3	4	15
Dodecanesulfonic acid	anionic	0.36	0.61	3	5	4
Octanesulfonic acid	anionic	0.33	0.27	3	6	13
STP	chelating	0.30	0.21	5	7	9
Biz detergent	enzymatic	0.22	0.11	3	8	5
Minncare	oxidizing	0.13	0.37	3	9	8
Peracetic acid	oxidizing	0.09	0.14	3	10	7
DBSA	anionic	0.08	0.16	3	11	11
Citric acid	chelating	0.08	0.59	3	12	29
Benzenesulfonic acid	anionic	0.06	0.51	3	13	22
Zwittergent 3-12	zwit	0.02	0.98	3	14	24
Protease	enzymatic	-0.01	0.10	3	15	21
Triton X-45	nonionic	-0.11	0.63	3	16	3
TEA	cationic	-0.16	0.27	3	17	23
Zwittergent 3-8	zwit	-0.31	0.11	3	18	18
Zosteric acid	anionic	-0.37	0.21	3	19	32
EDTA	enzymatic	-0.40	0.23	3	20	27
Butanesulfonic acid	anionic	-0.44	0.03	3	21	25
Mega 8	nonionic	-0.46	0.60	3	22	6
Nonylglucopyranoside	nonionic	-0.48	0.23	3	23	28
Tween 80	nonionic	-0.62	0.27	3	24	16
Zwittergent 3-16	zwit	-0.73	0.09	3	25	20
Endozime	enzymatic	-0.74	0.20	3	26	31
Empigen BB	zwit	-0.85	0.15	3	27	2
Tween 20	nonionic	-0.85	0.27	3	28	30
Genapol X80	nonionic	-0.87	0.18	3	29	26
Triton X-100	nonionic	-0.95	0.03	3	30	36
DecyltrimethylammBr	cationic	-1.04	0.26	3	31	19
Mega 10	nonionic	-1.12	0.28	3	32	33
Genapol C-100	nonionic	-1.42	0.03	3	33	35
DTAB	cationic	-1.58	0.07	2	34	34
Benzalkonium Cl	cationic	-1.74	1.45	3	35	17
CTAB	cationic	-1.99	0.04	3	36	37
Cetylpyridinium Cl	cationic	-3.02	0.30	3	37	12
Avg of all 37 Cleaning Agents:		**-.041**				

Table 13. Average Change in Specific Water Flux (L/m^2·day/psi) for Hyrdanautics ESPA2 RO Membrane After 1 Hr Exposure to Cleaning Agent.

					Ranking by flux change	
Cleaning Agent	**Class**	Avg	SDEV	N	Water	Solute
Diamite BFT	oxidizing	1.71	0.27	3	1	2
DBSA + STP	anion-chelatg	1.49	0.04	3	2	1
STP	chelating	0.80	1.16	6	3	23
Endozime	enzymatic	0.37	0.09	3	4	3
Biz detergent	enzymatic	0.05	0.05	3	5	28
DBSA	anionic	0.02	0.25	2	6	12
CTAB	cationic	0.01	0.55	3	7	9
Triton X-100	nonionic	-0.02	0.09	3	8	7
DecyltrimethylammBr	cationic	-0.05	0.05	2	9	4
Tween 80	nonionic	-0.07	0.09	3	10	19
Zwittergent 3-8	zwit	-0.16	0.09	3	11	10
Hydrogen Peroxide	oxidizing	-0.18	0.26	3	12	30
Mega 8	nonionic	-0.21	0.15	3	13	32
EDTA	enzymatic	-0.21	0.17	3	14	18
Protease	enzymatic	-0.23	0.09	3	15	20
Zwittergent 3-16	zwit	-0.24	0.27	3	16	26
Butanesulfonic acid	anionic	-0.35	0.02	3	17	5
Dodecanesulfonic acid	anionic	-0.36	0.02	2	18	6
Citric acid	chelating	-0.36	0.20	3	19	21
SDS	anionic	-0.36	0.06	3	20	29
DTAB	cationic	-0.38	0.13	6	21	16
Octanesulfonic acid	anionic	-0.38	0.04	3	22	22
Triton X-45	nonionic	-0.51	0.09	3	23	15
Tween 20	nonionic	-0.53	0.20	3	24	27
Benzenesulfonic acid	anionic	-0.57	0.24	6	25	17
TEA	cationic	-0.67	0.19	3	26	14
Zosteric acid	anionic	-0.71	0.44	3	27	35
Zwittergent 3-12	zwit	-0.94	0.08	3	28	11
Minncare	oxidizing	-1.11	0.17	3	29	31
Mega 10	nonionic	-1.17	0.13	3	30	25
Cetylpyridinium Cl	cationic	-1.29	0.54	3	31	36
Peracetic acid	oxidizing	-1.39	11.10	3	32	34
Nonylglucopyranoside	nonionic	-1.56	0.22	3	33	33
Empigen BB	zwit	-1.71	0.29	3	34	24
Genapol C-100	nonionic	-2.21	0.31	3	35	13
Genapol X80	nonionic	-3.26	0.18	3	36	8
Benzalkonium Cl	cationic	-5.67	0.18	3	37	37
Avg of all 37 Cleaning Agents:		**-0.61**				

Table 14. Average Change in Specific Water Flux (L/m^2·day/psi) for Koch TFC-HR RO Membrane After 1 Hr Exposure to Cleaning Agent.

					Ranking by flux change	
Cleaning Agent	Class	Avg	SDEV	N	Water	Solute
Diamite BFT	oxidizing	2.14	0.12	3	1	1
DBSA + STP	anion-chelatg	0.34	0.12	3	2	14
Minncare	oxidizing	0.02	0.08	3	3	4
Dodecanesulfonic acid	anionic	-0.01	0.09	3	4	3
Protease	enzymatic	-0.20	0.06	3	5	18
SDS	anionic	-0.22	0.11	3	6	16
Hydrogen Peroxide	oxidizing	-0.34	0.08	3	7	28
Zwittergent 3-12	zwit	-0.67	0.14	3	8	5
Peracetic acid	oxidizing	-0.77	0.08	3	9	15
Zwittergent 3-8	zwit	-0.78	0.05	3	10	31
Octanesulfonic acid	anionic	-0.87	0.05	3	11	24
Triton X-100	nonionic	-0.89	0.13	3	12	9
DTAB	cationic	-0.90	0.25	3	13	2
Biz detergent	enzymatic	-0.96	0.10	3	14	7
TEA	cationic	-1.05	0.27	3	15	13
CTAB	cationic	-1.05	0.31	3	16	11
DBSA	anionic	-1.09	0.19	3	17	34
STP	chelating	-1.16	0.11	3	18	33
DecyltrimethylammBr	cationic	-1.18	0.13	3	19	12
Zwittergent 3-16	zwit	-1.21	0.29	3	20	21
EDTA	enzymatic	-1.29	0.34	3	21	10
Benzenesulfonic acid	anionic	-1.30	0.18	6	22	20
Zosteric acid	anionic	-1.36	0.08	3	23	36
Empigen BB	zwit	-1.44	0.17	3	24	29
Mega 10	nonionic	-1.46	0.10	3	25	26
Tween 80	nonionic	-1.58	0.41	3	26	22
Nonylglucopyranoside	nonionic	-1.58	0.19	3	27	17
Mega 8	nonionic	-1.63	0.11	3	28	32
Citric acid	chelating	-1.70	0.17	3	29	30
Endozime	enzymatic	-1.73	0.08	3	30	6
Butanesulfonic acid	anionic	-1.77	0.22	3	31	23
Triton X-45	nonionic	-1.89	0.27	3	32	8
Genapol X80	nonionic	-1.95	0.69	6	33	19
Tween 20	nonionic	-2.21	0.24	3	34	27
Genapol C-100	nonionic	-3.18	0.23	3	35	35
Cetylpyridinium Cl	cationic	-4.33	0.52	6	36	25
Benzalkonium Cl	cationic	-5.29	0.46	3	37	37
Avg of all 37 Cleaning Agents:		**-1.26**				

Table 15. Average Change in Specific Water Flux (L/m^2·day/psi) for Koch TFC-ULP RO Membrane After 1 Hr Exposure to Cleaning Agent.

					Ranking by flux change	
Cleaning Agent	Class	Avg	SDEV	N	Water	Solute
Diamite BFT	oxidizing	4.46	0.29	3	1	1
DBSA + STP	anion-chelatg	1.84	0.23	3	2	5
Protease	enzymatic	0.86	0.08	3	3	4
SDS	anionic	-0.31	0.09	3	4	25
Zosteric acid	anionic	-0.41	0.36	3	5	26
Biz detergent	enzymatic	-0.42	0.20	3	6	10
DBSA	nonionic	-0.45	0.34	9	7	18
Dodecanesulfonic acid	anionic	-0.57	0.20	3	8	22
Minncare	oxidizing	-0.59	0.52	3	9	7
Peracetic acid	oxidizing	-0.61	0.03	3	10	2
TEA	cationic	-0.64	0.37	3	11	19
STP	chelating	-0.78	0.67	9	12	6
DecyltrimethylammBr	cationic	-0.78	0.18	3	13	11
Butanesulfonic acid	anionic	-0.86	0.41	3	14	9
Hydrogen Peroxide	oxidizing	-0.93	0.06	3	15	16
Octanesulfonic acid	anionic	-0.96	0.18	3	16	15
Zwittergent 3-12	zwit	-1.06	0.15	3	17	3
Citric acid	chelating	-1.28	0.17	3	18	30
Triton X-45	nonionic	-1.44	0.31	3	19	23
Zwittergent 3-8	zwit	-1.58	0.28	3	20	34
Zwittergent 3-16	zwit	-1.72	0.49	3	21	36
EDTA	enzymatic	-1.97	0.05	3	22	29
Nonylglucopyranoside	nonionic	-2.10	0.17	3	23	8
Triton X-100	nonionic	-2.30	0.10	3	24	13
Genapol X80	nonionic	-2.35	0.13	3	25	27
Mega 10	nonionic	-2.58	0.10	3	26	32
DTAB	cationic	-2.94	0.30	3	27	17
Tween 20	nonionic	-2.98	0.28	3	28	31
Genapol C-100	nonionic	-3.09	0.09	3	29	21
Empigen BB	zwit	-3.35	0.76	3	30	35
Cetylpyridinium Cl	cationic	-3.72	0.64	3	31	12
Mega 8	nonionic	-3.85	0.34	3	32	24
Benzenesulfonic acid	anionic	-3.93	0.22	3	33	14
CTAB	cationic	-4.40	0.34	3	34	37
Tween 80	nonionic	-4.40	0.31	3	35	20
Benzalkonium Cl	cationic	-4.60	0.42	6	36	33
Endozime	enzymatic	-4.82	1.05	3	37	28
Avg of all 37 Cleaning Agents:		**-1.67**				

Table 16. Average Change in Specific Water Flux (L/m^2·day/psi) for Trisep X-201 RO Membrane After 1 Hr Exposure to Cleaning Agent.

					Ranking by flux change	
Cleaning Agent	Class	Avg	SDEV	N	Water	Solute
Diamite BFT	oxidizing	0.61	0.11	3	1	1
STP	chelating	0.03	0.12	6	2	2
Protease	enzymatic	-0.07	0.04	3	3	17
Hydrogen Peroxide	oxidizing	-0.10	0.07	3	4	5
Minncare	oxidizing	-0.14	0.06	3	5	3
Biz detergent	enzymatic	-0.17	0.10	3	6	34
DBSA + STP	anion-chelatg	-0.21	0.08	3	7	9
Octanesulfonic acid	anionic	-0.22	0.03	3	8	14
Peracetic acid	oxidizing	-0.25	0.18	3	9	8
Benzenesulfonic acid	anionic	-0.31	0.26	3	10	16
Zosteric acid	anionic	-0.32	0.13	3	11	12
Mega 8	nonionic	-0.35	0.17	3	12	32
TEA	cationic	-0.41	0.04	3	13	24
Empigen BB	zwit	-0.41	0.10	3	14	7
SDS	anionic	-0.43	0.03	3	15	4
Citric acid	chelating	-0.45	0.08	3	16	28
Butanesulfonic acid	anionic	-0.48	0.01	3	17	22
Nonylglucopyranoside	nonionic	-0.50	0.08	3	18	23
DBSA	anionic	-0.50	0.13	3	19	21
EDTA	enzymatic	-0.50	0.07	3	20	13
Triton X-45	nonionic	-0.52	0.01	3	21	31
Endozime	enzymatic	-0.62	0.14	3	22	33
Mega 10	nonionic	-0.67	0.31	3	23	6
Zwittergent 3-8	zwit	-0.75	0.02	3	24	36
Tween 80	nonionic	-0.88	0.10	3	25	18
DecyltrimethylammBr	cationic	-0.89	0.11	3	26	11
DTAB	cationic	-0.92	0.17	3	27	15
Zwittergent 3-16	zwit	-1.01	0.13	3	28	20
Dodecanesulfonic acid	anionic	-1.01	0.13	3	29	10
Zwittergent 3-12	zwit	-1.04	0.22	3	30	27
Genapol X80	nonionic	-1.18	0.05	3	31	26
Triton X-100	nonionic	-1.21	0.12	3	32	35
Cetylpyridinium Cl	cationic	-1.34	0.54	3	33	19
CTAB	cationic	-1.40	0.08	3	34	25
Tween 20	nonionic	-1.42	0.12	3	35	37
Genapol C-100	nonionic	-1.49	0.06	3	36	29
Benzalkonium Cl	cationic	-2.38	0.25	3	37	30
Avg of all 37 Cleaning Agents:		**-0.65**				

Table 17. Average Change in Specific Water Flux (L/m^2·day/psi) for GE Osmonics Desal CA RO Membrane After 1 Hr Exposure to Cleaning Agent.

					Ranking by flux change	
Cleaning Agent	Class	Avg	SDEV	N	Water	Solute
Diamite BFT	oxidizing	5.12	-	-	1	1
Protease	enzymatic	0.57	0.11	3	2	5
SDS	anionic	0.28	0.05	3	3	7
STP	chelating	0.27	0.23	6	4	22
Tween 20	nonionic	0.21	0.08	3	5	25
Biz detergent	enzymatic	0.15	0.06	3	6	3
Mega 8	nonionic	0.08	0.10	3	7	10
TEA	cationic	0.04	0.10	3	8	16
Hydrogen Peroxide	oxidizing	0.03	0.09	3	9	17
Butanesulfonic acid	anionic	0.01	0.10	3	10	15
Tween 80	nonionic	0.00	0.02	3	11	14
DBSA + STP	anion-chelatg	-0.003	0.02	3	12	36
Minncare	oxidizing	-0.02	0.08	3	13	9
Mega 10	nonionic	-0.03	0.08	3	14	21
EDTA	enzymatic	-0.05	0.02	3	15	13
Cetylpyridinium Cl	cationic	-0.05	0.05	3	16	19
Nonylglucopyranoside	nonionic	-0.07	0.01	3	17	4
Benzenesulfonic acid	anionic	-0.08	0.06	3	18	27
Zwittergent 3-12	zwit	-0.09	0.06	3	19	6
DecyltrimethylammBr	cationic	-0.09	0.17	3	20	18
Peracetic acid	oxidizing	-0.09	0.04	3	21	12
Triton X-100	nonionic	-0.11	0.03	3	22	29
Octanesulfonic acid	anionic	-0.12	0.06	3	23	11
Genapol C-100	nonionic	-0.13	0.09	3	24	8
Dodecanesulfonic acid	anionic	-0.13	0.12	3	25	23
Endozime	enzymatic	-0.15	0.09	3	26	24
DBSA	anionic	-0.17	0.03	2	27	28
DTAB	cationic	-0.17	0.03	2	28	2
Zwittergent 3-8	zwit	-0.18	0.06	3	29	26
Citric acid	chelating	-0.21	0.13	3	30	30
CTAB	cationic	-0.27	0.41	3	31	20
Zwittergent 3-16	zwit	-0.29	0.11	3	32	32
Benzalkonium Cl	cationic	-0.32	0.09	5	33	35
Genapol X80	nonionic	-0.33	0.17	3	34	31
Zosteric acid	anionic	-0.37	0.05	3	35	34
Triton X-45	nonionic	-0.64	0.06	3	36	33
Empigen BB	zwit	-1.34	0.03	3	37	37
Avg of all 37 cleaning compounds:		**0.03**				
Avg without BFT:		**-0.11**				

Table 18. Average Change in Solute Flux (moles/m^2·day) for FilmTec BW-30 RO Membrane After 1 Hr Exposure to Cleaning Agent.

					Ranking by flux change	
Compound	Class	Avg	SDEV	N	Solute	Water
Empigen BB	zwitterionic	48	11	3	3	1
Diamite BFT	oxidizing	no data	-	3	1	2
Protease	enzymatic	-5.7	39	3	5	3
CTAB	cationic	-41	50	3	13	4
Triton X-100	nonionic	-102	40	3	19	5
DecyltrimethylammBr	cationic	-16	70	2	6	6
Citric acid	chelating	-49	126	3	15	7
Tween 80	nonionic	-170	24	3	25	8
STP	chelating	-171	178	6	27	9
Hydrogen Peroxide	oxidizing	-110	14	3	21	10
Minncare	oxidizing	-182	90	3	29	11
Zwittergent 3-8	zwitterionic	-28	71	3	9	12
Peracetic acid	oxidizing	-170	57	3	26	13
Mega 8	nonionic	-31	11	3	11	14
EDTA	enzymatic	-103	33	3	20	15
Zwittergent 3-16	zwitterionic	0.3	56	3	4	16
Biz detergent	enzymatic	-18	11	3	8	17
Mega 10	nonionic	-47	24	3	14	18
Butanesulfonic acid	anionic	-74	53	3	17	19
DBSA	anionic	-202	49	6	31	20
Dodecanesulfonic acid	anionic	-31	30	2	10	21
SDS	anionic	-151	13	3	23	22
Benzenesulfonic acid	anionic	-38	39	5	12	23
DTAB	cationic	175	86	6	2	24
Octanesulfonic acid	anionic	-182	11	3	28	25
DBSA + STP	anion-cheltg	-290	59	3	34	26
Endozime	enzymatic	-68	6.2	3	16	27
Triton X-45	nonionic	-163	7	3	24	28
Tween 20	nonionic	-275	57	3	33	29
Nonylglucopyranoside	nonionic	-112	47	3	22	30
TEA	cationic	-17	37	3	7	31
Zosteric acid	anionic	-183	94	3	30	32
Zwittergent 3-12	zwitterionic	-215	26	3	32	33
Benzalkonium Cl	cationic	-407	106	3	37	34
Cetylpyridinium Cl	cationic	-338	26	3	35	35
Genapol X80	nonionic	-359	4	3	36	36
Genapol C-100	nonionic	-86	47	3	18	37
Avg of 36 compounds (without BFT):		**-117**				

Table 19. Average Change in Solute Flux (moles/m^2·day) for Hydranautics LFC3 RO Membrane After 1 Hr Exposure to Cleaning Agent.

					Ranking by flux change	
Compound	Class	Avg	SDEV	N	Solute	Water
Diamite BFT	oxidizing	1509	599	3	1	1
DBSA + STP	anion-cheltg	57	25	3	14	2
SDS	anionic	87	25	3	10	3
Hydrogen Peroxide	oxidizing	54	46	3	15	4
Dodecanesulfonic acid	anionic	161	275	3	4	5
Octanesulfonic acid	anionic	59	86	3	13	6
STP	chelating	88	148	5	9	7
Biz detergent	enzymatic	140	161	3	5	8
Minncare	oxidizing	92	50	3	8	9
Peracetic acid	oxidizing	92	14	3	7	10
DBSA	anionic	86	133	3	11	11
Citric acid	chelating	-13	3.1	3	29	12
Benzenesulfonic acid	anionic	8	25	3	22	13
Zwittergent 3-12	zwitterionic	6	36	3	24	14
Protease	enzymatic	8.9	14	3	21	15
Triton X-45	nonionic	206	326	3	3	16
TEA	cationic	8	8	3	23	17
Zwittergent 3-8	zwitterionic	26	21	3	18	18
Zosteric acid	anionic	-25	18	3	32	19
EDTA	enzymatic	-10	6	3	27	20
Butanesulfonic acid	anionic	-2	26	3	25	21
Mega 8	nonionic	133	178	3	6	22
Nonylglucopyranoside	nonionic	-13	7.6	3	28	23
Tween 80	nonionic	42	68	3	16	24
Zwittergent 3-16	zwitterionic	12	10	3	20	25
Endozime	enzymatic	-17	14	3	31	26
Empigen BB	zwitterionic	356	340	3	2	27
Tween 20	nonionic	-15	6.0	3	30	28
Genapol X80	nonionic	-4	7	3	26	29
Triton X-100	nonionic	-61	11	3	36	30
DecyltrimethylammBr	cationic	19	13	3	19	31
Mega 10	nonionic	-35	54	3	33	32
Genapol C-100	nonionic	-43	39	3	35	33
DTAB	cationic	-39	10	2	34	34
Benzalkonium Cl	cationic	37	142	3	17	35
CTAB	cationic	-77	12	3	37	36
Cetylpyridinium Cl	cationic	62	100	3	12	37
Avg of all 37 compounds:		**81**				

Table 20. Average Change in Solute Flux (moles/m^2·day) for Hydranautics ESPA2 RO Membrane After 1 Hr Exposure to Cleaning Agent.

					Ranking by flux change	
Compound	Class	Avg	SDEV	N	Solute	Water
Diamite BFT	oxidizing	266	48	3	2	1
DBSA + STP	anion-cheltg	351	391	3	1	2
STP	chelating	-20	20	6	23	3
Endozime	enzymatic	154	24	2	3	4
Biz detergent	enzymatic	-55	16	3	28	5
DBSA	anionic	46	35	2	12	6
CTAB	cationic	52	52	3	9	7
Triton X-100	nonionic	60	9	3	7	8
Decyltrimethylamm Br	cationic	153	151	5	4	9
Tween 80	nonionic	14	10	3	19	10
Zwittergent 3-8	zwitterionic	52	52	3	10	11
Hydrogen Peroxide	oxidizing	-58	13	3	30	12
Mega 8	nonionic	-139	48	3	32	13
EDTA	enzymatic	14	10	3	18	14
Protease	enzymatic	13	4.1	3	20	15
Zwittergent 3-16	zwitterionic	-36	110	3	26	16
Butanesulfonic acid	anionic	93	26	3	5	17
Dodecanesulfonic acid	anionic	69	10	3	6	18
Citric acid	chelating	5	18	3	21	19
SDS	anionic	-57	10	3	29	20
DTAB	cationic	27	47	3	16	21
Octanesulfonic acid	anionic	-12	26	3	22	22
Triton X-45	nonionic	36	35	3	15	23
Tween 20	nonionic	-45	95	3	27	24
Benzenesulfonic acid	anionic	15	113	6	17	25
TEA	cationic	37	7	3	14	26
Zosteric acid	anionic	-303	65	3	35	27
Zwittergent 3-12	zwitterionic	48	15	3	11	28
Minncare	oxidizing	-134	17	3	31	29
Mega 10	nonionic	-34	31	3	25	30
Cetylpyridinium Cl	cationic	-341	100	3	36	31
Peracetic acid	oxidizing	-222	11	3	34	32
Nonylglucopyranoside	nonionic	-175	19	3	33	33
Empigen BB	zwitterionic	-29	28	3	24	34
Genapol C-100	nonionic	43	47	3	13	35
Genapol X80	nonionic	53	72	6	8	36
Benzalkonium Cl	cationic	-385	63	3	37	37
Avg of all 37 compounds:		**-12**				

Table 21. Average Change in Solute Flux (moles/m^2·day) for Koch TFC-HR RO Membrane After 1 Hr Exposure to Cleaning Agent.

					Ranking by flux change	
Compound	Class	Avg	SDEV	N	Solute	Water
Diamite BFT	oxidizing	320	49	3	1	1
DBSA + STP	anion-cheltg	-6	33	3	14	2
Minncare	oxidizing	60	25	3	4	3
Dodecanesulfonic acid	anionic	67	22	3	3	4
Protease	enzymatic	-10	8.9	3	18	5
SDS	anionic	-7	36	3	16	6
Hydrogen Peroxide	oxidizing	-34	24	3	28	7
Zwittergent 3-12	zwitterionic	49	14	3	5	8
Peracetic acid	oxidizing	-6.5	4.0	3	15	9
Zwittergent 3-8	zwitterionic	-46	13	3	31	10
Octanesulfonic acid	anionic	-24	25	3	24	11
Triton X-100	nonionic	3	11	3	9	12
DTAB	cationic	119	5.2	3	2	13
Biz detergent	enzymatic	32	44	3	7	14
TEA	cationic	-4	12	3	13	15
CTAB	cationic	-3	6.6	3	11	16
DBSA	anionic	-69	56	3	34	17
STP	chelating	-58	23	3	33	18
DecyltrimethylammBr	cationic	-4	2	3	12	19
Zwittergent 3-16	zwitterionic	-21	42	3	21	20
EDTA	enzymatic	-1	44	3	10	21
Benzenesulfonic acid	anionic	-17	22	6	20	22
Zosteric acid	anionic	-129	40	3	36	23
Empigen BB	zwitterionic	-42	8.4	3	29	24
Mega 10	nonionic	-31	22	3	26	25
Tween 80	nonionic	-23	7	3	22	26
Nonylglucopyranoside	nonionic	-8	76	3	17	27
Mega 8	nonionic	-49	62	3	32	28
Citric acid	chelating	-44	21	3	30	29
Endozime	enzymatic	48	28	3	6	30
Butanesulfonic acid	anionic	-24	8.8	3	23	31
Triton X-45	nonionic	13	4.0	3	8	32
Genapol X80	nonionic	-15	25	6	19	33
Tween 20	nonionic	-31	1.0	3	27	34
Genapol C-100	nonionic	-74	10	3	35	35
Cetylpyridinium Cl	cationic	-30	12	6	25	36
Benzalkonium Cl	cationic	-254	84	3	37	37
Avg of all 37 compounds:		**-10**				

Table 22. Average Change in Solute Flux (moles/m^2·day) for Koch TFC-ULP RO Membrane After 1 Hr Exposure to Cleaning Agent.

					Ranking by flux change	
Compound	Class	Avg	SDEV	N	Solute	Water
Diamite BFT	oxidizing	565	32	3	1	1
DBSA + STP	anion-cheltg	34	17	3	5	2
Protease	enzymatic	37	2.0	3	4	3
SDS	anionic	-106	30	3	25	4
Zosteric acid	anionic	-130	17	3	26	5
Biz detergent	enzymatic	-25	15	3	10	6
DBSA	anionic	-38	22	9	18	7
Dodecanesulfonic acid	anionic	-80	10	3	22	8
Minncare	oxidizing	-7.6	1.7	3	7	9
Peracetic acid	oxidizing	57	84	3	2	10
TEA	cationic	-54	24	3	19	11
STP	chelating	19	9.2	9	6	12
DecyltrimethylammBr	cationic	-25	22	3	11	13
Butanesulfonic acid	anionic	-24	4	3	9	14
Hydrogen Peroxide	oxidizing	-30	18	3	16	15
Octanesulfonic acid	anionic	-29	5	3	15	16
Zwittergent 3-12	zwitterionic	48	19	3	3	17
Citric acid	chelating	-147	26	3	30	18
Triton X-45	nonionic	-81	12	3	23	19
Zwittergent 3-8	zwitterionic	-320	75	3	34	20
Zwittergent 3-16	zwitterionic	-366	63	3	36	21
EDTA	enzymatic	-143	32	3	29	22
Nonylglucopyranoside	nonionic	-24	16	3	8	23
Benzenesulfonic acid	anionic	-27	16	3	13	23
Triton X-100	nonionic	-133	17	3	27	24
Genapol X80	nonionic	-257	56	3	32	25
Mega 10	nonionic	-31	22	3	17	26
DTAB	cationic	-229	7	3	31	27
Tween 20	nonionic	-71	11	3	21	28
Genapol C-100	nonionic	-340	23	3	35	29
Empigen BB	zwitterionic	-26	14	3	12	30
Cetylpyridinium Cl	cationic	-83	10	3	24	31
Mega 8	nonionic	-29	5	3	14	32
CTAB	cationic	-497	40	3	37	34
Tween 80	nonionic	-59	21	3	20	35
Benzalkonium Cl	cationic	-311	37	6	33	36
Endozime	enzymatic	-136	52	3	28	37
Avg of all 37 compounds:		**-84**				

Table 23. Average Change in Solute Flux (moles/m^2·day) for Trisep X-201 RO Membrane After 1 Hr Exposure to Cleaning Agent.

					Ranking by flux change	
Compound	Class	Avg	SDEV	N	Solute	Water
Diamite BFT	oxidizing	1588	1182	3	1	1
STP	chelating	292	223	6	2	2
Protease	enzymatic	-38	10.2	3	17	3
Hydrogen Peroxide	oxidizing	85	64	3	5	4
Minncare	oxidizing	172	143	3	3	5
Biz detergent	enzymatic	-132	43	3	34	6
DBSA + STP	anion-cheltg	4	84	3	9	7
Octanesulfonic acid	anionic	-28	130	3	14	8
Peracetic acid	oxidizing	9	38	3	8	9
Benzenesulfonic acid	anionic	-38	-35	3	16	10
Zosteric acid	anionic	-13	-57	3	12	11
Mega 8	nonionic	-127	-187	3	32	12
TEA	cationic	-74	-63	3	24	13
Empigen BB	zwitterionic	28	-25	3	7	14
SDS	anionic	98	117	3	4	15
Citric acid	chelating	-91	-88	3	28	16
Butanesulfonic acid	anionic	-69	-82	3	22	17
Nonylglucopyranoside	nonionic	-73	-119	3	23	18
DBSA	anionic	-52	-72	3	21	19
EDTA	enzymatic	-15	-22	3	13	20
Triton X-45	nonionic	-109	-88	3	31	21
Endozime	enzymatic	-128	44	3	33	22
Mega 10	nonionic	84	32	3	6	23
Zwittergent 3-8	zwitterionic	-169	-125	3	36	24
Tween 80	nonionic	-38	-36	3	18	25
DecyltrimethylammBr	cationic	2	34	3	11	26
DTAB	cationic	-29	-123	3	15	27
Zwittergent 3-16	zwitterionic	-50	-60	3	20	28
Dodecanesulfonic acid	anionic	4	-23	3	10	29
Zwittergent 3-12	zwitterionic	-87	-295	3	27	30
Genapol X80	nonionic	-87	-60	3	26	31
Triton X-100	nonionic	-152	-178	3	35	32
Cetylpyridinium Cl	cationic	-46	188	3	19	33
CTAB	cationic	-86	-56	3	25	34
Tween 20	nonionic	-237	-231	3	37	35
Genapol C-100	nonionic	-100	-56	3	29	36
Benzalkonium Cl	cationic	-109	7.7	3	30	37
Avg. of all 37 compounds		**5**				

Table 24. Average Change in Solute Flux (moles/m^2·day) for GE Osmonics Desal CA RO Membrane After 1 Hr Exposure to Cleaning Agent.

					Ranking by flux change	
Compound	Class	Avg	SDEV	N	Solute	Water
Diamite BFT	oxidizing	20048	-	-	1	1
Protease	enzymatic	124	10	3	5	2
SDS	anionic	89	26	3	7	3
STP	chelating	33	69	6	22	4
Tween 20	nonionic	27	4.4	3	25	5
Biz detergent	enzymatic	253	2.4	3	3	6
Mega 8	nonionic	81	37	3	10	7
TEA	cationic	59	12	3	16	8
Hydrogen Peroxide	oxidizing	58	25	3	17	9
Butanesulfonic acid	anionic	65	21	3	15	10
Tween 80	nonionic	70	23	3	14	11
DBSA + STP	anion-cheltg	-78	58	3	36	12
Minncare	oxidizing	87	8.2	3	9	13
Mega 10	nonionic	41	22	3	21	14
EDTA	enzymatic	76	22	3	13	15
Cetylpyridinium Cl	cationic	47	63	3	19	16
Nonylglucopyranoside	nonionic	185	47	3	4	17
Benzenesulfonic acid	anionic	24	14	3	27	18
Zwittergent 3-12	zwitterionic	107	68	3	6	19
DecyltrimethylammBr	cationic	55	32	3	18	20
Peracetic acid	oxidizing	77	23	3	12	21
Triton X-100	nonionic	12	6.1	3	29	22
Octanesulfonic acid	anionic	81	37	3	11	23
Genapol C-100	nonionic	88	31	3	8	24
Dodecanesulfonic acid	anionic	32	19	3	23	25
Endozime	enzymatic	31	21	3	24	26
DBSA	anionic	21	23	3	28	27
DTAB	cationic	644	45	2	2	28
Zwittergent 3-8	zwitterionic	24	31	3	26	29
Citric acid	chelating	1.2	66	3	30	30
CTAB	cationic	43	13	3	20	31
Zwittergent 3-16	zwitterionic	-28	35	3	32	32
Benzalkonium Cl	cationic	-62	89	6	35	33
Genapol X80	nonionic	-2.5	88	3	31	34
Zosteric acid	anionic	-53	14	3	34	35
Triton X-45	nonionic	-43	29	3	33	36
Empigen BB	zwitterionic	-178	21	3	37	37
Avg of all 37 compounds:		**598**				
Avg without BFT:		**58**				

Table 25. Average Change in Specific Water Flux (L/m^2·day/psi) for Five PA RO Membranes After 1 Hr Exposure to Cleaning Agent.

					Ranking by flux change	
Cleaning Agent	Class	Avg	SDEV	N	Water	Solute
Diamite BFT	oxidizing	1.97	1.46	15	1	37
DBSA + STP	anion-cheltg	0.87	0.86	15	2	32
Protease	enzymatic	0.10	0.42	15	3	30
Dodecanesulfonic acid	anionic	0.00	0.49	14	4	33
SDS	anionic	-0.15	0.40	15	5	16
Hydrogen Peroxide	oxidizing	-0.23	0.56	15	6	18
STP	chelating	-0.24	1.02	29	7	22
Biz detergent	enzymatic	-0.27	0.47	15	8	31
Minncare	oxidizing	-0.38	0.56	15	9	19
DBSA	anionic	-0.40	0.44	23	10	11
Octanesulfonic acid	anionic	-0.41	0.50	15	11	12
Zwittergent 3-12	zwit	-0.46	0.69	15	12	24
TEA	cationic	-0.55	0.40	15	13	27
Peracetic acid	oxidizing	-0.57	0.54	15	14	13
Zwittergent 3-8	zwit	-0.58	0.62	15	15	9
Citric acid	chelating	-0.67	0.85	15	16	14
Zosteric acid	anionic	-0.68	0.44	15	17	2
Decyltrimethylamm Br	cationic	-0.78	0.39	17	18	35
Zwittergent 3-16	zwit	-0.81	0.74	17	19	8
EDTA	enzymatic	-0.82	0.75	15	20	15
Butanesulfonic acid	anionic	-0.87	0.56	15	21	26
Triton X-100	nonionic	-0.99	0.77	15	22	17
Benzenesulfonic acid	anionic	-1.07	1.24	23	23	25
DTAB	cationic	-1.17	0.94	17	24	34
Empigen BB	zwit	-1.27	1.50	15	25	36
Nonylglucopyranoside	nonionic	-1.28	0.66	15	26	10
Mega 8	nonionic	-1.32	0.78	15	27	21
Triton X-45	nonionic	-1.39	1.11	15	28	29
Endozime	enzymatic	-1.48	1.90	15	29	28
Mega 10	nonionic	-1.50	1.36	15	30	23
CTAB	cationic	-1.53	1.67	15	31	4
Genapol X80	nonionic	-1.65	1.11	21	32	7
Tween 80	nonionic	-1.86	1.61	15	33	20
Tween 20	nonionic	-2.03	1.24	15	34	6
Genapol C-100	nonionic	-2.65	0.78	15	35	5
Cetylpyridinium Cl	cationic	-3.08	1.31	19	36	3
Benzalkonium Cl	cationic	-3.90	1.81	18	37	1
Avg of 37 Cleaning Agents:		**-0.921**				
Avg (without BFT):		**-1.00**				

Table 26. Average Change in Solute Flux (moles/m^2·day) for Five PA RO Membrane After 1 Hr Exposure to Cleaning Agent.

					Ranking by flux change	
Compound	Class	Avg	SDEV	N	Solute	Water
Diamite BFT	oxidizing	665	583	15	1	1
DBSA + STP	anion-chelatg	41	275	15	6	2
Protease	enzymatic	8.6	24	15	8	3
Dodecanesulfonic acid	anionic	42	140	14	5	4
SDS	anionic	-47	88	15	22	5
Hydrogen Peroxide	oxidizing	-36	59	15	20	6
STP	chelating	-28	125	29	16	7
Biz detergent	enzymatic	15	101	15	7	8
Minncare	oxidizing	-34	119	15	19	9
DBSA	anionic	-61	111	23	27	10
Octanesulfonic acid	anionic	-52	92	15	26	11
Zwittergent 3-12	zwit	-13	108	15	14	12
TEA	cationic	-6	36	15	11	13
Peracetic acid	oxidizing	-50	135	15	25	14
Zwittergent 3-8	zwit	-67	141	15	29	15
Citric acid	chelating	-50	74	15	24	16
Zosteric acid	anionic	-188	104	15	36	17
DecyltrimethylammBr	cationic	50	117	17	3	18
Zwittergent 3-16	zwit	-75	150	17	30	19
EDTA	enzymatic	-48	69	15	23	20
Butanesulfonic acid	anionic	-6	75	15	12	21
Triton X-100	nonionic	-47	75	15	21	22
Benzenesulfonic acid	anionic	-12	43	23	13	23
DTAB	cationic	43	158	17	4	24
Empigen BB	zwit	62	202	15	2	25
Nonylglucopyranoside	nonionic	-66	77	15	28	26
Mega 8	nonionic	-33	30	15	17	27
Triton X-45	nonionic	2	179	15	9	28
Endozime	enzymatic	-3.8	100	14	10	29
MEGA-10	nonionic	-23	117	15	15	30
CTAB	cationic	-113	206	15	34	31
Genapol X80	nonionic	-78	160	21	31	32
Tween 80	nonionic	-33	87	15	18	33
Tween 20	nonionic	-87	107	15	32	34
Genapol C100	nonionic	-100	136	15	33	35
Cetylpyridinium Cl	cationic	-123	165	19	35	36
Benzalkonium Cl	cationic	-264	168	18	37	37
Avg of 36 compounds (w/o BFT):		**-15**				

Table 27. Average Change in Water Flux (L/m^2·day/psi) by Chemical Class of the Cleaning Agent

Cleaning Agent Type / Class	SST TMC/MPD	Hydranautics LFC3	Trisep X-201	Koch TFC-ULP	Koch TFC-HR	Hydranautics ESPA2	FilmTec BW-30	**Average Change Water Flux**
Anionic	-0.17	0.16	-0.33	-0.66	-0.88	-0.12	-0.37	**-0.34**
Anionic-chelating	0.28	1.11	-0.21	1.84	0.34	1.49	-0.41	**0.63**
Cationic	-1.18	-1.57	-1.22	-2.85	-2.30	-1.44	-0.79	**-1.62**
Chelating	0.07	0.07	-0.22	-0.78	-1.39	0.25	-0.10	**-0.30**
Enzymatic	-0.28	-0.18	-0.29	-1.46	-0.97	0.06	-48.4	**-7.35**
Nonionic	-0.85	-0.77	-0.91	-2.54	-1.86	-0.76	-1.98	**-1.38**
Oxidizing	-0.09	0.27	-0.16	-0.44	-0.36	-0.89	-0.15	**-0.26**
Oxidizing/BFT	-	1.33	0.61	4.46	2.14	1.71	0.22	**1.74**
Zwitterionic	-0.63	-0.60	-0.99	-2.00	-1.04	-0.34	0.04	**-0.79**

Table 28. Average Change in Solute Flux (moles/m^2·day) by Chemical Class of Cleaning Agent

Cleaning Agent Type / Class	SST TMC/MPD	Hydranautics LFC3	Trisep X-201	Koch TFC-ULP	Koch TFC-HR	Hydranautics ESPA2	FilmTec BW-30	**Average Change Solute Flux**
Anionic	28	50	9.4	106	-28	5.8	-51	**17.1**
Anionic-chelating	42	57	14	34	-6.3	351	-290	**29**
Cationic	-38	8.0	-59	-24	-30	-2.0	-133	**-39.7**
Chelating	8.1	25	1.26	24	-34	1.7	-35	**16.5**
Enzymatic	-1.1	45	-102	37	23	41	-48	**-0.58**
Nonionic	15	16	-96	-3.2	-24	5.0	-141	**-32.6**
Oxidizing	13	88	70.3	56	7.2	-138	4.0	**14.4**
Oxidizing/BFT	---	1540	1602	510	321	266	---	**848**
Zwitterionic	-14	24	-95	202	-9.2	11	-45	**10.4**

Table 29. Average Change in Performance of GE Osmonics Desal CA Membrane

Chemical Agent Type / Class	Average Change Water Flux (L/m^2 day/psi)	Average Change Solute Flux (moles/m^2·day)
Anionic	-0.003	-78
Anionic-chelating	-0.061	45
Cationic	-0.196	96
Chelating	0.071	37
Enzymatic	0.191	136
Nonionic	-0.117	45
Oxidizing	0.021	72
Oxidizing / BFT	5.117	20048
Zwitterionic	-0.605	-17

Table 30 Molecular Interactions with Membrane Surface / Separation Index

		CA	TMC/MPD	BW-30	LFC3	HR	ULP	ESPA2	X-201	**Ave**
Benzalkonium chloride	cationic	2	2	1	1	2	2	2	2	**1.8**
Benzensulfonic acid	cationic	2	2	1	1	2	1.5	2	2	**1.7**
Biz	anionic	2	1	1.5	1.5	2	2	2	2	**1.8**
Cetylpyridinium chloride	anionic	1.5	1.5	1.5	2	2	2	2	2	**1.8**
Citric acid	chelator	1.5	2	1	1.5	2	2	2	1.5	**1.7**
DBSA	anionic	2	2	1.5	1.5	1.5	1.5	2	2	**1.8**
DBSA and STP	anionic	2	1.5	1	1	2	2	2	1.5	**1.6**
Diamite BFT	oxidizing	2	NA	2	1.5	2	1.5	2	2	**1.9**
Empigen BB	zwittergent	2	1.5	2	1	2	1	1	2	**1.6**
Endozime	enzymatic	2	2	2	1.5	2	1.5	1.5	2	**1.8**
Genapol C-100	nonionic	2	2	2	1	2	2	2	1.5	**1.8**
Mega-10	nonionic	1	2	1.5	2	1	1.5	1	1	**1.4**
Minncare	oxidizing	2	NA	2	1.5	2	1	2	1.5	**1.7**
Nonylglucopyranoside	nonionic	1.5	2	1	1.5	2	2	2	1.5	**1.7**
Protease	enzymatic	1.5	1	2	2	2	2	2	1.5	**1.8**
SDS	anionic	2	2	1	1	2	1	2	1.5	**1.6**
STP	chelator	2	2	1.5	1.5	2	1.5	2	1.5	**1.8**
Triton X-100	nonionic	2	2	1	1	2	1.5	2	2	**1.7**
Tween 20	nonionic	2	2	2	1	2	1.5	2	2	**1.8**
Zosteric Acid	anionic	2	1.5	1.5	1	2	1	1.5	2	**1.6**
Zwittergent 1.5-16	zwittergent	2	2	1	1	2	2	2	2	**1.8**
Sum		39	34	31	28	40.5	34	39	37	
Average		**1.9**	**1.2**	**1.5**	**1.3**	**1.9**	**1.6**	**1.9**	**1.8**	

1 – No separation
1.5 – Partial separation
2 – Separation

Table 31. Cleaning Compound Association with Membrane Surface

Membrane Type	Separation Index 2 Complete Separation (Strong Association)	1.5 Partial Separation (Partial Association)	1 No Separation (No Association)
All membranes	57.8%	24.7%	17.5%
CA	76.2%	19.0%	4.8%
TMC/MPD*	68.4%	21.1%	10.5%
BW-30	33.3%	28.6%	38.1%
LFC3	14.3%	38.1%	47.6%
TFC-HR	90.5%	4.75%	4.75%
TFC-ULP	42.9%	38.1%	19.0%
ESPA2	81.0%	9.5%	9.5%
X-201	57.1%	38.1%	4.8%

*-based on exposure to 19 of 21 chemical cleaning compounds excluding Diamite BFT and Minncare.

Table 32. Sensitivity Indices of Molecular Descriptors

	Change in Water Flux			Change in Solute Flux		
	PA	**CA**	**PA-Urea**	**PA**	**CA**	**PA-Urea**
Charge / Polarity						
Zeta potential slope	0.4718					
Dipole	0.1445					
MaxNeg			-0.4795	-0.6646		
Py		0.0024				
Pz		29.0442				
Dx		-10.2415			-12.4020	
Dz						-5.4917
Qxx						-12.7533
Qyy		-0.9572				-1.2787
Sumdel1				-2.8423		
Tets2				-0.4554		
ssCH3	0.2961					
SdssC					21.4926	
SHother	-4.2971					
Hmax						1.2612
Hmin					-11.0764	
Gmin	-0.5802					
Molecular Complexity						
COO^-/AMII	0.0017	NA	NA		NA	NA
AMII/874	0.2643	NA	NA	0.2997	NA	NA
Projected Area				0.6818		
xpc4						-0.6113
xvpc4						0.2355
xvc3		-0.4530				
nxc3					-1.6797	
LD50			-0.1138			
phia		0.4327				
IC			-2.4014			
numHBa					1.6945	
SHHBd					12.4138	
nelem			0.4392		-0.1215	
HBP (Hydrophobicity)						
LogP					2.5910	

Table 33. Predicted Change in Specific Water Flux ($L/m^2 \cdot day/psi$) by ANN Models

Compound	Membrane					
	BW-30	**ESPA-2**	**TFC-HR**	**TFC-ULP**	**X-201**	**CA**
Formic acid	-0.63	-0.53	-1.72	-0.12	-0.21	-0.13
Propionic acid	-0.83	-0.41	-1.90	0.70	-0.23	-0.15
Acetic acid	-0.81	-0.67	-2.29	0.49	-0.24	-0.12
Butyric acid	-0.90	-0.50	-1.91	0.68	-0.21	-0.19
Capric acid	-1.02	-0.92	-2.29	-2.46	-0.43	-0.02
Caproic acid	-0.92	-0.51	-1.90	0.58	-0.26	-0.23
Lauric acid	-1.02	-0.90	-2.18	-2.60	-0.52	0.07
Hexadecanoic acid	-1.28	-1.31	-1.82	-1.57	-0.47	0.25
Octadecanoic acid	-1.44	-1.33	-2.17	-2.10	-0.35	0.24
Benzalkonium chloride	-2.44	-4.45	-4.02	-4.21	-1.86	-0.26
Cetylpyridinium chloride	-2.90	-1.46	-3.43	-4.19	-1.44	-0.03
Zosteric acid	-1.24	-0.58	-1.23	-0.66	-0.30	-0.38
Benzenesulfonic acid	-1.08	-0.40	-0.72	-1.94	-0.18	-0.13
p-toluenesulfonic acid	0.03	0.12	-0.13	0.24	-0.03	-0.10
Ethylbenzenesulfonic acid	0.06	0.09	-0.15	0.10	-0.11	-0.11
Octylbenzenesulfonic acid	0.03	-0.12	-0.38	0.00	-0.37	-0.17
DBSA	0.04	-0.09	-1.00	0.02	-0.43	-0.15
Butanesulfonic acid	-0.48	-1.17	-2.37	-2.72	-0.44	0.01
Pentanesulfonic acid	-0.16	-1.53	-2.79	-3.11	-0.32	0.02
Heptanesulfonic acid	0.18	-1.18	-1.28	-3.21	-0.19	0.01
Hexanesulfonic acid	0.01	-1.39	-2.49	-3.15	-0.54	0.01
Octanesulfonic acid	0.23	-0.62	-0.46	-2.77	-0.10	-0.01
Nonanesulfonic acid	0.23	-0.11	-0.35	-0.46	-0.14	-0.02
Decanesulfonic acid	0.20	0.07	-0.37	-0.07	-0.19	-0.04
Dodecanesulfonic acid	0.10	0.06	-0.43	-0.33	-0.29	-0.11
Hexadecanesulfonic acid	-0.12	-0.69	-0.52	-0.88	-0.55	-0.40
SDS	0.41	-0.16	-0.76	-0.34	-0.42	0.28
HEXglucopyranoside	-1.64	-1.46	-1.88	-2.33	-1.14	0.08
HEPglucopyranoside	-1.67	-1.46	-2.01	-2.36	-1.26	0.01
OCTglucopyranoside	-1.78	-1.73	-2.10	-2.50	-1.29	-0.09
NONglucopyranoside	-1.81	-1.74	-2.20	-2.52	-0.56	-0.08
DECglucopyranoside	-1.85	-1.78	-2.28	-2.55	-0.42	-0.08
DODglucopyranoside	-1.92	-1.82	-2.43	-2.59	-0.37	-0.07
EDTA	-0.84	-0.18	-0.79	-1.66	-0.60	-0.04
Citric acid	-0.33	-0.34	-0.89	-1.24	-0.49	-0.18
Genapol C-100	-2.84	-2.03	-3.39	-2.80	-1.34	-0.12
Genapol X-80	-2.01	-0.57	-3.06	-2.81	-1.30	-0.25

Table 32 (continued). Predicted Change in Specific Water Flux (L/m^2·day/psi) by ANN Models

Compound	Membrane					
	BW-30	**ESPA2**	**TFC-HR**	**TFC-ULP**	**X-201**	**CA**
Mega 8	-0.27	-1.25	-2.92	-2.54	-0.61	-0.05
Mega 9	-0.53	-1.07	-2.90	-2.40	-0.37	0.00
Mega 10	-0.32	-1.13	-3.01	-2.58	-0.35	0.08
Nonyltrimethylammonium Br	-0.57	-0.56	-3.27	-3.30	-0.77	-0.15
Decyltrimethylammonium Br	-0.70	-0.53	-3.43	-3.28	-0.85	-0.14
DTAB	-0.95	-0.52	-3.68	-3.25	-1.04	-0.11
Tetradecyltrimethylamm Br	-1.16	-0.56	-3.87	-3.25	-1.28	-0.09
CTAB	-1.36	-0.63	-4.01	-3.27	-1.52	-0.07
Octadecyltrimethylamm Br	-1.53	-0.71	-4.11	-3.29	-1.73	-0.05
Tetrabutylammonium bromide	-1.67	-0.75	-4.00	-3.68	-0.68	0.11
TEA	-0.62	-0.54	-2.38	-1.78	-0.49	0.05
Tetrapentylammonium bromide	-1.99	-1.03	-4.28	-3.66	-0.90	0.16
Tetraheptylammonium bromide	-2.41	-1.47	-4.51	-3.61	-1.09	0.21
Tetrahexylammonium bromide	-2.23	-1.27	-4.42	-3.64	-0.54	0.18
Tetraoctylammonium bromide	-2.57	-1.63	-4.57	-3.59	-1.67	0.22
Tetradecylammonium bromide	-2.97	-1.82	-4.64	-3.54	-1.51	0.27
Tetrahexyldecylammonium Br	-2.07	-1.78	-4.73	-3.36	-1.27	0.24
Triton X-45	-0.57	-0.47	-1.91	-2.30	-0.42	-0.63
Triton X-100	-1.12	0.06	-2.42	-2.38	-1.22	-0.09
Tween 20	-3.51	-0.34	-3.44	-2.71	-1.13	0.24
Tween 40	-3.38	-0.64	-3.62	-2.97	-1.10	0.04
Tween 60	-3.47	-0.27	-3.38	-2.61	-1.06	-1.34
Tween 80	-3.46	-0.14	-3.29	-2.47	-1.04	0.00
Zwit 3-8	0.59	-0.13	-1.96	-0.98	-0.71	-0.19
Zwit 3-10	0.69	-0.20	-1.54	-0.97	-0.80	-0.14
Zwit 3-12	0.59	-0.31	-1.29	-0.95	-0.89	-0.14
Zwit 3-14	0.49	-0.46	-1.32	-1.05	-0.97	-0.25
Zwit 3-16	0.42	-0.66	-1.70	-1.24	-1.04	-0.33
Empigen BB	-0.26	-1.99	-2.60	-3.29	-0.44	-1.33

Table 34. Predicted Change in Solute Flux (moles/m^2·day) by ANN Models

Compound	Membrane						
	BW-30	**ESPA2**	**LFC3**	**TFC-HR**	**TFC-ULP**	**X-201**	**CA**
Formic acid	91.2	81.4	3.0	5.4	54.0	115	1270
Propionic acid	94.3	90.6	9.7	41.3	58.1	-3.1	1270
Acetic acid	96.8	89.2	7.2	35.9	58.9	-1.9	1270
Butyric acid	90.8	90.7	10.8	42.9	57.1	-8.5	1270
Capric acid	71.1	87.7	-12.4	15.0	57.3	3.8	647
Caproic acid	84.9	90.3	11.9	43.8	55.8	-4.5	1270
Lauric acid	67.4	84.3	-29.4	-10.0	57.9	9.6	847
Hexadecanoic acid	76.7	17.7	98.8	11.7	0.0	23.5	1270
Octadecanoic acid	36.8	18.7	91.7	0.1	38.3	27.5	1270
Benzalkonium chloride	-430	-416	56.6	-282	-370	-109	-87.1
Cetylpyridinium chloride	-356	-305	35.5	-37.1	-77.3	-45.7	63.4
Zosteric acid	-133	-91.7	-6.1	-56.3	-99.6	-13.1	-44.8
Benzenesulfonic acid	-58.8	23.1	-10.8	9.7	-25.3	-37.8	26.8
p-toluenesulfonic acid	-26.6	-77.7	48.9	14.1	-27.4	-19.7	1270
Ethylbenzenesulfonic acid	-27.4	-65.0	70.0	-19.3	-68.8	-2.6	768
Octylbenzenesulfonic acid	-75.0	-2.4	51.0	-43.5	-67.6	-45.7	564
DBSA	-168	24.0	54.7	-30.6	-77.1	-52.4	19.7
Butanesulfonic acid	-80.8	60.2	14.6	-61.8	-18.5	-69.0	39.2
Pentanesulfonic acid	-93.4	49.8	6.5	-73.3	-14.1	-79.4	3.2
Hexanesulfonic acid	-96.9	39.2	-12.4	-75.2	-7.4	-48.9	-16.8
Heptanesulfonic acid	-91.2	30.5	-31.6	-61.4	-0.3	-55.7	8.8
Octanesulfonic acid	-77.4	24.8	-37.4	-33.1	4.7	-28.3	48.6
Nonanesulfonic acid	-59.7	22.4	-24.5	-2.2	-0.6	-33.8	69.8
Decanesulfonic acid	-42.1	22.7	1.9	18.9	-32.3	-10.8	71.7
Dodecanesulfonic acid	-13.1	25.5	13.5	8.2	-159	3.9	39.4
Hexadecanesulfonic acid	-131	19.4	36.9	-45.6	-183	26.4	-59.3
SDS	-93.3	-6.0	54.5	-44.2	-99.6	98.3	61.9
HEXglucopyranoside	-115	-115	-31.0	-59.2	-110	-64.3	706
HEPglucopyranoside	-118	-157	-29.1	-51.7	-110	-77.1	495
OCTglucopyranoside	-122	-197	-25.4	-45.3	-111	-86.3	270
NONglucopyranoside	-127	-241	-20.8	-39.9	-113	-73.3	157
DECglucopyranoside	-134	-274	-16.1	-35.5	-115	-69.1	76.6
DODglucopyranoside	-146	-263	-7.2	-28.8	-122	-55.7	-24.9

Table 33 (continued). Predicted Change in Solute Flux (moles/m^2·day) by ANN Models

Compound	Membrane						
	BW-30	**ESPA2**	**LFC3**	**TFC-HR**	**TFC-ULP**	**X-201**	**CA**
EDTA	-67.3	34.5	7.7	-3.3	-118	-14.8	75.0
Citric acid	-68.0	-48.1	-16.5	-85.3	-165	-91.1	-1.1
Genapol C-100	-162	61.1	-32.9	-27.2	-216	-99.5	88.7
Genapol X-80	-171	49.9	-5.1	-23.6	-182	-87.0	-9.1
Mega 8	-29.1	-88.7	14.4	-24.2	-17.9	-127	143
Mega 9	-30.8	-95.9	24.1	-31.4	-37.8	-130	78.4
Mega 10	-39.5	-102	35.2	-34.2	-35.8	83.7	30.0
Nonyltrimethylamm Br	21.8	88.8	9.4	19.1	-34.4	13.9	-119
Decyltrimethylamm Br	16.8	91.0	27.2	16.2	-18.2	2.0	53.5
Dodecyltrimethylamm Br	7.5	83.1	47.1	2.7	-205	-28.5	594
Tetradecyltrimethylamm Br	-5.5	73.1	10.4	-16.7	-344	-58.4	333
Hexadecyltrimethylamm Br	-70.8	26.2	-56.4	-38.7	-332	-86.3	74.8
Octadecyltrimethylamm Br	-318	-112	-3.4	-66.3	-321	-111	-80.2
Tetrabutylammonium Br	-10.3	67.0	-44.1	-21.4	-347	51.8	-286
Tetraethylamm Br	-2.3	54.9	17.0	-10.1	-50.9	-74.0	55.3
Tetrapentylamm Br	-397	-215	38.0	-88.7	-324	29.2	-287
Tetraheptylamm Br	-444	-432	44.6	-347	-399	77.4	-325
Tetrahexylamm Br	-430	-404	55.8	-212	-355	28.1	-314
Tetraoctylamm Br	-451	-436	28.6	-421	-431	51.4	-330
Tetradecylamm Br	-460	-435	-5.5	-461	-463	-132	-231
Tetrahexyldecylamm Br	-470	-358	-82.6	-472	-482	-191	87.1
Triton X-45	-147	-80.3	17.1	-31.0	-50.1	-109	-53.5
Triton X-100	-169	64.4	-24.1	-25.2	-217	-152	10.1
Tween 20	-196	8.4	12.4	-27.3	-58.1	-237	27.1
Tween 40	-196	8.7	12.6	-27.3	-58.3	-223	-81.9
Tween 60	-197	8.5	12.6	-26.2	-56.6	-51.8	-82.0
Tween 80	-197	8.6	12.7	-26.2	-56.7	-38.2	69.5
Zwit 3-8	-54.0	38.7	38.9	-42.5	-213	-169	22.3
Zwit 3-10	-148	45.2	42.6	-50.9	-217	-188	62.5
Zwit 3-12	-130	24.7	43.3	-48.9	-215	-87.5	62.7
Zwit 3-14	-23.9	-13.3	46.6	-45.2	-217	-71.7	18.3
Zwit 3-16	7.5	-12.6	51.4	-41.5	-224	-49.9	-21.0
Empigen BB	50.7	-26.0	81.6	20.3	-6.8	28.1	-178

Table 35. Chemical Cleaning of Fouled RO Membranes

Membrane	DBSA		Genapol C-100		Zwittergent 3-16		Protease	
	%Change Solute Flux	% Change Water Flux	%Change Solute Flux	% Change Water Flux	%Change Solute Flux	% Change Water Flux	%Change Solute Flux	% Change Water Flux
FilmTec BW-30	-1.7	-5.6	12.1	-25.6	25.1	6.6	9.0	1.3
Hydranautics ESPA2	-49.1	-13.1	20.6	-17.4	-27.5	-17.7	16.9	-0.7
Hydranautics LFC3	29.1	9.8	22.7	-15.1	29.7	2.1	32.0	1.4
Koch TFC-HR	-2.0	-9.5	10	-32.2	37.6	4	23.9	-0.9

List of Figures

List of Tables

List of Appendices

Appendix I. Chemical Structures of Chemical Compounds

benzenesulfonic acid

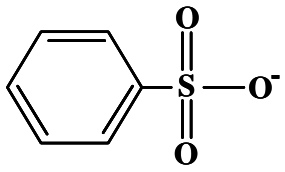

DBSA

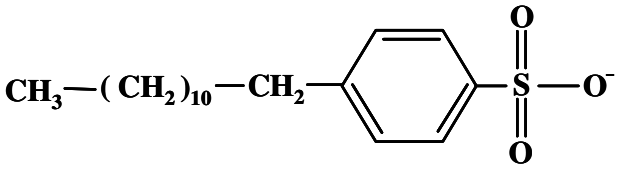

butane sulfonic acid

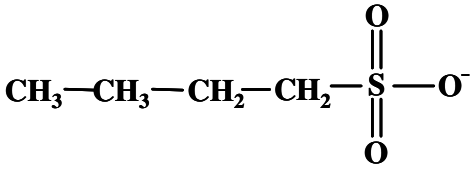

octane sulfonic acid

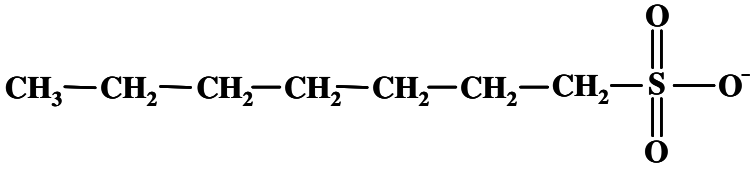

dodecanesulfonic acid

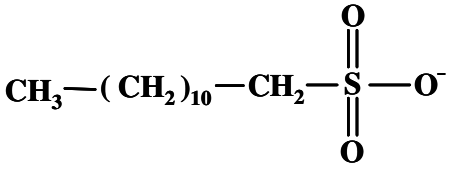

sodium dodecylsulfate

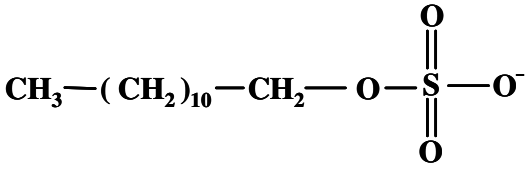

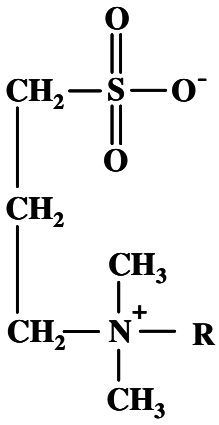

Zwittergent 3-08 **R =** $-CH_2-(CH_2)_6-CH_3$

Zwittergent 3-12 **R =** $-CH_2-(CH_2)_{10}-CH_3$

Zwittergent 3-16 **R =** $-CH_2-(CH_2)_{14}-CH_3$

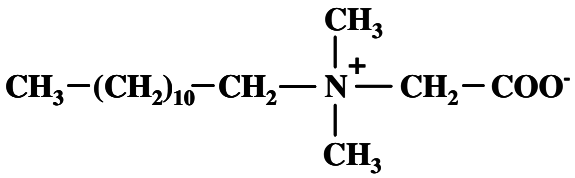

n-dodecyl-N,N-dimethylglycine

EMPIGEN BB 30% solution

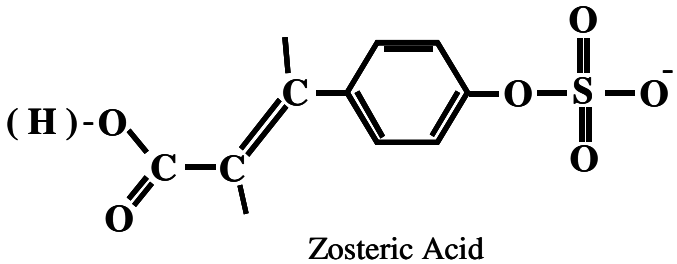

Zosteric Acid

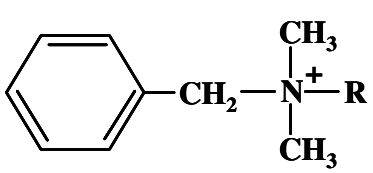

R = $C_{12}H_{25}$, $C_{14}H_{29}$, $C_{16}H_{33}$

Benzalkonium chloride

Decyltrimethylammonium bromide

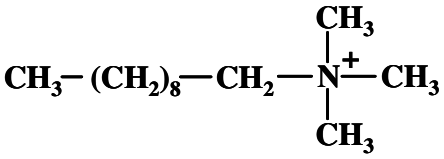

Dodecyltrimethylammonium bromide

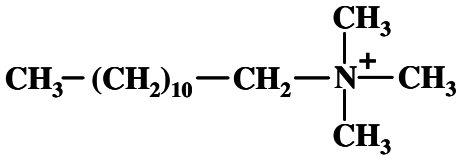

Hexadecyltrimethylammonium bromide

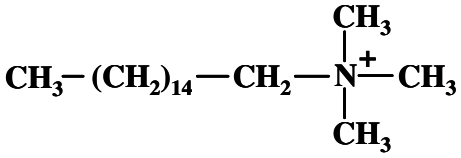

Tetraethylammonium bromide

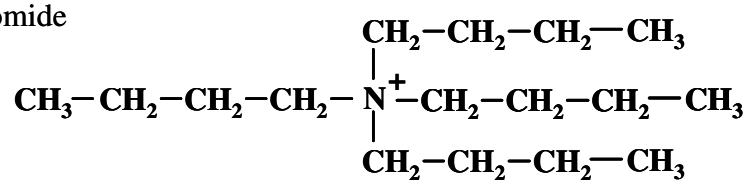

Cetylpyridinium chloride

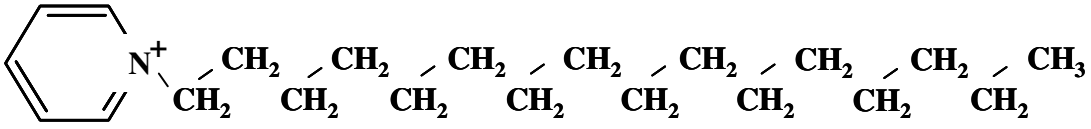

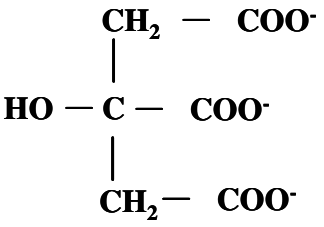

Citric Acid

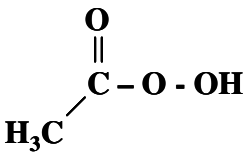

Peracetic Acid

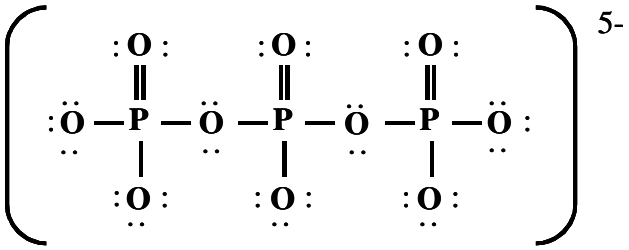

Tripolyphosphate ion

Hydrogen peroxide

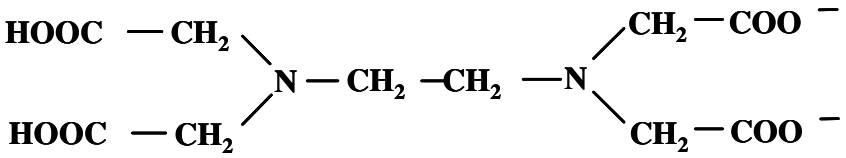

Ethylenediaminetetraacetic acid

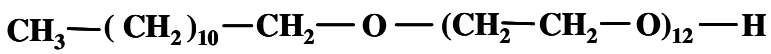

Polyethyleneglycol laurylether (Genapol C-100)

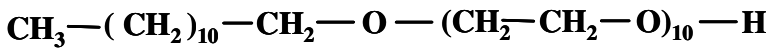

Polyethyleneglycol dodecylether (Genapol X-80)

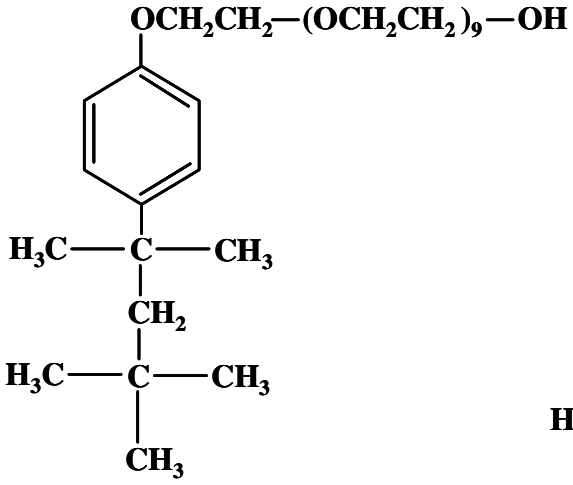

Triton X-100
N = 9.5

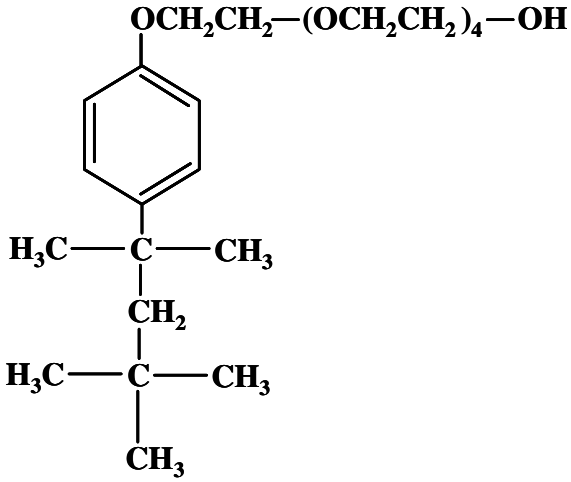

Triton X-45
N = 5

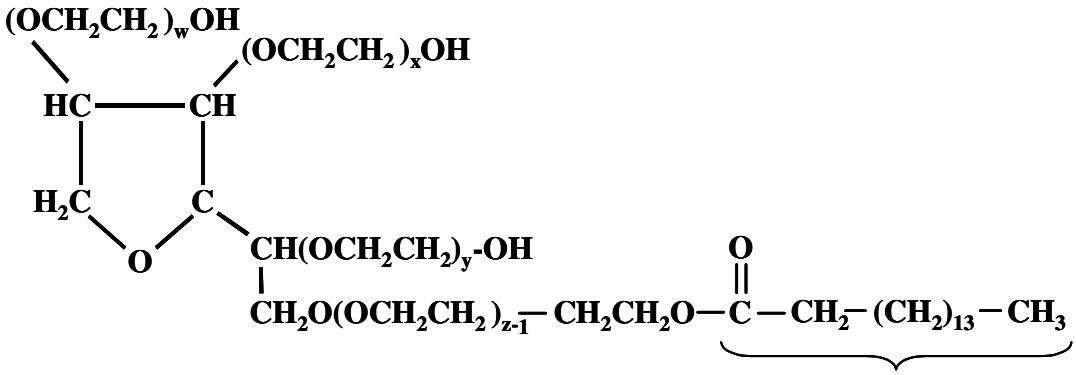

w + x + y + z = 20

Polyoxyethylene (20) sorbitan monolaurate	Tween 20	$R = C_{12}$
Polyoxyethylene (20) sorbitan monopalmitate	Tween 80	$R = C_{18}$

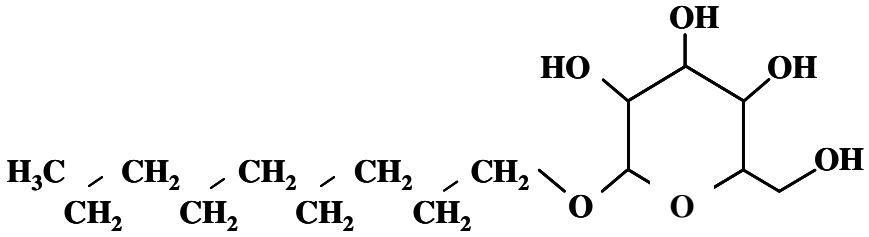

n-nonyl-β-*D*-glucopyranoside

Appendix II. Box and Whiskers Plot

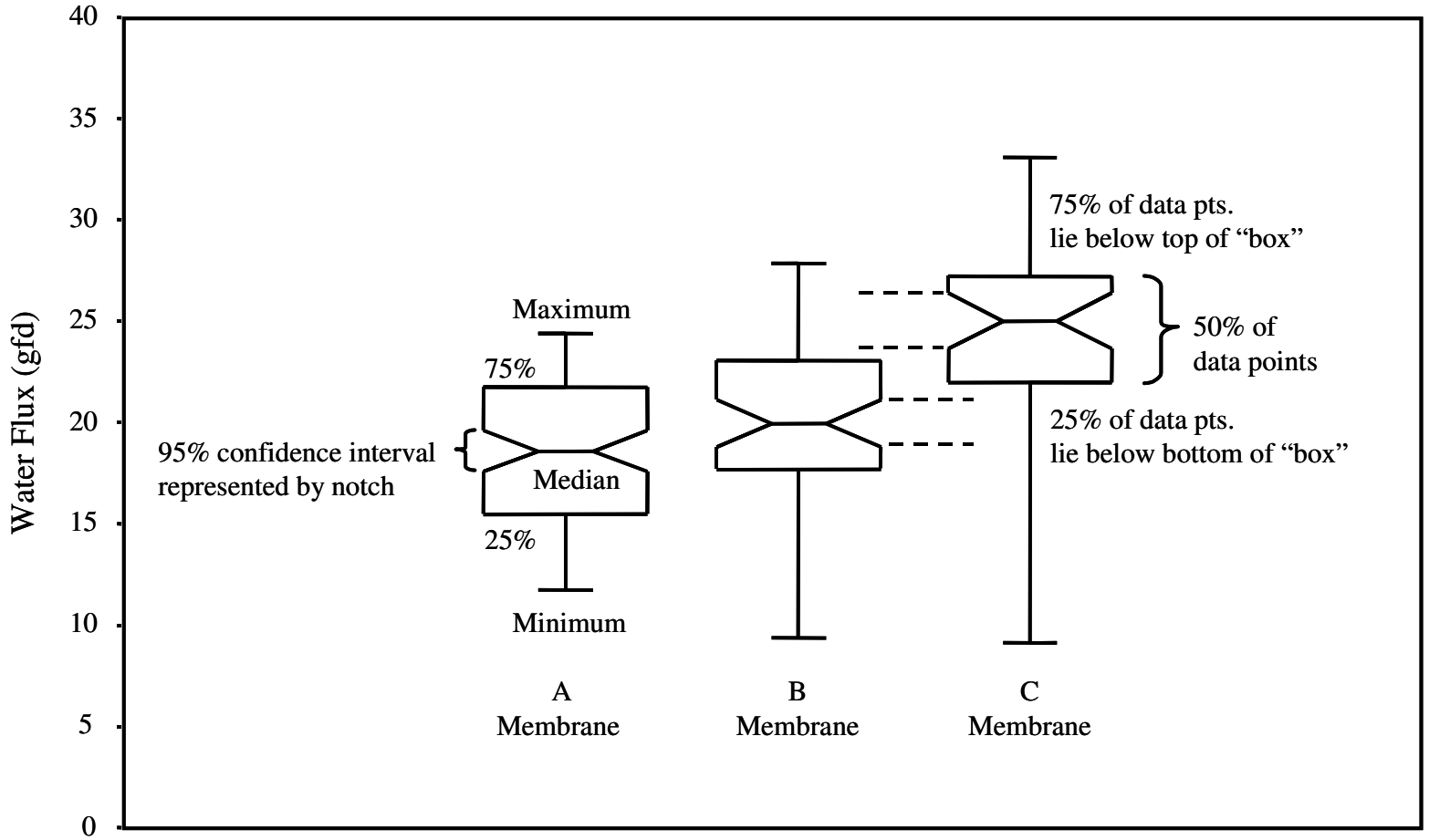

Appendix III. PCA of Chemical Cleaning Agents Exposed to RO Membranes

Benzalkonium chloride

The scores plots of the ATR/FTIR spectra of the Desal CA and the SST TMC/MPD RO membranes exposed to benzalkonium chloride are shown in Figure 35. The spectra of the surfactant-exposed membrane completely separated from the control membrane spectra suggesting a strong interaction of the surfactant with the membrane. Scores plots of the ATR/FTIR spectra of the FilmTec BW-30 and Hydranautics LFC3 RO membranes exposed to benzalkonium chloride are shown in Figure 36. Neither surfactant exposed membrane separated from the control set of spectra. Scores plots of the ATR/FTIR spectra of the Koch TFC-HR and TFC-ULP membranes are shown in Figure 37. The surfactant-exposed membrane spectra of both membranes completely separated from the spectra of control membranes. The scores plots of the Hydranautics ESPA2 and the Trisep X-201 RO membranes exposed to benzalkonium chloride are shown in Figure 38. Both sets of detergent-exposed membrane spectra separated from the spectra of the control membranes.

Benzenesulfonic acid

The scores plots of the ATR/FTIR spectra of the Desal CA and the SST TMC/MPD RO membranes exposed to benzenesulfonic acid are shown in Figure 39. The chemical-exposed spectra of both membranes completely separated from the control membrane spectra suggesting a strong interaction of the surfactant with the membrane. Scores plots of the ATR/FTIR spectra of the FilmTec BW-30 and Hydranautics LFC3 RO membranes exposed to benzenesulfonic acid are shown in Figure 40. Neither set of surfactant-exposed membrane spectra separated from the control set of spectra. This indicates that this compound did not strongly adsorb to the surface of the membrane. Scores plots of the ATR/FTIR spectra of the Koch TFC-HR and TFC-ULP membranes are shown in Figure 41. The surfactant-exposed membrane spectra of both membranes completely separated from the spectra of control membranes. The scores plots of the Hydranautics ESPA2 and the Trisep X-201 RO membranes exposed to benzalkonium chloride are shown in Figure 42. Both sets of detergent-exposed membrane spectra separated from the spectra of the control membranes.

Biz detergent

The scores plots of the ATR/FTIR spectra of the Desal CA and the SST TMC/MPD RO membranes exposed to benzalkonium chloride are shown in Figure 43. The spectra of the detergent-exposed CA membrane completely separated from the control membrane spectra suggesting a strong interaction of the surfactant with the membrane. However, the detergent-exposed membrane spectra of the SST TMC/MPD membrane did not completely separate from the control membrane spectra. This indicates a lack of association of the detergent with the membrane surface. Scores plots of the ATR/FTIR spectra of the FilmTec BW-30 and Hydranautics LFC3 RO membranes exposed to Biz detergent are shown in Figure 44. Both sets of surfactant-exposed membrane spectra

separated from the control set of spectra. However, one spectrum of each of the control membranes fell amongst the detergent-exposed spectra. Scores plots of the spectra of the Koch TFC-HR and TFC-ULP membranes are shown in Figure 45. The surfactant-exposed membrane spectra of both membranes completely separated from the spectra of control membranes. The scores plots of the Hydranautics ESPA2 and the Trisep X-201 RO membranes exposed to Biz detergent are shown in Figure 46. Both sets of detergent-exposed membrane spectra separated from the spectra of the control membranes indicating a strong association or interaction with the surface of the membranes.

Cetylpyridinum chloride

The scores plots of the ATR/FTIR spectra of the Desal CA and the SST TMC/MPD RO membranes exposed to cetylpyridinium chloride are shown in Figure 47. Two of the surfactant-exposed spectra of the CA membrane grouped with the control membrane spectra. This may have resulted from sampling that occurred in an area not affected by the surfactant. The line or plane that delineates the test spectra from the control spectra less well defined suggesting that the association of cetylpyridinium chloride is not as strong as other chemical cleaning agents. Scores plots of the ATR/FTIR spectra of the FilmTec BW-30 and Hydranautics LFC3 RO membranes exposed to cetylpyridinium chloride are shown in Figure 48. The separation between the test spectra and the control spectra are well defined; however, one of the control spectra fell very close to the group of test spectra of the surfactant-exposed BW-30 membrane. Scores plots of the ATR/FTIR spectra of the Koch TFC-HR and TFC-ULP membranes are shown in Figure **49**. The surfactant-exposed membrane spectra of both membranes clearly separated from the spectra of control membranes. The scores plots of the Hydranautics ESPA2 and the Trisep X-201 RO membranes exposed to cetylpyridinium chloride are shown in Figure 50. Both sets of detergent-exposed membrane spectra separated from the spectra of the control membranes. However, one of the control spectra associated with the Trisep X-201 control was located close to the test group of membrane spectra exposed to the surfactant.

Citric acid

The scores plots of the ATR/FTIR spectra of the Desal CA and the SST TMC/MPD RO membranes exposed to citric acid are shown in Figure 51. Most of the spectra of the citric acid-exposed membrane separated from the control membrane spectra. Three of the citric acid membrane spectra appeared to be more closely associated with control set of spectra. The spectra for citric acid actually appear to separate into four independent groups. Further, investigation into the data set is needed. However, it is outside the scope of this project. Scores plots of the ATR/FTIR spectra of the FilmTec BW-30 and Hydranautics LFC3 RO membranes exposed to citric acid are shown in Figure 52. The test spectra of the FilmTec BW-30 membrane exposed to citric acid did not separate from the control set of spectra. This indicates that the association of citric acid is very weak. The test spectra of the Hydranautics LFC3 membrane separated from the control spectra for the most part. However, the separation is not as clean as other samples. Anywhere from 1 to 3 test spectra maybe associated with the control spectra. It just depends on

where the plane of separation is drawn. This suggests that the interaction of citric acid is not real strong and that spread of the data is due to the random sampling. Scores plots of the ATR/FTIR spectra of the Koch TFC-HR and TFC-ULP membranes are shown in Figure 53. The surfactant-exposed membrane spectra of both membranes completely separated from the spectra of control membranes. The scores plots of the Hydranautics ESPA2 and the Trisep X-201 RO membranes exposed to citric acid are shown in Figure **54**. Both sets of detergent-exposed membrane spectra separated from the spectra of the control membranes. However, up to 4 of the Hydranautics ESPA2 spectra exposed to citric acid appear as if they could be associated with the control spectra. One of the control spectra of the Trisep X-201 grouped with the test spectra.

Dodecylbenzenesulfonic acid (DBSA)

The scores plots of the ATR/FTIR spectra of the Desal CA and the SST TMC/MPD RO membranes exposed to DBSA (2X CMC) are shown in Figure 55. The spectra of the surfactant-exposed CA membrane completely separated from the control membrane spectra suggesting a strong interaction of the surfactant with the membrane. The separation of the test spectra from the SST TMC/MPD control spectra while separate is less well defined. Two control spectra are grouped with the test spectra and one test spectrum group with the control spectra. Scores plots of the ATR/FTIR spectra of the FilmTec BW-30 and Hydranautics LFC3 RO membranes exposed to DBSA (2X CMC) are shown in Figure 56. Neither surfactant exposed membrane separated from the control set of spectra. Scores plots of the ATR/FTIR spectra of the Koch TFC-HR and TFC-ULP membranes are shown in Figure 57. The surfactant-exposed membrane spectra of both membranes completely separated from the spectra of control membranes. Several of the test spectra of the TFC-ULP membrane grouped with the control membrane spectra. The scores plots of the Hydranautics ESPA2 and the Trisep X-201 RO membranes exposed to DBSA (2X CMC) are shown in Figure 58. Both sets of detergent-exposed membrane spectra did not cleaning separate from the sets of control membrane spectra.

DBSA and STP

The scores plots of the ATR/FTIR spectra of the Desal CA and the SST TMC/MPD RO membranes exposed to DBSA and STP are shown in Figure 59. The test spectra of the CA membrane completely separated from the control membrane spectra suggesting a strong interaction of the surfactant with the membrane. The separation between test and control spectra of the SST TMC/MPD membrane is less well defined. Two of the test membrane spectra lie across the plane separating the test spectra from the control spectra. Scores plots of the ATR/FTIR spectra of the FilmTec BW-30 and Hydranautics LFC3 RO membranes exposed to DBSA and STP are shown in Figure 60. Neither set of membrane spectra exposed to DBSA and STP separated from the control spectra. This indicates that the two compounds are to not strongly adsorb or associate with these membranes. Scores plots of the ATR/FTIR spectra of the Koch TFC-HR and TFC-ULP membranes are shown in Figure 61. The surfactant-exposed membrane spectra of both membranes clearly separated from the spectra of control membranes. The scores plots of the Hydranautics ESPA2 and the Trisep X-201 RO membranes exposed to DBSA and

STP are shown in Figure 62. The test set of spectra from the Hydranautics ESPA2 membrane spectra separated from the spectra of the control membranes. However, the separation of the test spectra from the control spectra of Trisep X-201 was not as clear. One spectrum from the test group more closely associated the control spectra. This may only indicate this one area of the membrane was not affected by the chemical exposure.

Diamite BFT

The scores plots of the ATR/FTIR spectra of the Desal CA and the SST TMC/MPD RO membranes exposed to Diamite BFT are shown in Figure 63. The spectra of the chemical-exposed membrane completely separated from the control membrane spectra. This was readily apparent looking at the individual infrared spectra (data not shown). The CA membrane spectra that were exposed to Diamite BFT were deacetylated. The acetate functional group was removed resulting significant changes in the infrared spectrum (Figure 3.5). Scores plots of the ATR/FTIR spectra of the FilmTec BW-30 and Hydranautics LFC3 RO membranes exposed to Diamite BFT are shown in Figure 64. The Diamite BFT-exposed FilmTec BW-30 spectra separated from the control spectra. However, one of the control spectra grouped with detergent-exposed membrane spectra. The test spectra of the Hydranautics LFC3 also separated from the control spectra with three of the test spectra grouping with the control spectra. Scores plots of the ATR/FTIR spectra of the Koch TFC-HR and TFC-ULP membranes are shown in Figure 65. The Diamite BFT-exposed Koch TFC-HR membrane spectra completely separated from the spectra of control membranes. The test membranes of the Koch TFC-ULP separated from the control spectra but not as prominently as the TFC-HR membrane. One of the test TFC-HR spectra grouped with the control spectra. The scores plots of the Hydranautics ESPA2 and the Trisep X-201 RO membranes exposed to Diamite BFT are shown in Figure 66. The test spectra of both membranes completely separated from the control membrane spectra suggesting a strong interaction of the surfactant with the membrane.

Empigen BB

The scores plots of the ATR/FTIR spectra of the Desal CA and the SST TMC/MPD RO membranes exposed to Empigen BB are shown in Figure 67. The spectra of the surfactant-exposed membrane completely separated from the control CA membrane spectra suggesting a strong interaction of the surfactant with the membrane. The surfactant-exposed SST TMC/MPD spectra barely separated form the control spectra. One of the test spectra grouped with the control spectra. Scores plots of the ATR/FTIR spectra of the FilmTec BW-30 and Hydranautics LFC3 RO membranes exposed to Empigen BB are shown in Figure 68. The test spectra of the FilmTec BW-30 spectra completely separated from the control spectra. The Empigen BB-exposed membrane spectra did not separate from the control spectra of the Hydranautics LFC3 indicating that the Empigen BB did not interact strongly with the membrane surface. Scores plots of the ATR/FTIR spectra of the Koch TFC-HR and TFC-ULP membranes are shown in Figure **69**. The surfactant-exposed membrane spectra completely separated from the spectra of TFC-HR control membranes. The test spectra of the TFC-ULP membrane did not

completely separate from the control membrane spectra. The scores plots of the Hydranautics ESPA2 and the Trisep X-201 RO membranes exposed to Empigen BB are shown in Figure 70. Both sets of detergent-exposed membrane spectra separated from the spectra of the control membranes.

Endozime

The scores plots of the ATR/FTIR spectra of the Desal CA and the SST TMC/MPD RO membranes exposed to Endozime are shown in Figure 71. The spectra of the surfactant-exposed membrane completely separated from the control CA membrane spectra suggesting a strong interaction of the surfactant with the membrane. The test spectra also separated from the control spectra of the SST TMC/MPD membrane. However, it was necessary display the factors 1, 2, and 3 in order to completely visualize the separation between these two sets of membranes. Scores plots of the ATR/FTIR spectra of the FilmTec BW-30 and Hydranautics LFC3 RO membranes exposed to Endozime are shown in Figure 72. Both sets of test spectra separated from the control spectra. However, one of the control spectra of the Hydranautics LFC3 membrane grouped with the Endozime-treated membrane spectra. Scores plots of the ATR/FTIR spectra of the Koch TFC-HR and TFC-ULP membranes are shown in Figure 73. The surfactant-treated membrane spectra of the TFC-HR membrane spectra separated from the control spectra. The Endozime BB-treated TFC-ULP separated from the control spectra. However, four of the test membranes grouped with the control membrane spectra. The scores plots of the Hydranautics ESPA2 and the Trisep X-201 RO membranes exposed to Endozime are shown in Figure 74. Both sets of detergent-exposed membrane spectra separated from the spectra of the control membranes. However, one of the Hydranautics ESPA2 test membrane spectra grouped with the control spectra.

Genapol C-100

The scores plots of the ATR/FTIR spectra of the Desal CA and the SST TMC/MPD RO membranes exposed to Genapol C-100 are shown in Figure 75. The surfactant-exposed spectra from both membranes completely separated from the control spectra suggesting a strong interaction of the surfactant with the membrane. Scores plots of the ATR/FTIR spectra of the FilmTec BW-30 and Hydranautics LFC3 RO membranes exposed to Genapol GC-100 are shown in Figure 76. Neither surfactant exposed membrane separated from the control set of spectra. Scores plots of the ATR/FTIR spectra of the Koch TFC-HR and TFC-ULP membranes are shown in Figure 77. The surfactant-exposed membrane spectra of both membranes completely separated from the spectra of control membranes. The scores plots of the Hydranautics ESPA2 and the Trisep X-201 RO membranes exposed to Genapol GC-100 are shown in Figure 78. Both sets of detergent-exposed membrane spectra separated from the spectra of the control membranes.

Mega 10

The scores plots of the ATR/FTIR spectra of the Desal CA and the SST TMC/MPD RO membranes exposed to Mega 10 are shown in Figure 79. The spectra of the surfactant-exposed CA membrane only partially separated from the control membrane spectra. The treated spectra of the SST TMC/MPD membrane separated from the control spectra. Scores plots of the ATR/FTIR spectra of the FilmTec BW-30 and Hydranautics LFC3 RO membranes exposed to Mega 10 are shown in Figure 80. Neither surfactant exposed membrane separated from the control set of spectra. Scores plots of the ATR/FTIR spectra of the Koch TFC-HR and TFC-ULP membranes are shown in Figure 81. The surfactant-exposed membrane spectra of both membranes completely separated from the spectra of control membranes. However, one of the control spectra of the FilmTec BW-30 membranes grouped with the surfactant-exposed membrane spectra. The scores plots of the Hydranautics ESPA2 and the Trisep X-201 RO membranes exposed to Mega 10 are shown in Figure 82. The surfactant-treated Hydranautics ESPA2 spectra separated completely from the control membrane spectra. The surfactant-treated Hydranautics ESPA2 spectra also separated from the control spectra. However, the separation was not as great and the one of the control spectra grouped with the test spectra.

Minncare

The scores plots of the ATR/FTIR spectra of the Desal CA RO membranes exposed to Minncare are shown in Figure 83. The spectra of the surfactant-exposed membrane completely separated from the control membrane spectra. Minncare contains oxidizing agents that are not compatible with the CA membrane. Close examination of the ATR/FTIR spectra revealed a significant loss of vibrational bands in the O-H stretching region around 3300 cm^{-1}. However, the membrane was not damaged to the point where significant loss of acetate groups was observed. No data for the SST TMC/MPD membrane is available. Insufficient membrane was available to run this cleaning agent on the TMC/MPD membrane. Scores plots of the ATR/FTIR spectra of the FilmTec BW-30 and Hydranautics LFC3 RO membranes exposed to Minncare are shown in Figure 84. The test spectra of the FilmTec BW-30 membrane separated form the control spectra. The test spectra of the Hydranautics LFC3 membrane separated from the control spectra. However, the line separating the spectra is not as well defined. Two control spectra grouped with the test spectra and one control spectrum grouped with the test spectra. Scores plots of the ATR/FTIR spectra of the Koch TFC-HR and TFC-ULP membranes are shown in Figure 85. The Minncare-treated membrane spectra of the TFC-HR membranes separated from control spectra. However, all the test spectra of the TFC-ULP membrane did not separate from the control spectra. Nine Minncare-treated membrane grouped together away from the remaining test and control spectra. This may indicate that some areas on the membrane surface remained unaffected by exposure to the oxidizing cleaning agent. The scores plots of the Hydranautics ESPA2 and the Trisep X-201 RO membranes exposed to Minncare are shown in Figure 86. Both sets of membrane spectra separated from the control spectra. However, one test spectrum grouped with the control spectra.

Nonylglucopyranoside

The scores plots of the ATR/FTIR spectra of the Desal CA and the SST TMC/MPD RO membranes exposed to nonylglucopyranoside are shown in Figure 87. The spectra of the surfactant-exposed CA membrane separated from the control spectra but two of the test spectra grouped with the control. The surfactant-treated spectra of SST TMC/MPD completely separated from the control spectra. Scores plots of the ATR/FTIR spectra of the FilmTec BW-30 and Hydranautics LFC3 RO membranes exposed to nonylglucopyranoside are shown in Figure 88. The surfactant-exposed FilmTec BW-30 spectra did not separate from the control set of spectra. Three-D plot of factors 1, 2, and 3 reveal the separation between the test and control spectra. Scores plots of the ATR/FTIR spectra of the Koch TFC-HR and TFC-ULP membranes are shown in Figure 89. The surfactant-exposed membrane spectra of both membranes completely separated from the spectra of control membranes. The TFC-ULP data were plotted in 3-D in order to visualize the separation. The scores plots of the Hydranautics ESPA2 and the Trisep X-201 RO membranes exposed to nonylglucopyranoside are shown in Figure 90. The surfactant-exposed membrane spectra of Hydranautics ESPA2 separated from the spectra of the control membranes.

Protease

The scores plots of the ATR/FTIR spectra of the Desal CA RO membranes exposed to protease are shown in Figure 91. The spectra of the surfactant-exposed membrane completely separated from the control membrane spectra. Proteases are enzymatic proteins. Proteins are known to readily adsorb on the polymer surfaces. Therefore, a strong association and alteration of the infrared spectra of the membrane could be expected. No data for the SST TMC/MPD membrane is available. Insufficient membrane was available to run this cleaning agent on the TMC/MPD membrane. Scores plots of the ATR/FTIR spectra of the FilmTec BW-30 and Hydranautics LFC3 RO membranes exposed to protease are shown in Figure 92. It was necessary to plot factors 1, 2, and 3 in order to get the protease-treated FilmTec BW-30 membrane spectra to separate from the control spectra. The test and control spectra of the Hydranautics LFC3 membrane did not separation. There were some differences in the spectra but not enough to for them to be separated. Scores plots of the ATR/FTIR spectra of the Koch TFC-HR and TFC-ULP membranes are shown in Figure 93. The surfactant-exposed membrane spectra of both membranes completely separated from the spectra of control membranes. The scores plots of the Hydranautics ESPA2 and the Trisep X-201 RO membranes exposed to protease are shown in Figure 94. A plot of the scores of factors 1, 2, and 3 of the protease-treated Hydranautics ESPA2 membrane spectra reveal separation from the control spectra. The protease-exposed membrane spectra of the Trisep X-201 spectra separated from the spectra of the control membranes. However, two of the test spectra grouped with the control spectra.

Sodium Dodecylsulfate (SDS)

The scores plots of the ATR/FTIR spectra of the Desal CA and the SST TMC/MPD RO membranes exposed to sodium dodecylsulfate (SDS) are shown in Figure 95. The spectra from both surfactant-exposed membranes separated from the control membrane spectra. Scores plots of the ATR/FTIR spectra of the FilmTec BW-30 and Hydranautics LFC3 RO membranes exposed to SDS are shown in Figure 96. Neither surfactant exposed membrane separated from the control set of spectra. In both cases there appeared to be a line or plane of separation between a majority of the data points, but in both cases a few test or control spectra wound up grouped across the line. Scores plots of the ATR/FTIR spectra of the Koch TFC-HR and TFC-ULP membranes are shown in Figure 97. The SDS-exposed membrane spectra of the TFC-HR membranes completely separated from the spectra of control membranes. The test-spectra of the TFC-ULP spectra separated from the control spectra. However, on control spectrum grouped with the test spectra. The scores plots of the Hydranautics ESPA2 and the Trisep X-201 RO membranes exposed to SDS are shown in Figure 98. The detergent-exposed Hydranautics ESPA2 membrane spectra separated from the control spectra. The SDS-treated Trisep X-201 spectra did not completely separate from the control spectra. Two SDS-treated membrane spectra grouped with the control spectra and one control spectrum grouped with the test spectra.

Sodium Tripolyphosphate (STP)

The scores plots of the ATR/FTIR spectra of the Desal CA and the SST TMC/MPD RO membranes exposed to sodium tripolyphosphate are shown in Figure 99. Both sets of membrane test spectra separated from the control membrane spectra. Scores plots of the ATR/FTIR spectra of the FilmTec BW-30 and Hydranautics LFC3 RO membranes exposed to STP are shown in Figure 100. The STP-treated FilmTec BW-30 membrane spectra did not separate from the control set of spectra. A grouping of many of the treated spectra existed but the spectra did not completely separate from the control spectra. The STP-treated spectra of the Hydranautics LFC3 membrane separated from the control set of membrane spectra. However, one on the test spectra grouped with the control spectra. Scores plots of the ATR/FTIR spectra of the Koch TFC-HR and TFC-ULP membranes are shown in Figure 101. The surfactant-exposed membrane spectra of both membranes separated from the spectra of control membranes. However, one of the STP-treated membrane spectra of the TFC-ULP membrane grouped with the control spectra. The scores plots of the Hydranautics ESPA2 and the Trisep X-201 RO membranes exposed to STP are shown in Figure 102. The STP-treated Hydranautics ESPA2 spectra completely separated from the control spectra. The test spectra of the Trisep X-201 membrane did not completely separate from the control spectra. Two STP-treated spectra grouped with the control set and one control grouped with the test set.

Triton X-100

The scores plots of the ATR/FTIR spectra of the Desal CA and the SST TMC/MPD RO membranes exposed to Triton X-100 are shown in Figure 103. Both sets of surfactant-

exposed membrane spectra completely separated from the control membrane spectra suggesting a strong interaction of the surfactant with the membrane. Scores plots of the ATR/FTIR spectra of the FilmTec BW-30 and Hydranautics LFC3 RO membranes exposed to Triton X-100 are shown in Figure 104. Neither surfactant exposed membrane separated from the control set of spectra. The FilmTec BW-30 grouped together to some extent but did not completely separate from the control spectra. Scores plots of the ATR/FTIR spectra of the Koch TFC-HR and TFC-ULP membranes are shown in Figure **105**. The surfactant-exposed Koch TFC-HR membrane spectra separated from the control spectra but the surfactant-treated Koch TFC-ULP membrane did not. The scores plots of the Hydranautics ESPA2 and the Trisep X-201 RO membranes exposed to Triton X-100 are shown in Figure 106. Both sets of detergent-exposed membrane spectra separated from the spectra of the control membranes.

Tween 20

The scores plots of the ATR/FTIR spectra of the Desal CA and the SST TMC/MPD RO membranes exposed to Tween 20 are shown in Figure 107. Both sets of spectra of the surfactant-exposed membranes completely separated from the control membrane spectra suggesting a strong interaction of the surfactant with the membrane. Scores plots of the ATR/FTIR spectra of the FilmTec BW-30 and Hydranautics LFC3 RO membranes exposed to Tween 20 are shown in Figure 108. The surfactant-treated spectra of the FilmTec BW-30 completely separated from the control set of spectra. The Tween 20-treated spectra of the Hydranautics LFC3 membrane did not separate from the control spectra. Scores plots of the ATR/FTIR spectra of the Koch TFC-HR and TFC-ULP membranes are shown in Figure 109. The surfactant-exposed membrane spectra of both membranes separated from the spectra of control membranes. However, one of the control spectra grouped with the surfactant-treated spectra of the control spectra. The scores plots of the Hydranautics ESPA2 and the Trisep X-201 RO membranes exposed to Tween 20 are shown in Figure 110. Both sets of detergent-exposed membrane spectra completely separated from the spectra of the control membranes.

Zosteric acid

The scores plots of the ATR/FTIR spectra of the Desal CA and the SST TMC/MPD RO membranes exposed to zosteric acid are shown in Figure 111. The spectra of the surfactant-exposed membrane separated from the control membrane. However, in both cases one test spectrum grouped with the control spectra. Scores plots of the ATR/FTIR spectra of the FilmTec BW-30 and Hydranautics LFC3 RO membranes exposed to zosteric acid are shown in Figure 112. The treated FilmTec BW-30 did not quite separate from the control membranes. Two of the control membrane spectra grouped with the test spectra and one of the test spectra grouped with the control spectra. The zosteric acid-treated Hydranautics LFC3 spectra did not separate from the control spectra. Scores plots of the ATR/FTIR spectra of the Koch TFC-HR and TFC-ULP membranes are shown in Figure 113. The zosteric acid –treated Koch TFC-HR membrane spectra completely separated from the control membrane spectra. However, the test spectra of the Koch TFC-ULP spectra did not separate from the control spectra. The scores plots of the

Hydranautics ESPA2 and the Trisep X-201 RO membranes exposed to zosteric acid are shown in Figure 114. Both sets of membrane test spectra separated from the spectra of the controls.

Zwittergent 3-16

The scores plots of the ATR/FTIR spectra of the Desal CA and the SST TMC/MPD RO membranes exposed to Zwittergent 3-16 are shown in Figure 115. The spectra of the surfactant-exposed membrane completely separated from the control membrane spectra suggesting a strong interaction of the surfactant with the membrane. Scores plots of the ATR/FTIR spectra of the FilmTec BW-30 and Hydranautics LFC3 RO membranes exposed to Zwittergent 3-16 are shown in Figure 116. Neither surfactant exposed membrane separated from the control set of spectra. Scores plots of the ATR/FTIR spectra of the Koch TFC-HR and TFC-ULP membranes are shown in Figure 117. The surfactant-exposed membrane spectra of both membranes completely separated from the spectra of control membranes. The scores plots of the Hydranautics ESPA2 and the Trisep X-201 RO membranes exposed to Zwittergent 3-16 are shown in Figure 118. Both sets of detergent-exposed membrane spectra separated from the spectra of the control membranes.

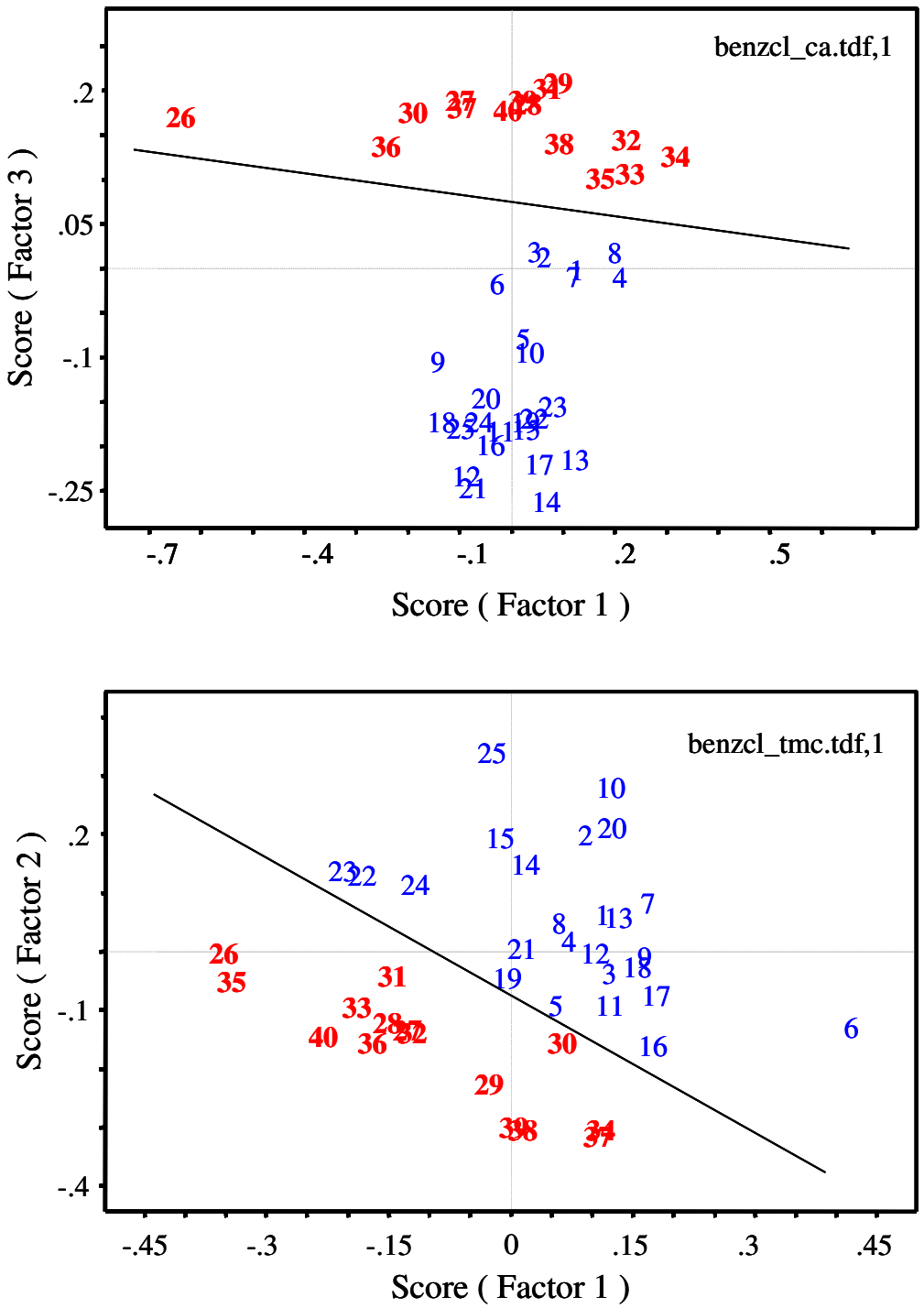

Figure 35. PCA scores plots of the IR spectra of Desal CA (top) and SST TMC/MPD (bottom) RO membrane exposed to benzalkonium chloride (26-40) and 1,000-ppm NaCl feedwater control (1-25).

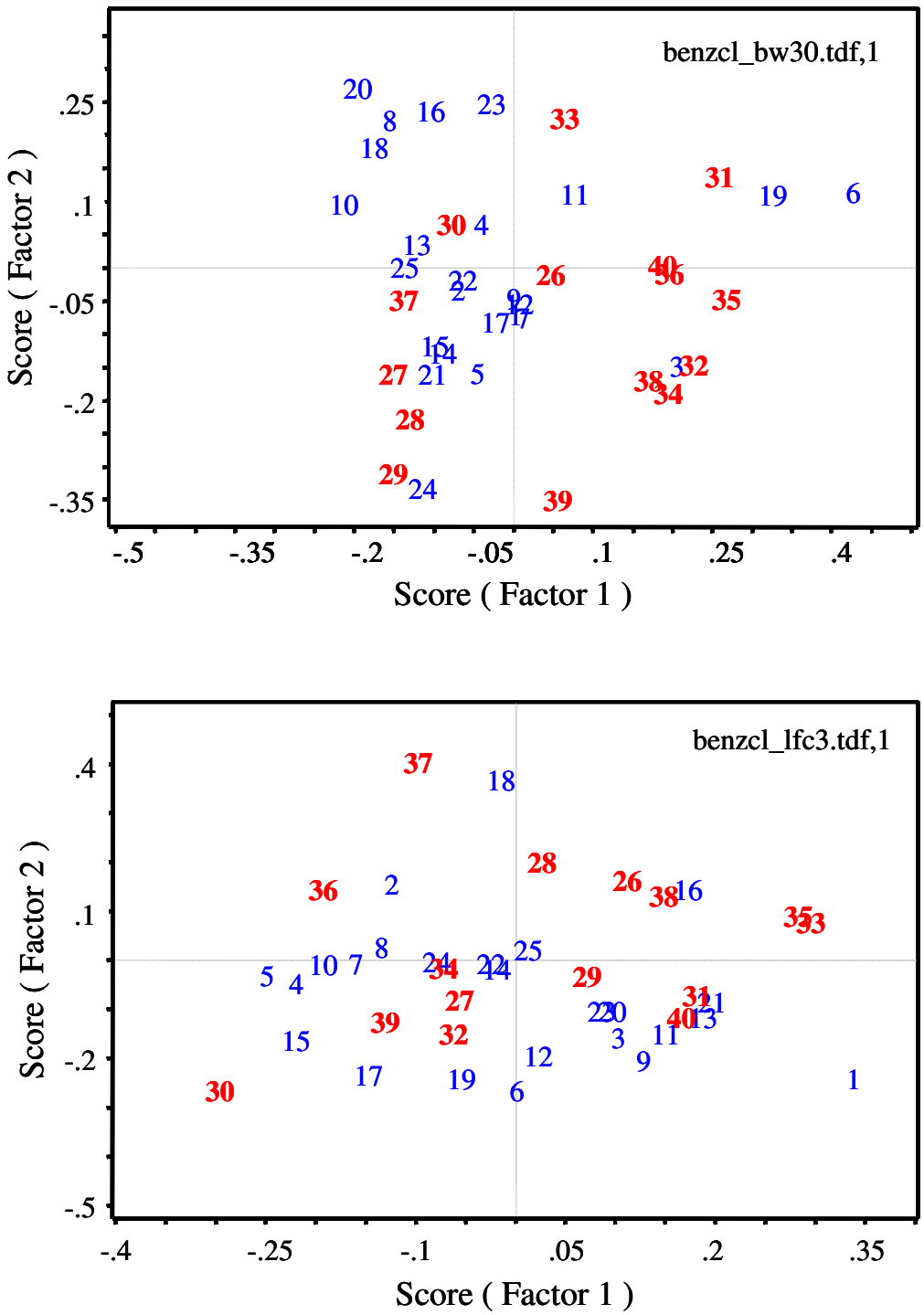

Figure 36. PCA scores plots of the IR spectra of FilmTec BW-30 (top) and Hydranautics LFC3 (bottom) RO membrane exposed to benzalkonium chloride (26-40) and 1,000-ppm NaCl feedwater control (1-25).

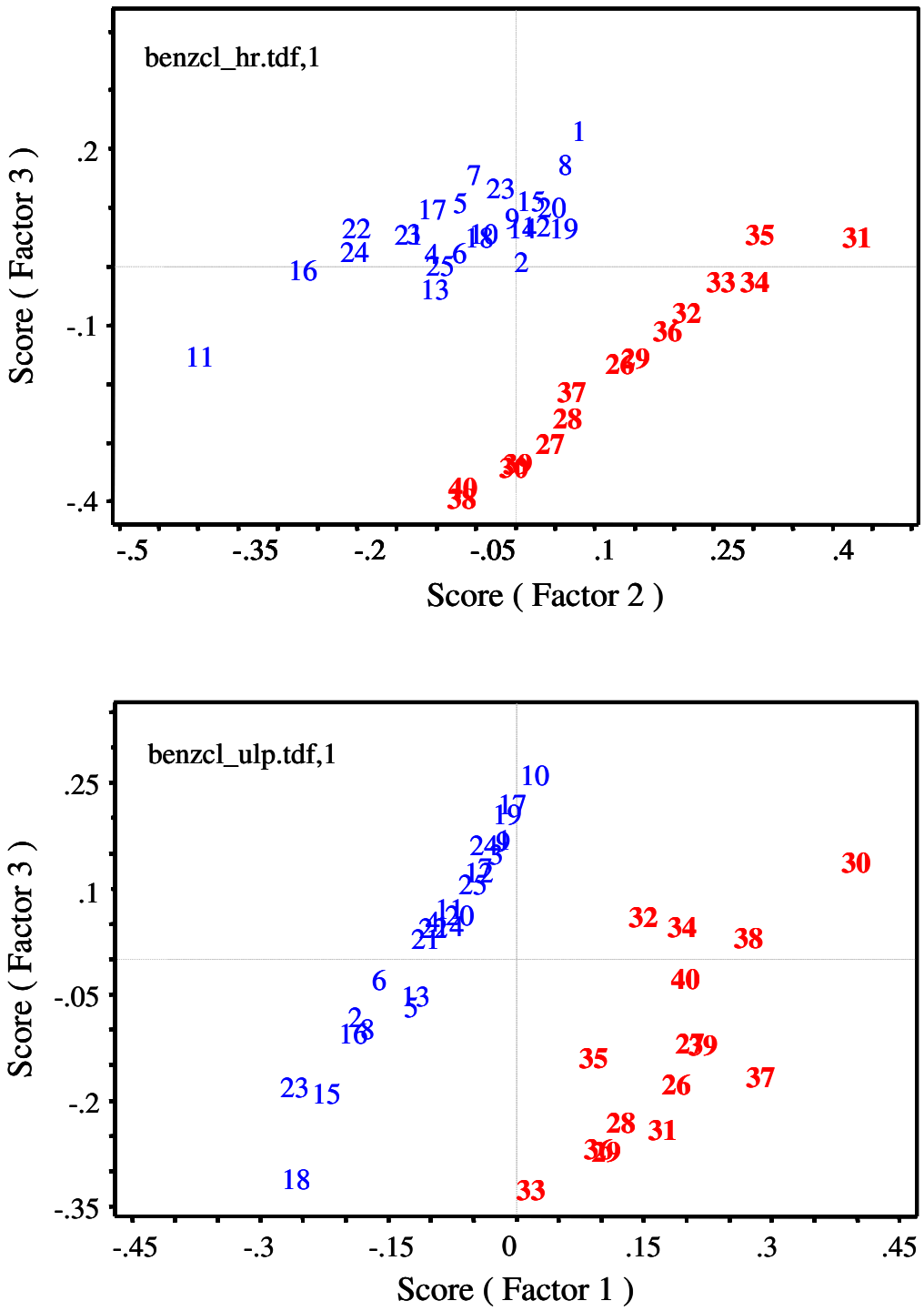

Figure 37. PCA scores plots of the IR spectra of Koch TFC-HR (top) and TFC-ULP (bottom) RO membrane exposed to benzalkonium chloride (26-40) and 1,000-ppm NaCl feedwater control (1-25).

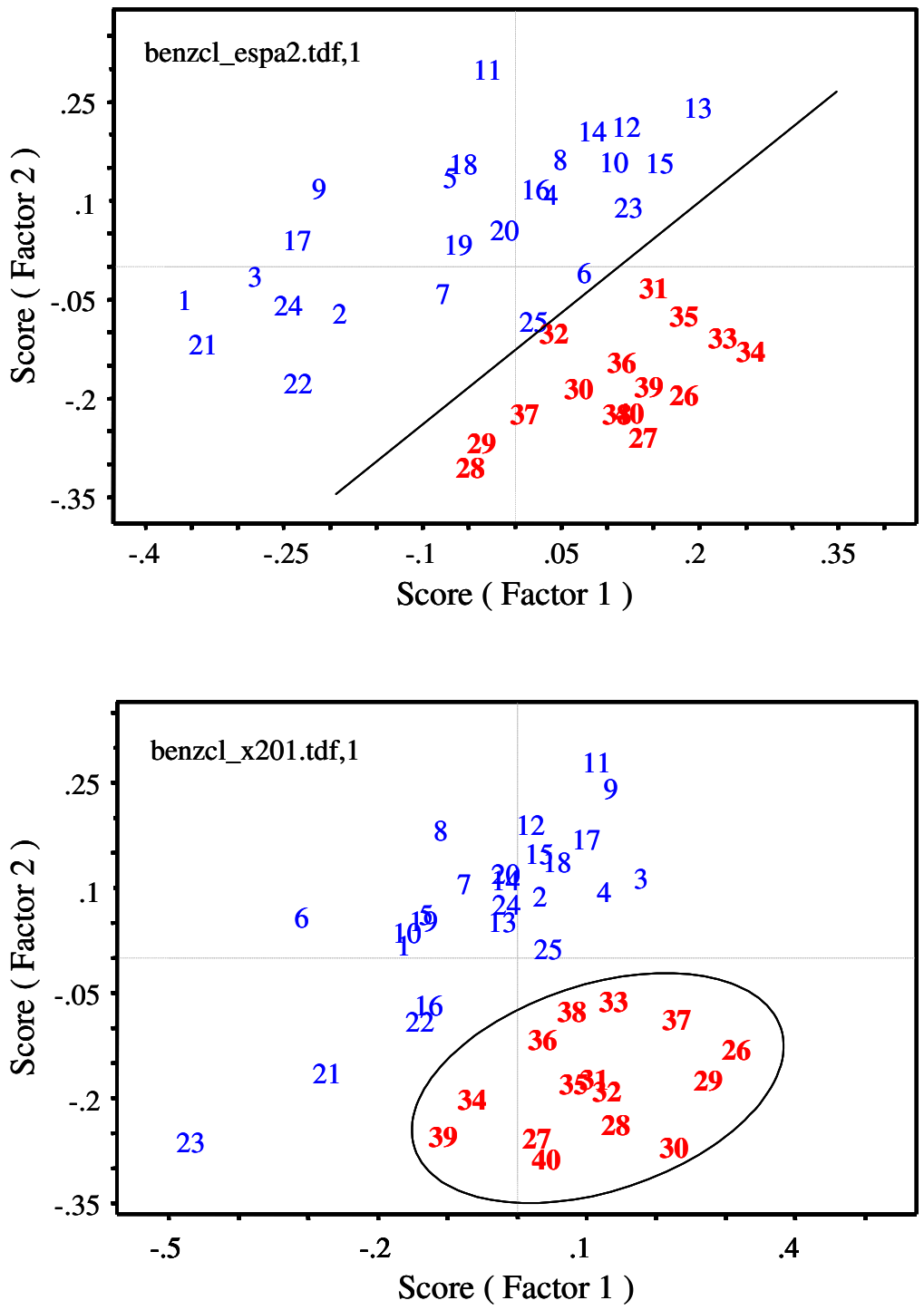

Figure 38. PCA scores plots of the IR spectra of Hydranautics ESPA2 (top) and Trisep X-201 (bottom) RO membrane exposed to benzalkonium chloride (26-40) and 1,000-ppm NaCl feedwater control (1-25).

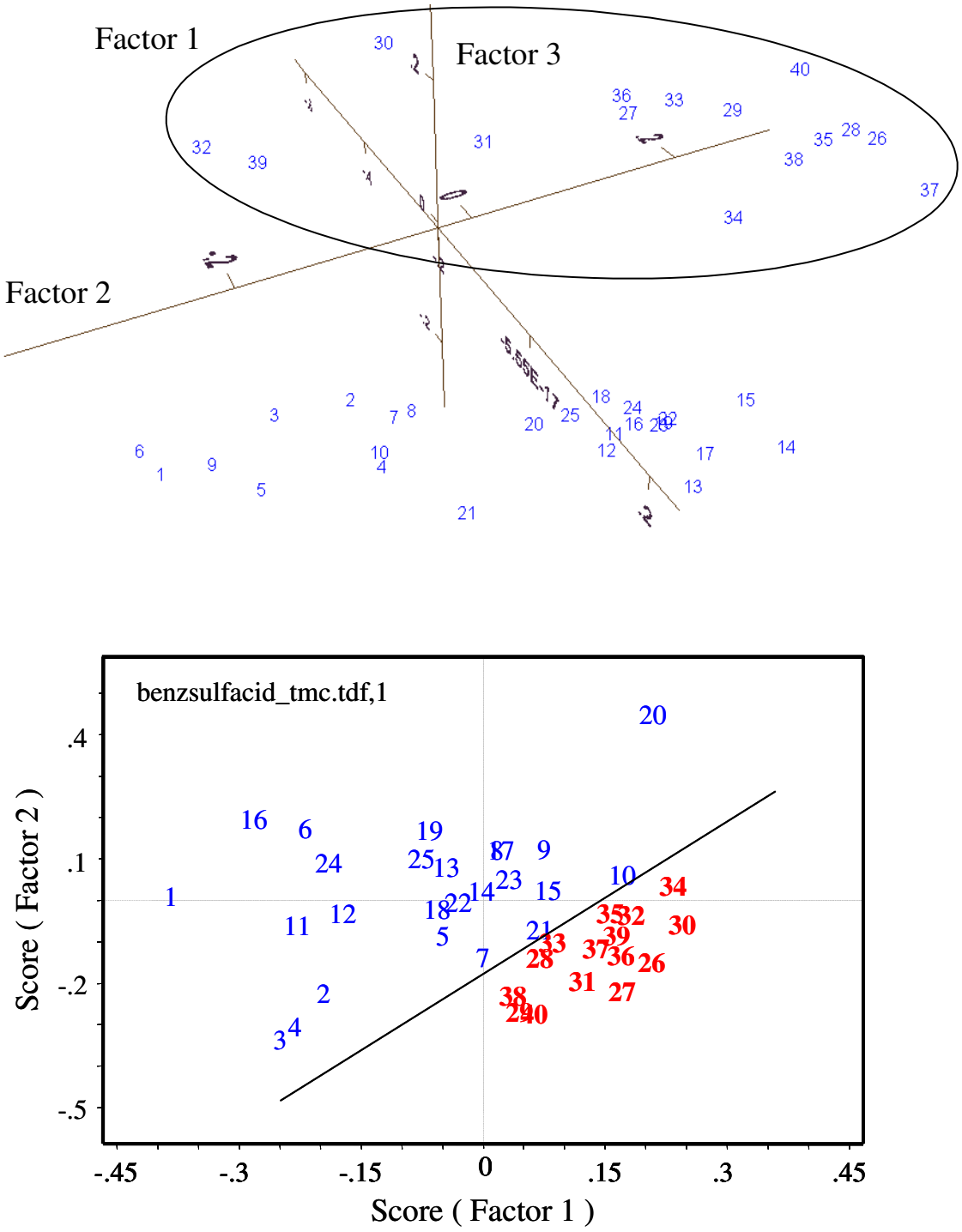

Figure 39. PCA scores plots of the IR spectra of Desal CA (top) and SST TMC/MPD (bottom) RO membrane exposed to benzenesulfonic acid (26-40) and 1,000-ppm NaCl feedwater control (1-25).

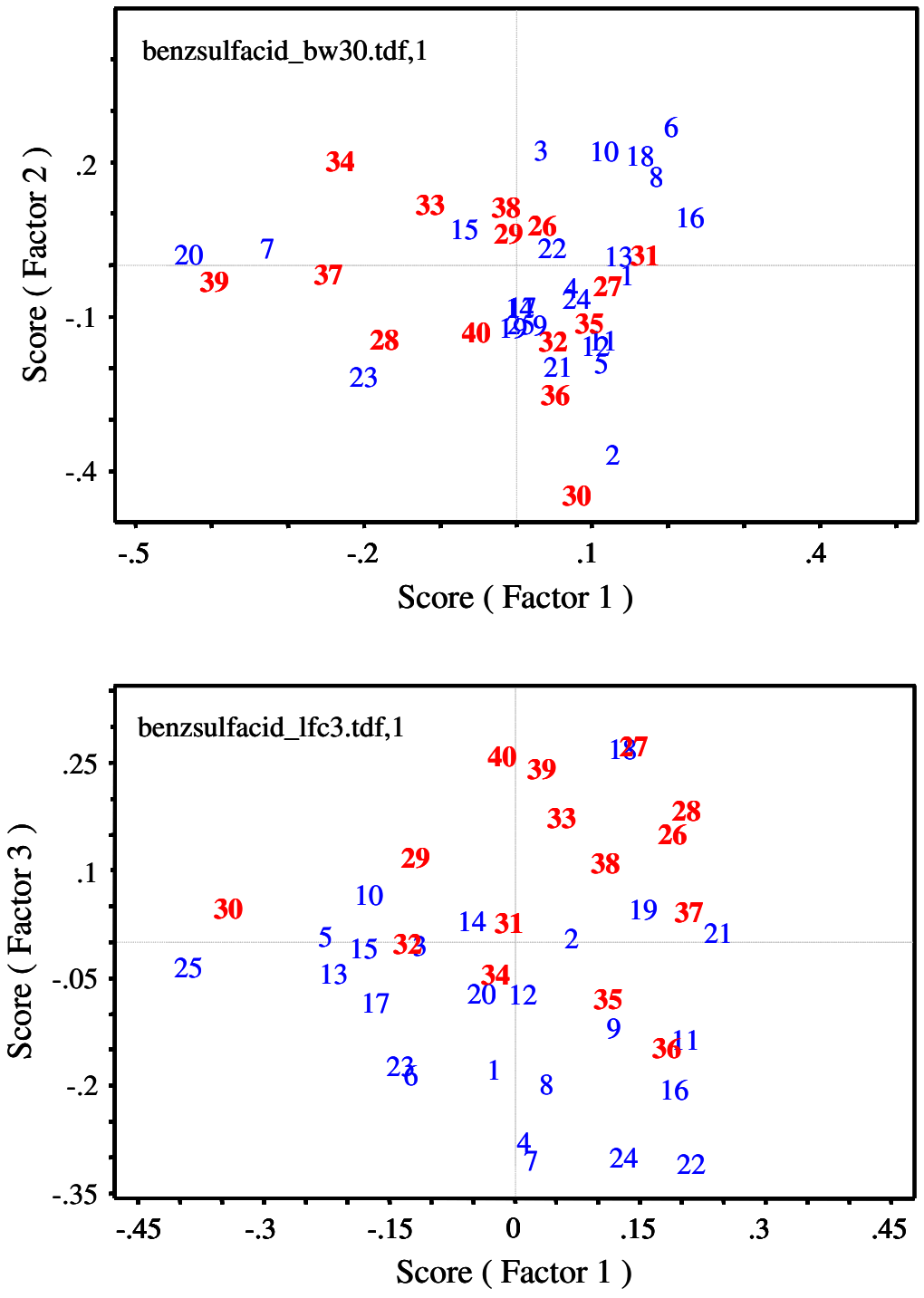

Figure 40. PCA scores plots of the IR spectra of FilmTec BW-30 (top) and Hydranautics LFC3 (bottom) RO membrane exposed to benzenesulfonic acid (26-40) and 1,000-ppm NaCl feedwater control (1-25).

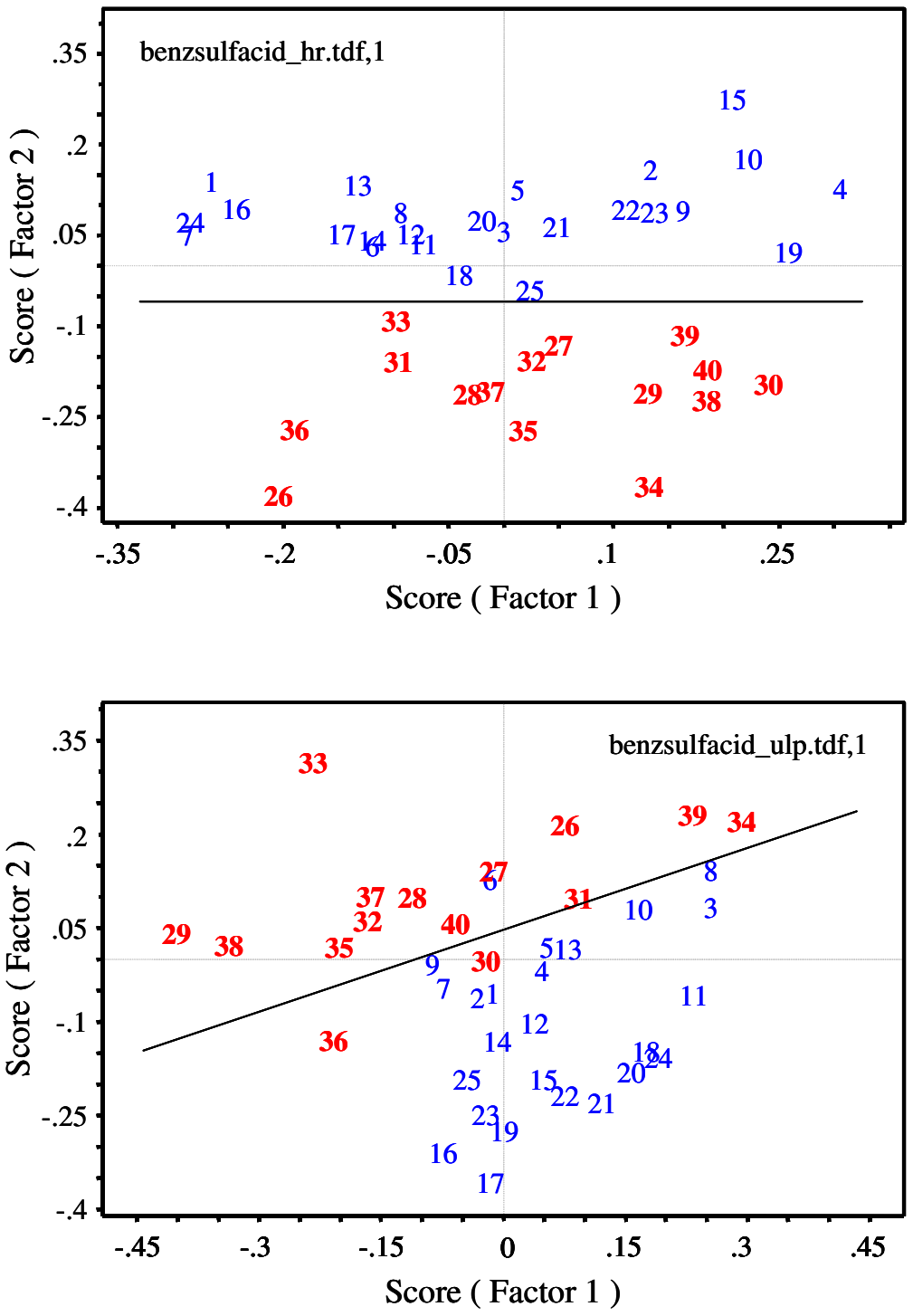

Figure 41. PCA scores plots of the IR spectra of Koch TFC-HR (top) and TFC-ULP (bottom) RO membrane exposed to benzenesulfonic acid (26-40) and 1,000-ppm NaCl feedwater control (1-25).

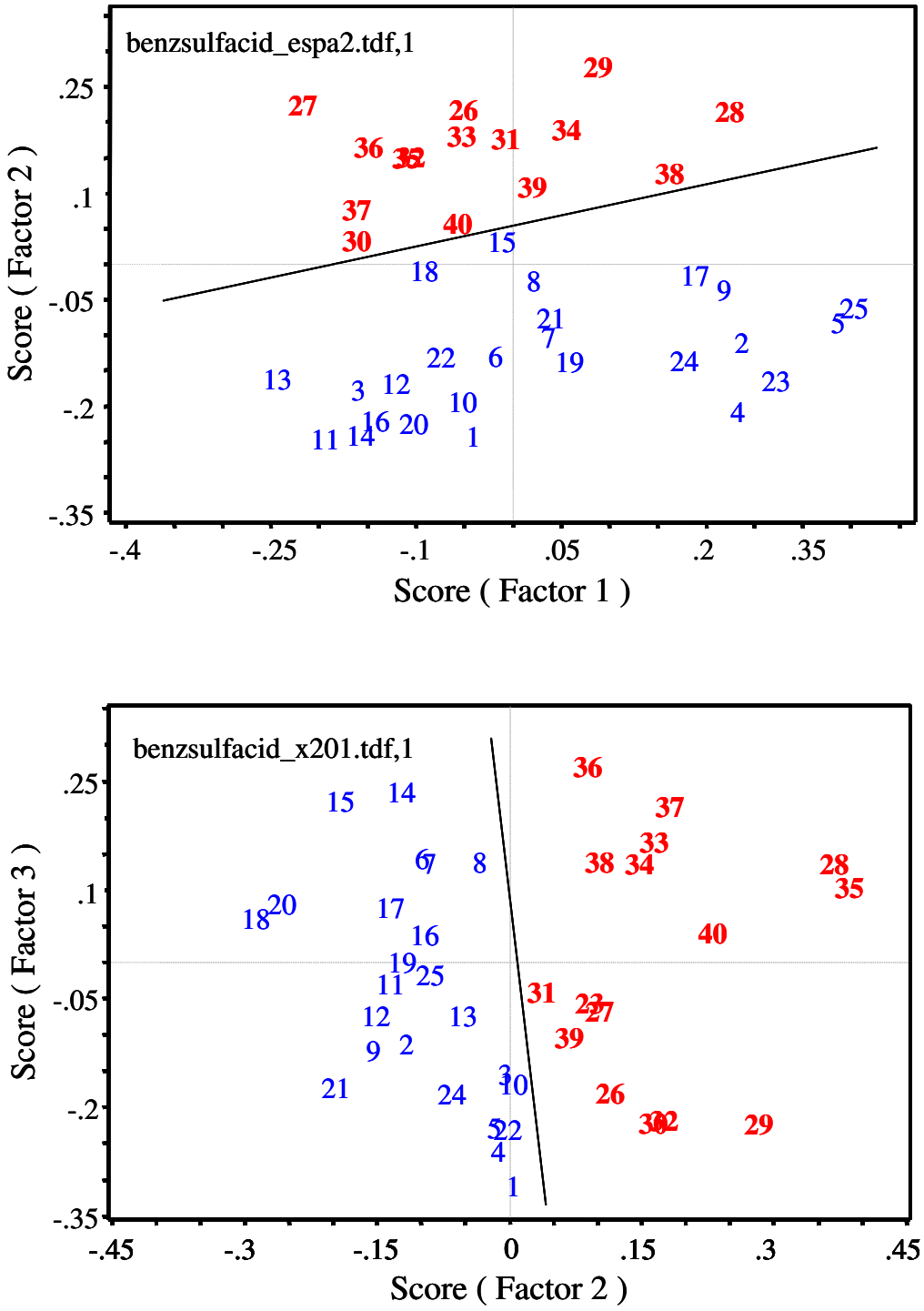

Figure 42. PCA scores plots of the IR spectra of Hydranautics ESPA2 (top) and Trisep X-201 (bottom) RO membrane exposed to benzenesulfonic acid (26-40) and 1,000-ppm NaCl feedwater control (1-25).

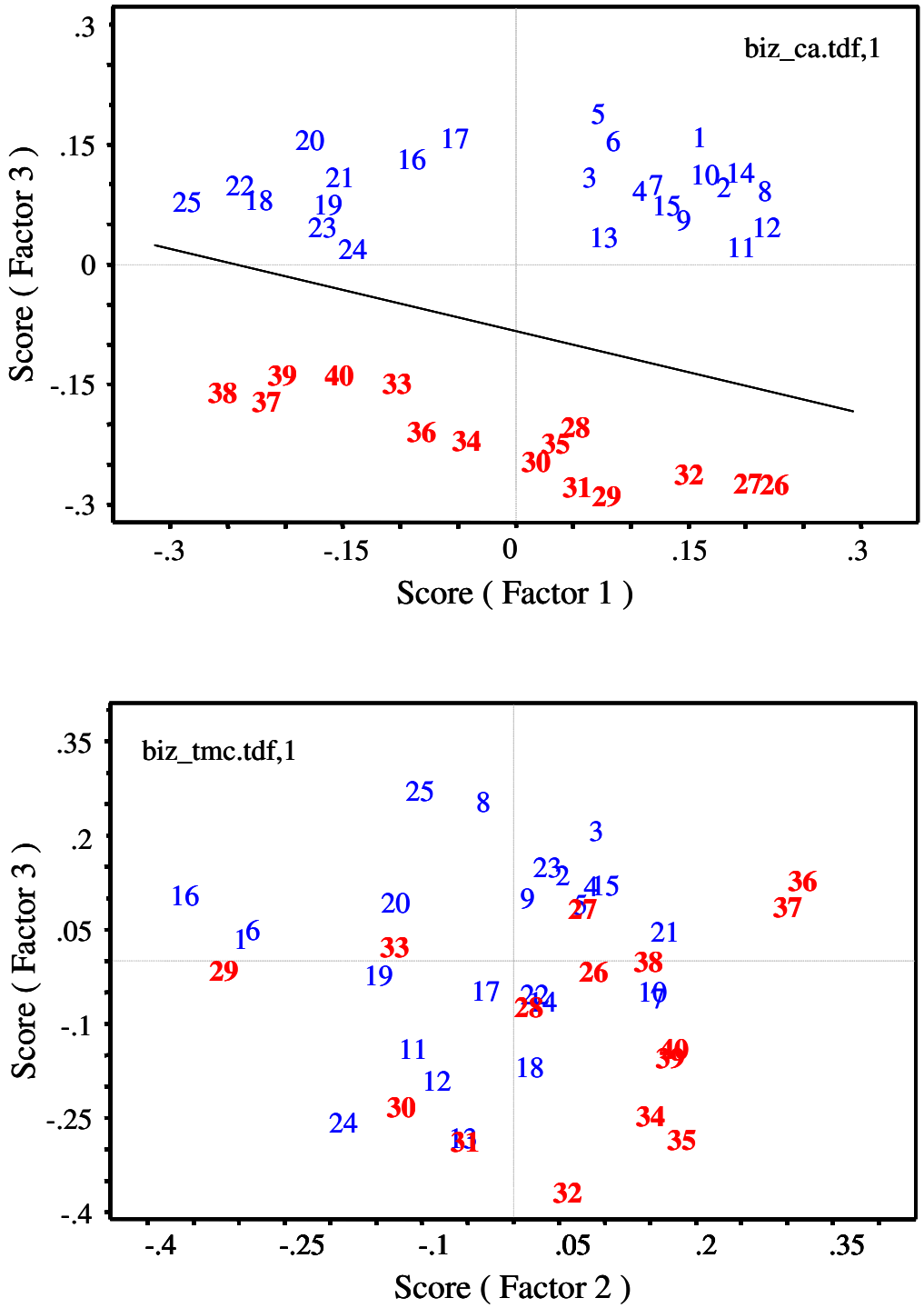

Figure 43. PCA scores plots of the IR spectra of Desal CA and SST TMC/MPD RO membrane exposed to Biz detergent (26-40) and 1,000-ppm NaCl feedwater control (1-25).

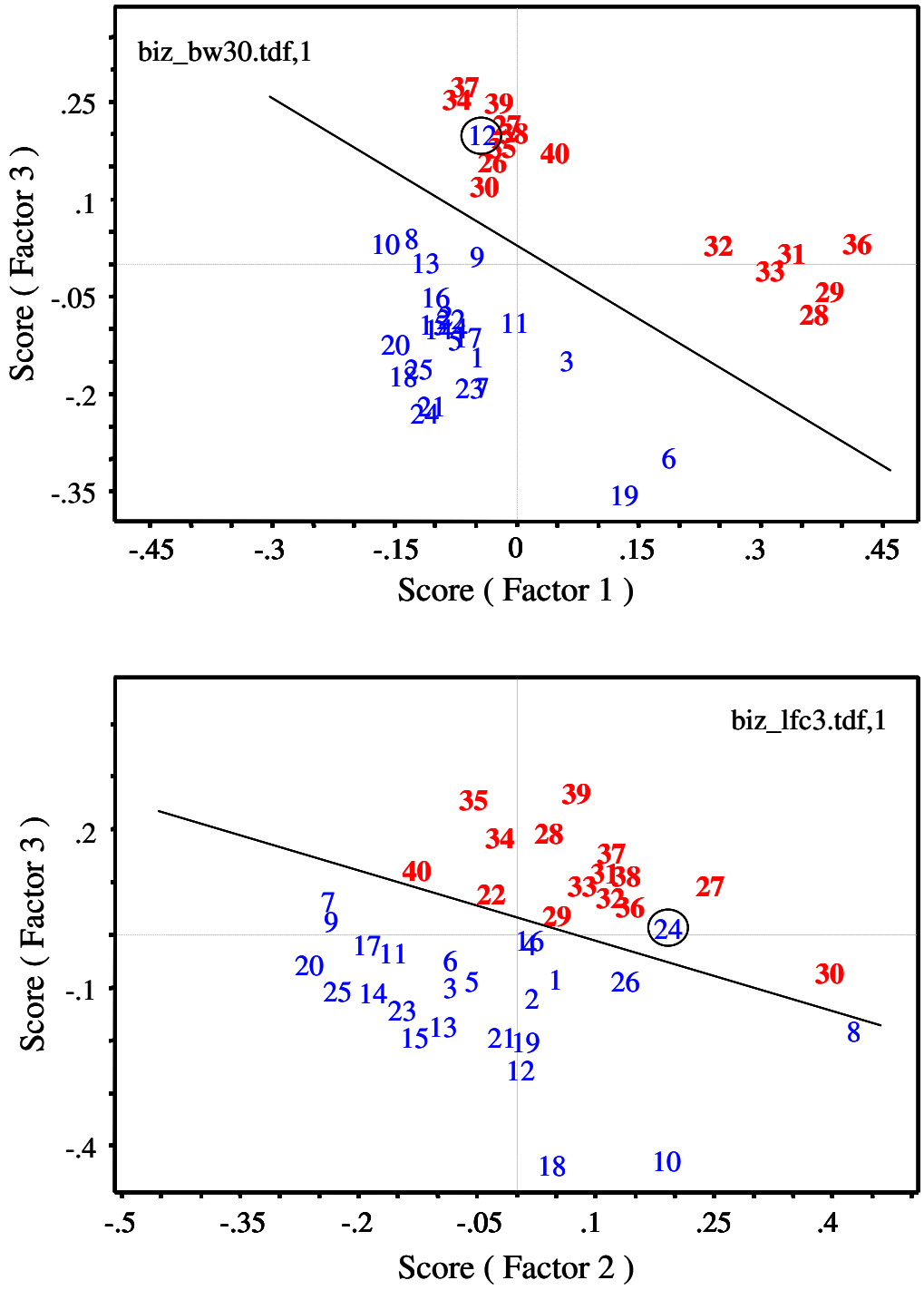

Figure 44. PCA scores plots of the IR spectra of FilmTec BW-30 (top) and Hydranautics LFC3 (bottom) RO membrane exposed to Biz detergent (26-40) and 1,000-ppm NaCl feedwater control (1-25).

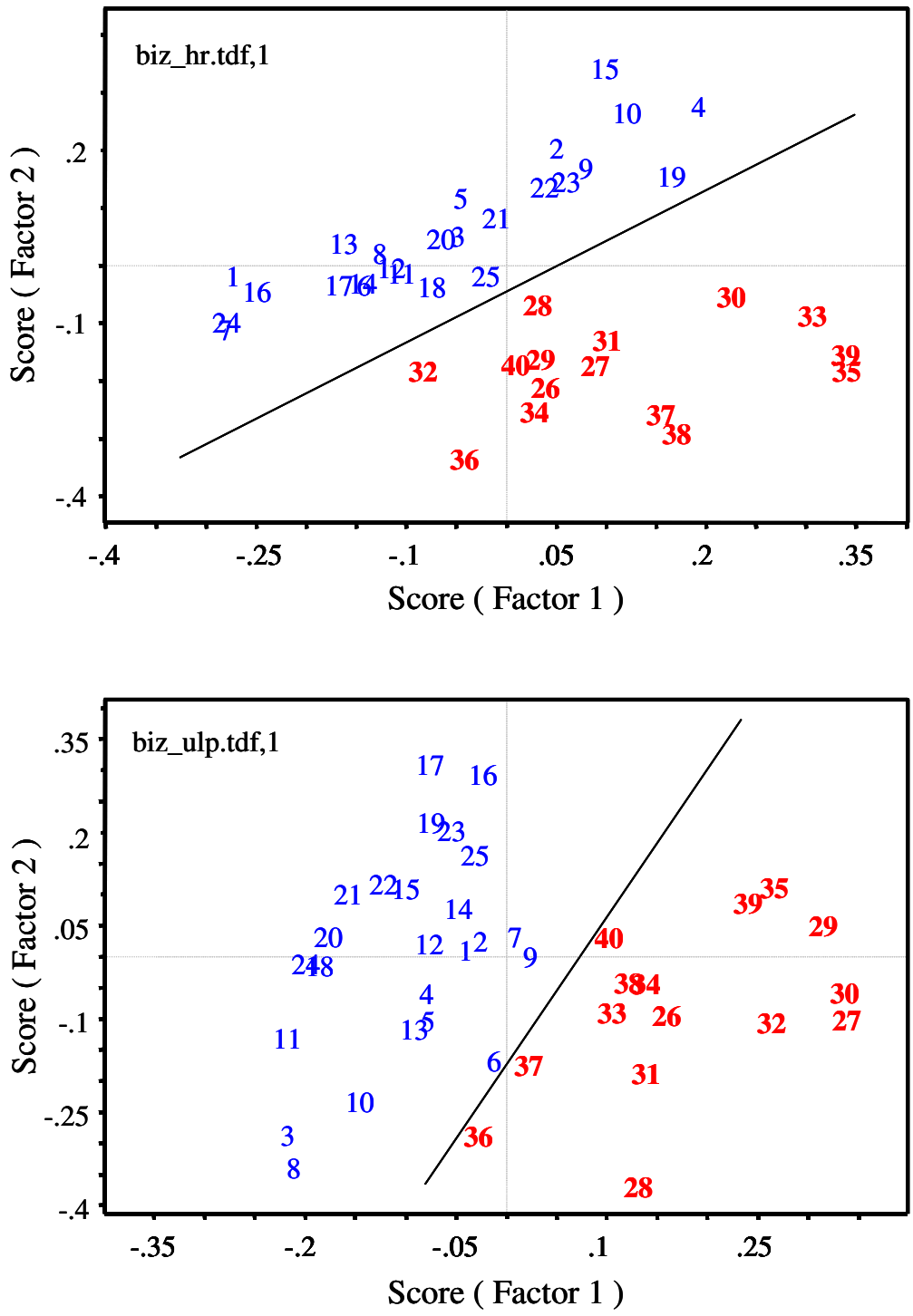

Figure 45. PCA scores plots of the IR spectra of Koch TFC-HR (top) and TFC-ULP (bottom) RO membrane exposed to Biz detergent (26-40) and 1,000-ppm NaCl feedwater control (1-25).

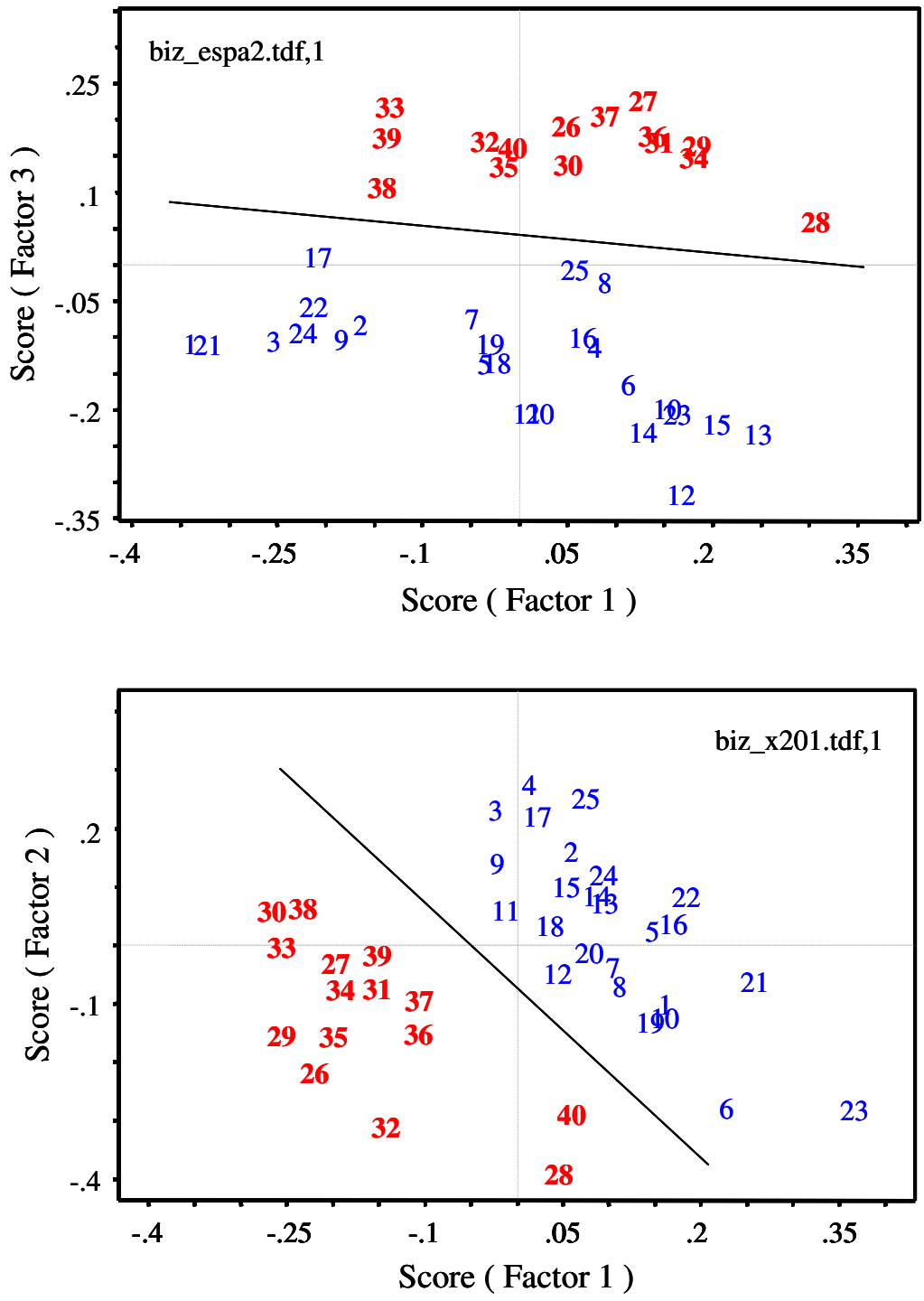

Figure 46. PCA scores plots of the IR spectra of Hydranautics ESPA2 (top) and Trisep X-201 (bottom) RO membrane exposed to Biz detergent (26-40) and 1,000-ppm NaCl feedwater control (1-25).

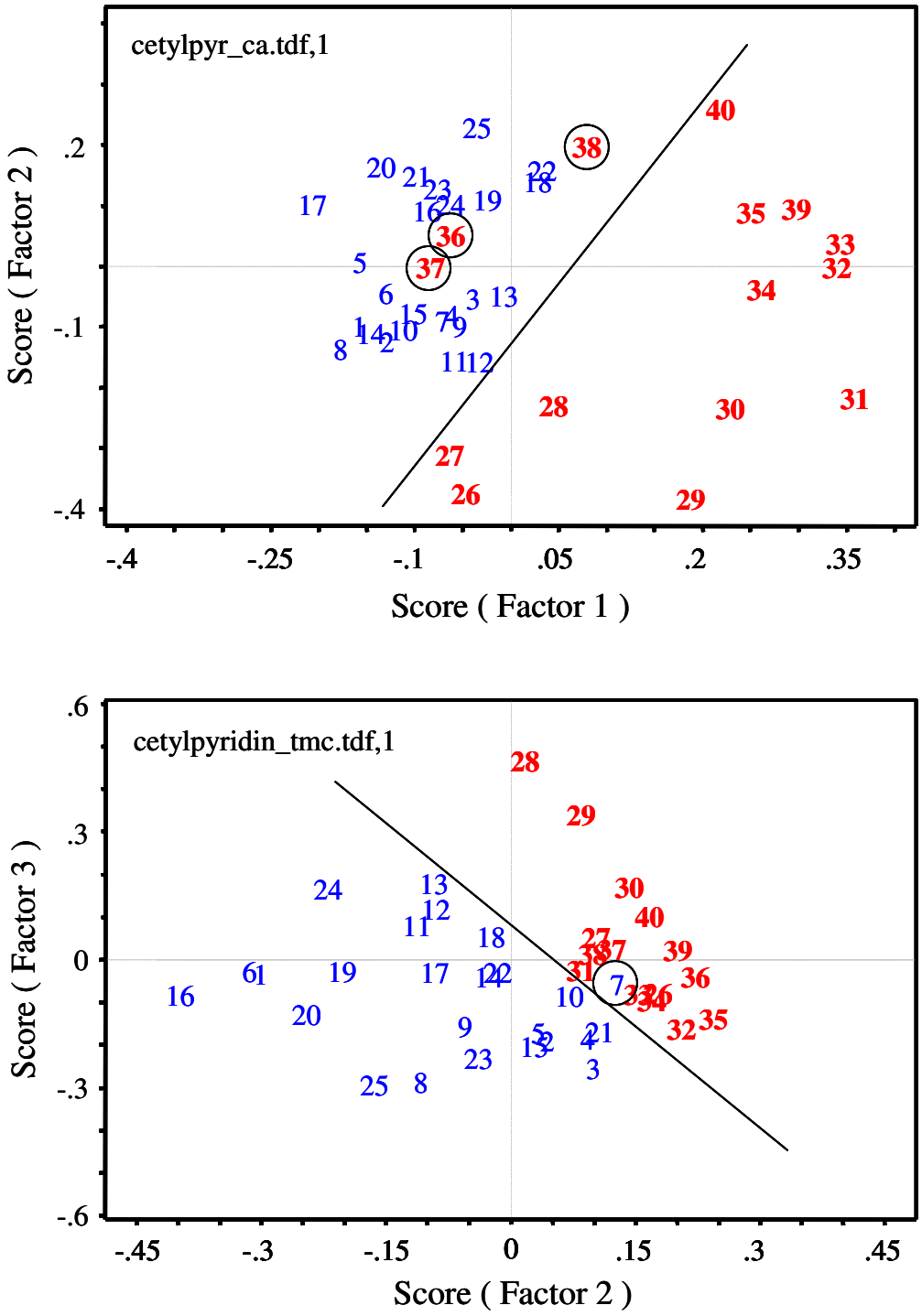

Figure 47. PCA scores plots of the IR spectra of Desal CA and SST TMC/MPD RO membrane exposed to cetylpyridinium chloride (26-40) and 1,000-ppm NaCl feedwater control (1-25).

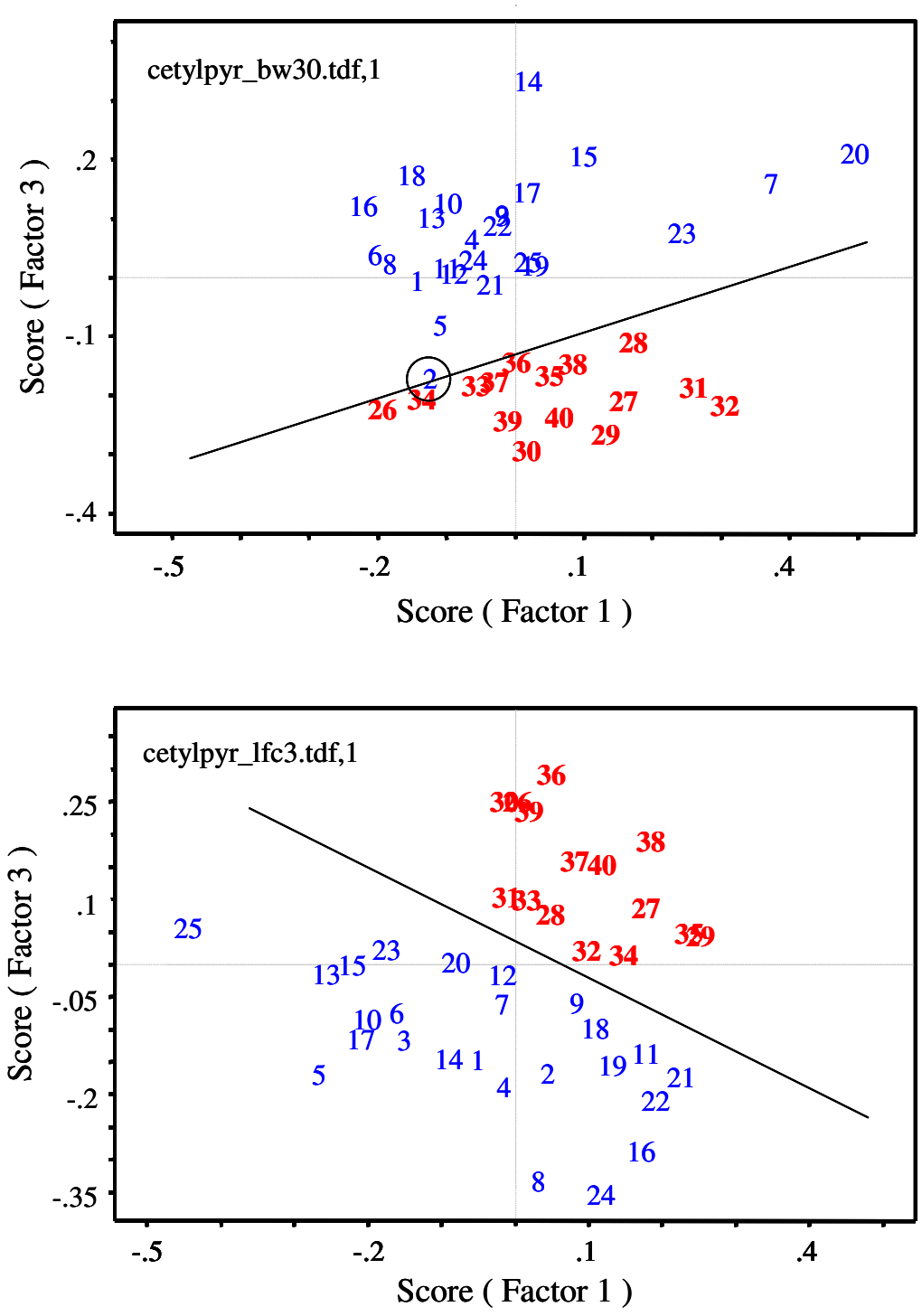

Figure 48. PCA scores plots of the IR spectra of FilmTec BW-30 (top) and Hydranautics LFC3 (bottom) RO membrane exposed to cetylpyridinium chloride (26-40) and 1,000-ppm NaCl feedwater control (1-25).

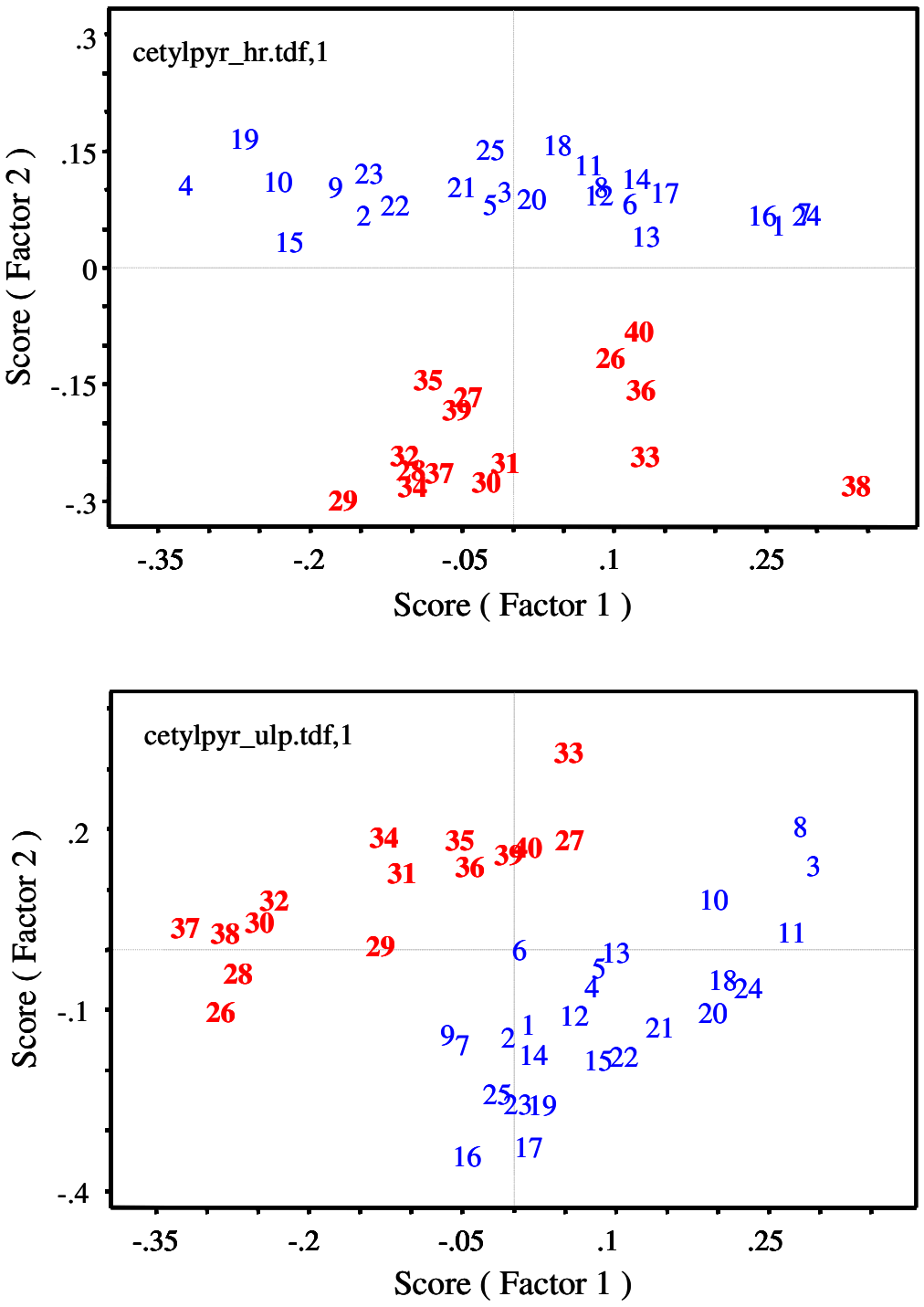

Figure 49. PCA scores plots of the IR spectra of Koch TFC-HR (top) and TFC-ULP (bottom) RO membrane exposed to cetylpyridinium chloride (26-40) and 1,000-ppm NaCl feedwater control (1-25).

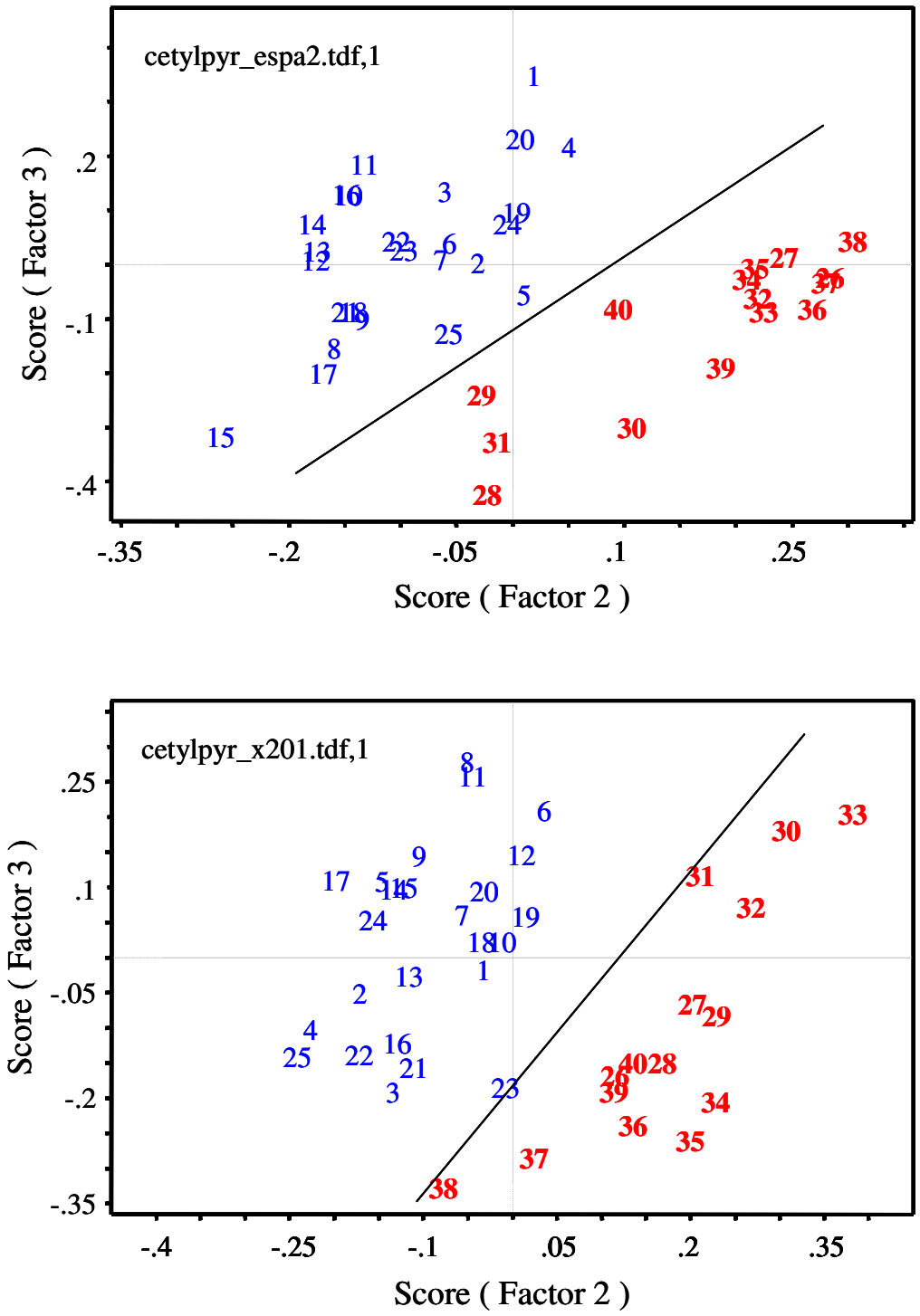

Figure 50. PCA scores plots of the IR spectra of Hydranautics ESPA2 (top) and Trisep X-201 (bottom) RO membrane exposed to cetylpyridinium chloride (26-40) and 1,000-ppm NaCl feedwater control (1-25).

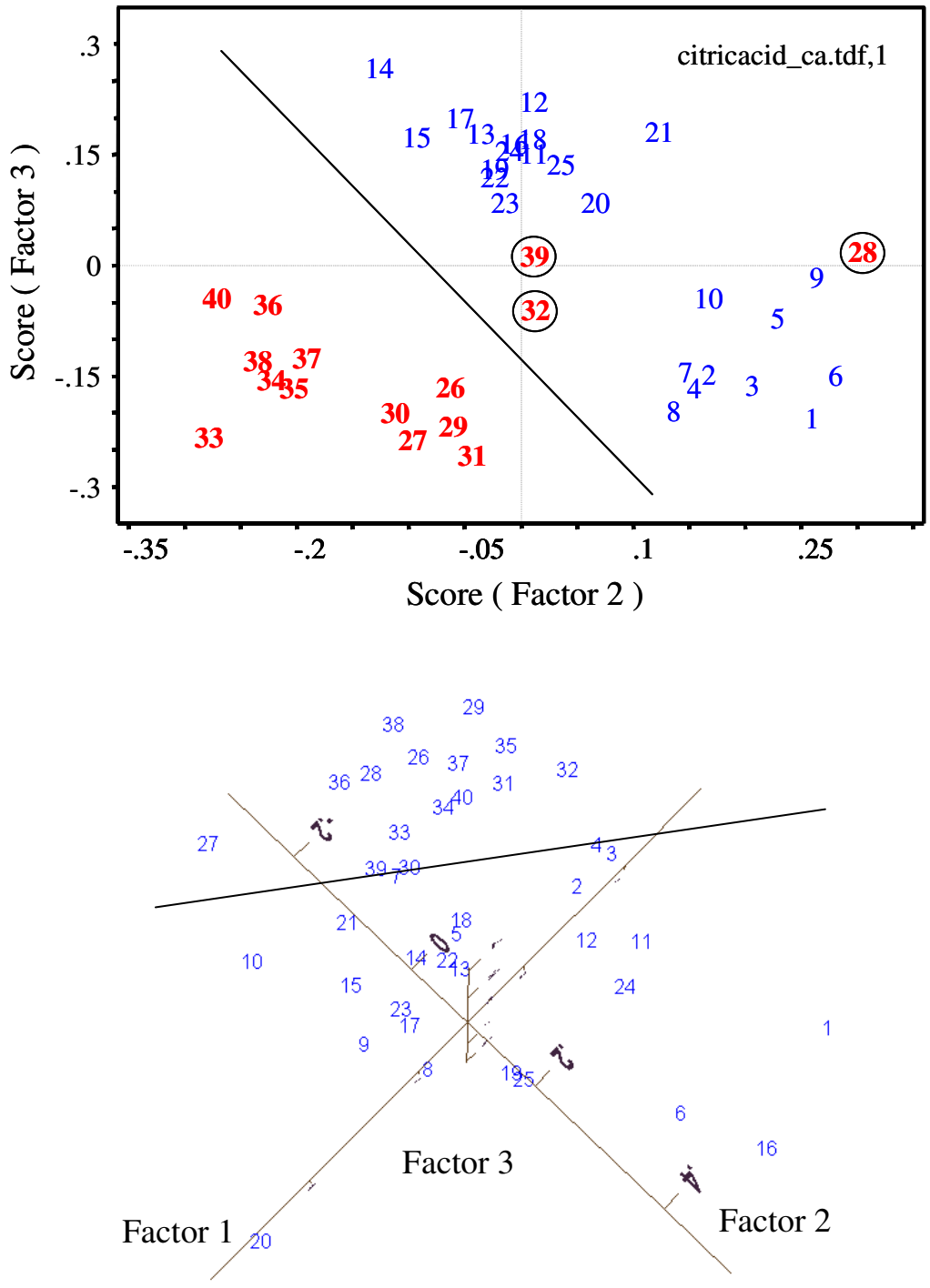

Figure 51. PCA scores plots of the IR spectra of Desal CA and SST TMC/MPD RO membrane exposed to citric acid (26-40) and 1,000-ppm NaCl feedwater control (1-25).

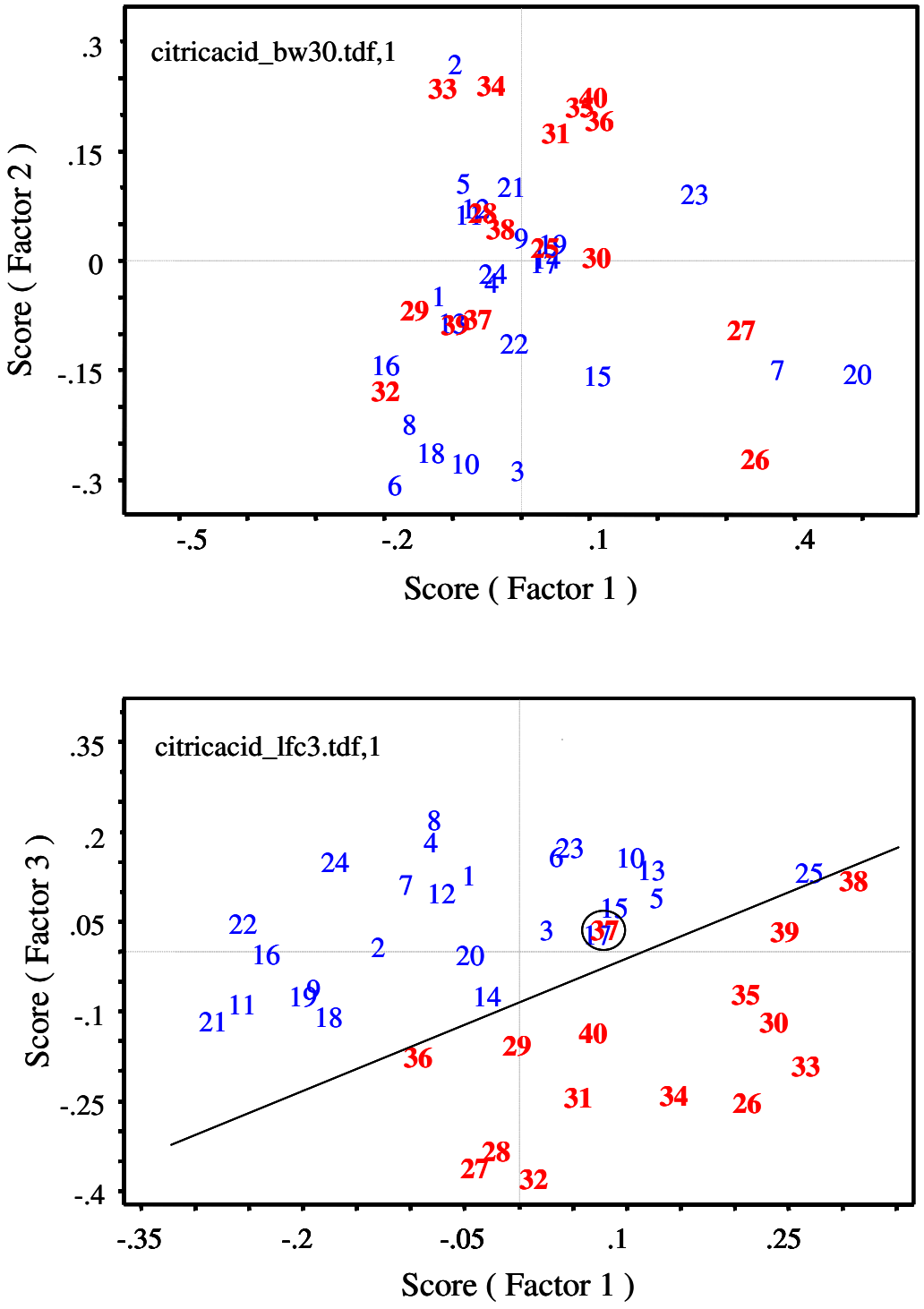

Figure 52. PCA scores plots of the IR spectra of FilmTec BW-30 (top) and Hydranautics LFC3 (bottom) RO membrane exposed to citric acid (26-40) and 1,000-ppm NaCl feedwater control (1-25).

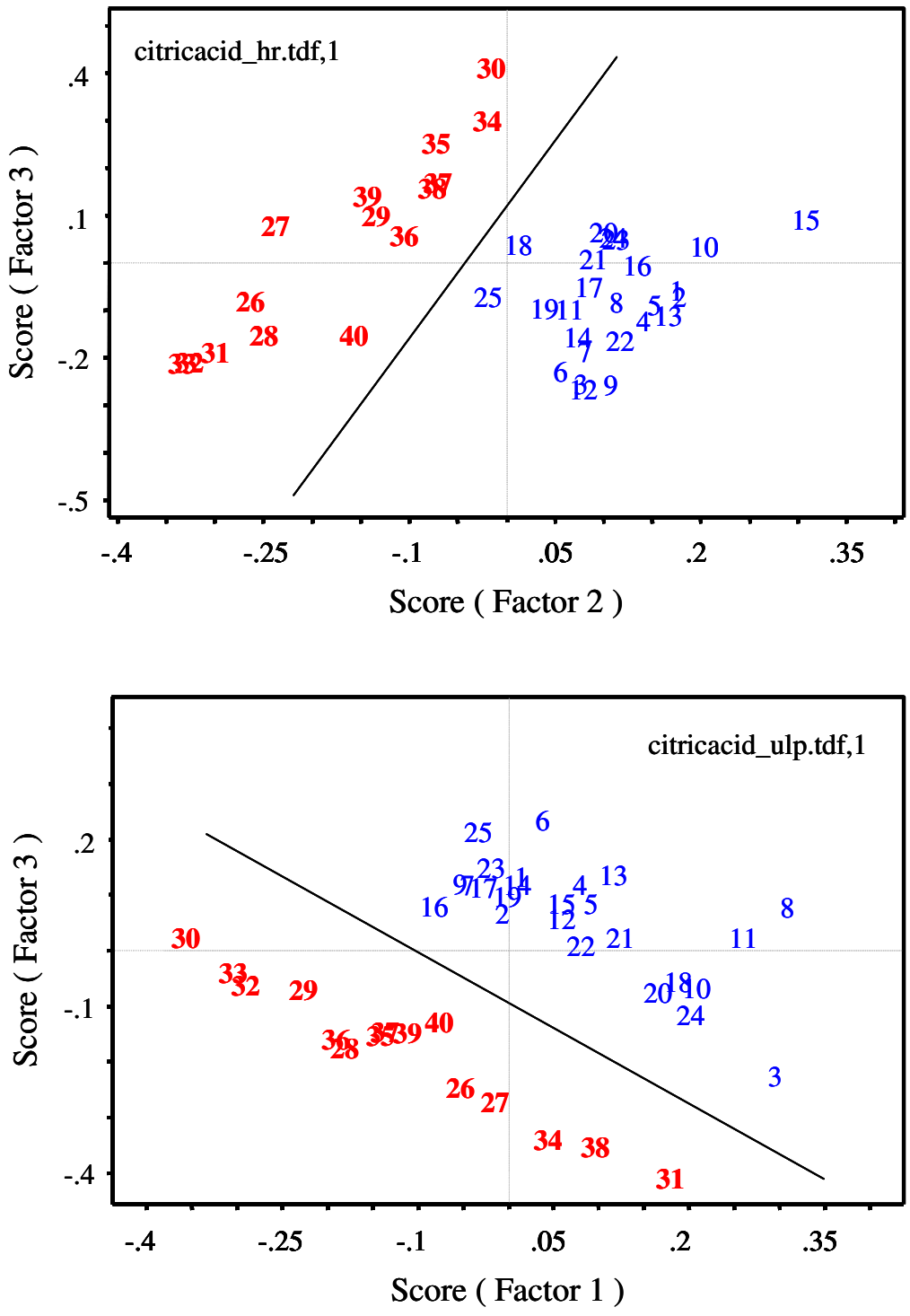

Figure 53. PCA scores plots of the IR spectra of Koch TFC-HR (top) and TFC-ULP (bottom) RO membrane exposed to citric acid (26-40) and 1,000-ppm NaCl feedwater control (1-25).

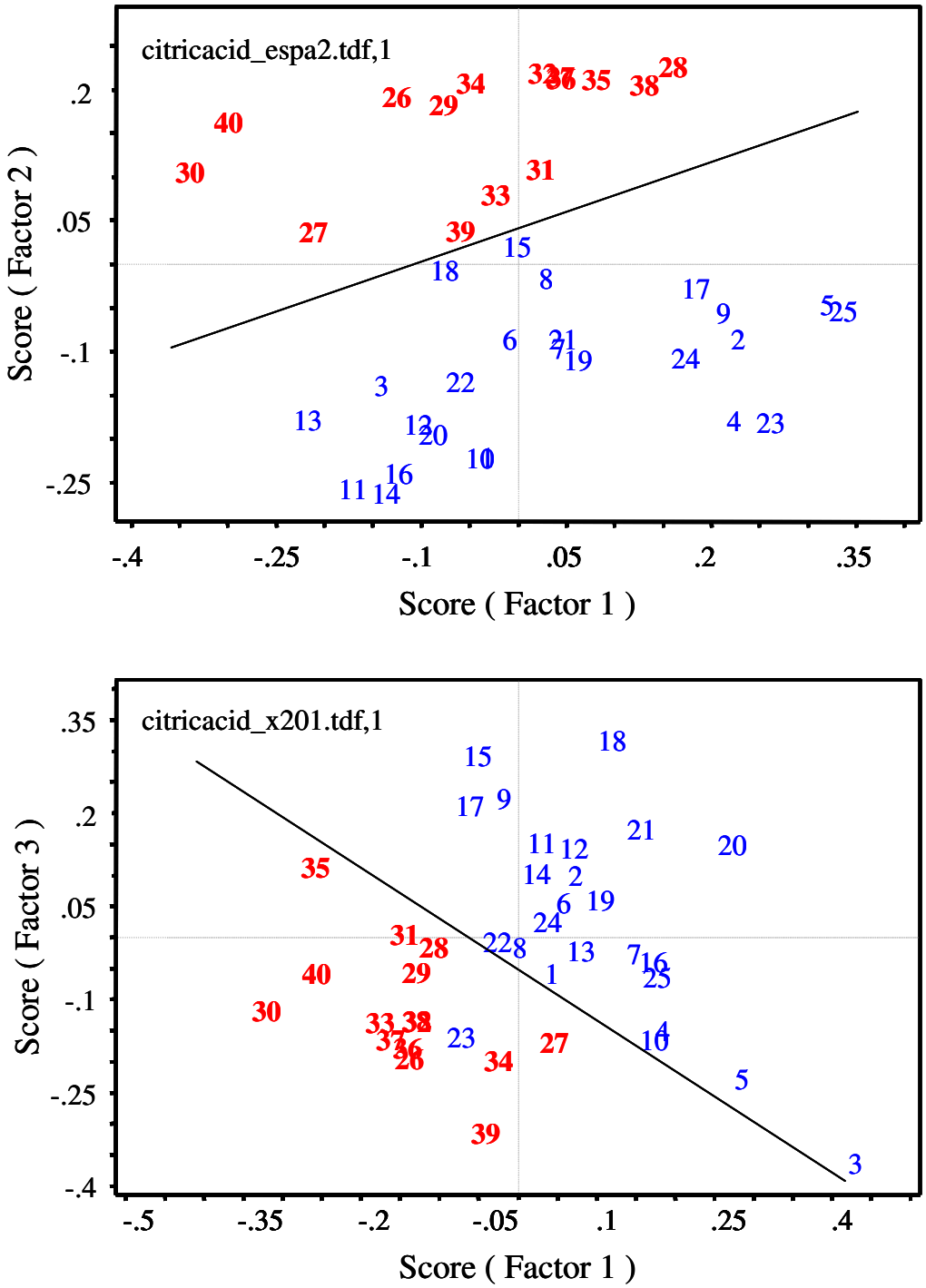

Figure 54. PCA scores plots of the IR spectra of Hydranautics ESPA2 (top) and TrisepX-201 (bottom) RO membrane exposed to citric acid (26-40) and 1,000-ppm NaCl feedwater control (1-25).

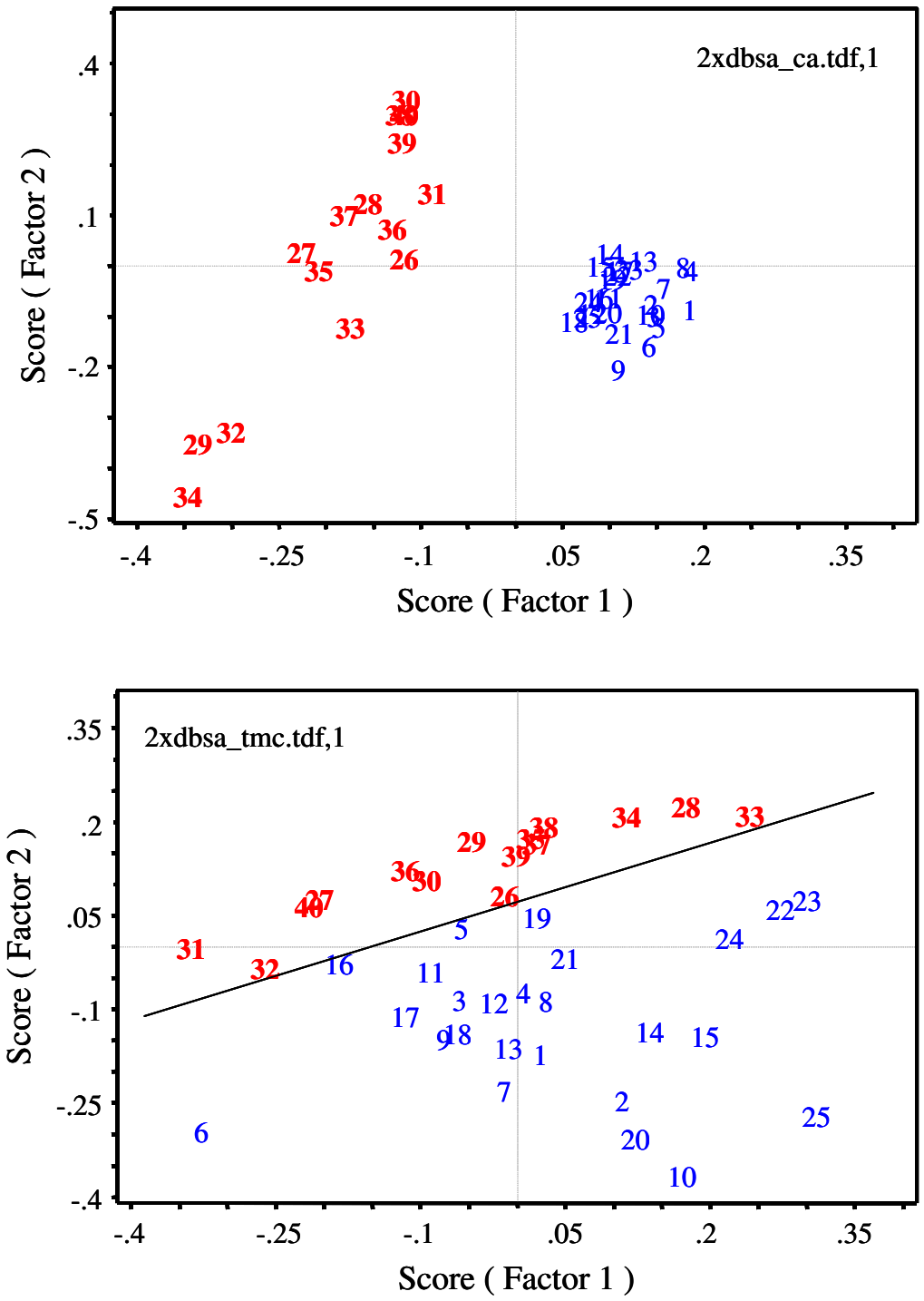

Figure 55. PCA scores plots of the IR spectra of Desal CA and SST TMC/MPD RO membrane exposed to DBSA at 2X's the CMC (26-40) and 1,000-ppm NaCl feedwater control (1-25).

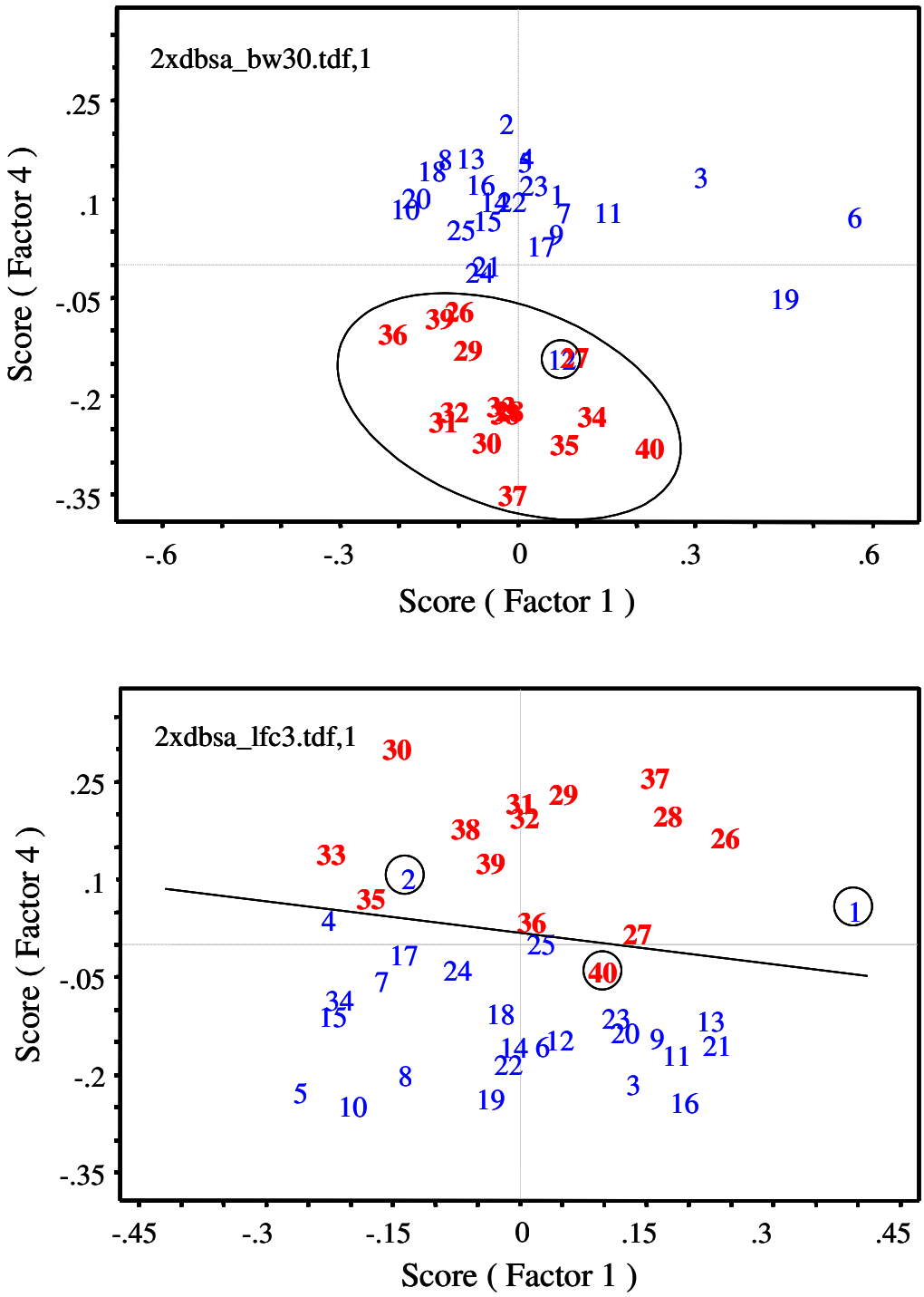

Figure 56. PCA scores plots of the IR spectra of FilmTec BW-30 (top) and Hydranautics LFC3 (bottom) RO membrane exposed to DBSA at 2X the CMC (26-40) and 1,000-ppm NaCl feedwater control (1-25).

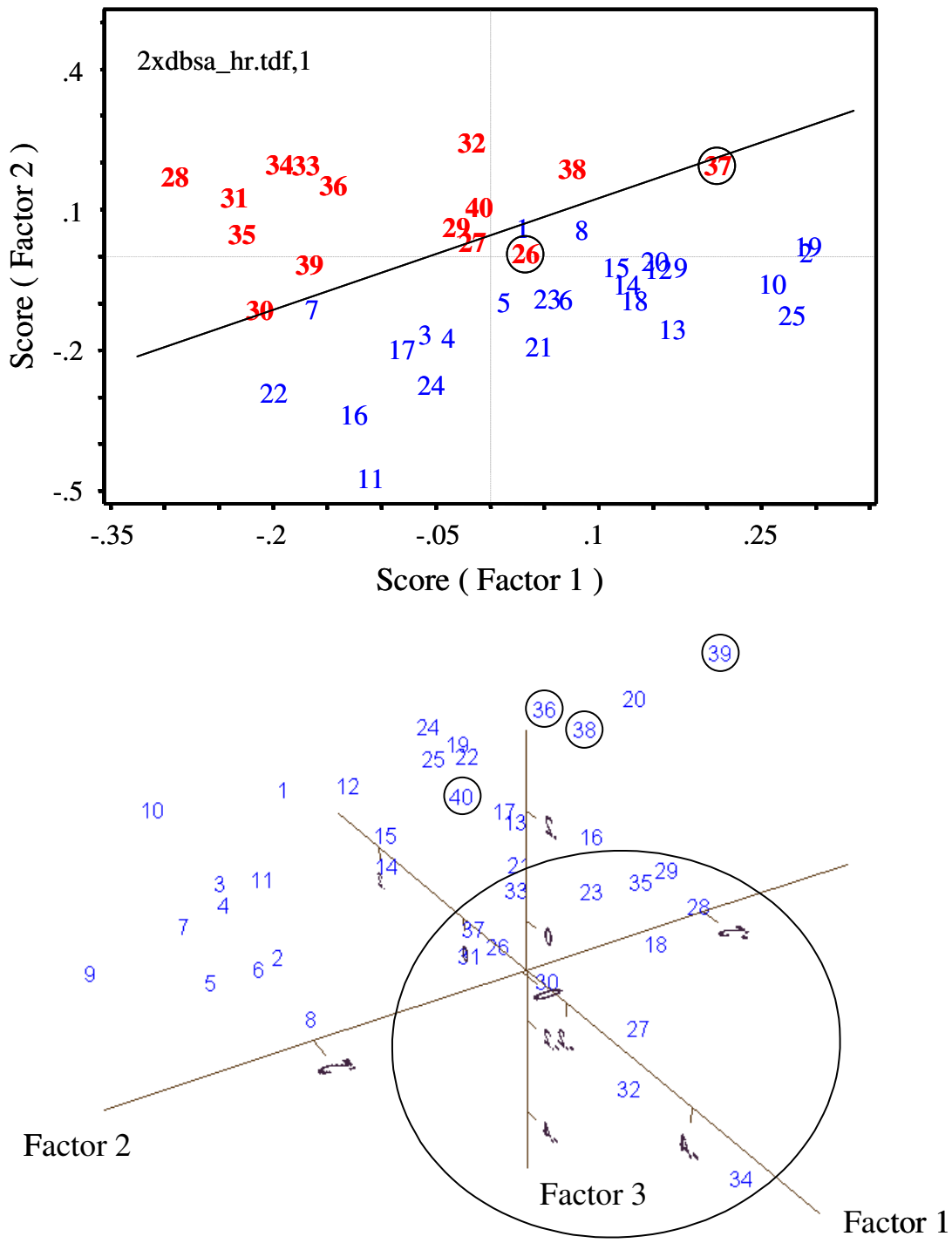

Figure 57. PCA scores plots of the IR spectra of Koch TFC-HR (top) and TFC-ULP (bottom) RO membrane exposed to DBSA at 2X the CMC (26-40) and 1,000-ppm NaCl feedwater control (1-25).

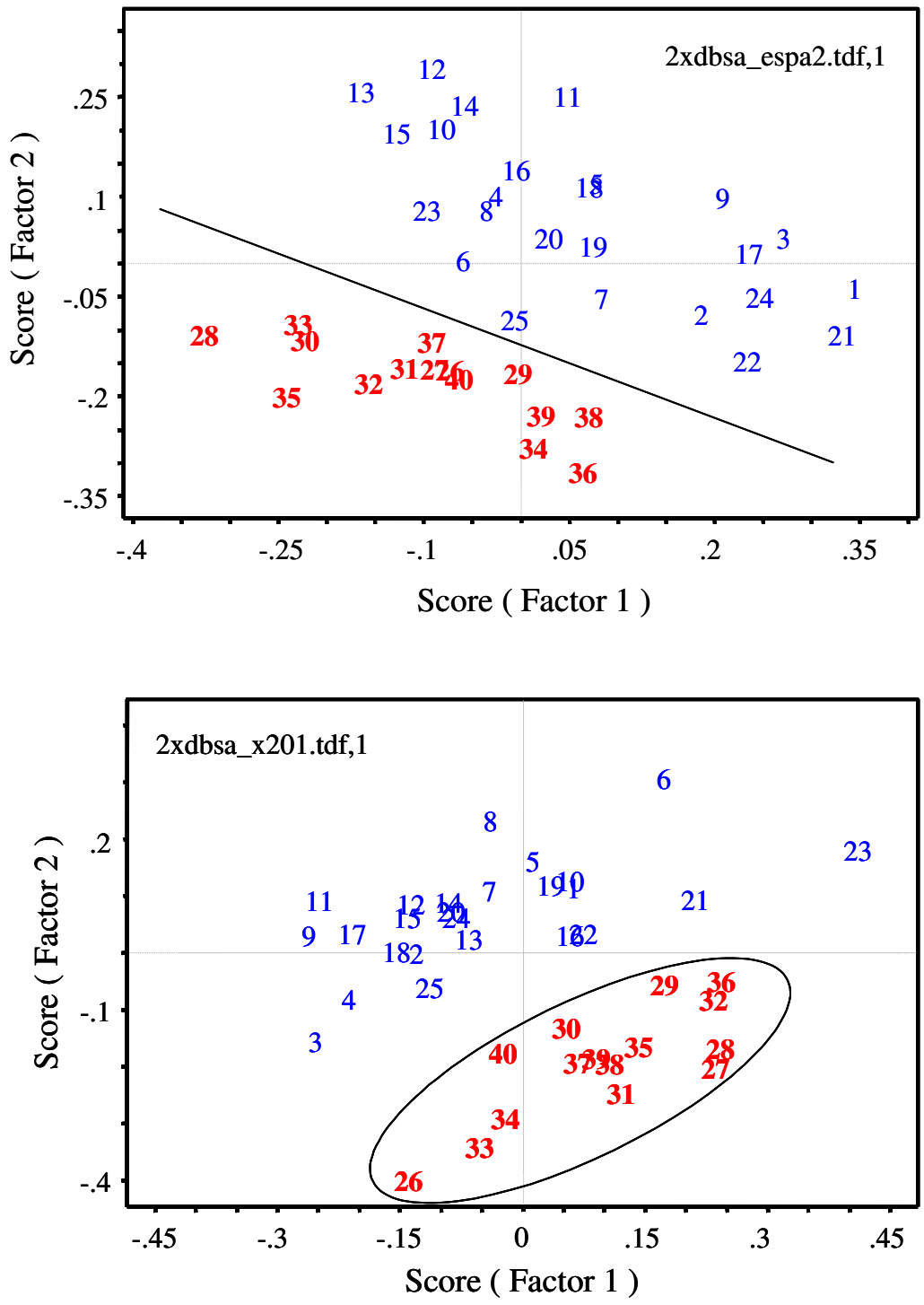

Figure 58. PCA scores plots of the IR spectra of Hydranautics ESPA2 (top) and Trisep X-201 (bottom) RO membrane exposed to DBSA at 2X the CMC (26-40) and 1,000-ppm NaCl feedwater control (1-25).

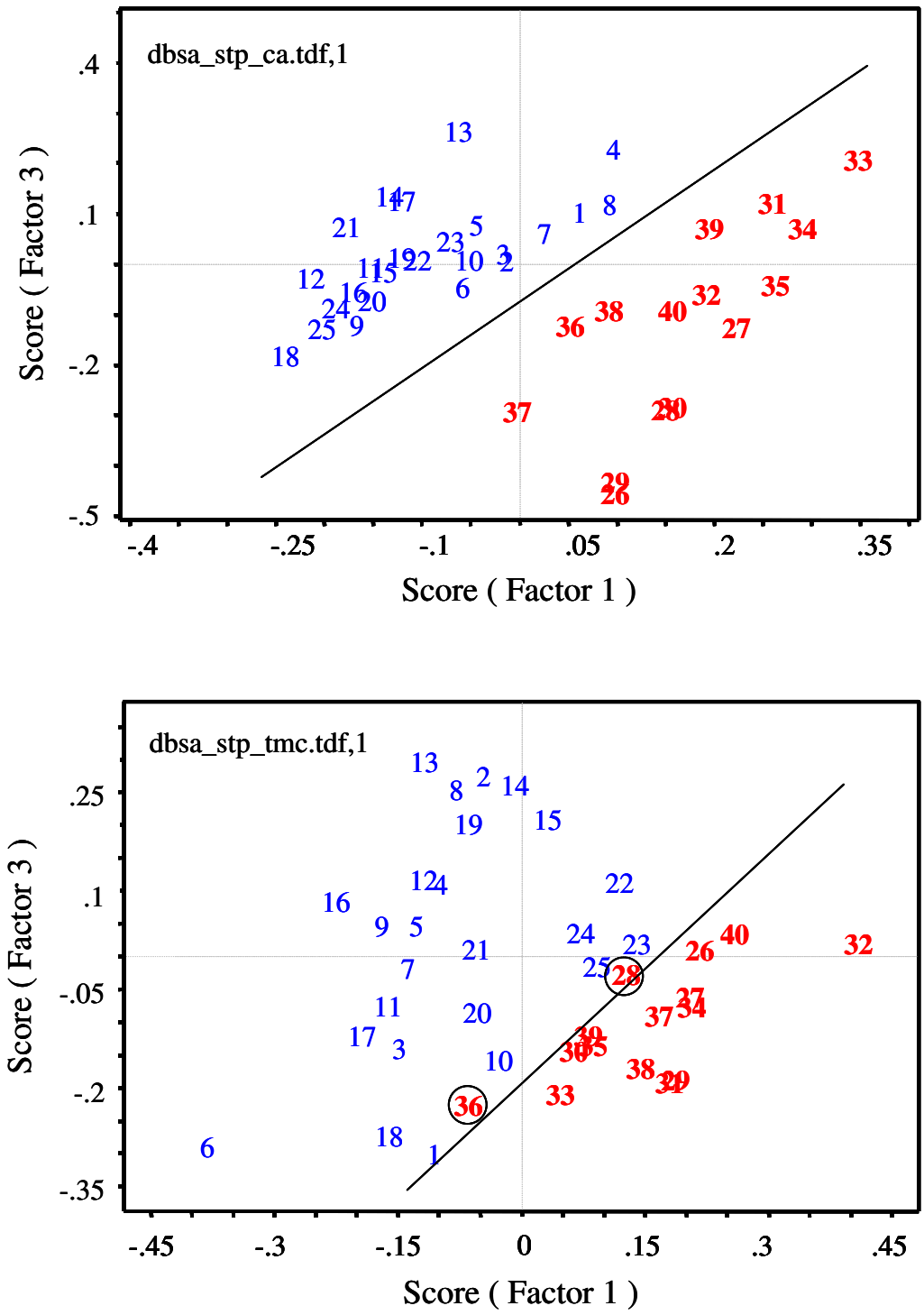

Figure 59. PCA scores plots of the IR spectra of Desal CA and SST TMC/MPD RO membrane exposed to DBSA and STP (26-40) and 1,000-ppm NaCl feedwater control (1-25).

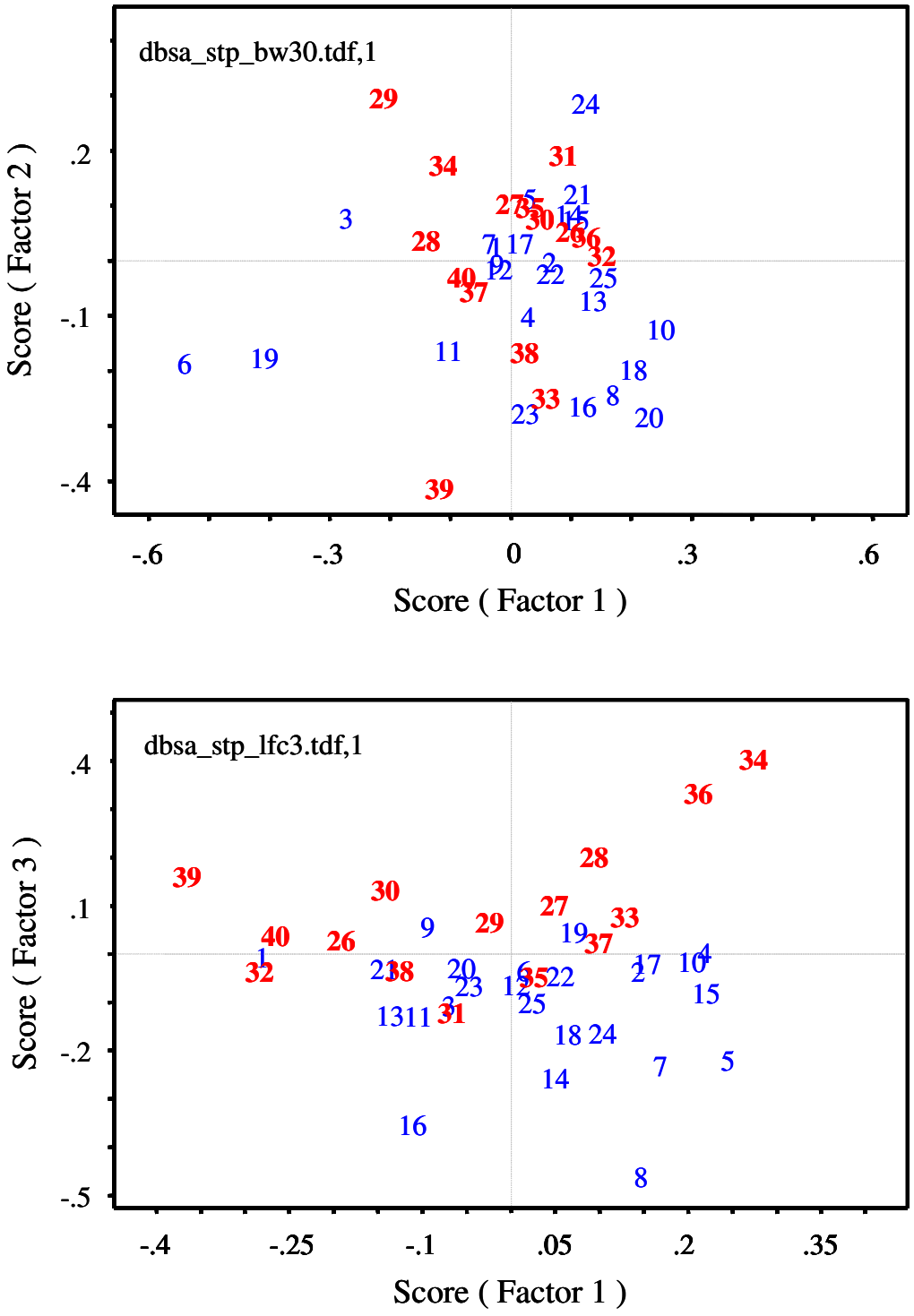

Figure 60. PCA scores plots of the IR spectra of FilmTec BW-30 (top) and Hydranautics LFC3 (bottom) RO membrane exposed to DBSA and STP (26-40) and 1,000-ppm NaCl feedwater control (1-25).

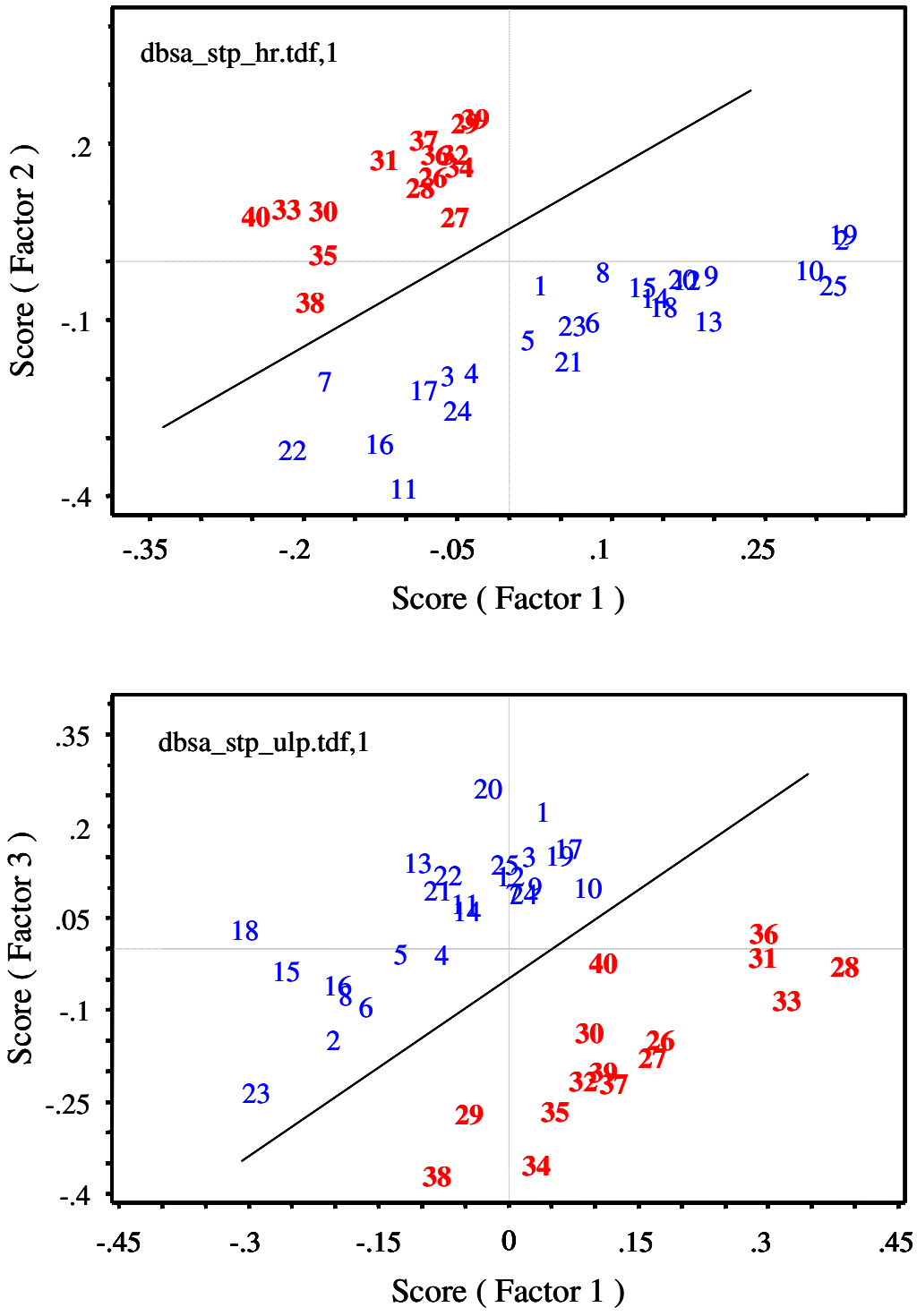

Figure 61. PCA scores plots of the IR spectra of Koch TFC-HR (top) and TFC-ULP (bottom) RO membrane exposed to DBSA and STP (26-40) and 1,000-ppm NaCl feedwater control (1-25).

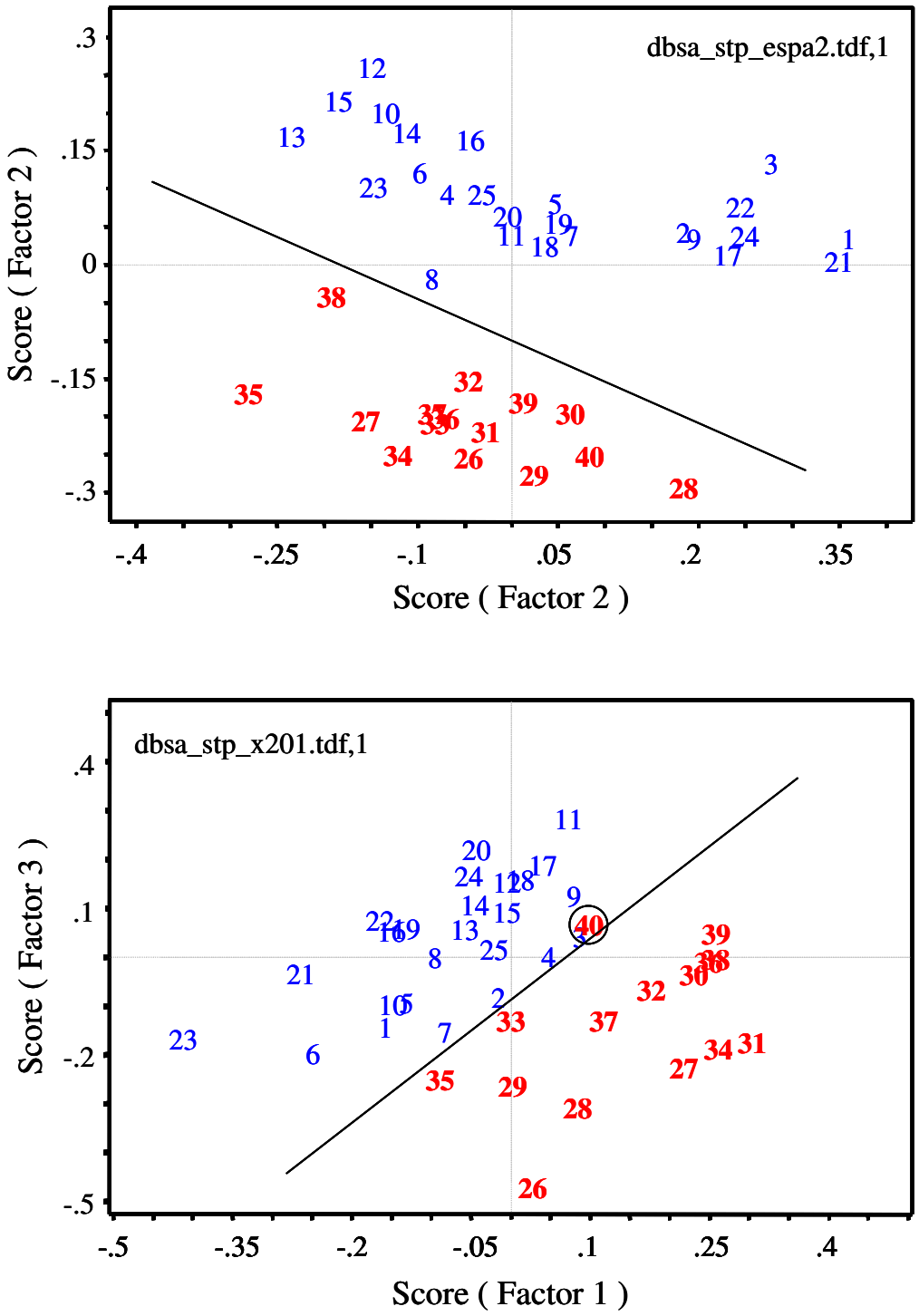

Figure 62. PCA scores plots of the IR spectra of Hydranautics ESPA2 (top) and Trisep X-201 (bottom) RO membrane exposed to DBSA and STP (26-40) and 1,000-ppm NaCl feedwater control (1-25).

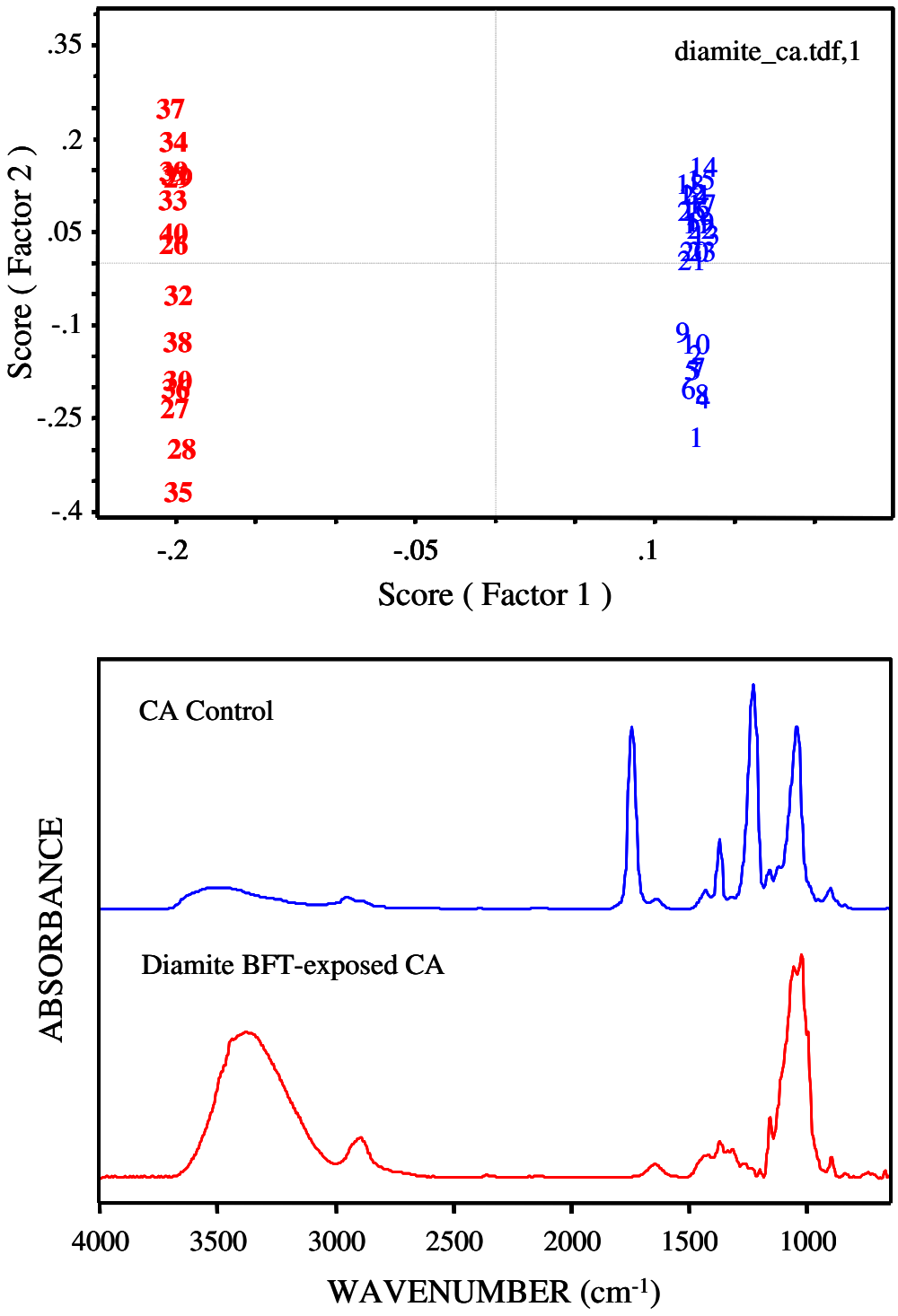

Figure 63. PCA scores plot (top) of the IR spectra of Desal CA (top) RO membrane exposed to Diamite BFT (26-40) and 1,000-ppm NaCl feedwater control (1-25). ATR/FTIR spectra (bottom) of CA control membrane and Diamite BFT-exposed CA membrane.

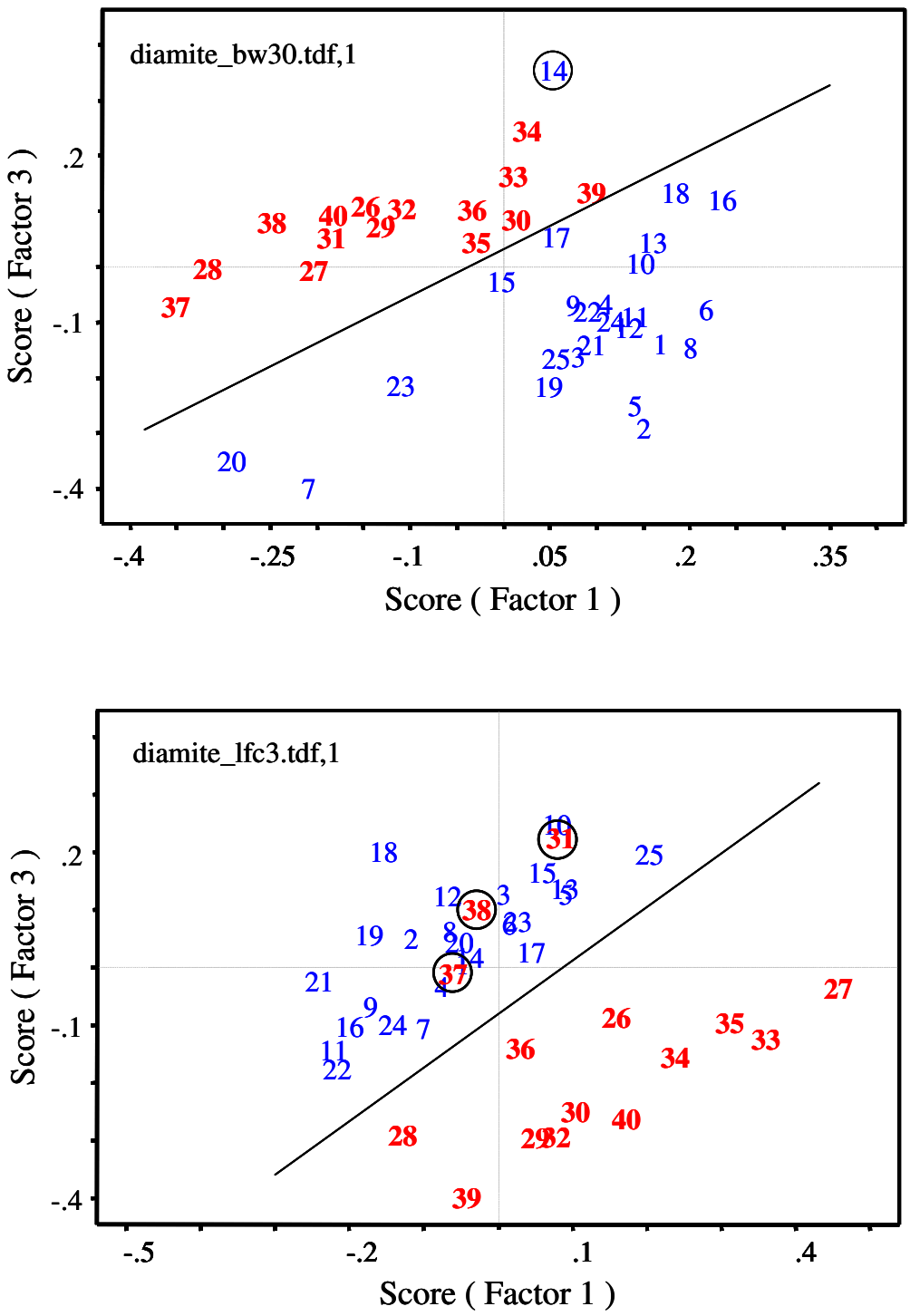

Figure 64. PCA scores plots of the IR spectra of FilmTec BW-30 (top) and Hydranautics LFC3 (bottom) RO membrane exposed to SDS (26-40) and 1,000-ppm NaCl feedwater control (1-25).

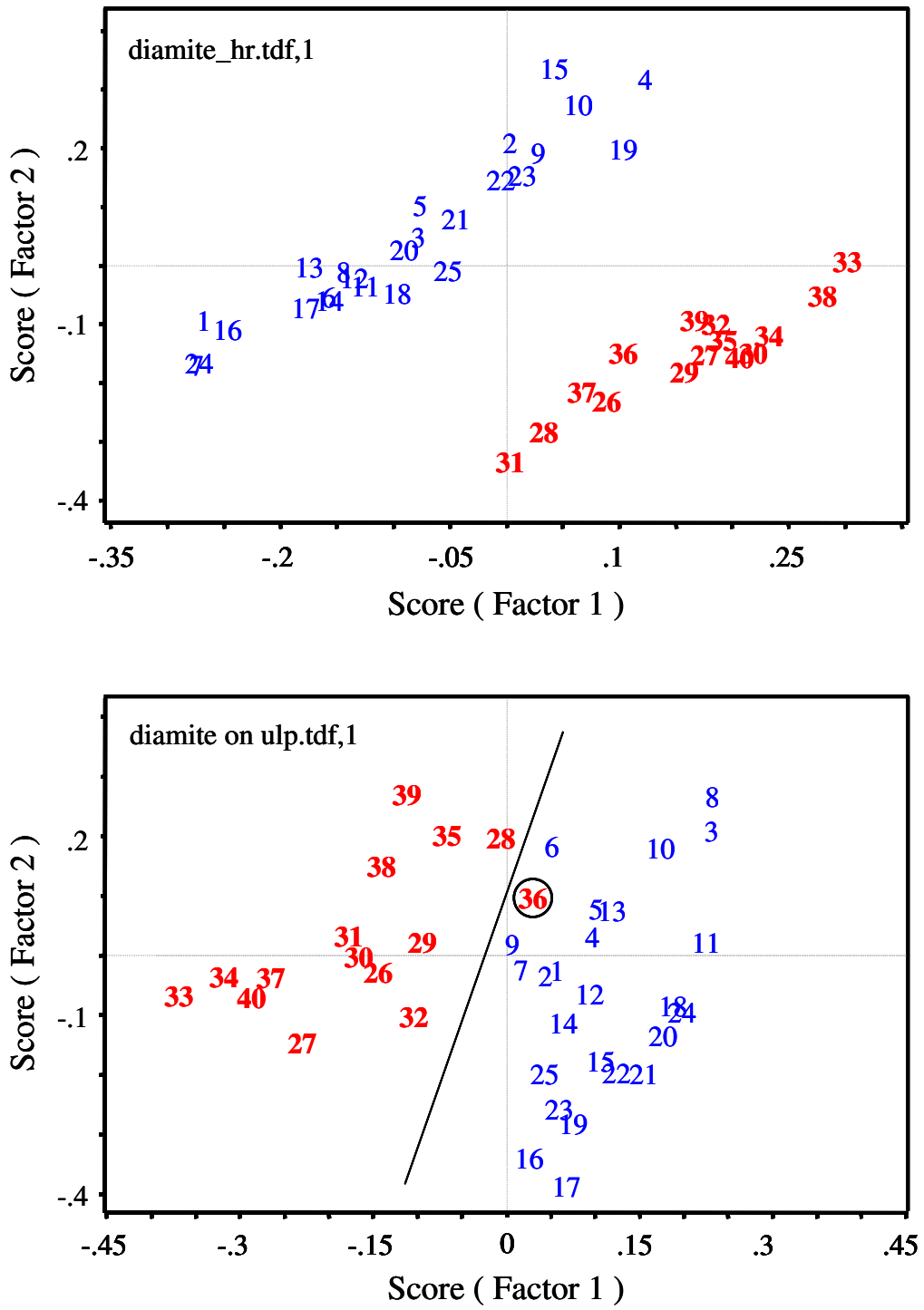

Figure 65. PCA scores plots of the IR spectra of Koch TFC-HR (top) and TFC-ULP (bottom) RO membrane exposed to SDS (26-40) and 1,000-ppm NaCl feedwater control (1-25).

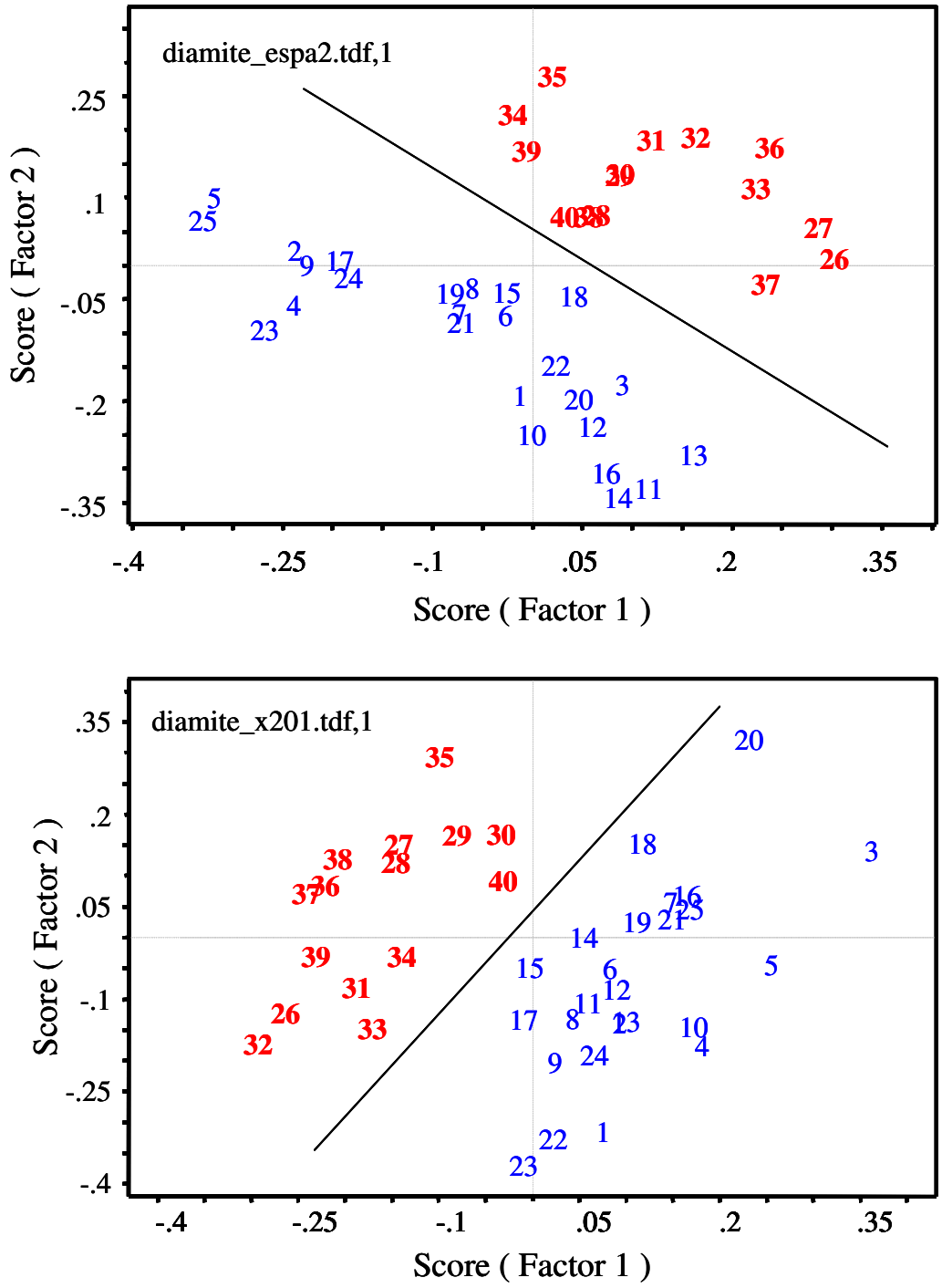

Figure 66. PCA scores plots of the IR spectra of Hydranautics ESPA2 (top) and Trisep X-201 (bottom) RO membrane exposed to Diamite BFT (26-40) and 1,000-ppm NaCl feedwater control (1-25).

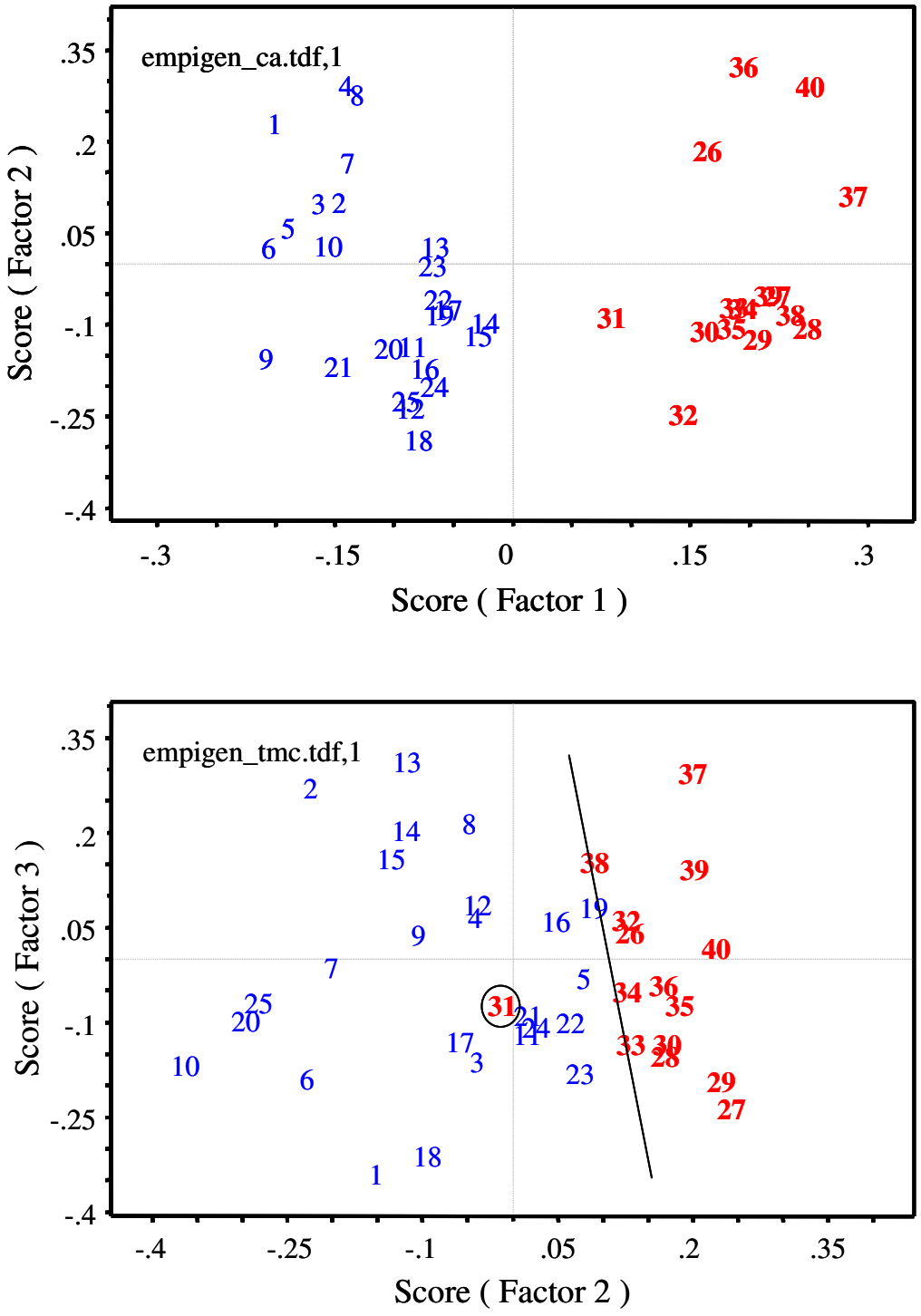

Figure 67. PCA scores plots of the IR spectra of Desal CA (top) and SST TMC/MPD (bottom) RO membrane exposed to n-dodecyl-N,N-dimethylglycine (Empigen BB) (26-40) and 1,000-ppm NaCl feedwater control (1-25).

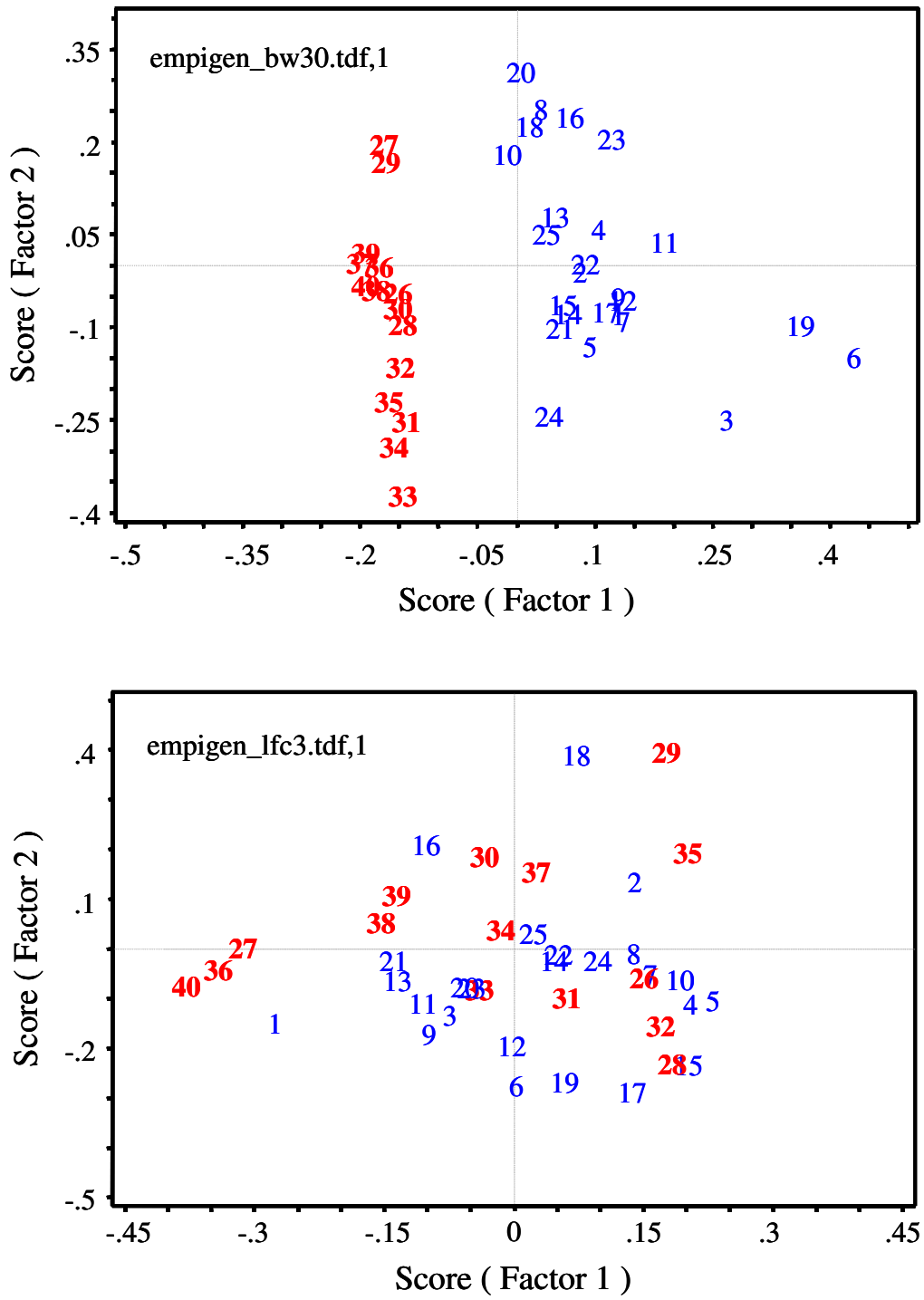

Figure 68. PCA scores plots of the IR spectra of FilmTec BW-30 (top) and Hydranautics LFC3 (bottom) RO membrane exposed to n-dodecyl-N,N-dimethylglycine (Empigen BB) (26-40) and 1,000-ppm NaCl feedwater control (1-25).

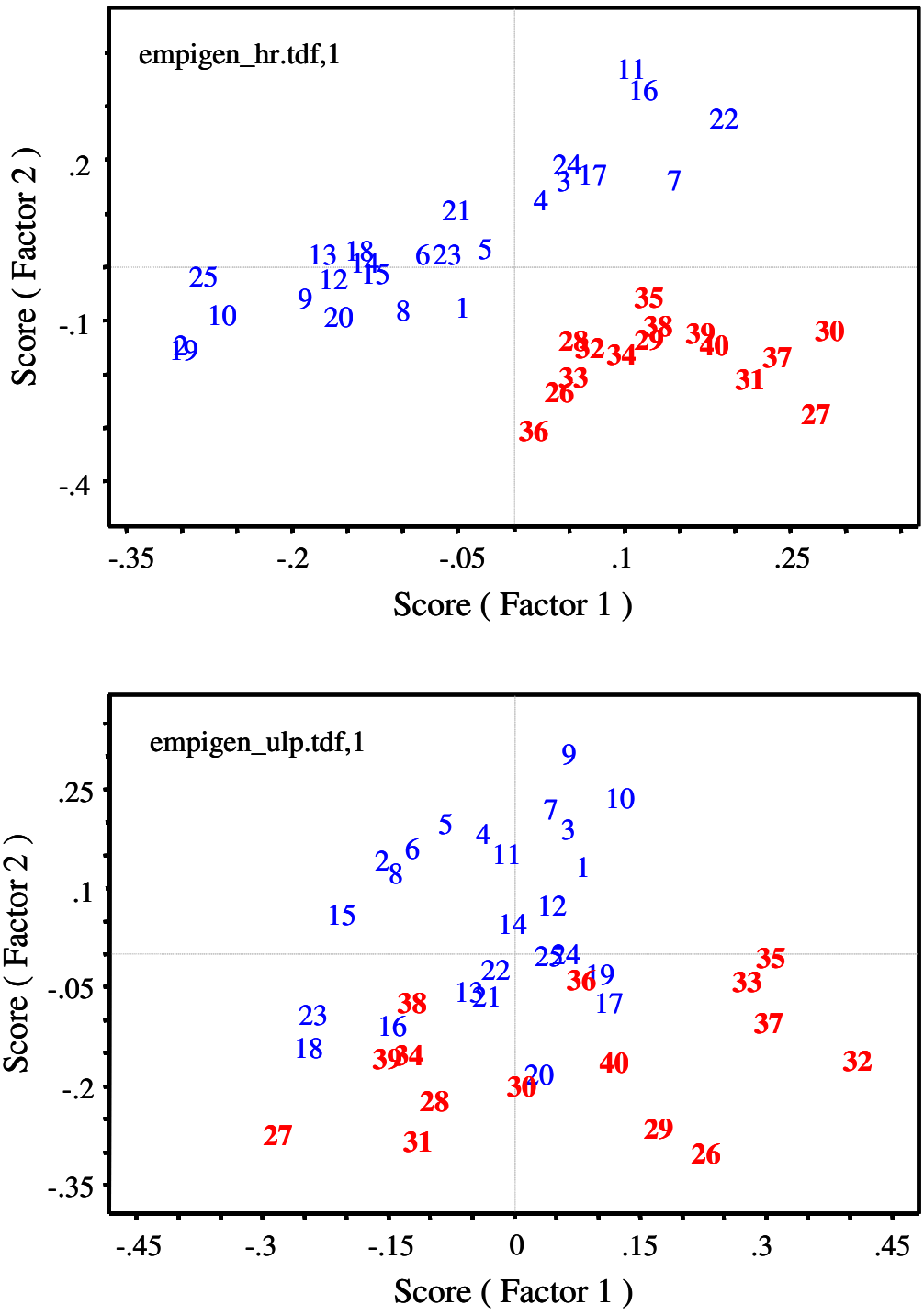

Figure 69. PCA scores plots of the IR spectra of Koch TFC-HR (top) and TFC-ULP (bottom) RO membrane exposed to n-dodecyl-N,N-dimethylglycine (Empigen BB) (26-40) and 1,000-ppm NaCl feedwater control (1-25).

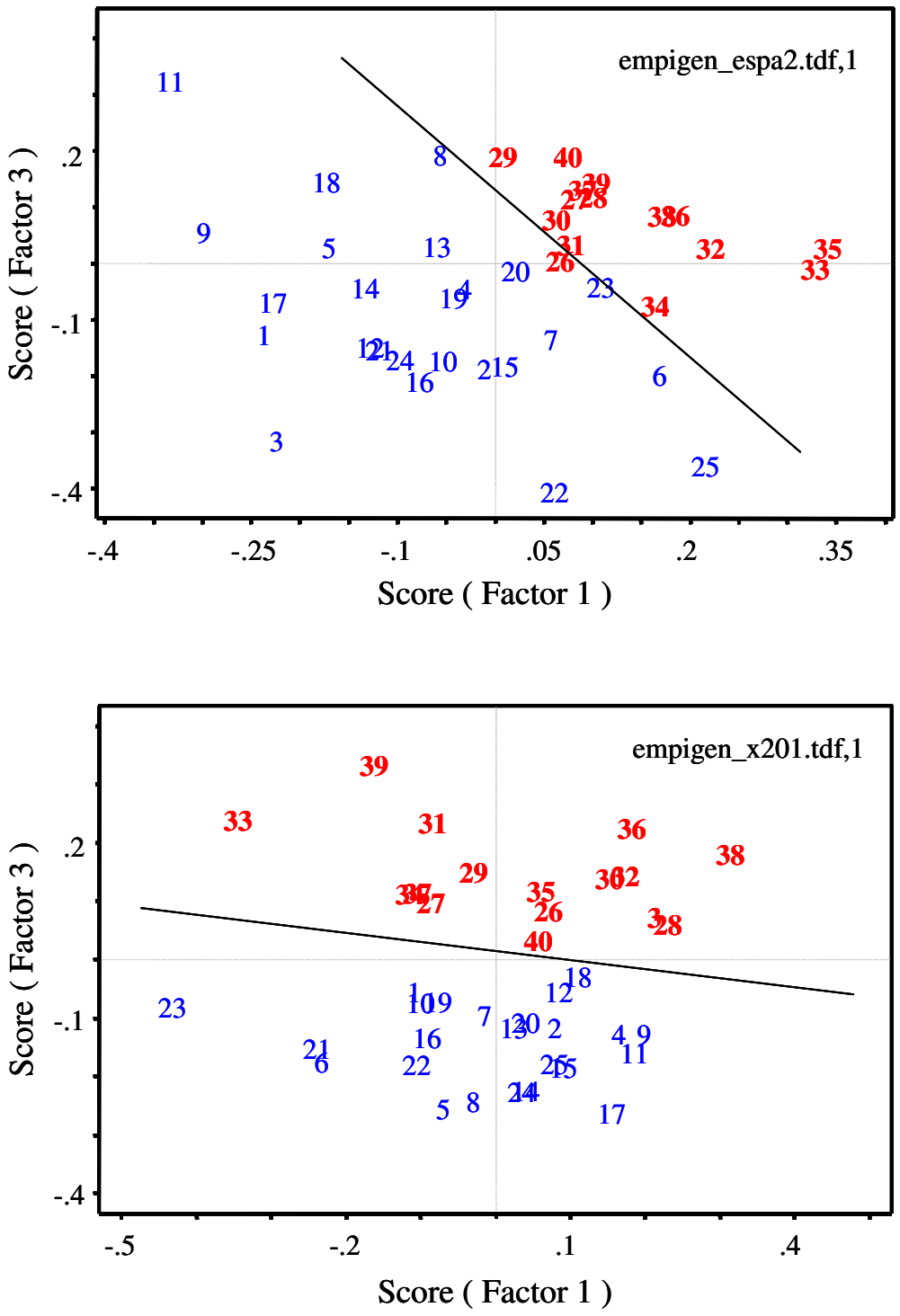

Figure 70. PCA scores plots of the IR spectra of Hydranautics ESPA2 (top) and Trisep X-201 (bottom) RO membrane exposed to n-dodecyl-N,N-dimethylglycine (Empigen BB) (26-40) and 1,000-ppm NaCl feedwater control (1-25).

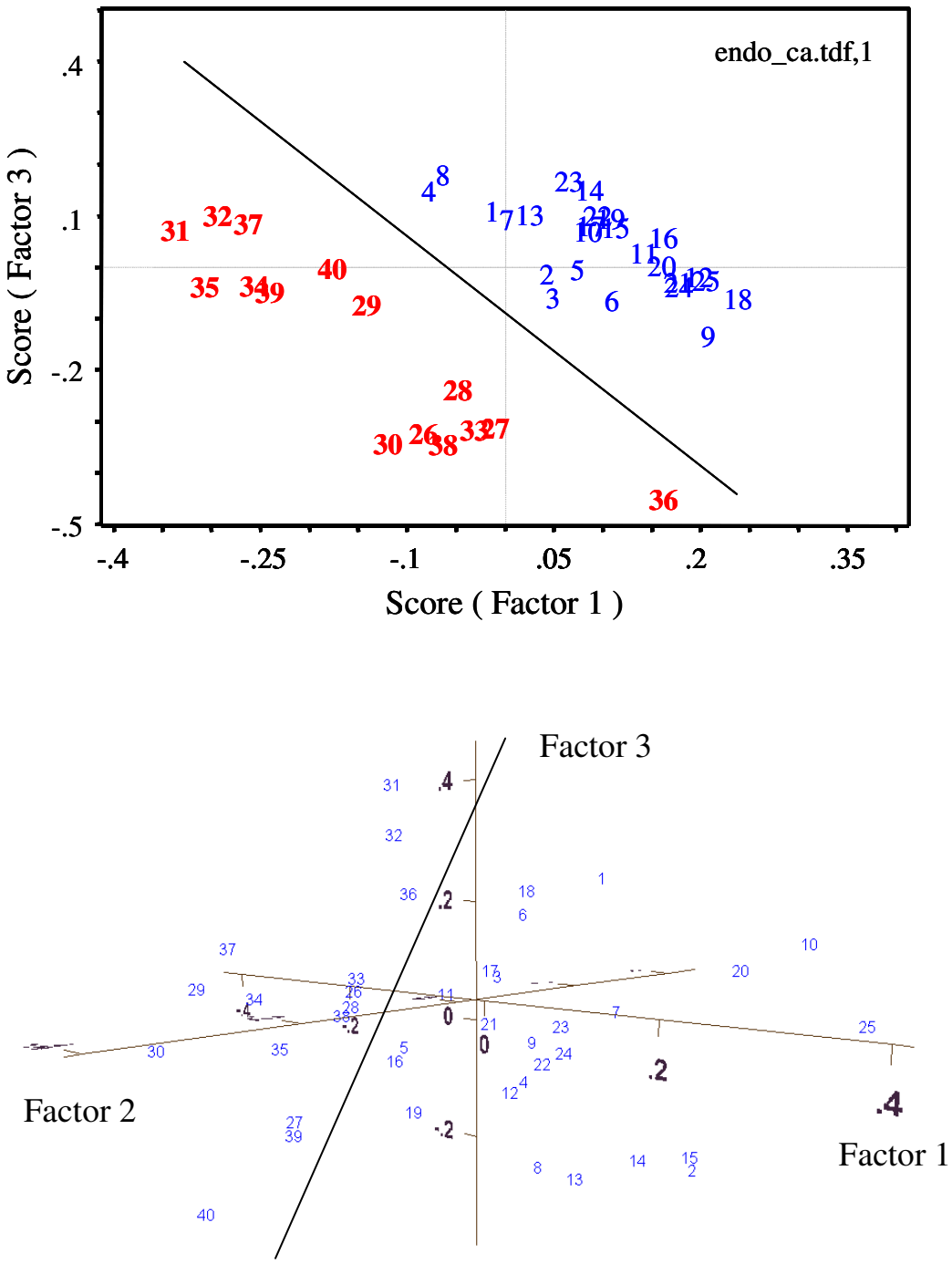

Figure 71. PCA scores plots of the IR spectra of Desal CA (top) and SST TMC/MPD (bottom) RO membrane exposed to Endozime (26-40) and 1,000-ppm NaCl feedwater control (1-25).

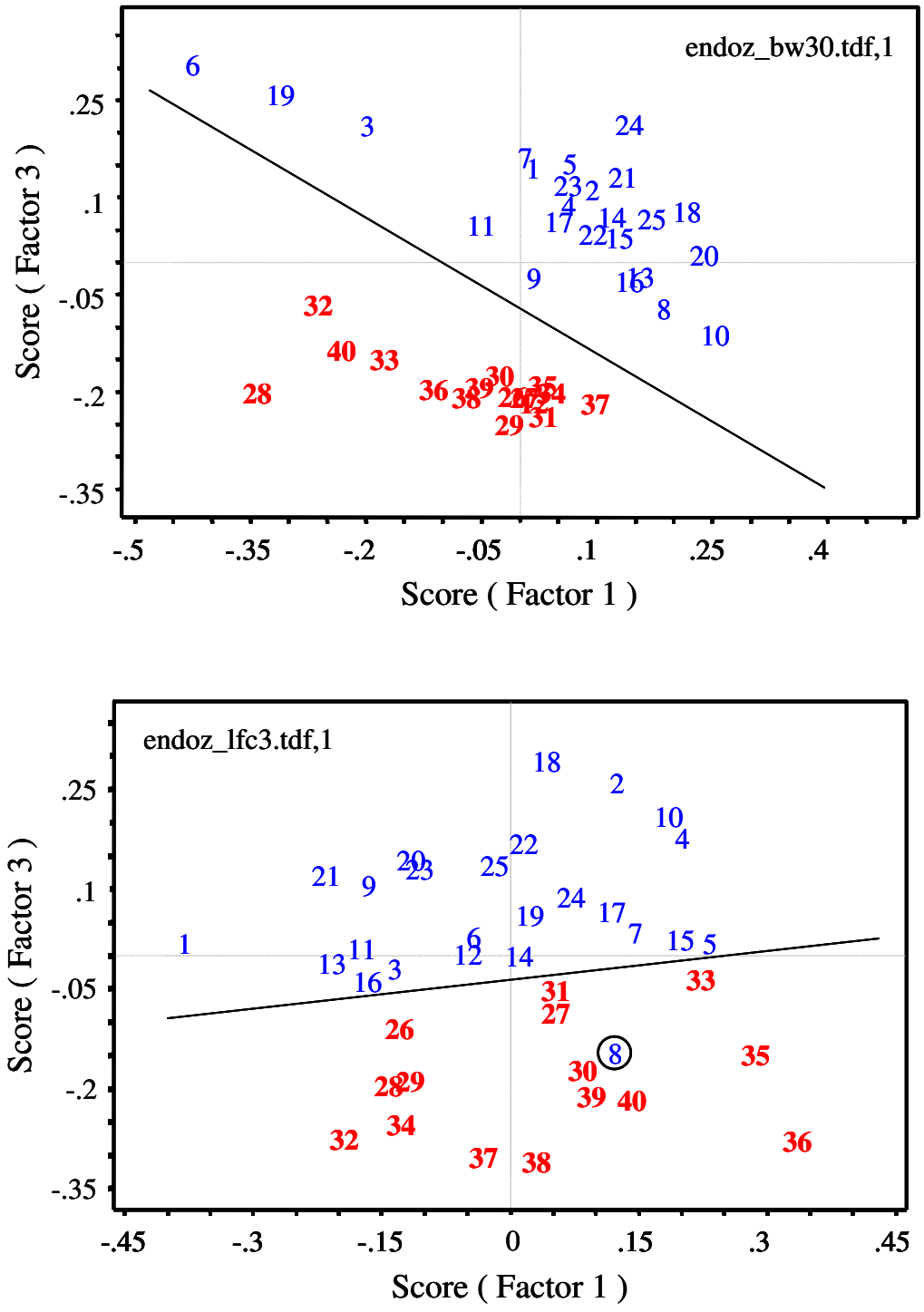

Figure 72. PCA scores plots of the IR spectra of FilmTec BW-30 (top) and Hydranautics LFC3 (bottom) RO membrane exposed to Endozime (26-40) and 1,000-ppm NaCl feedwater control (1-25).

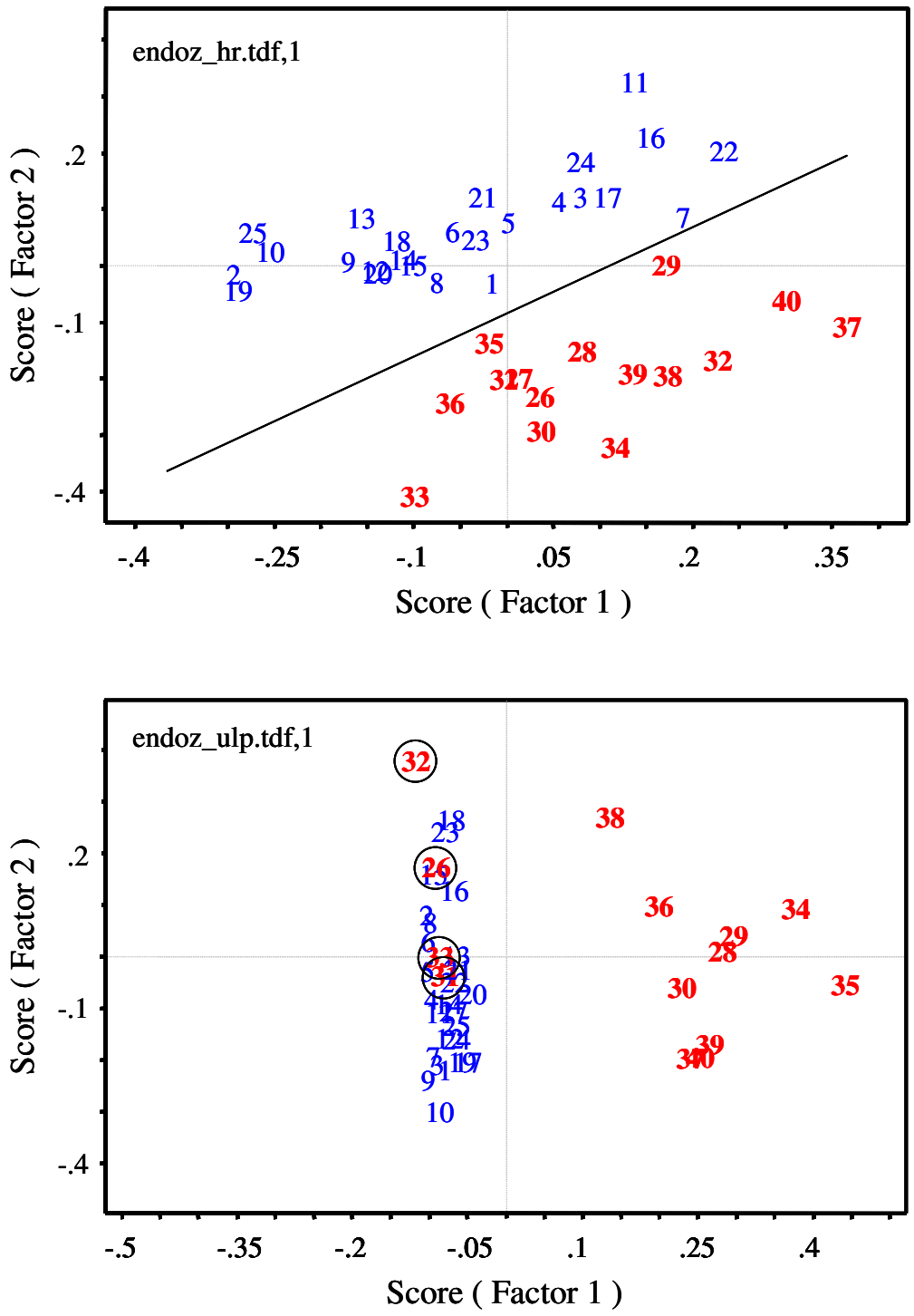

Figure 73. PCA scores plots of the IR spectra of Koch TFC-HR (top) and TFC-ULP (bottom) RO membrane exposed to Endozime (26-40) and 1,000-ppm NaCl feedwater control (1-25).

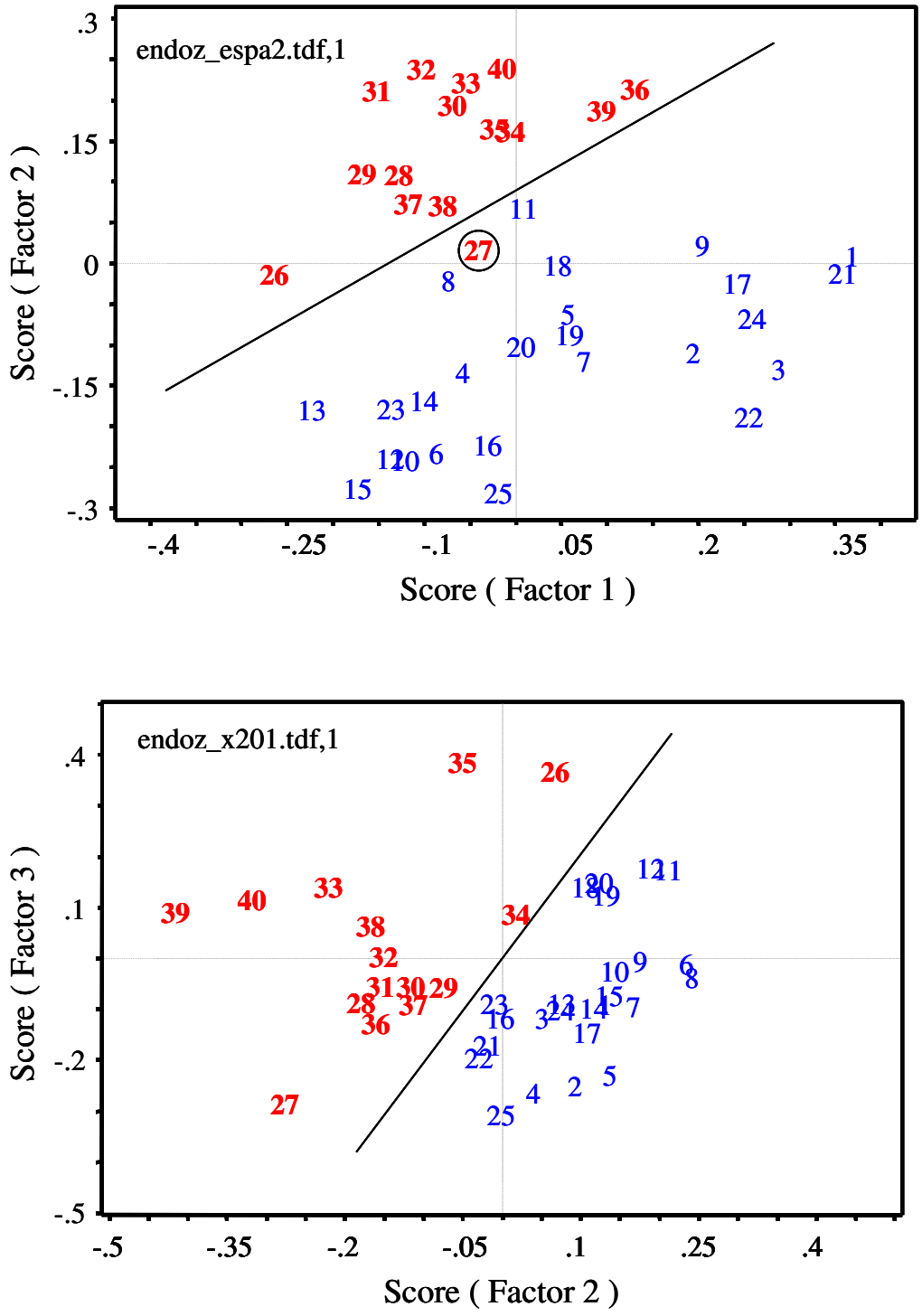

Figure 74. PCA scores plots of the IR spectra of Hydranautics ESPA2 (top) and Trisep X-201 (bottom) RO membrane exposed to Endozime (26-40) and 1,000-ppm NaCl feedwater control (1-25).

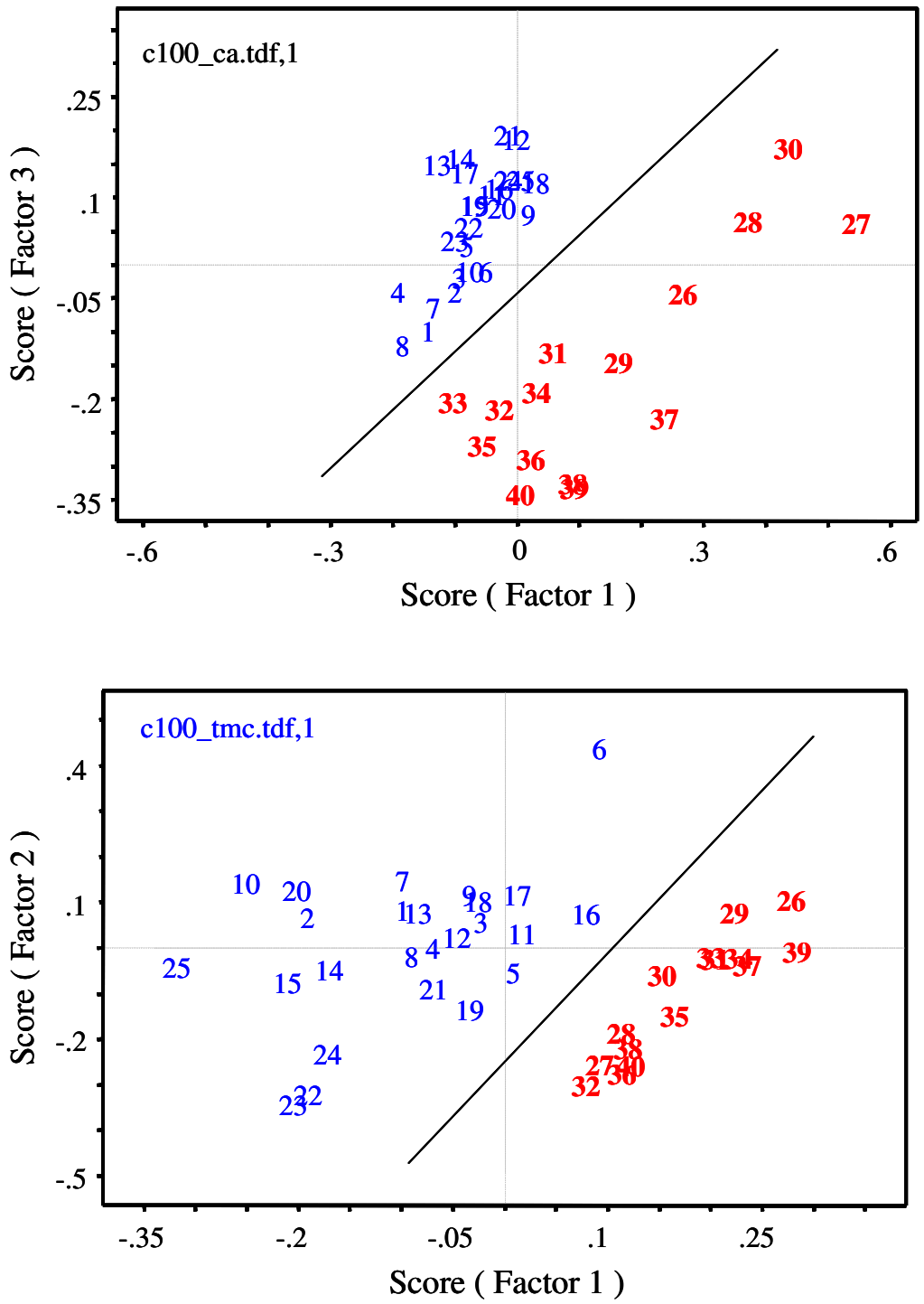

Figure 75. PCA scores plots of the IR spectra of Desal CA and SST TMC/MPD RO membrane exposed to polyethyleneglycollaurylether (26-40) and 1,000-ppm NaCl feedwater control (1-25).

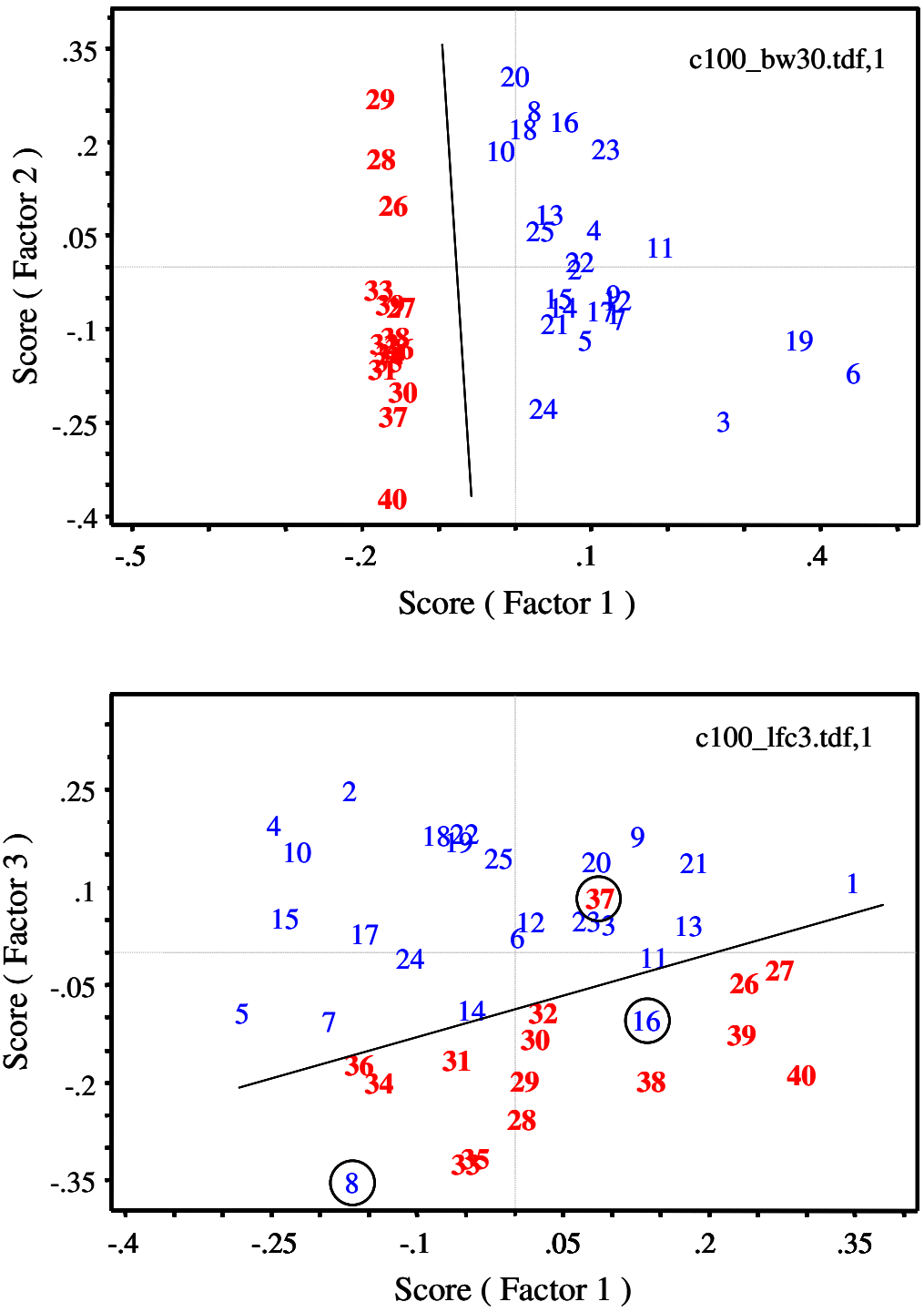

Figure 76. PCA scores plots of the IR spectra of FilmTec BW-30 (top) and Hydranautics LFC3 (bottom) RO membrane exposed to polyethylene glycol lauryl ether (Genapol C-100) (26-40) and 1,000-ppm NaCl feedwater control (1-25).

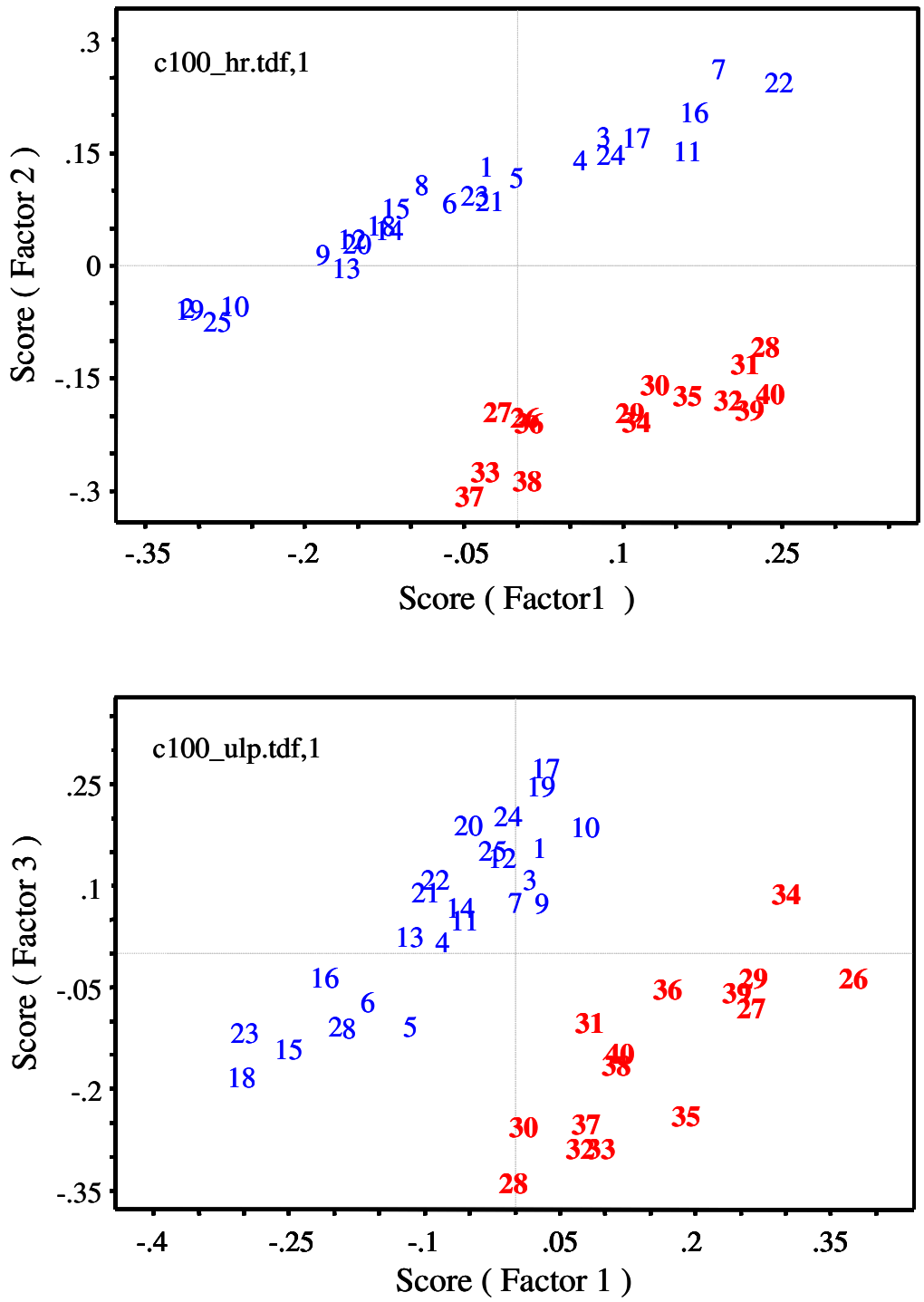

Figure 77. PCA scores plots of the IR spectra of Koch TFC-HR (top) and TFC-ULP (bottom) RO membrane exposed to polyethylene glycol lauryl ether (Genapol C-100) (26-40) and 1,000-ppm NaCl feedwater control (1-25).

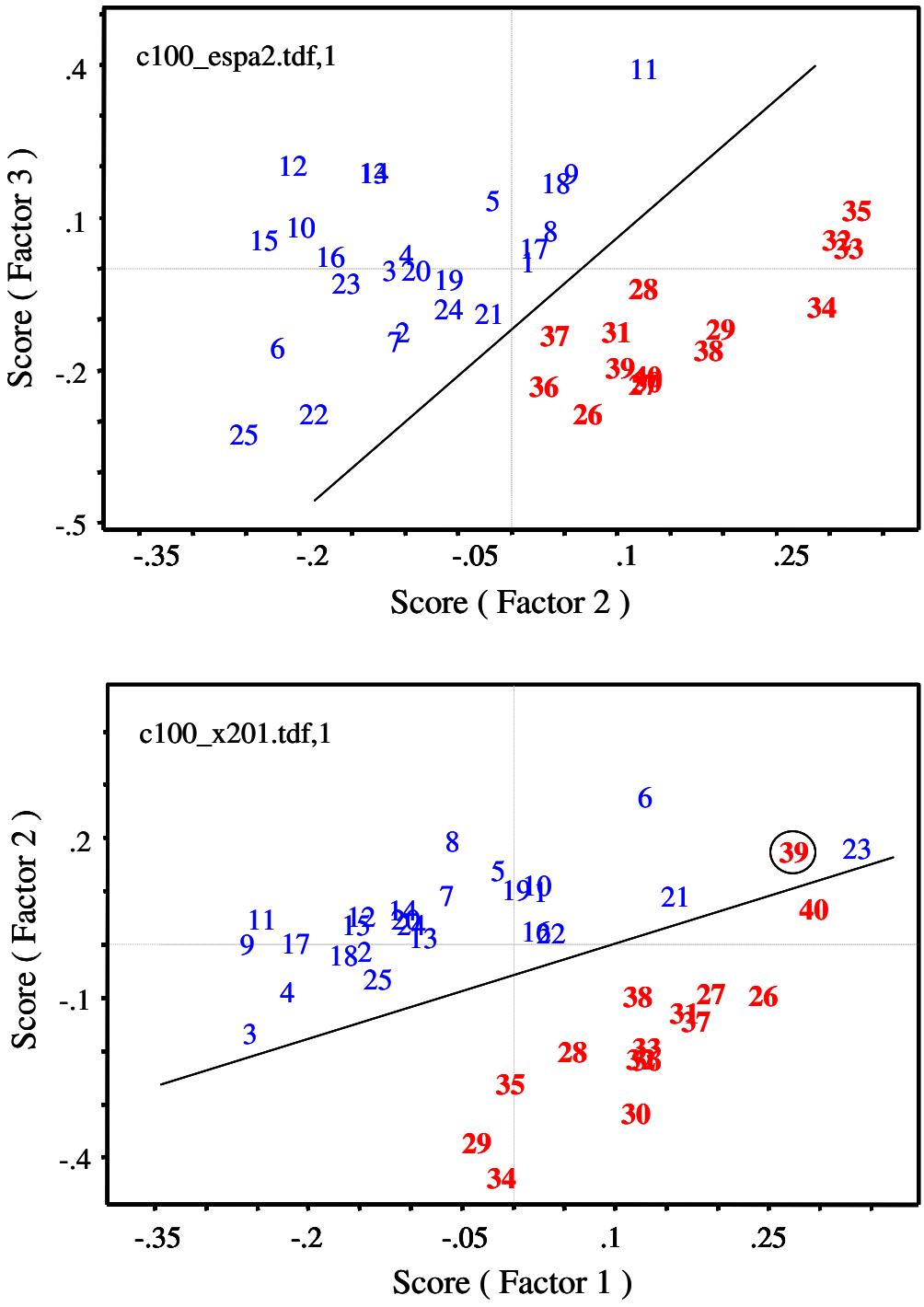

Figure 78. PCA scores plots of the IR spectra of Hydranautics ESPA2 (top) and Trisep X-201 (bottom) RO membrane exposed to polyethylene glycol lauryl ether (Genapol C-100) (26-40) and 1,000-ppm NaCl feedwater control (1-25).

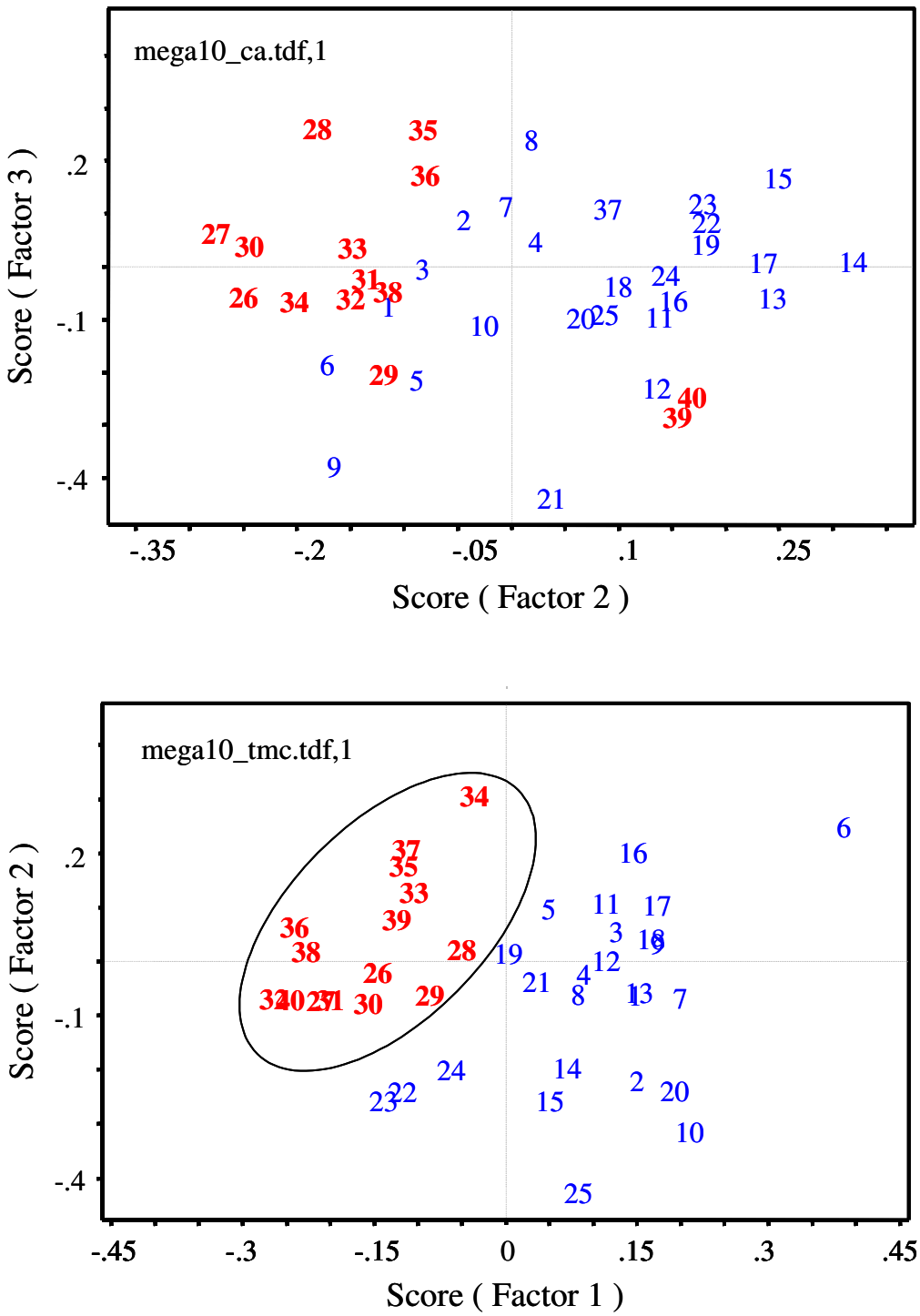

Figure 79. PCA scores plots of the IR spectra of Desal CA and SST TMC/MPD RO membrane exposed to deconyl-N-methylglucamide (Mega 10) (26-40) and 1,000-ppm NaCl feedwater control (1-25).

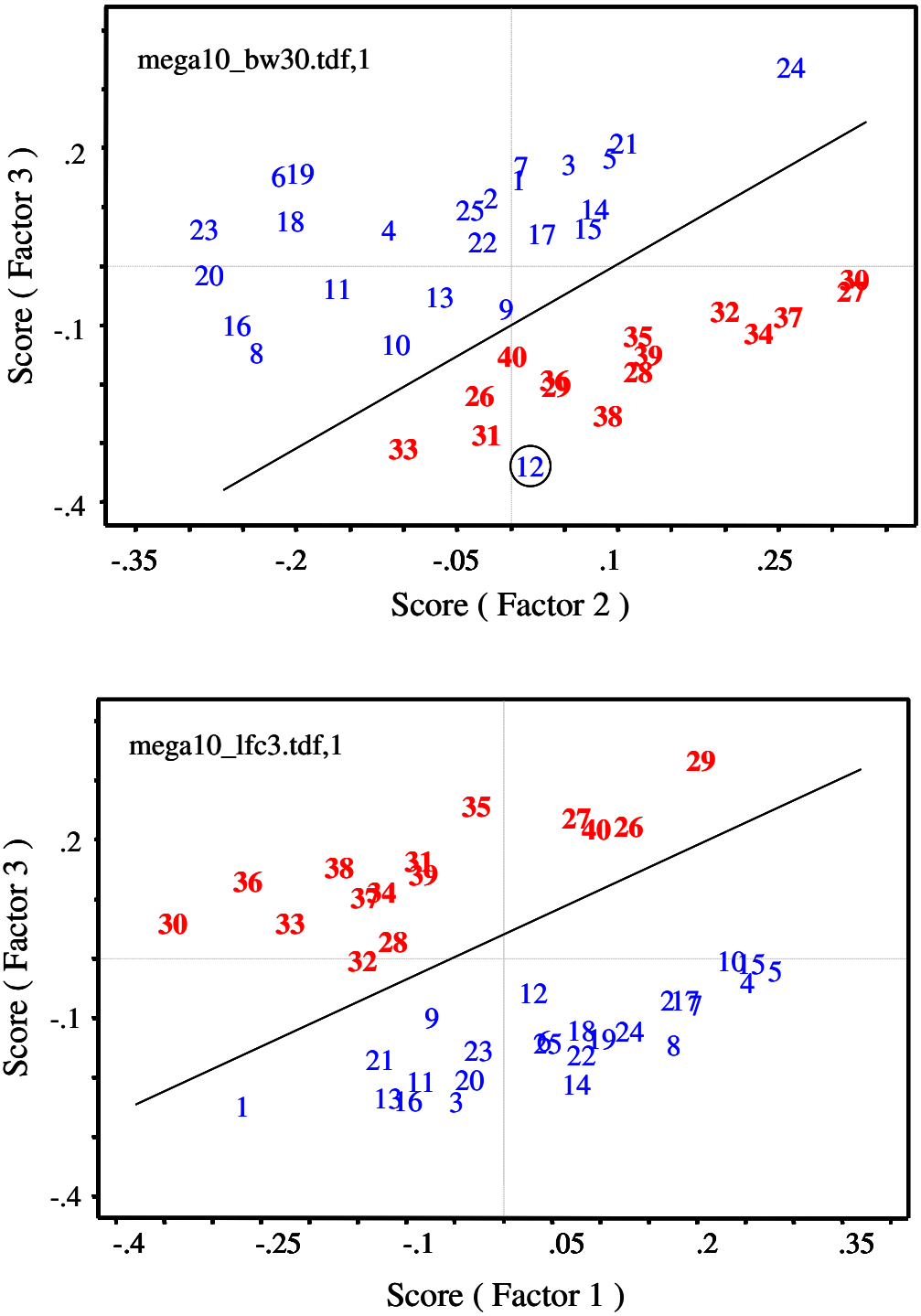

Figure 80. PCA scores plots of the IR spectra of FilmTec BW-30 (top) and Hydranautics LFC3 (bottom) RO membrane exposed to deconyl-N-methylglucamide (Mega 10) (26-40) and 1,000-ppm NaCl feedwater control (1-25).

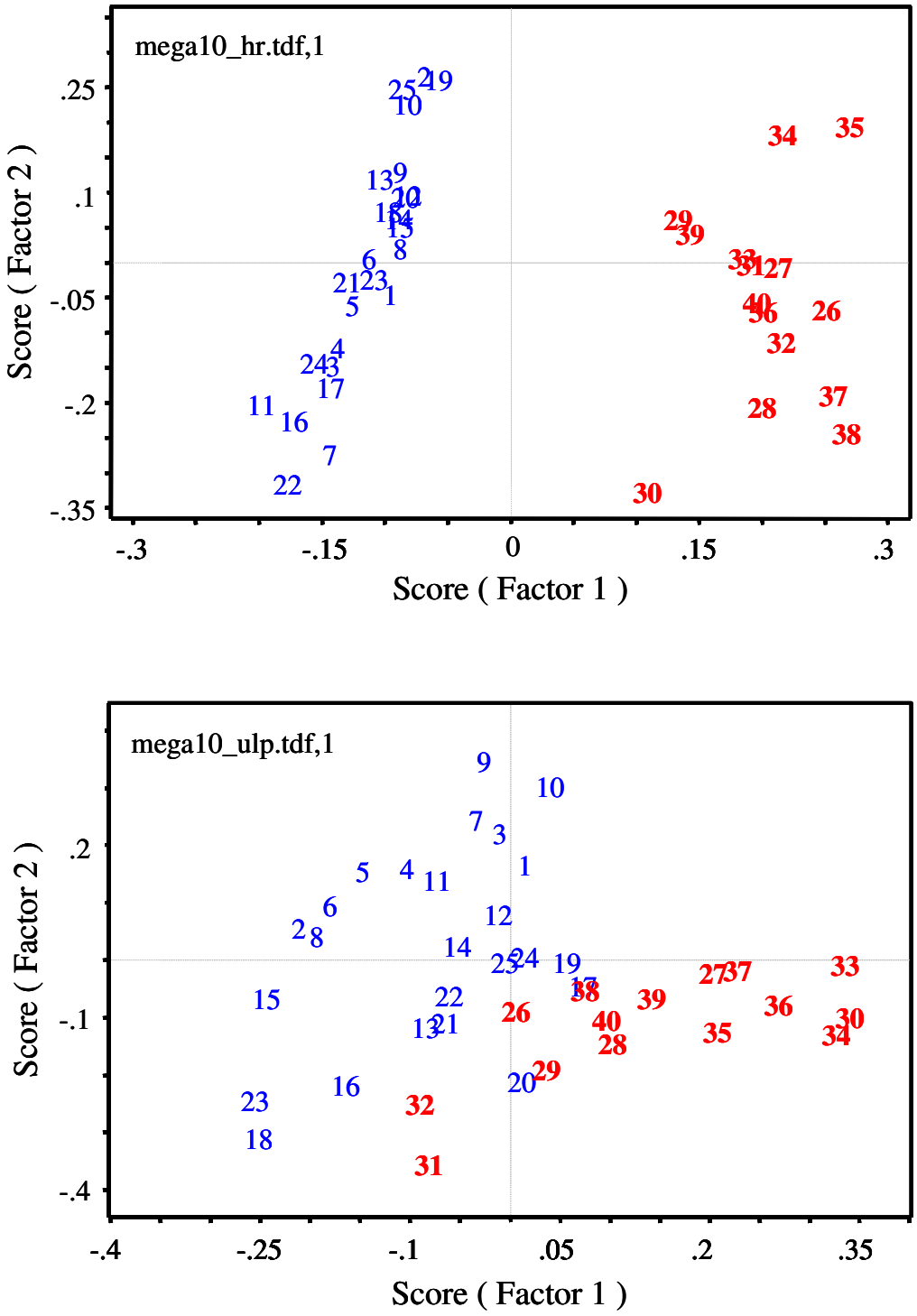

Figure 81. PCA scores plots of the IR spectra of Koch TFC-HR (top) and TFC-ULP (bottom) RO membrane exposed to deconyl-N-methylglucamide (Mega 10) (26-40) and 1,000-ppm NaCl feedwater control (1-25).

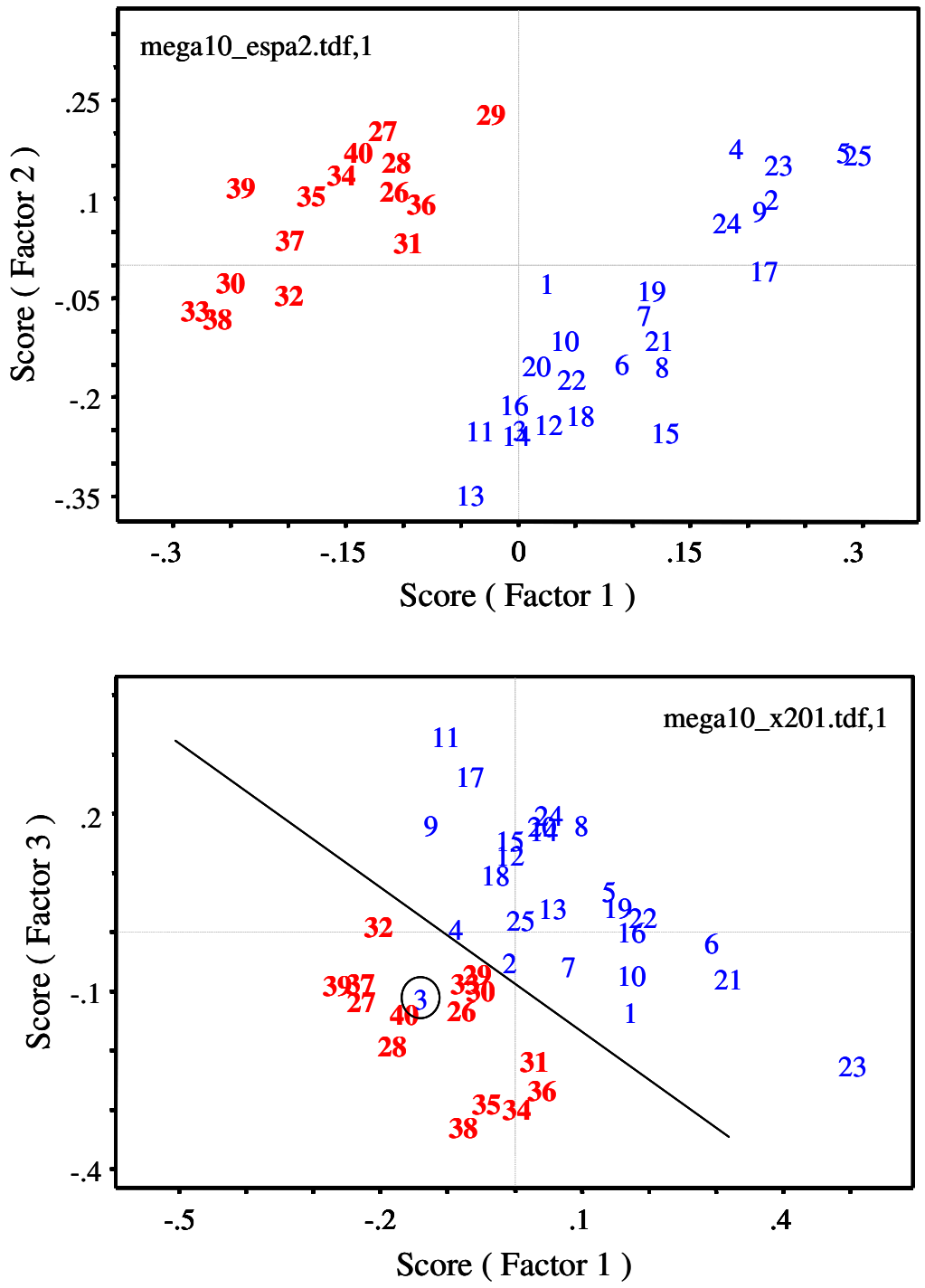

Figure 82. PCA scores plots of the IR spectra of Hydranautics ESPA2 (top) and Trisep X-201 (bottom) RO membrane exposed to deconyl-N-methylglucamide (Mega 10) (26-40) and 1,000-ppm NaCl feedwater control (1-25).

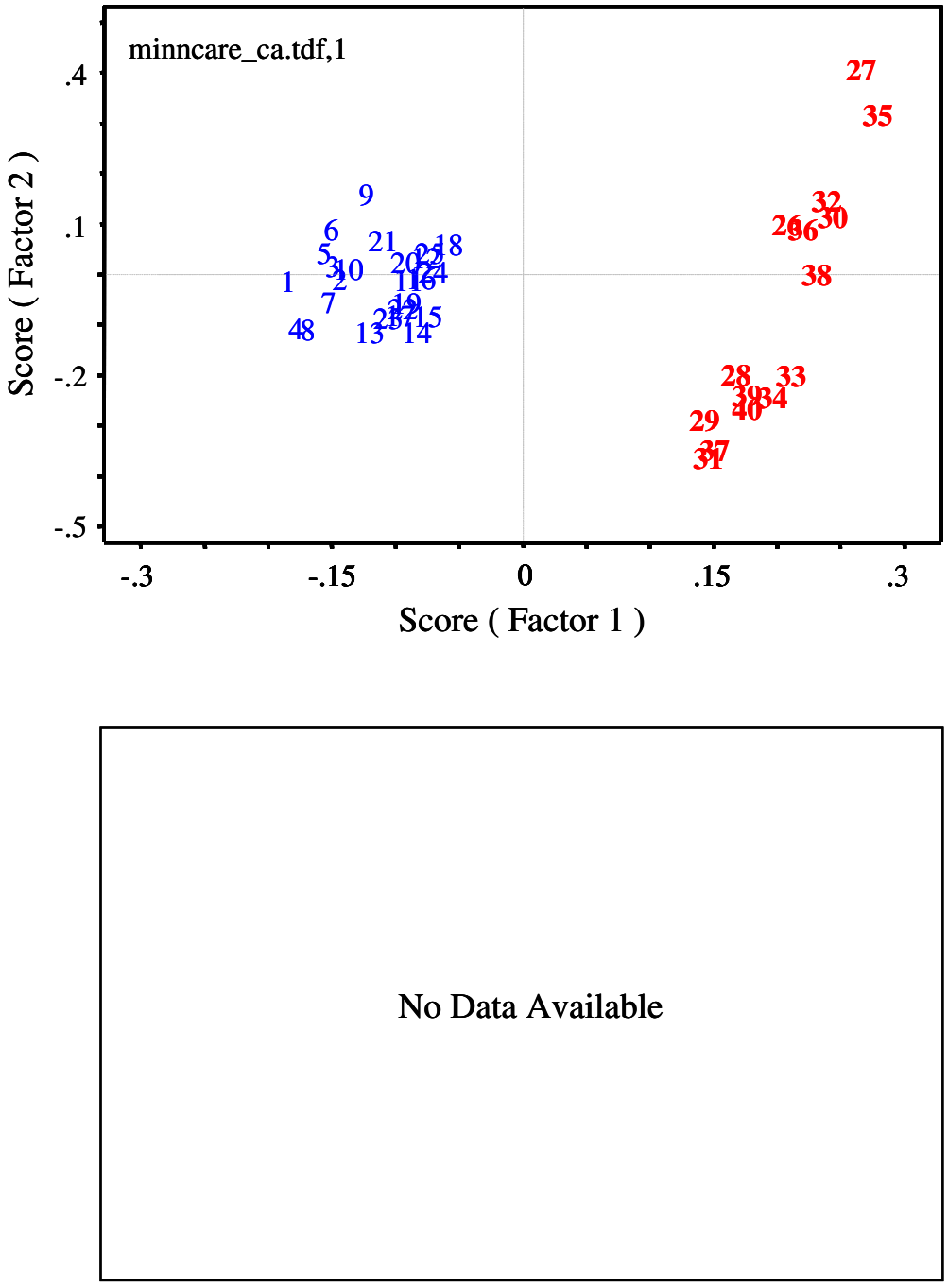

Figure 83. PCA scores plots of the IR spectra of Desal CA (top) and SST TMC/MPD (bottom) RO membrane exposed to Minncare (26-40) and 1,000-ppm NaCl feedwater control (1-25).

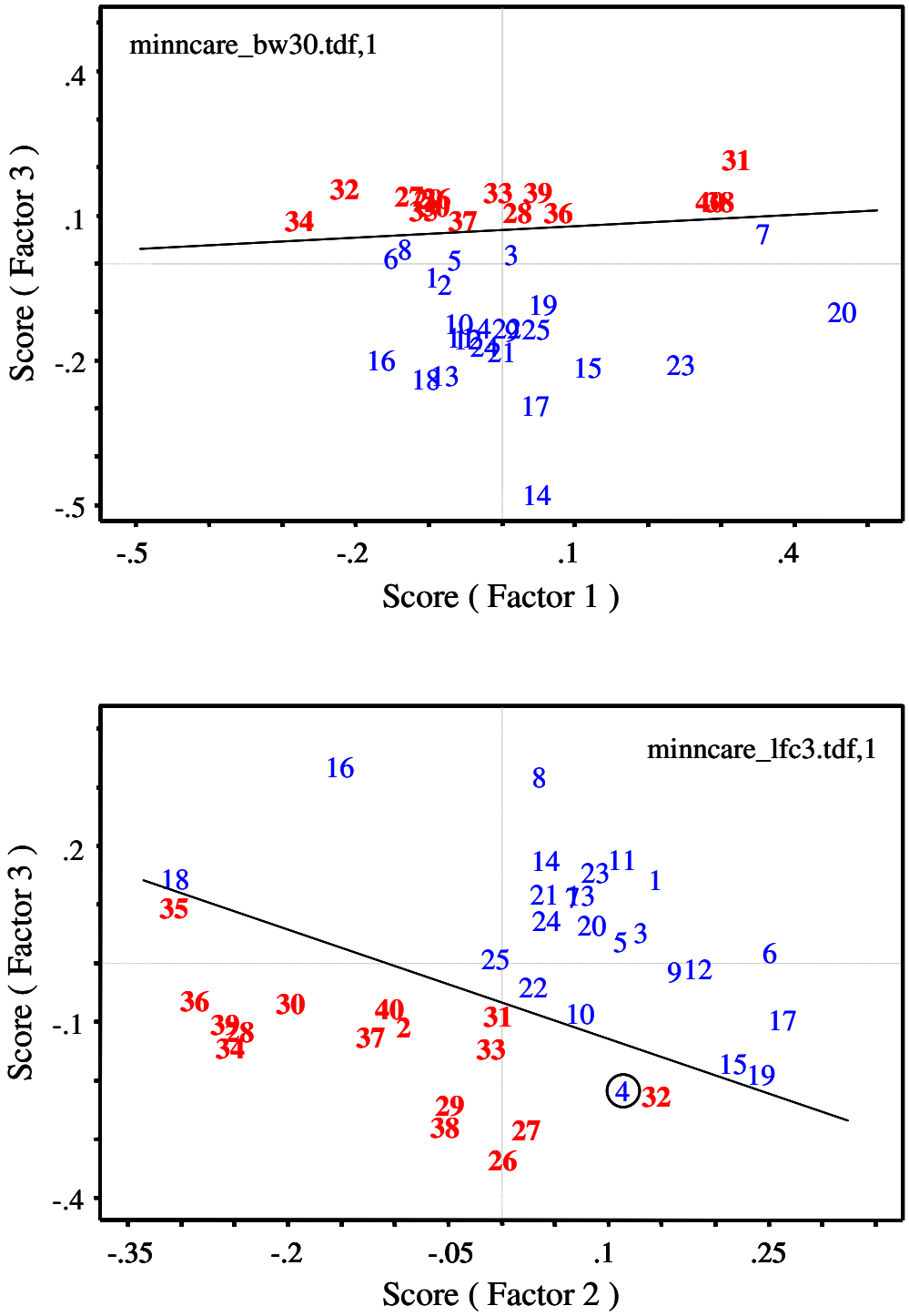

Figure 84. PCA scores plots of the IR spectra of FilmTec BW-30 (top) and Hydranautics LFC3 (bottom) RO membrane exposed to Minncare (26-40) and 1,000-ppm NaCl feedwater control (1-25).

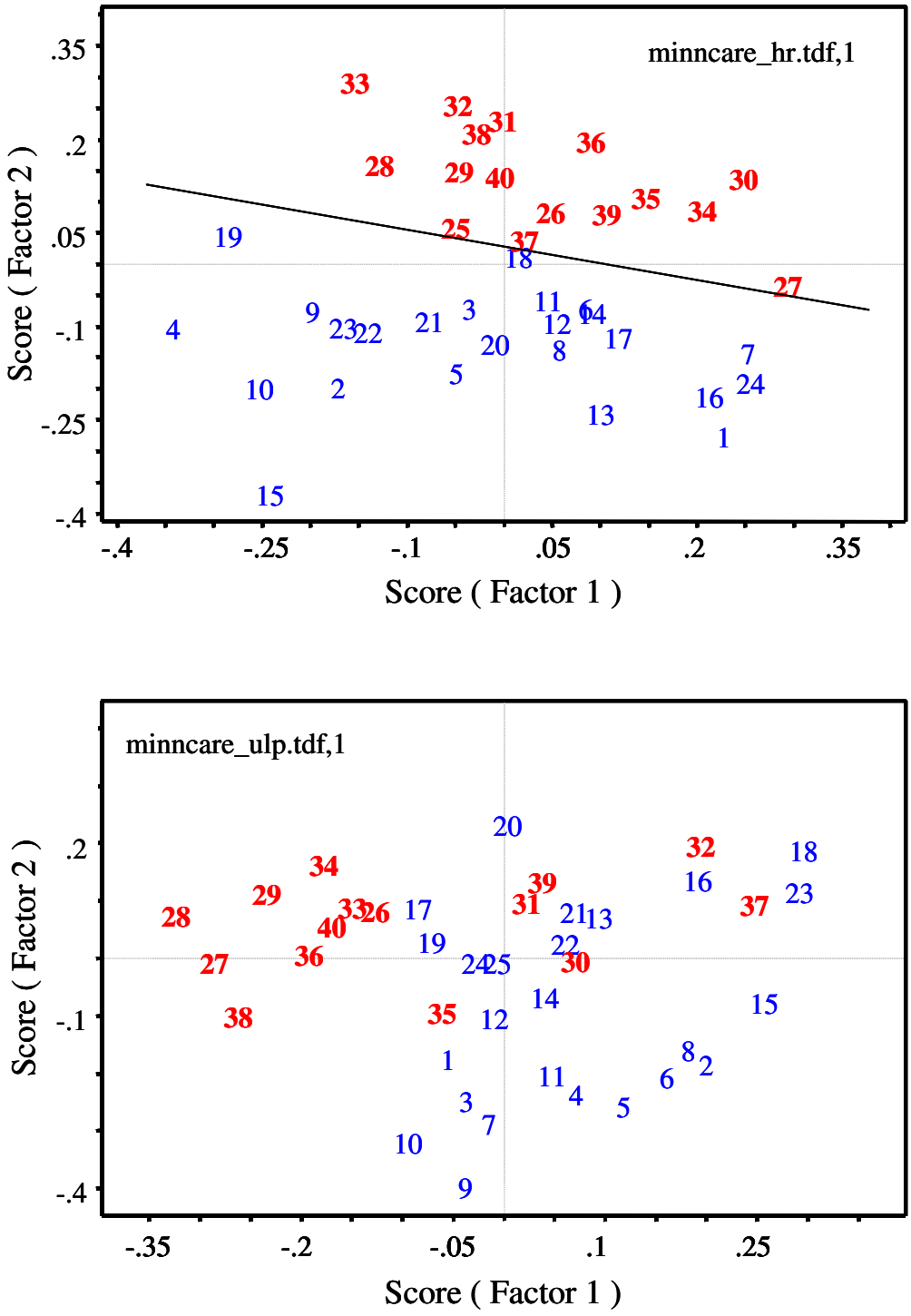

Figure 85. PCA scores plots of the IR spectra of Koch TFC-HR (top) and TFC-ULP (bottom) RO membrane exposed to Minncare (26-40) and 1,000-ppm NaCl feedwater control (1-25).

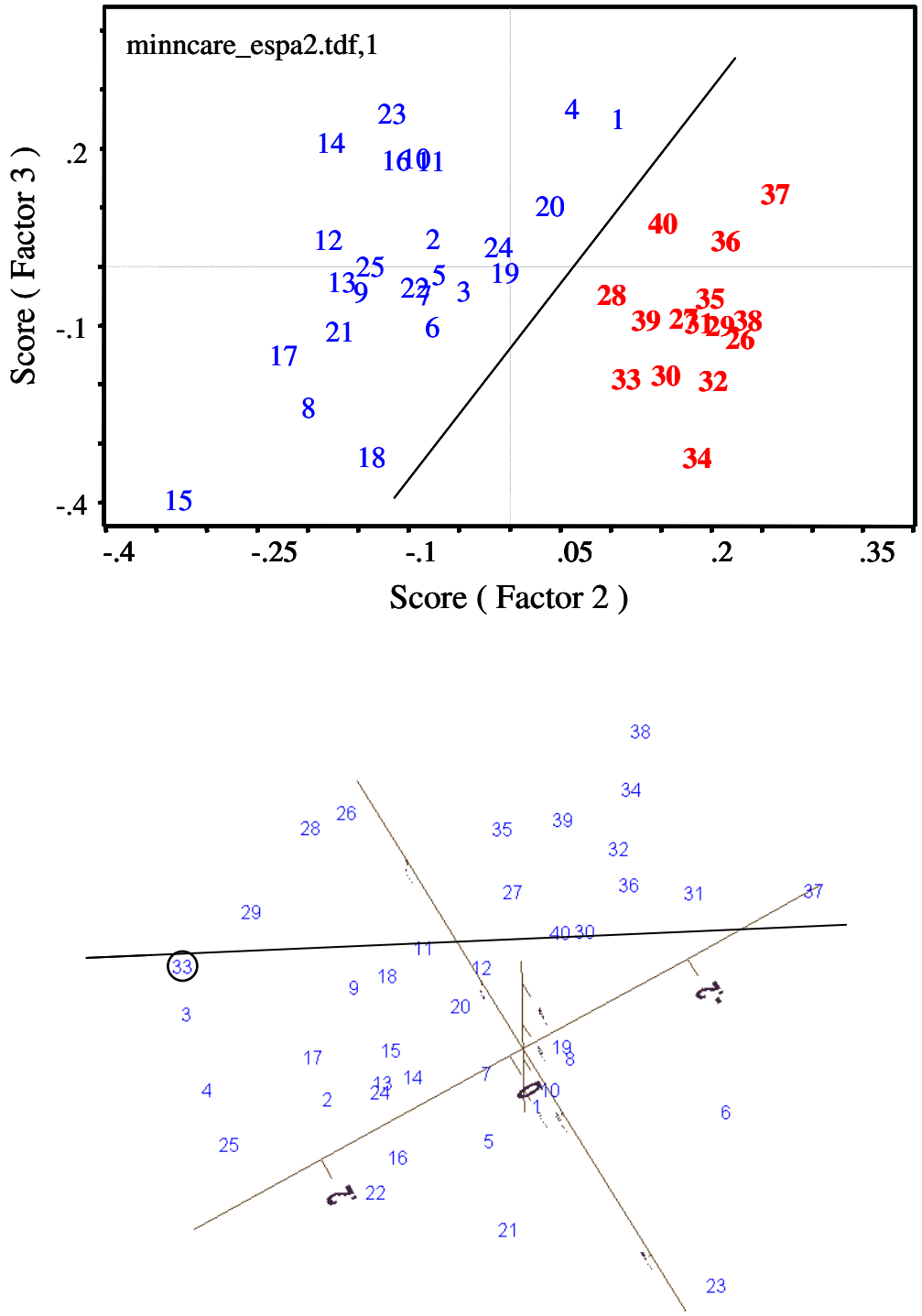

Figure 86. PCA scores plots of the IR spectra of Hydranautics ESPA2 (top) and Trisep X-201 (bottom) RO membrane exposed to SDS (26-40) and 1,000-ppm NaCl feedwater control (1-25).

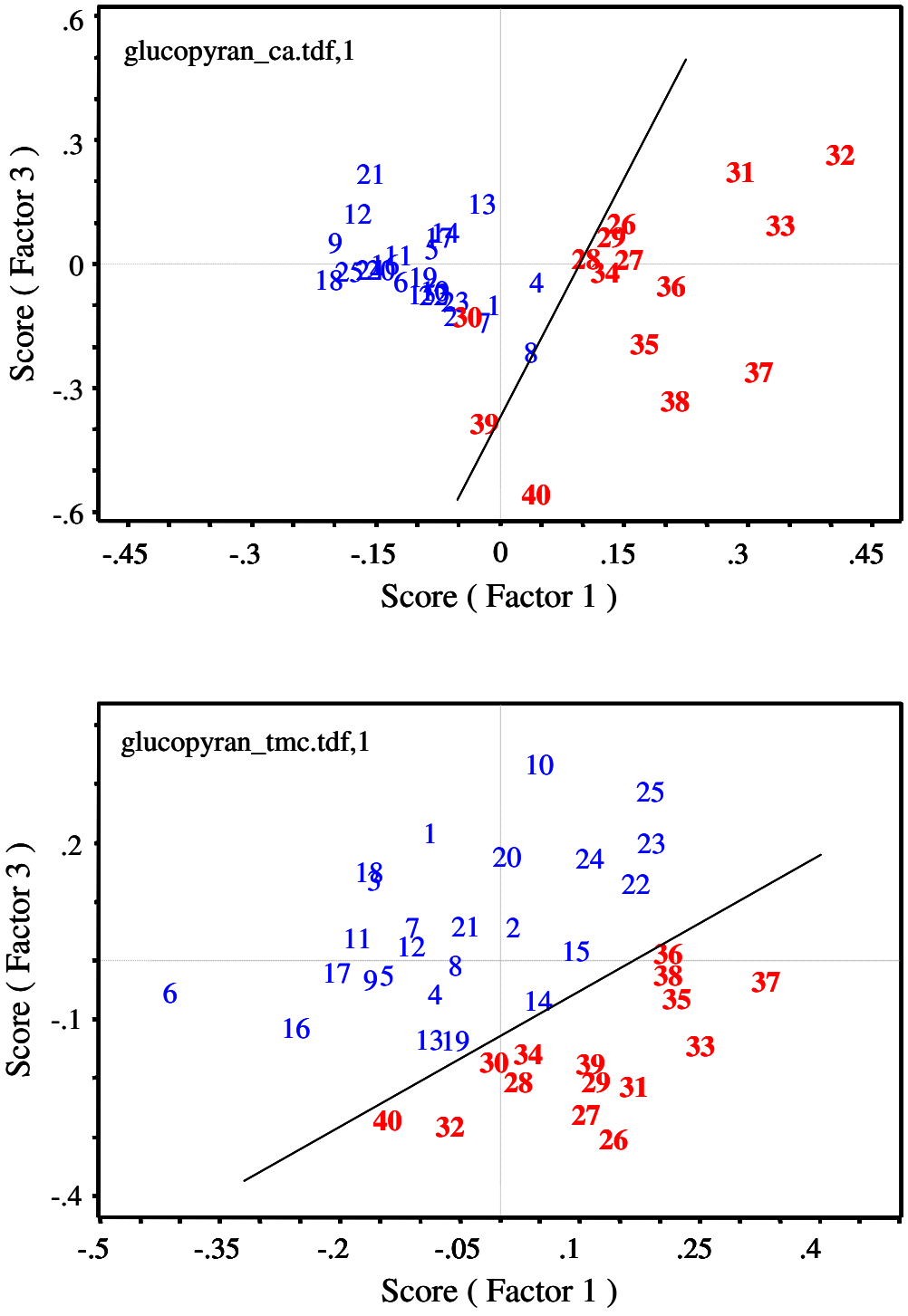

Figure 87. PCA scores plots of the IR spectra of Desal CA (top) and SST TMC/MPD (bottom) RO membrane exposed to n-nonyl-β-*D*-glucopyranoside (26-40) and 1,000-ppm NaCl feedwater control (1-25).

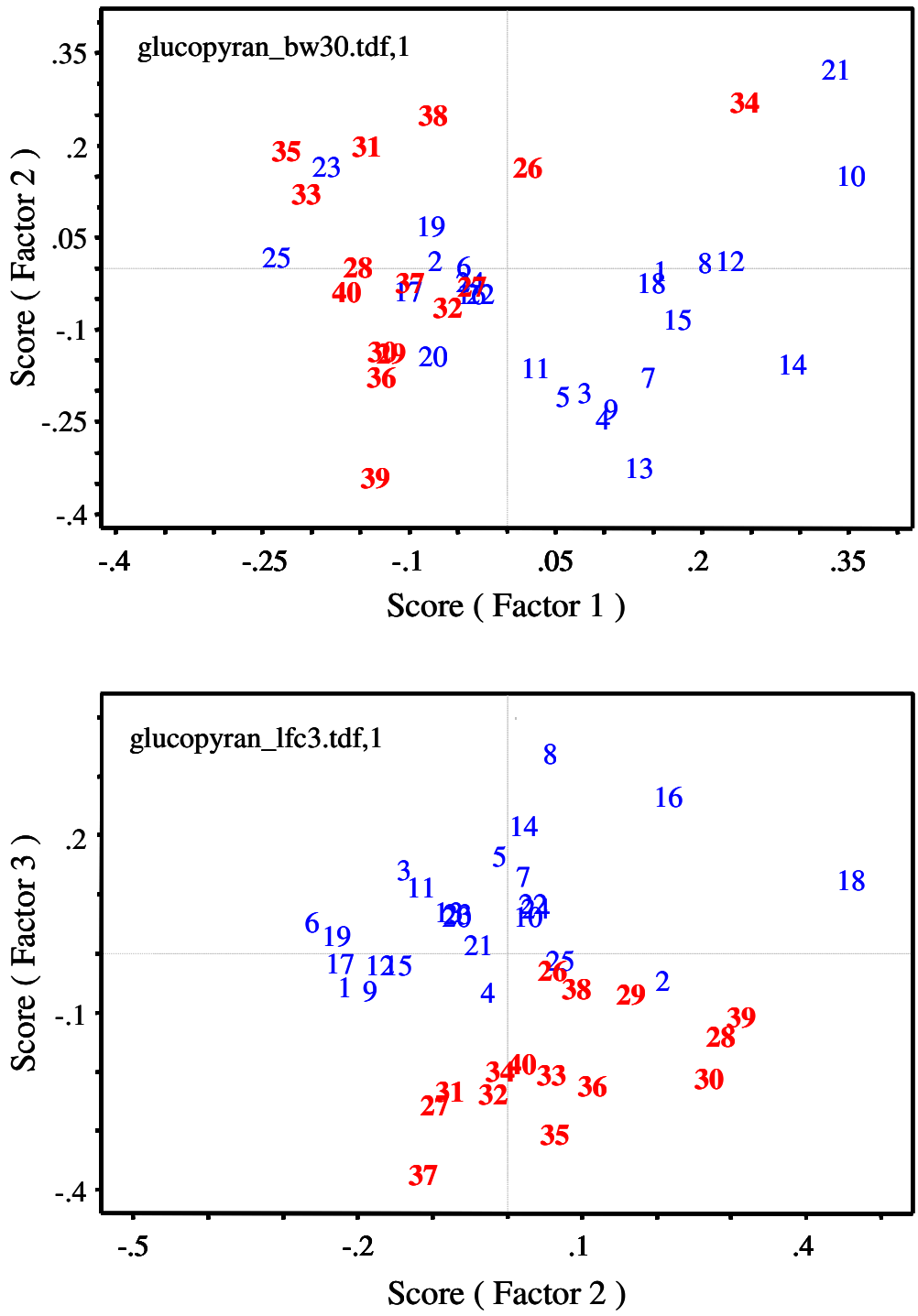

Figure 88. PCA scores plots of the IR spectra of FilmTec BW-30 (top) and Hydranautics LFC3 (bottom) RO membrane exposed to n-nonyl-β-*D*-glucopyranoside (26-40) and 1,000-ppm NaCl feedwater control (1-25).

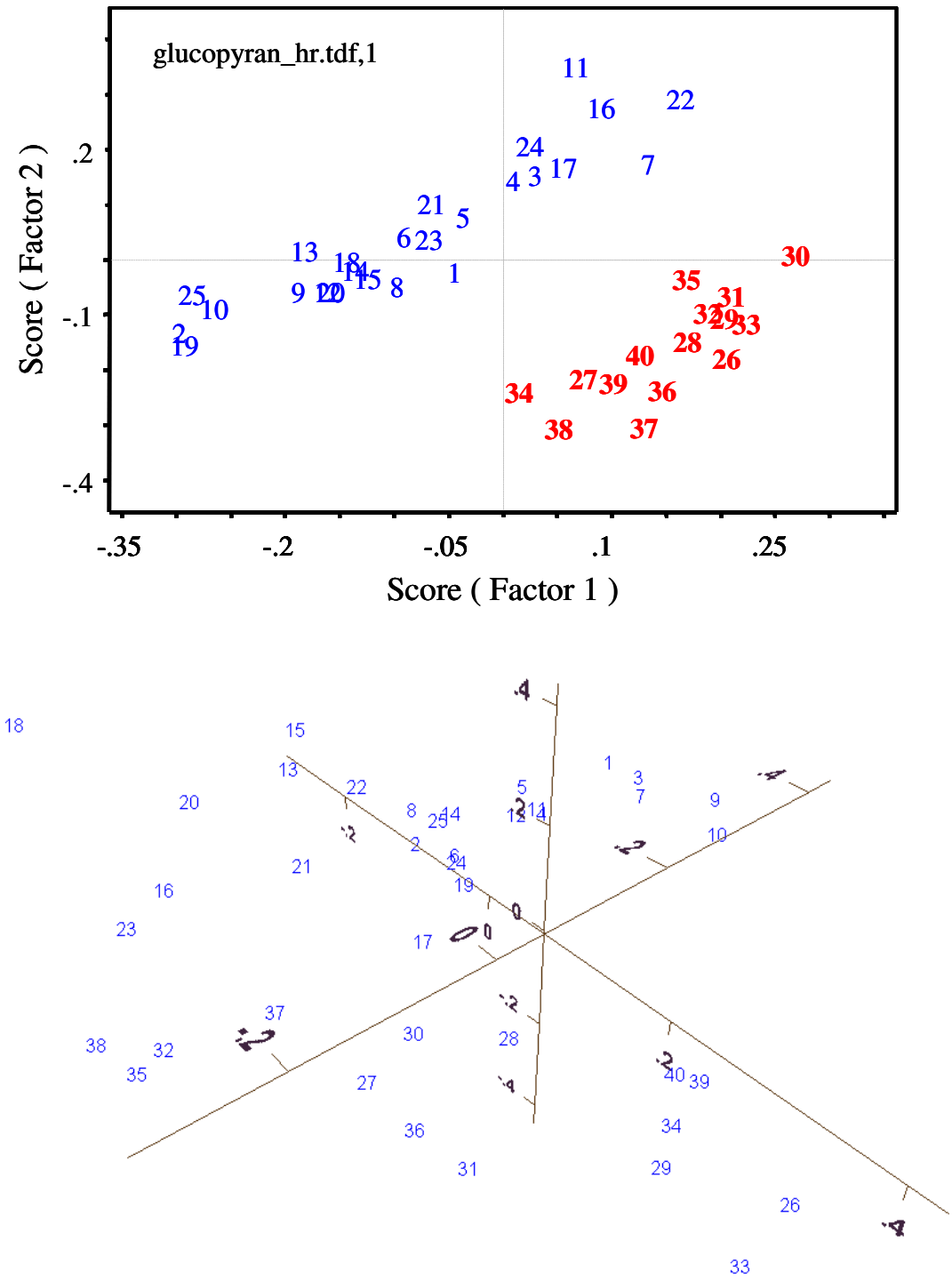

Figure 89. PCA scores plots of the IR spectra of Koch TFC-HR (top) and TFC-ULP (bottom) RO membrane exposed to n-nonyl-β-*D*-glucopyranoside (26-40) and 1,000-ppm NaCl feedwater control (1-25).

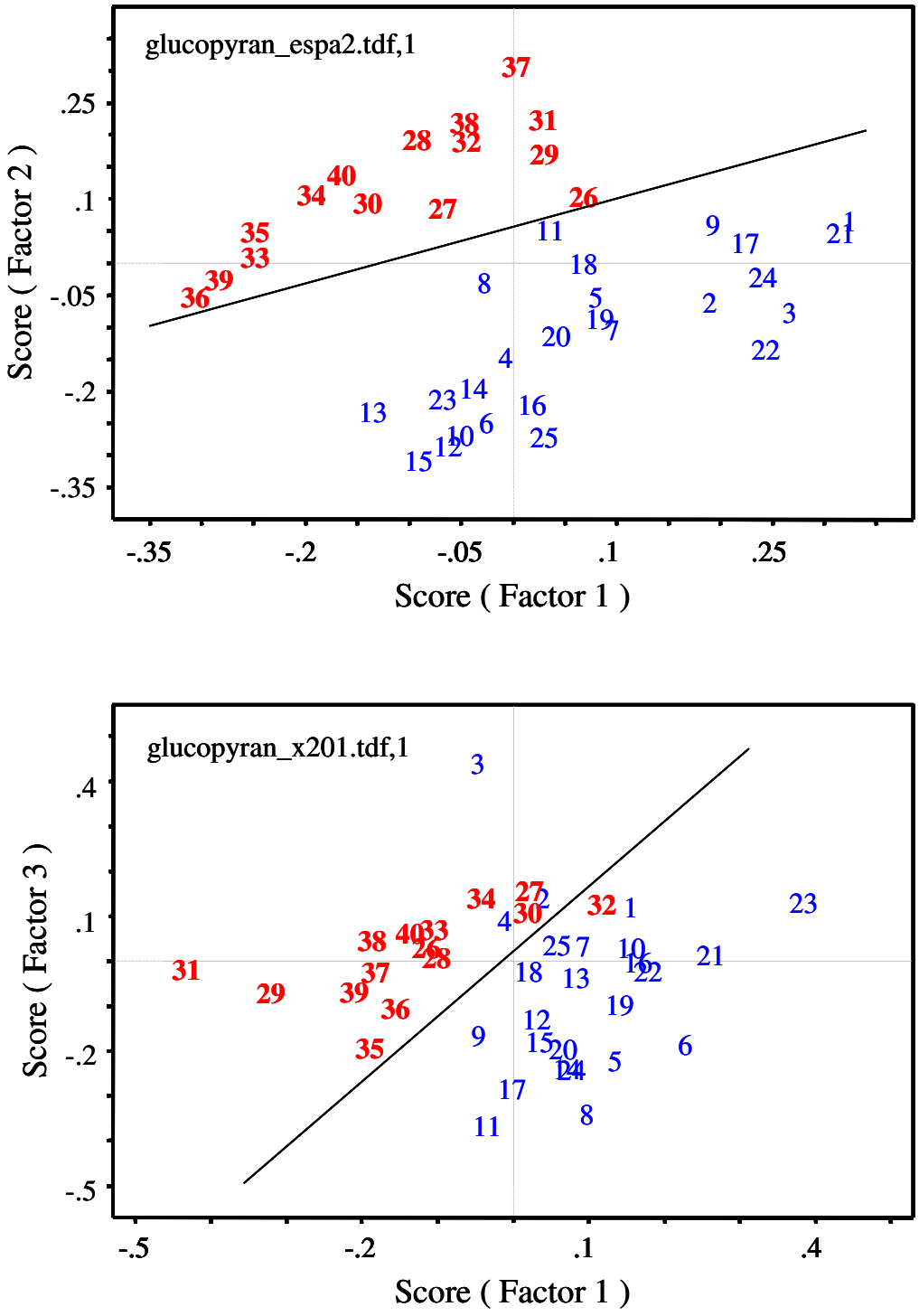

Figure 90. PCA scores plots of the IR spectra of Hydranautics ESPA2 (top) and Trisep X-201 (bottom) RO membrane exposed to n-nonyl-β-*D*-glucopyranoside (26-40) and 1,000-ppm NaCl feedwater control (1-25).

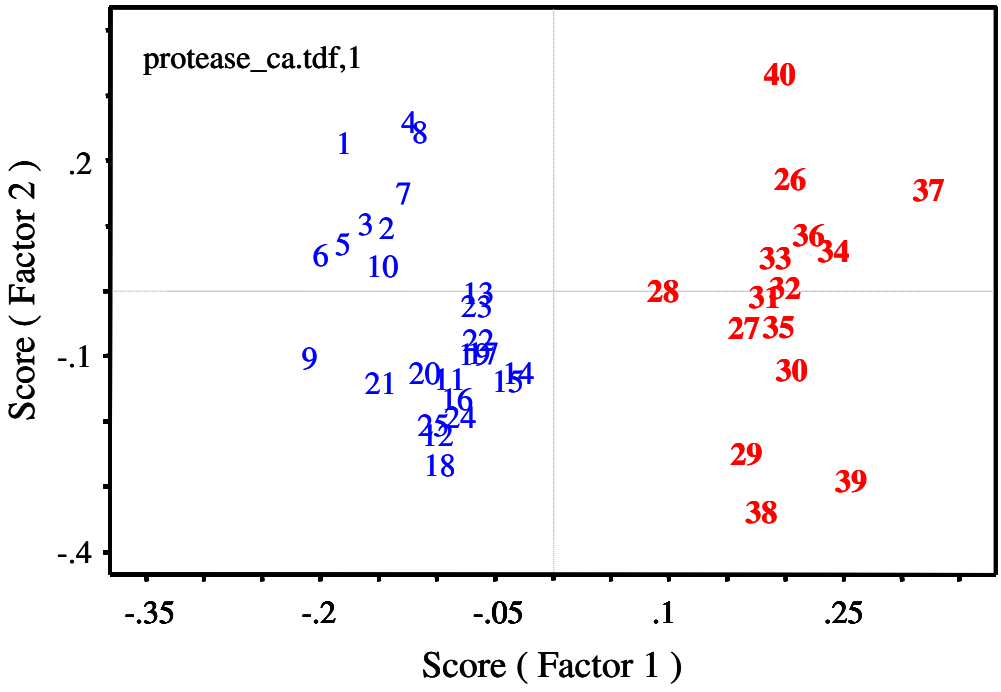

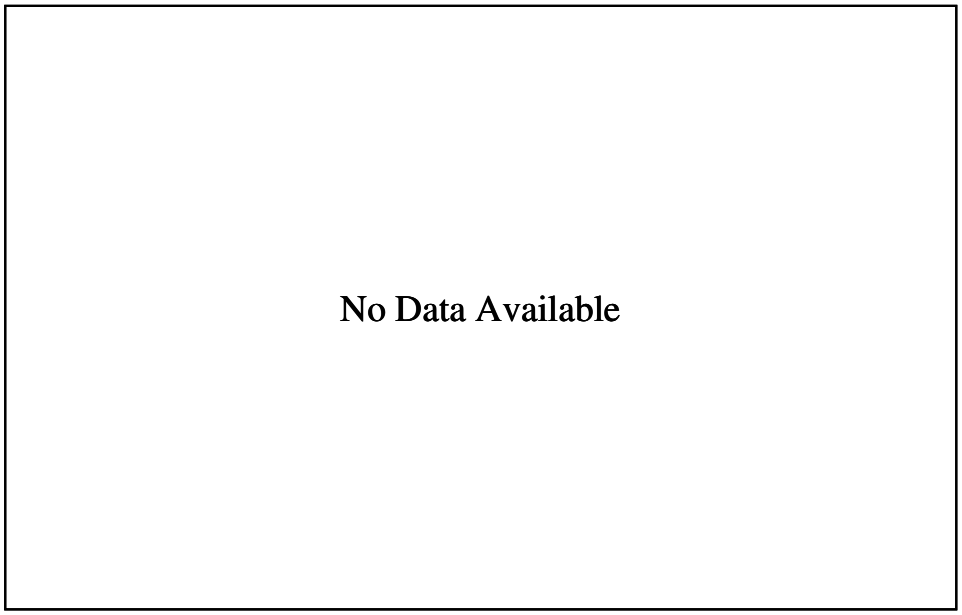

Figure 91. PCA scores plots of the IR spectra of Desal CA and protease TMC/MPD RO membrane exposed to protease (26-40) and 1,000-ppm NaCl feedwater control (1-25).

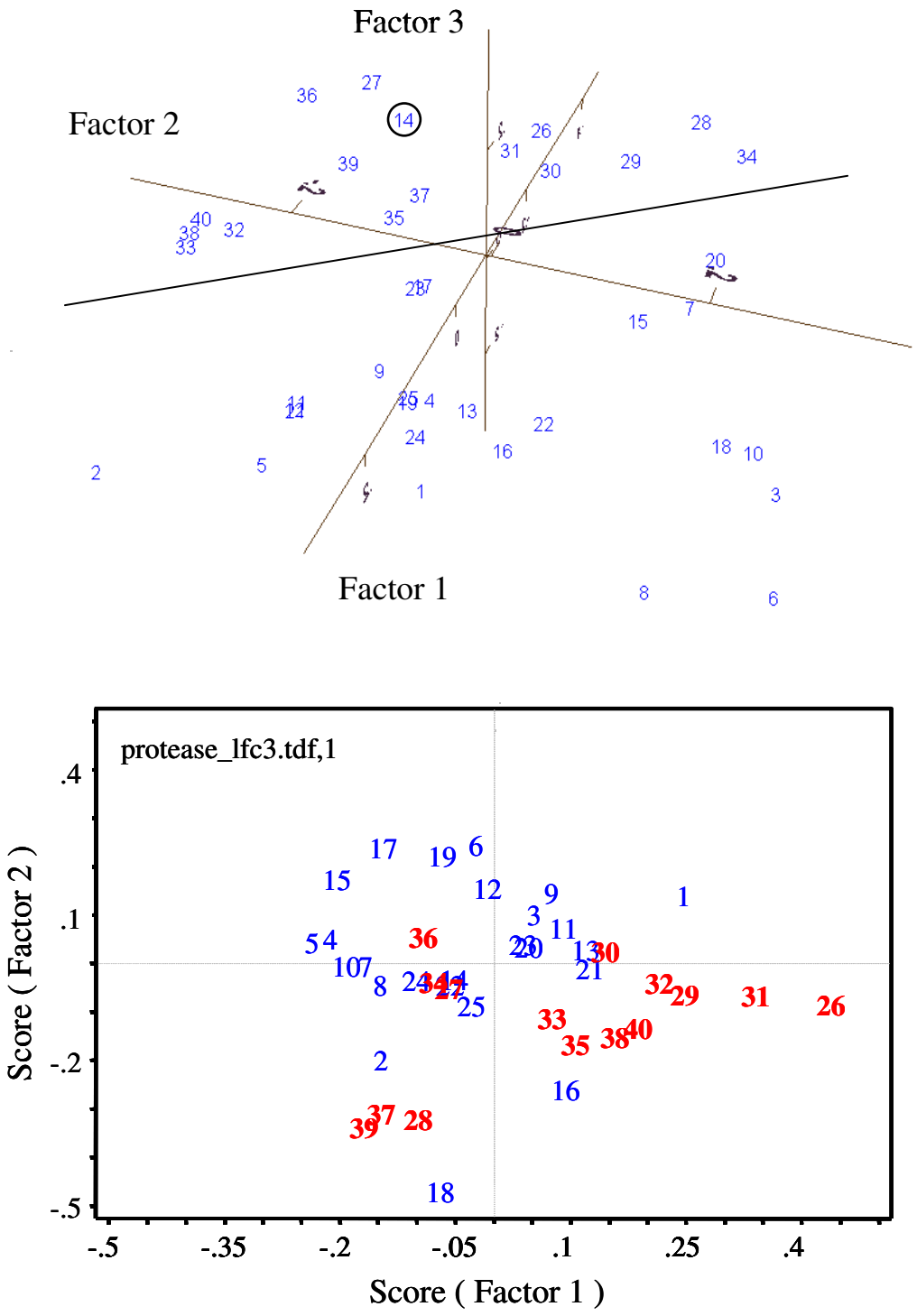

Figure 92. PCA scores plots of the IR spectra of FilmTec BW-30 (top) and Hydranautics LFC3 (bottom) RO membrane exposed to protease (26-40) and 1,000-ppm NaCl feedwater control (1-25).

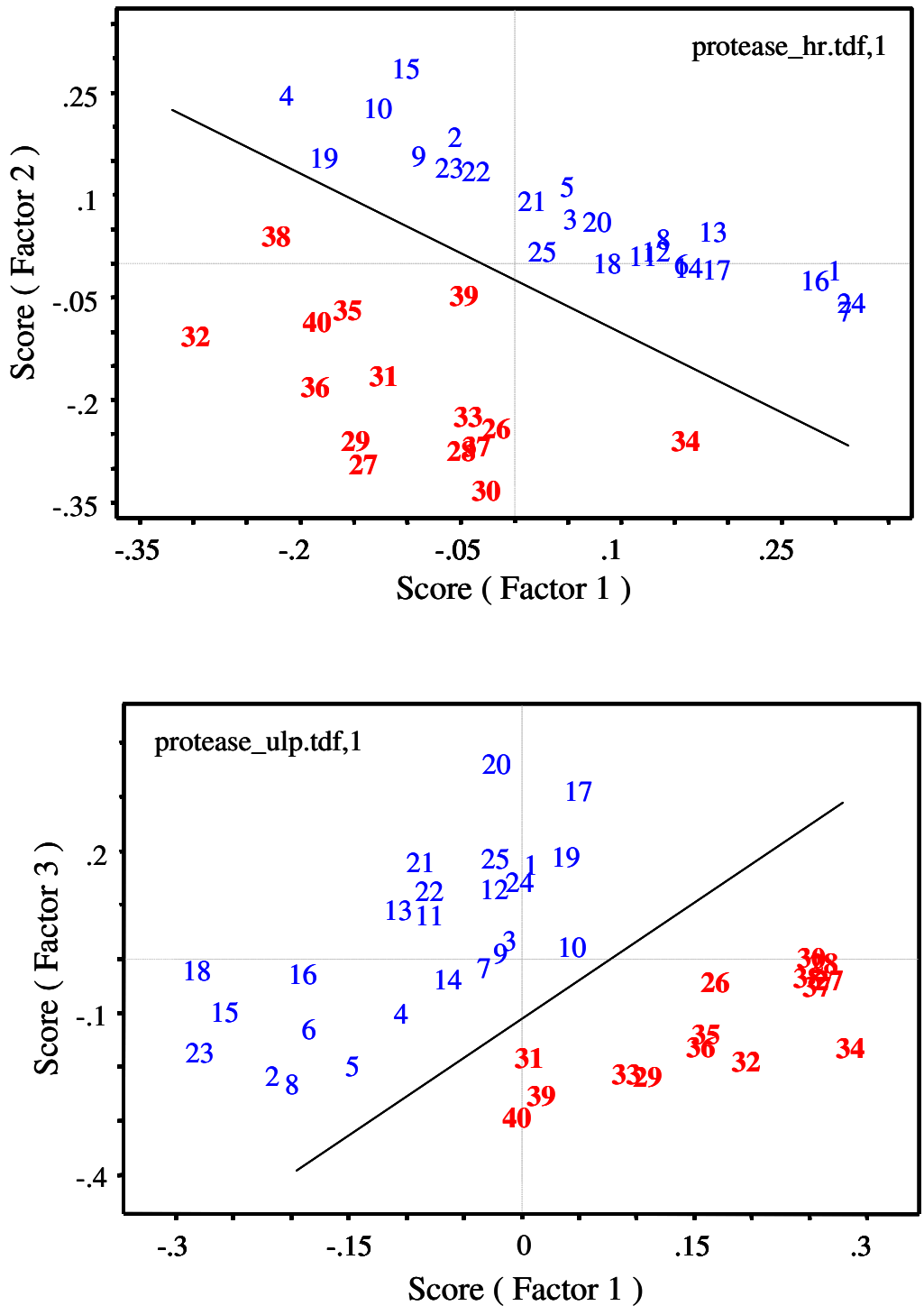

Figure 93. PCA scores plots of the IR spectra of Koch TFC-HR (top) and TFC-ULP (bottom) RO membrane exposed to protease (26-40) and 1,000-ppm NaCl feedwater control (1-25).

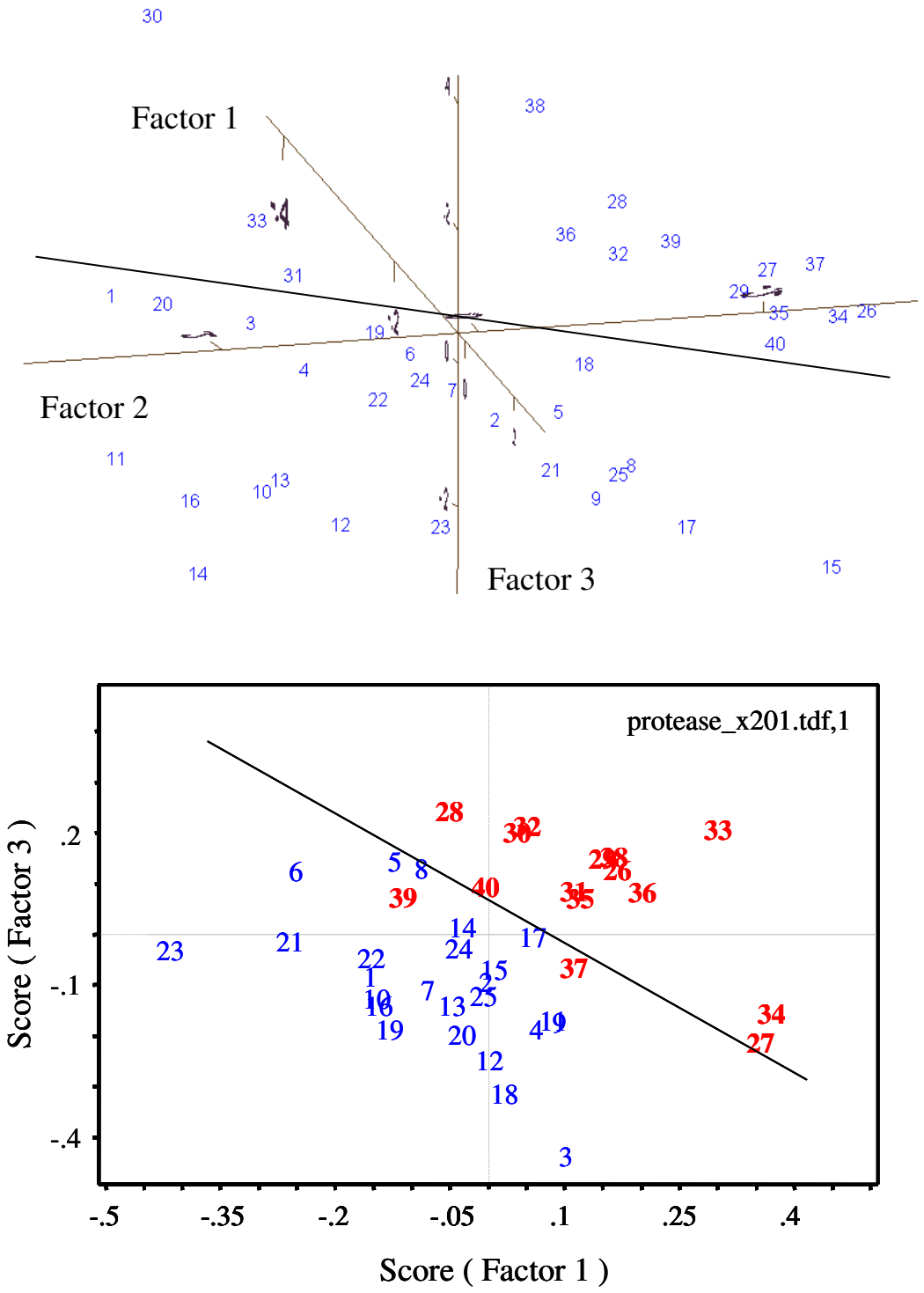

Figure 94. PCA scores plots of the IR spectra of Hydranautics ESPA2 (top) and Trisep X-201 (bottom) RO membrane exposed to protease (26-40) and 1,000-ppm NaCl feedwater control (1-25).

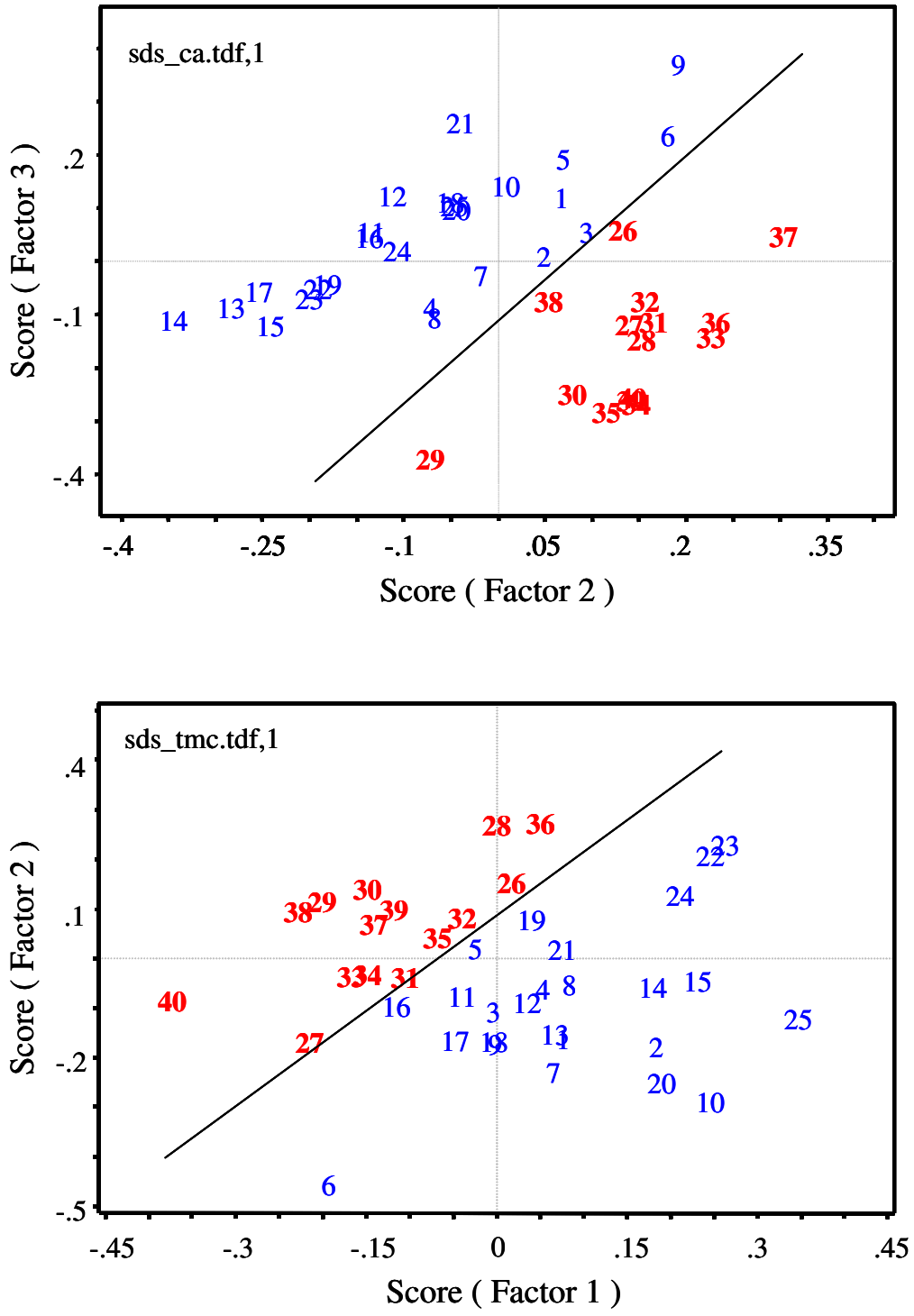

Figure 95. PCA scores plots of the IR spectra of Desal CA (top) and SST TMC/MPD (bottom) RO membrane exposed to SDS (26-40) and 1,000-ppm NaCl feedwater control (1-25).

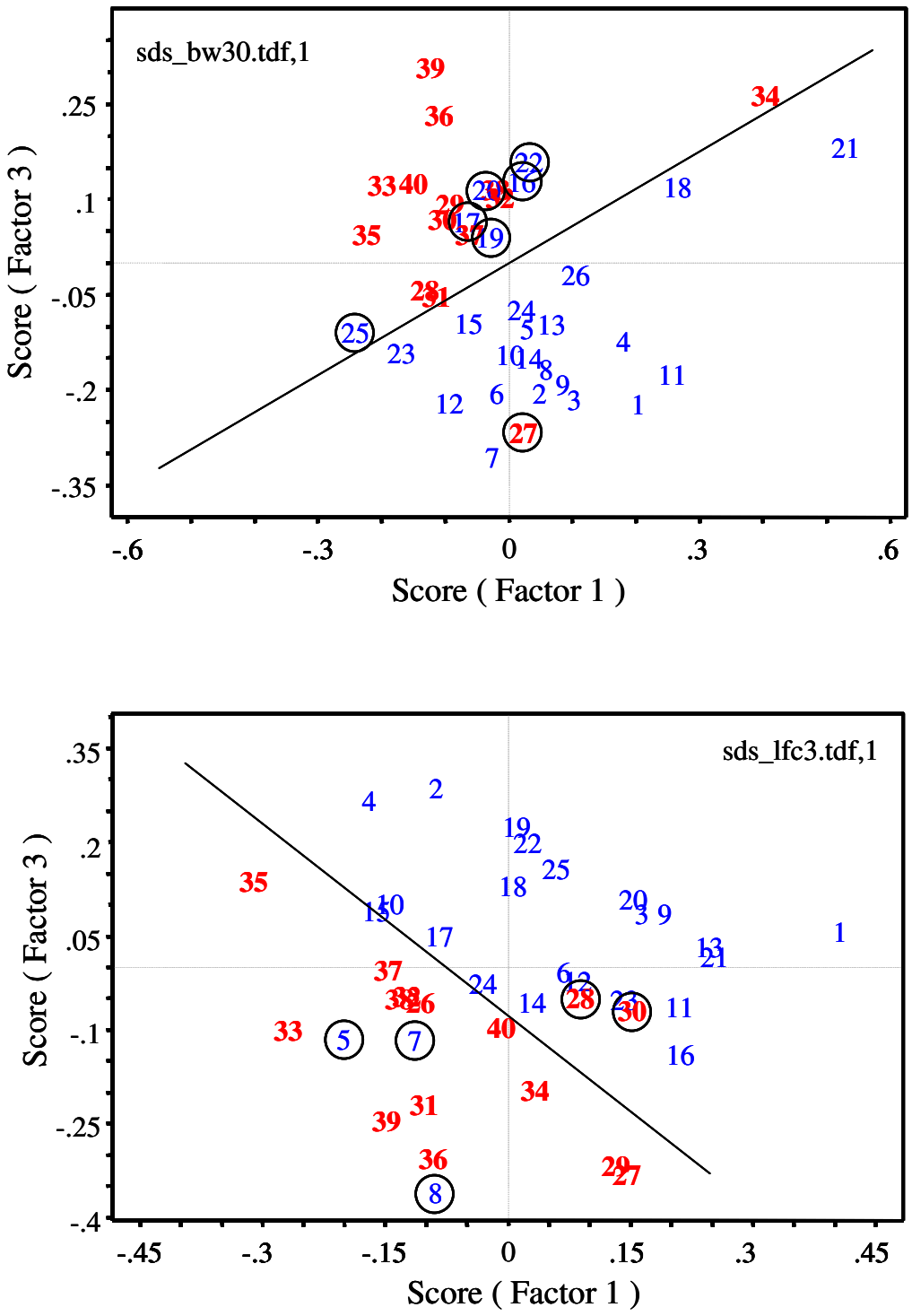

Figure 96. PCA scores plots of the IR spectra of FilmTec BW-30 (top) and Hydranautics LFC3 (bottom) RO membrane exposed to SDS (26-40) and 1,000-ppm NaCl feedwater control (1-25).

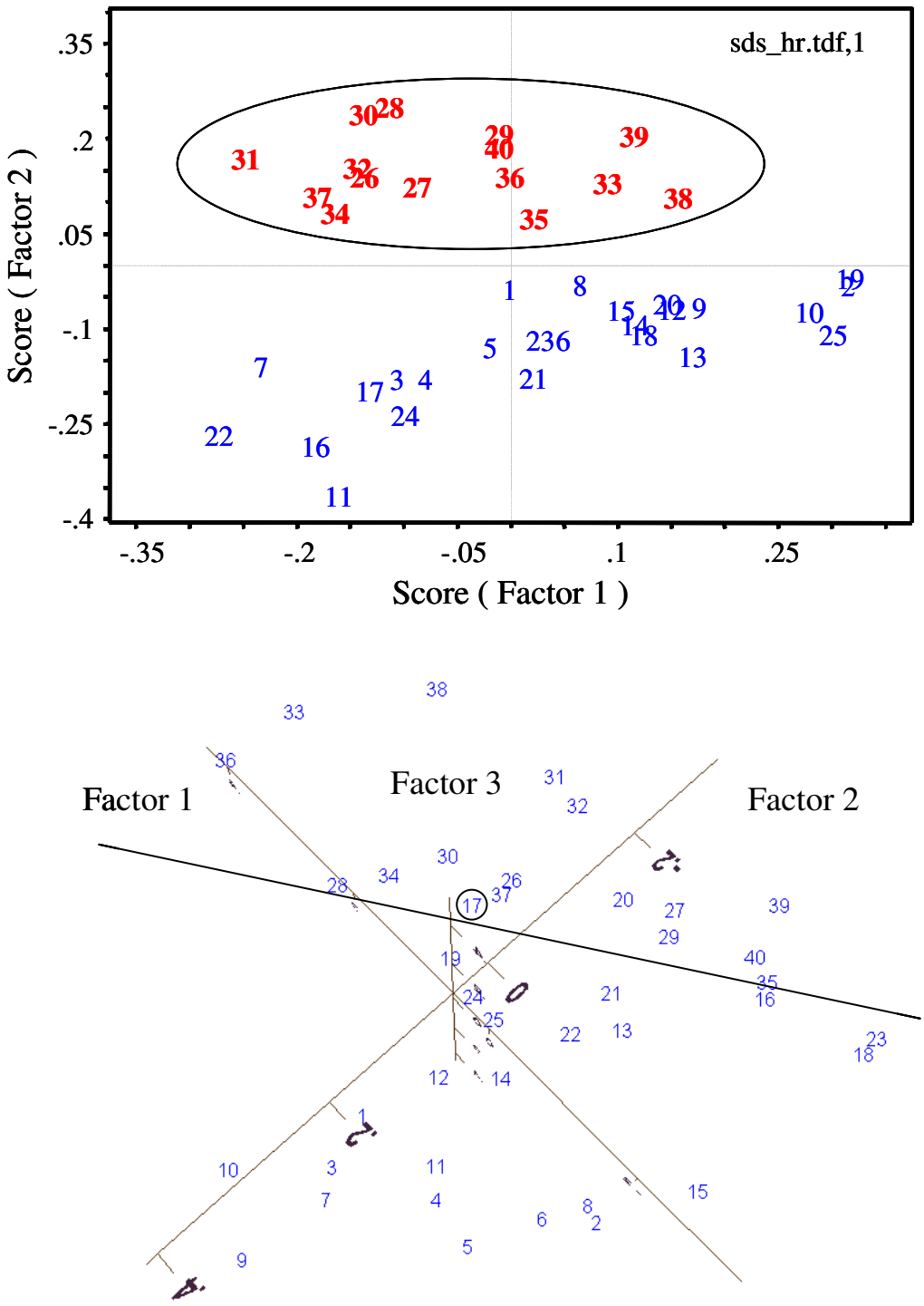

Figure 97. PCA scores plots of the IR spectra of Koch TFC-HR (top) and TFC-ULP (bottom) RO membrane exposed to SDS (26-40) and 1,000-ppm NaCl feedwater control (1-25).

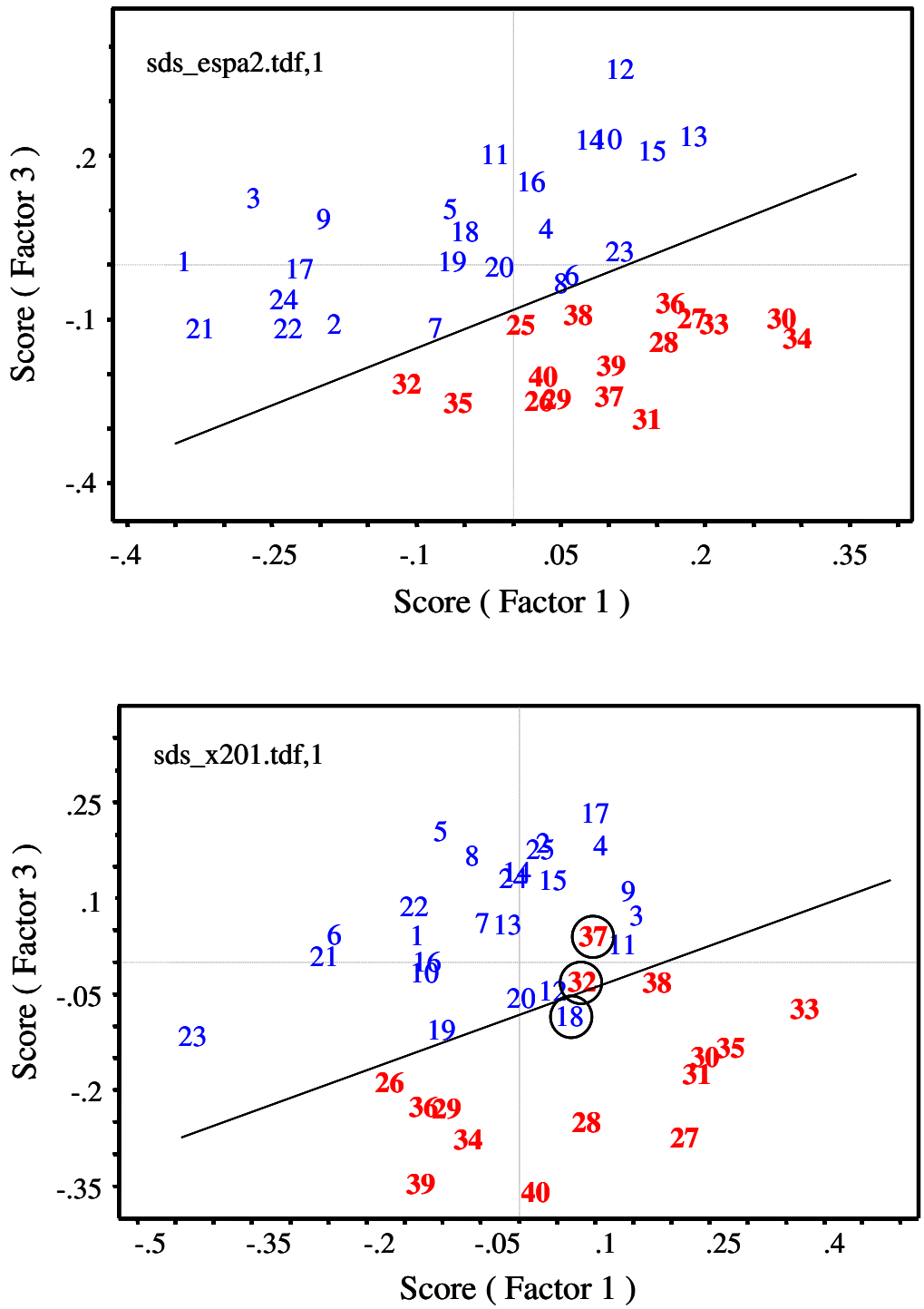

Figure 98. PCA scores plots of the IR spectra of Hydranautics ESPA2 (top) and Trisep X-201 (bottom) RO membrane exposed to SDS (26-40) and 1,000-ppm NaCl feedwater control (1-25).

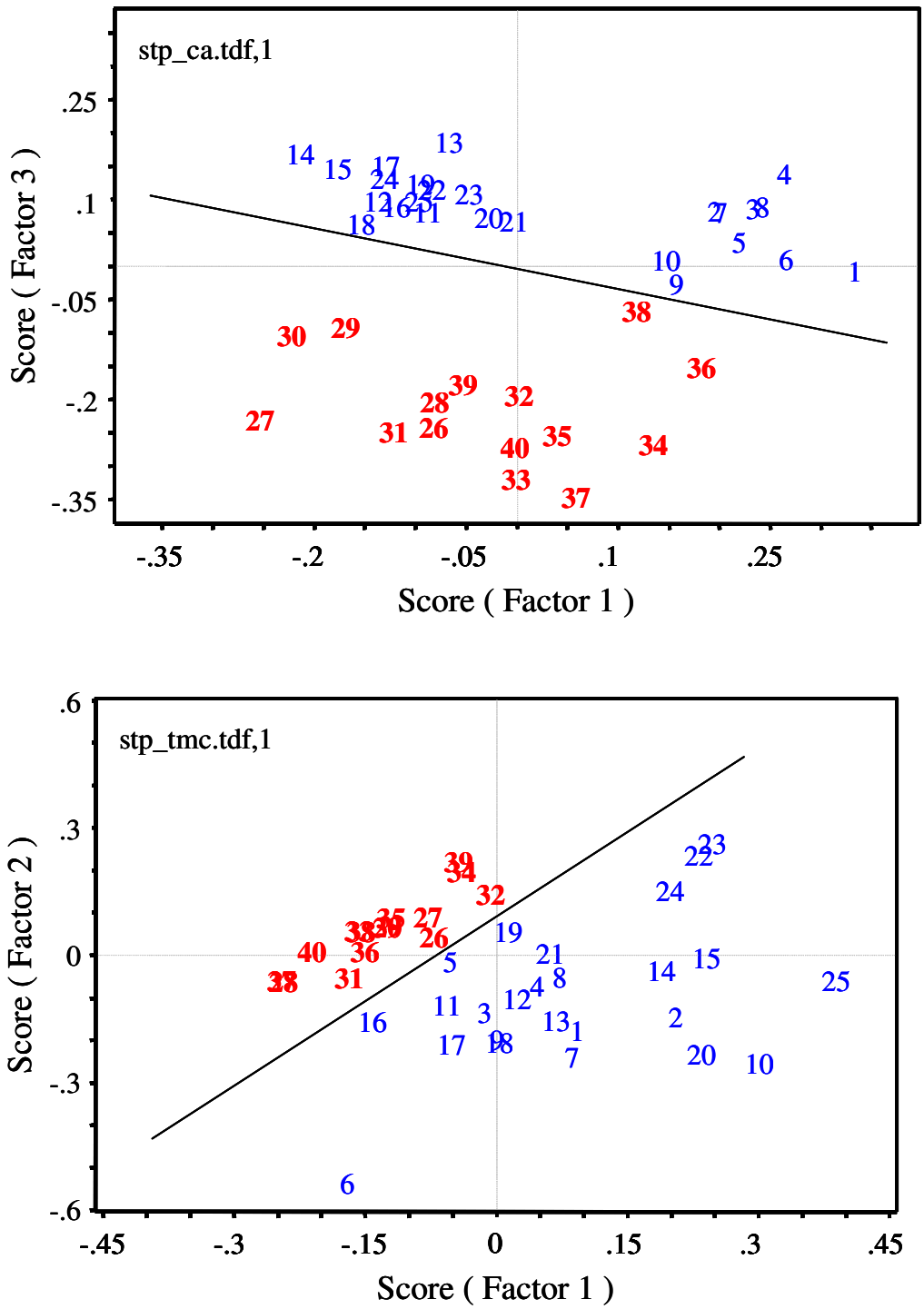

Figure 99. PCA scores plots of the IR spectra of Desal CA (top) and SST TMC/MPD (bottom) RO membrane exposed to STP (26-40) and 1,000-ppm NaCl feedwater control (1-25).

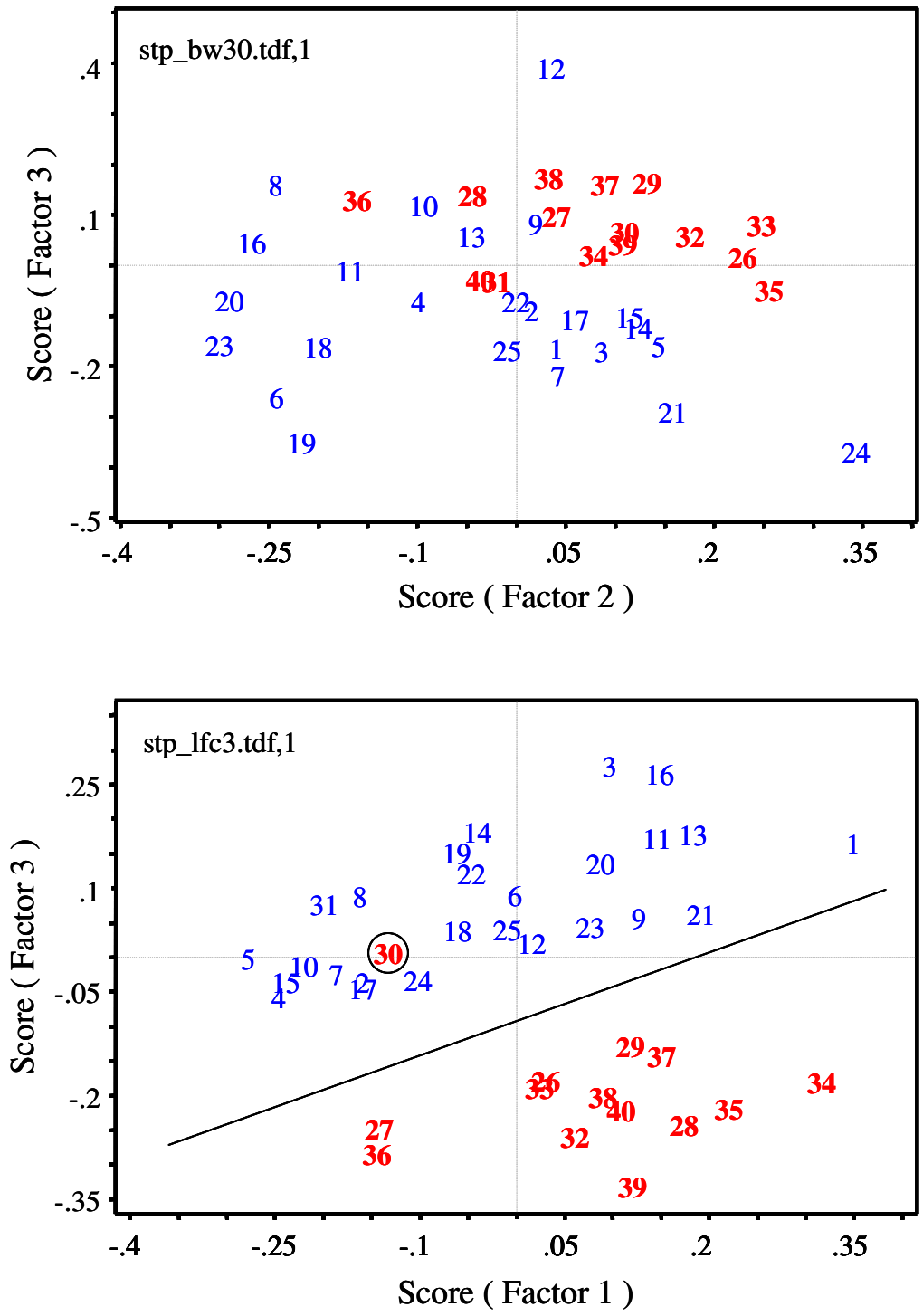

Figure 100. PCA scores plots of the IR spectra of FilmTec BW-30 (top) and Hydranautics LFC3 (bottom) RO membrane exposed to STP (26-40) and 1,000-ppm NaCl feedwater control (1-25).

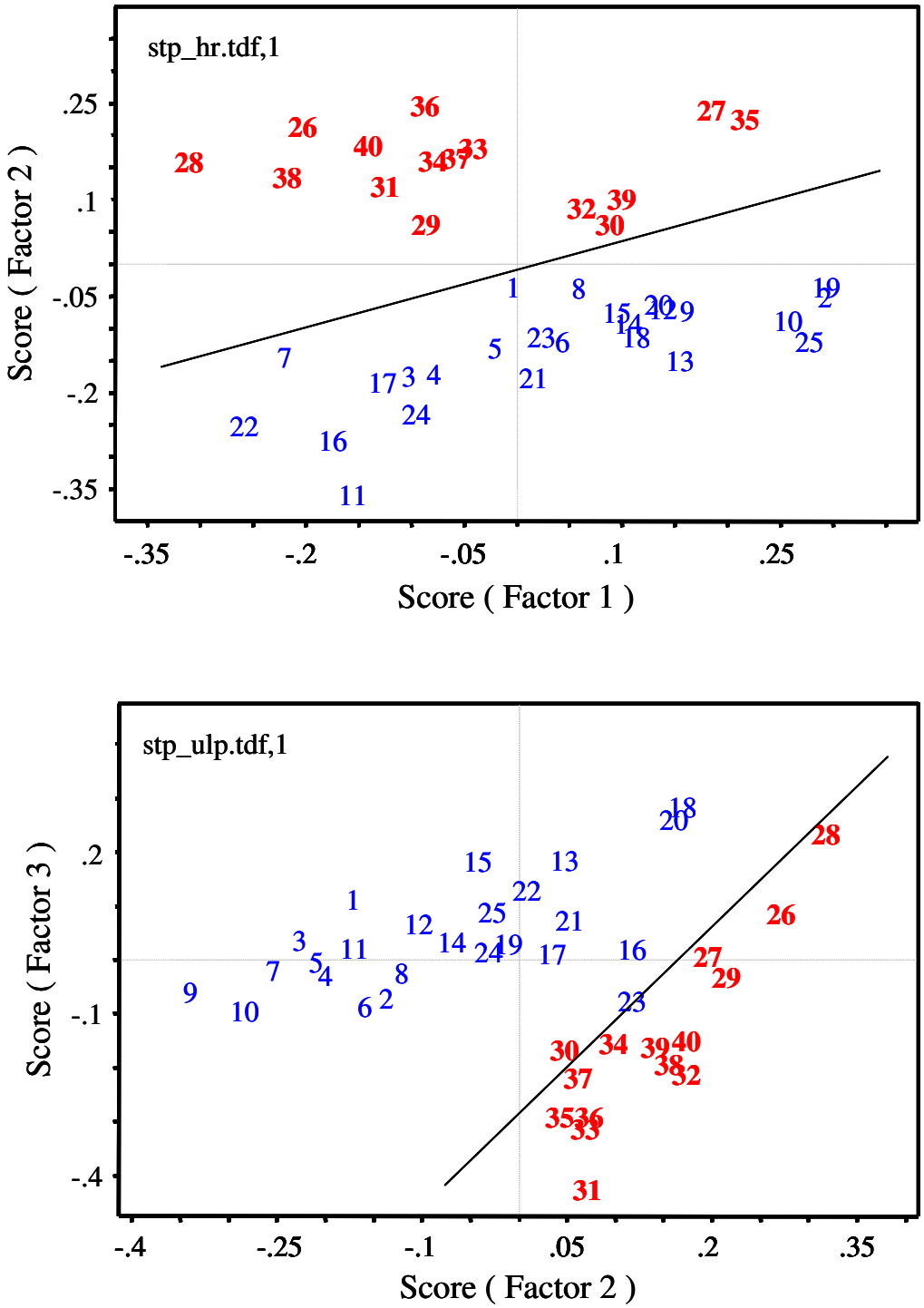

Figure 101. PCA scores plots of the IR spectra of Koch TFC-HR (top) and TFC-ULP (bottom) RO membrane exposed to STP (26-40) and 1,000-ppm NaCl feedwater control (1-25).

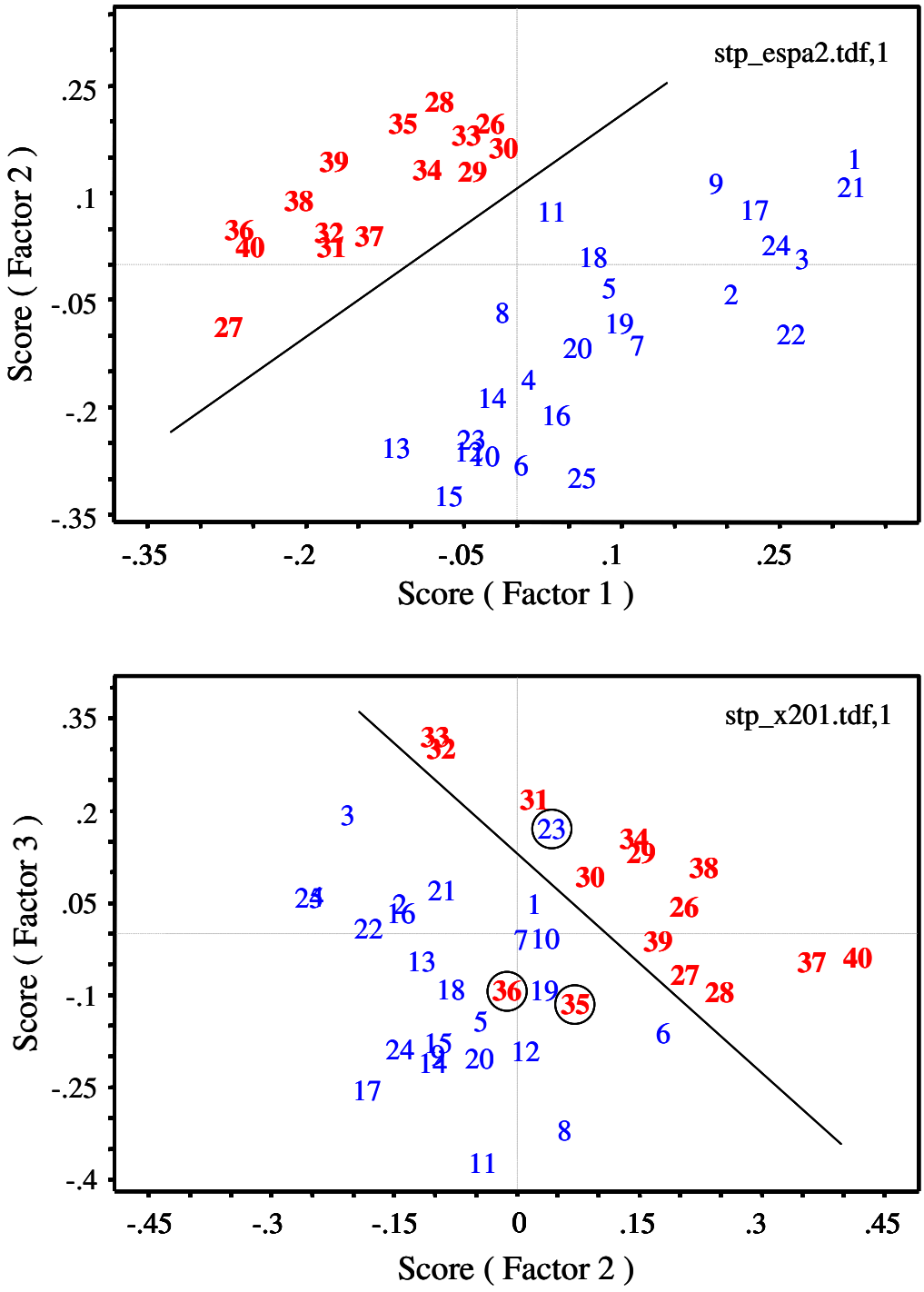

Figure 102. PCA scores plots of the IR spectra of Hydranautics ESPA2 (top) and Trisep X-201 (bottom) RO membrane exposed to SDS (26-40) and 1,000-ppm NaCl feedwater control (1-25).

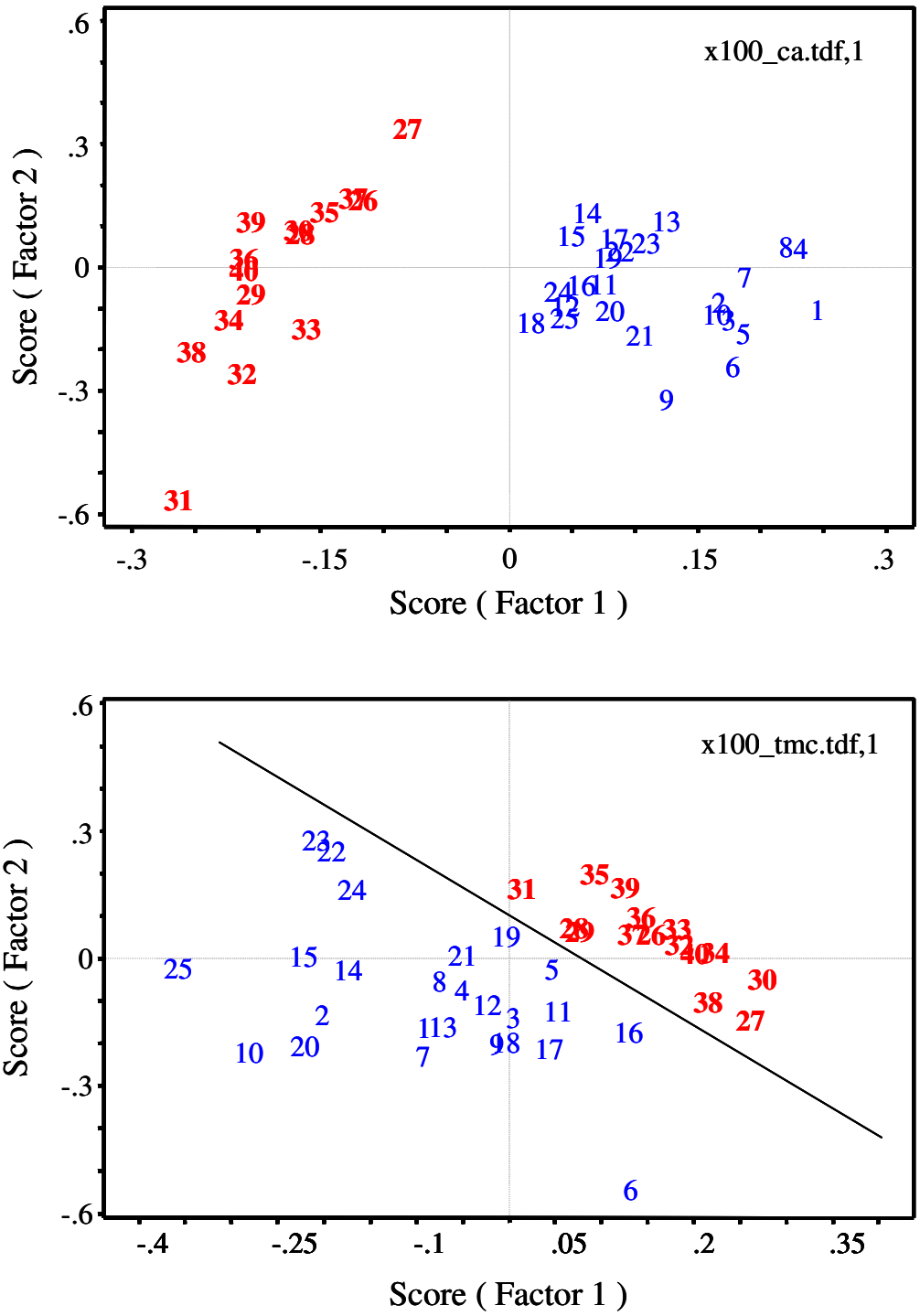

Figure 103. PCA scores plots of the IR spectra of Desal CA (top) and SST TMC/MPD (bottom) RO membrane exposed to Triton X-100 (26-40) and 1,000-ppm NaCl feedwater control (1-25).

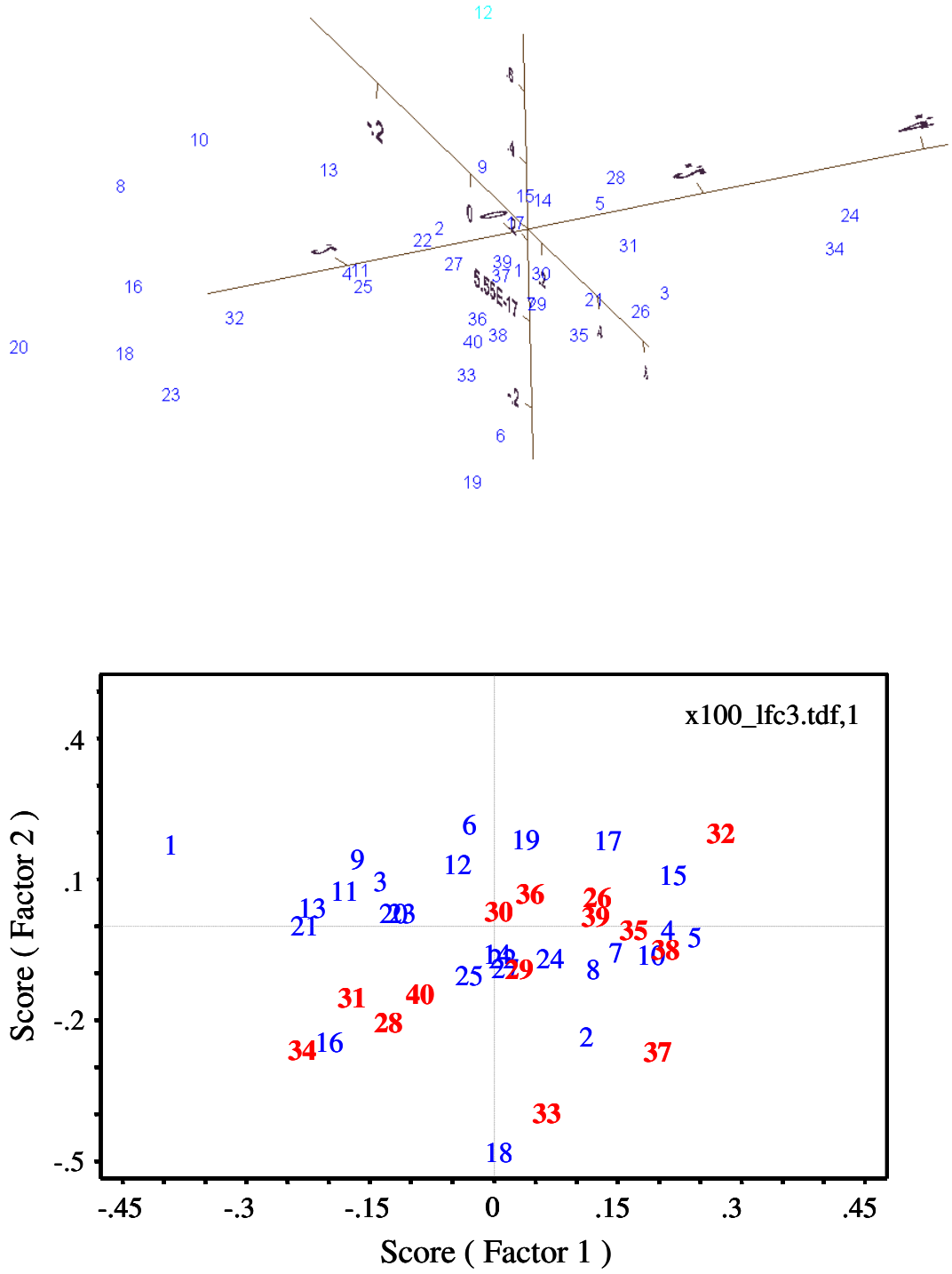

Figure 104. PCA scores plots of the IR spectra of FilmTec BW-30 (top) and Hydranautics LFC3 (bottom) RO membrane exposed to Triton X-100 (26-40) and 1,000-ppm NaCl feedwater control (1-25).

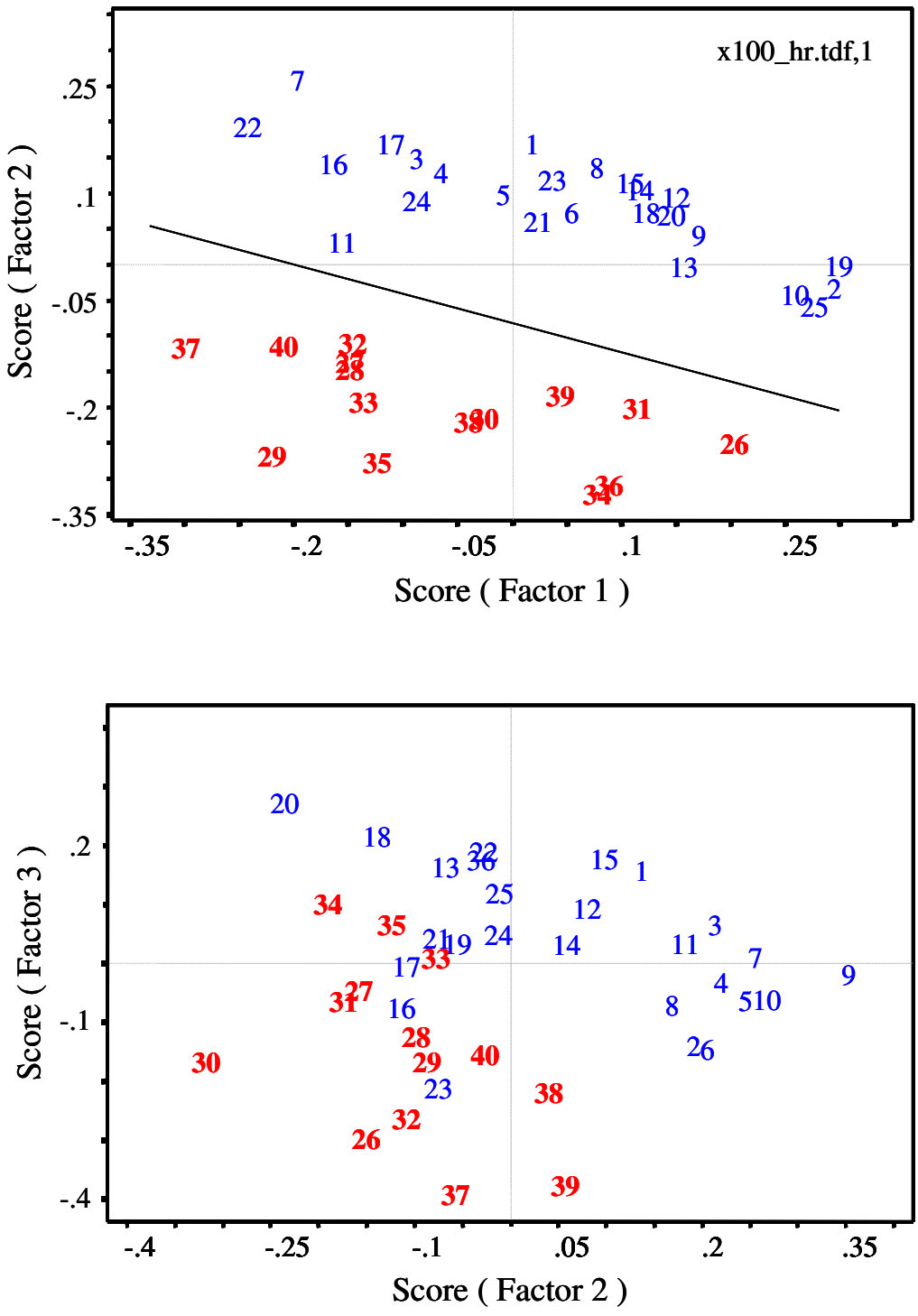

Figure 105. PCA scores plots of the IR spectra of Koch TFC-HR (top) and TFC-ULP (bottom) RO membrane exposed to Triton X-100 (26-40) and 1,000-ppm NaCl feedwater control (1-25).

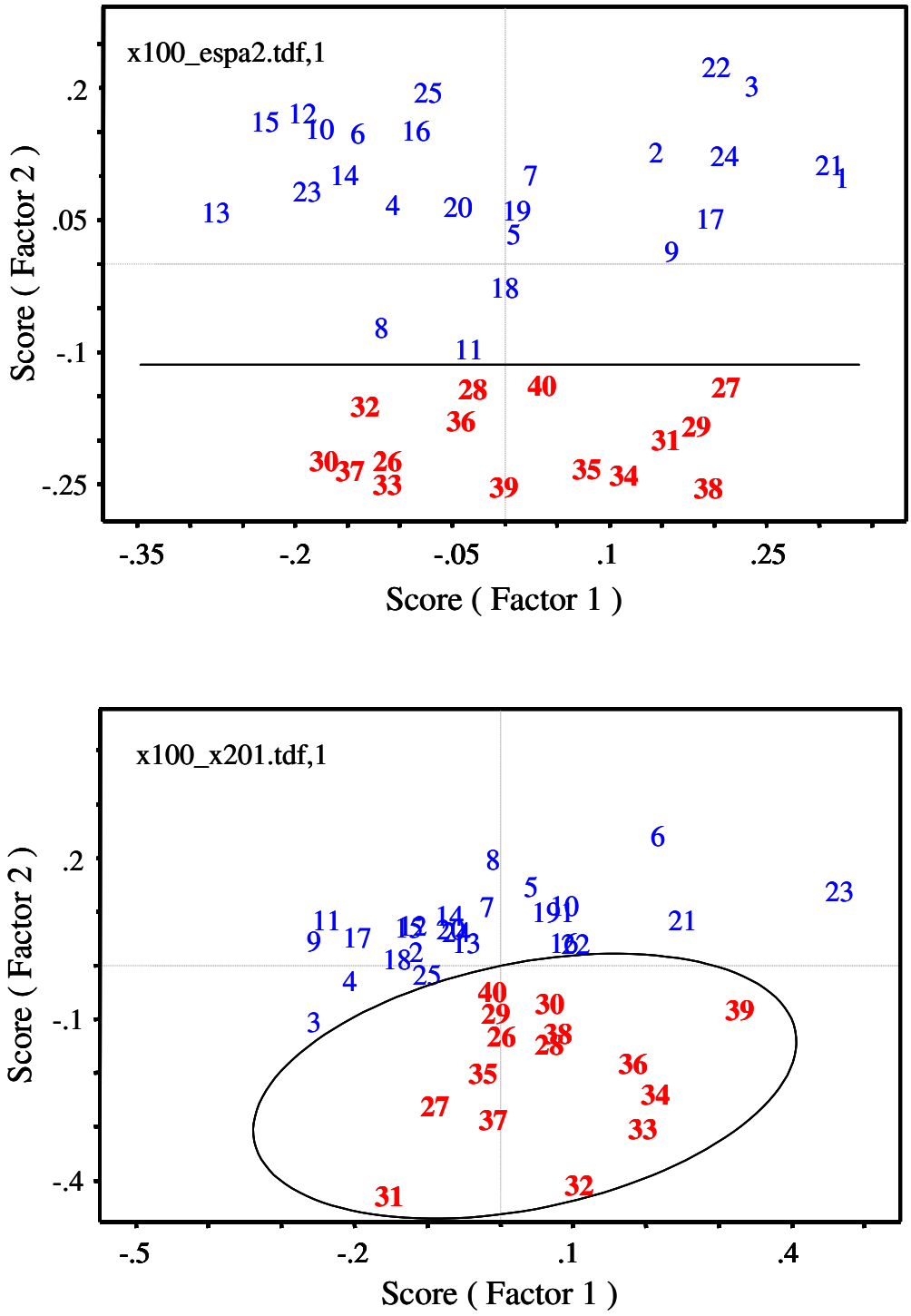

Figure 106. PCA scores plots of the IR spectra of Hydranautics ESPA2 (top) and Trisep X-100 (bottom) RO membrane exposed to Triton X-100 (26-40) and 1,000-ppm NaCl feedwater control (1-25).

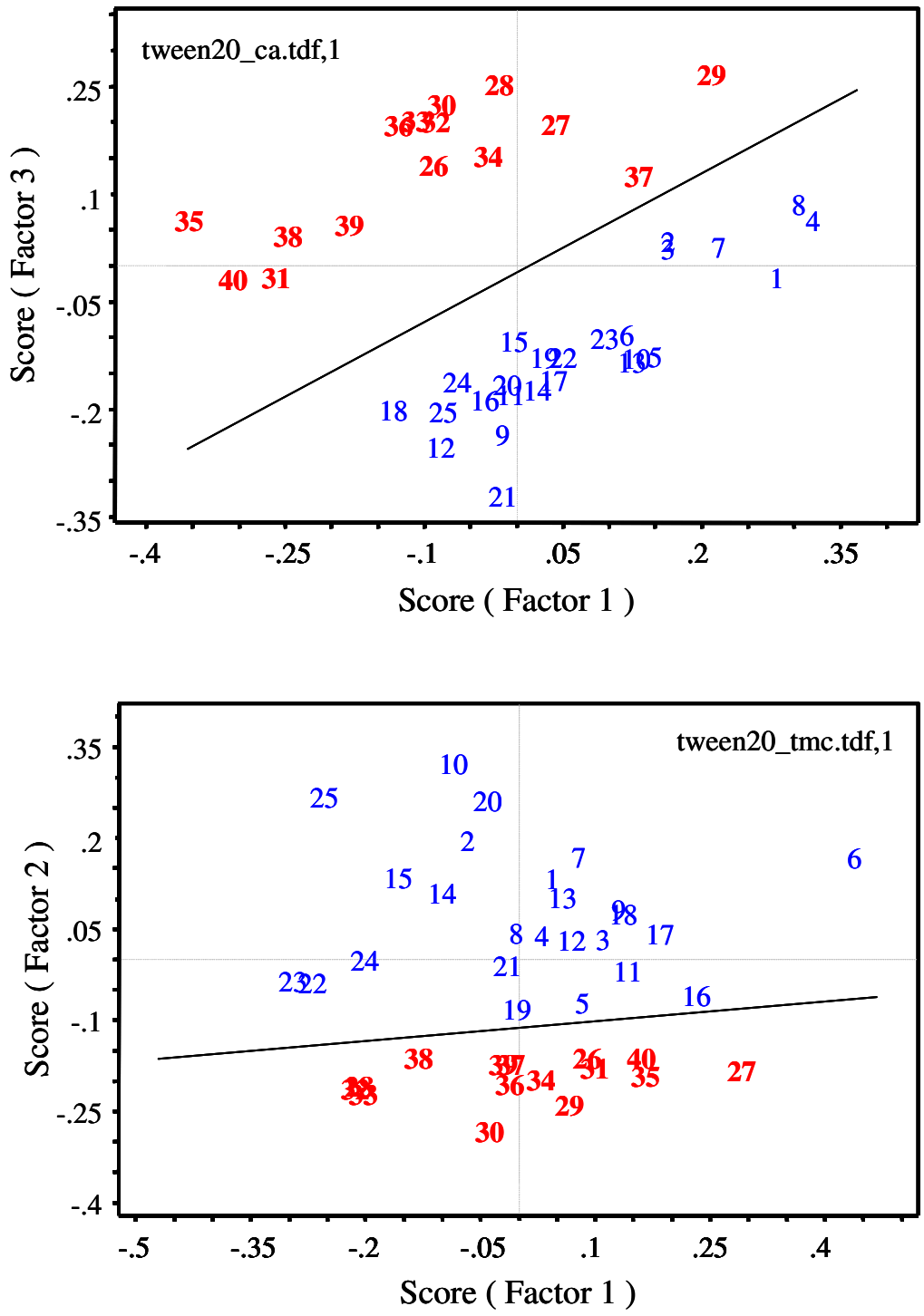

Figure 107. PCA scores plots of the IR spectra of Desal CA and SST TMC/MPD RO membrane exposed to Tween 20 (26-40) and 1,000-ppm NaCl feedwater control (1-25).

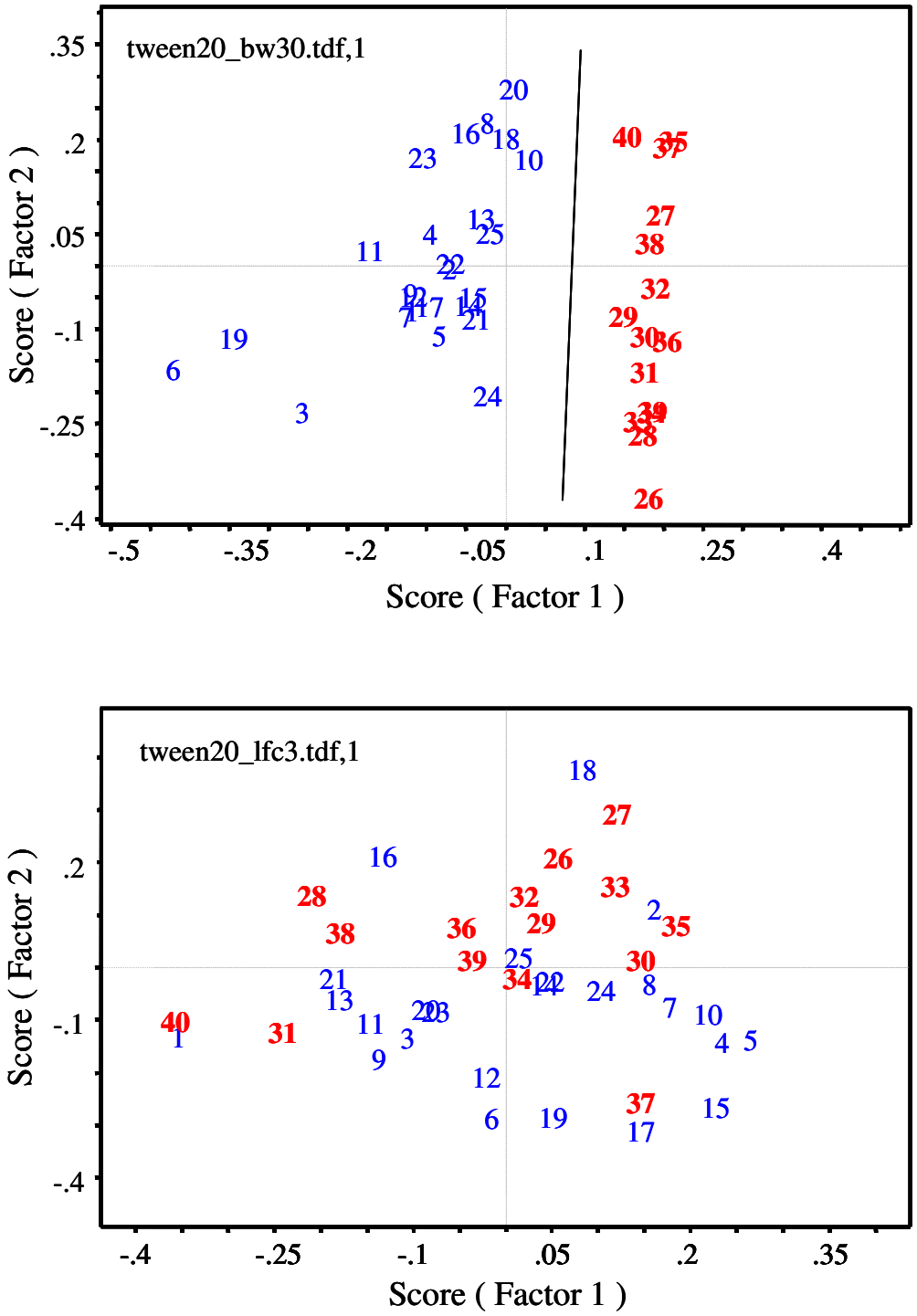

Figure 108. PCA scores plots of the IR spectra of FilmTec BW-30 (top) and Hydranautics LFC3 (bottom) RO membrane exposed to Tween 20 (26-40) and 1,000-ppm NaCl feedwater control (1-25).

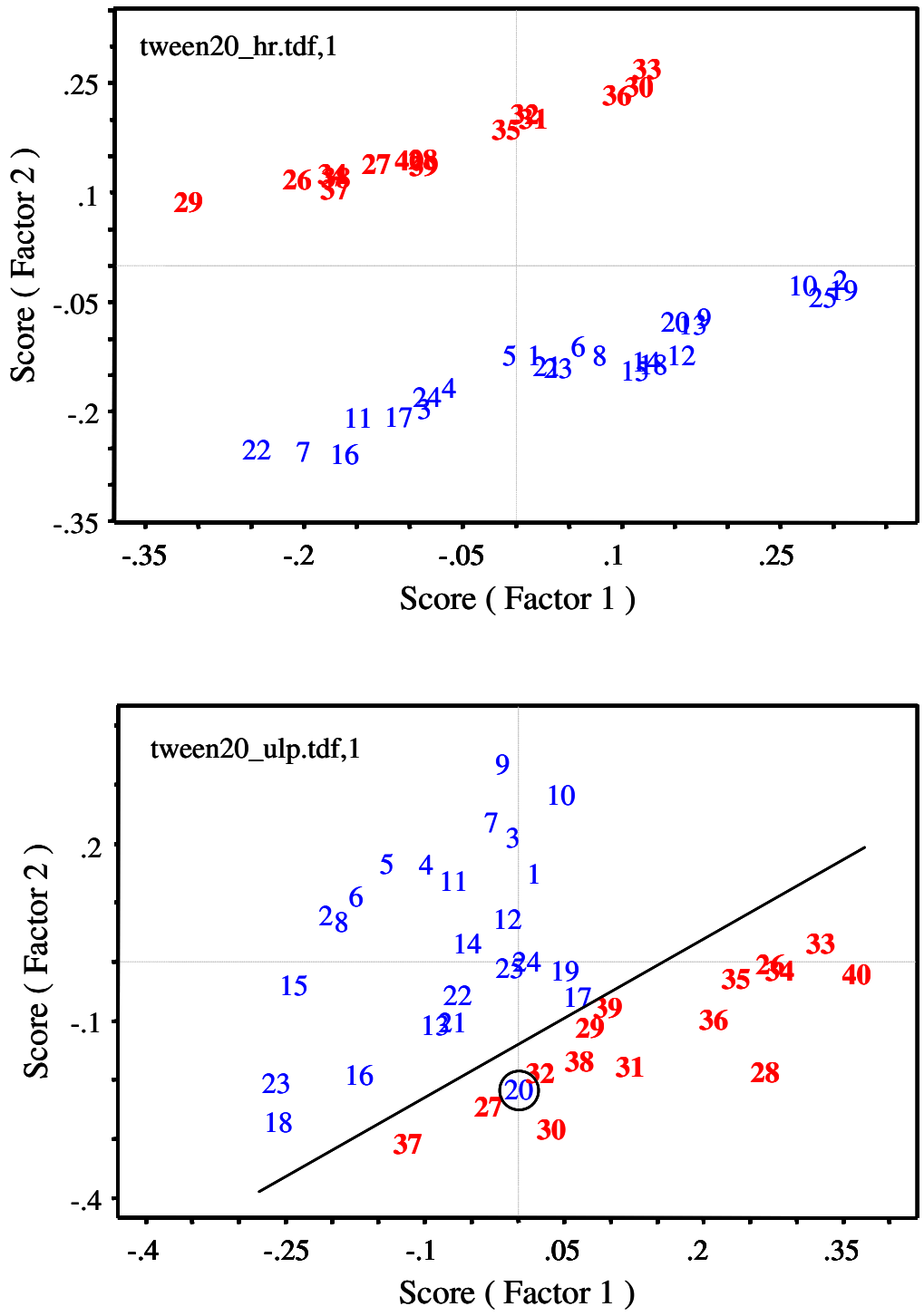

Figure 109. PCA scores plots of the IR spectra of Koch TFC-HR (top) and TFC-ULP (bottom) RO membrane exposed to Tween 20 (26-40) and 1,000-ppm NaCl feedwater control (1-25).

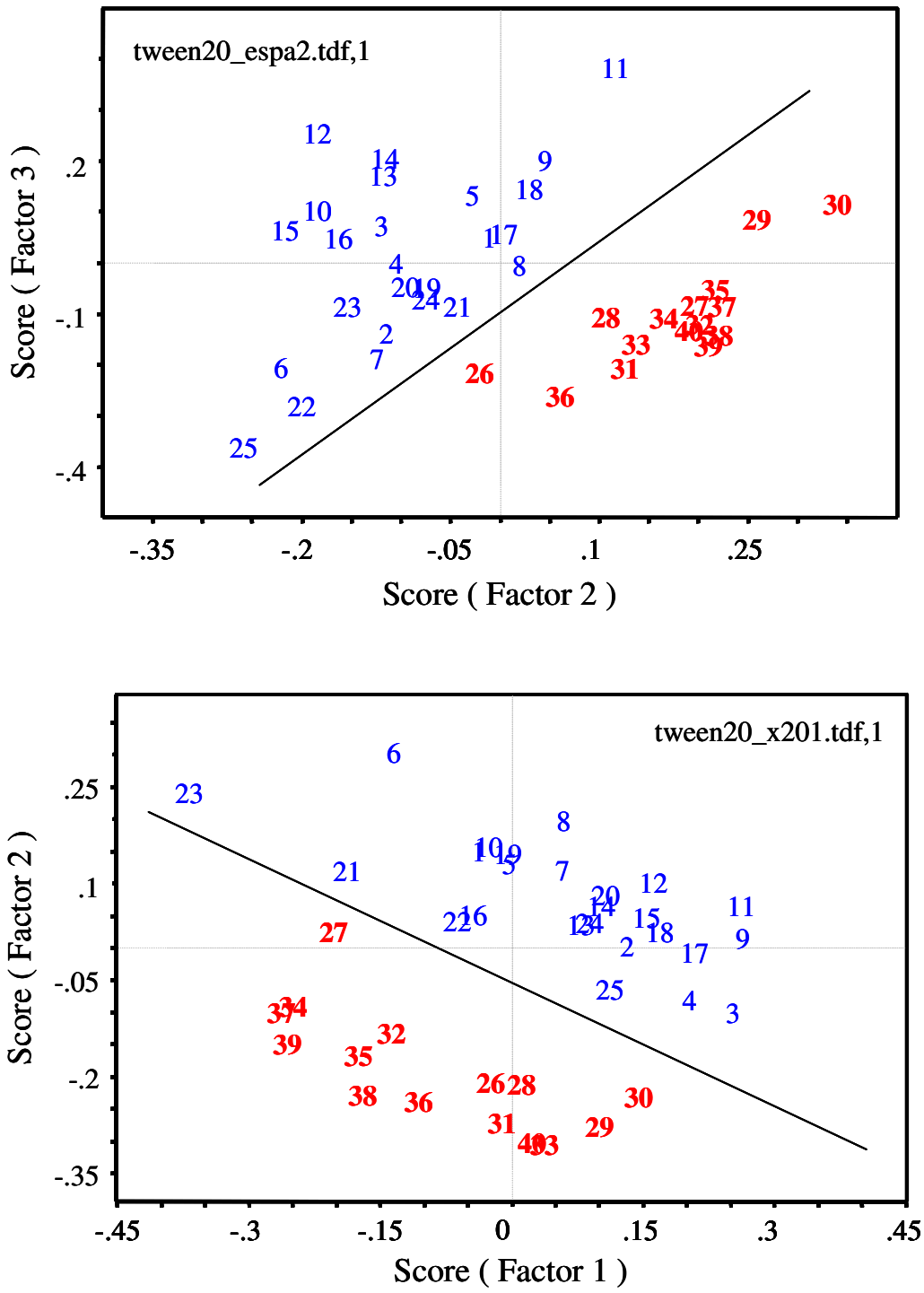

Figure 110. PCA scores plots of the IR spectra of Hydranautics ESPA2 (top) and Trisep X-201 (bottom) RO membrane exposed to Tween 20 (26-40) and 1,000-ppm NaCl feedwater control (1-25).

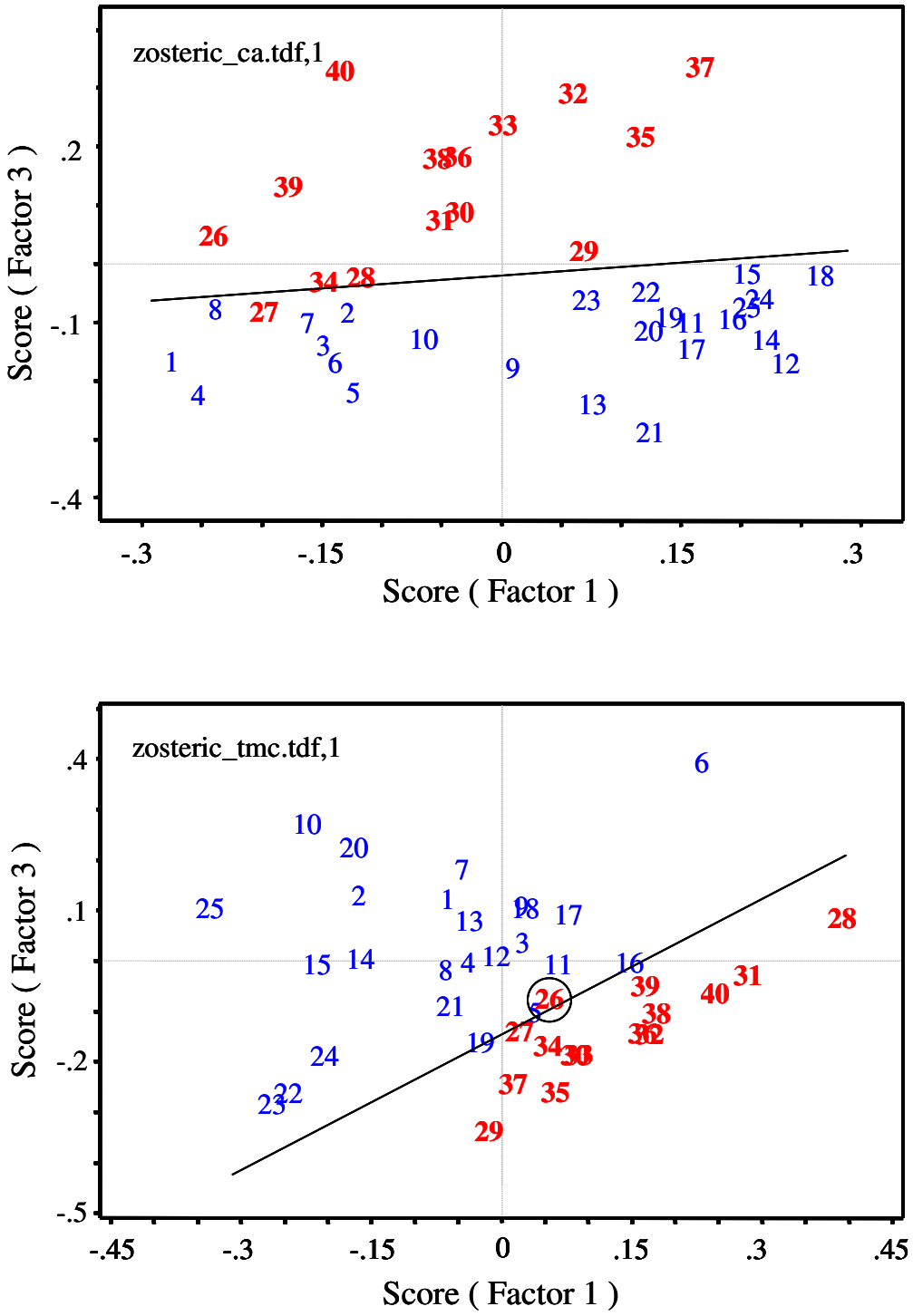

Figure 111. PCA scores plots of the IR spectra of Desal CA (top) and SST TMC/MPD (bottom) RO membrane exposed to zosteric acid (26-40) and 1,000-ppm NaCl feedwater control (1-25).

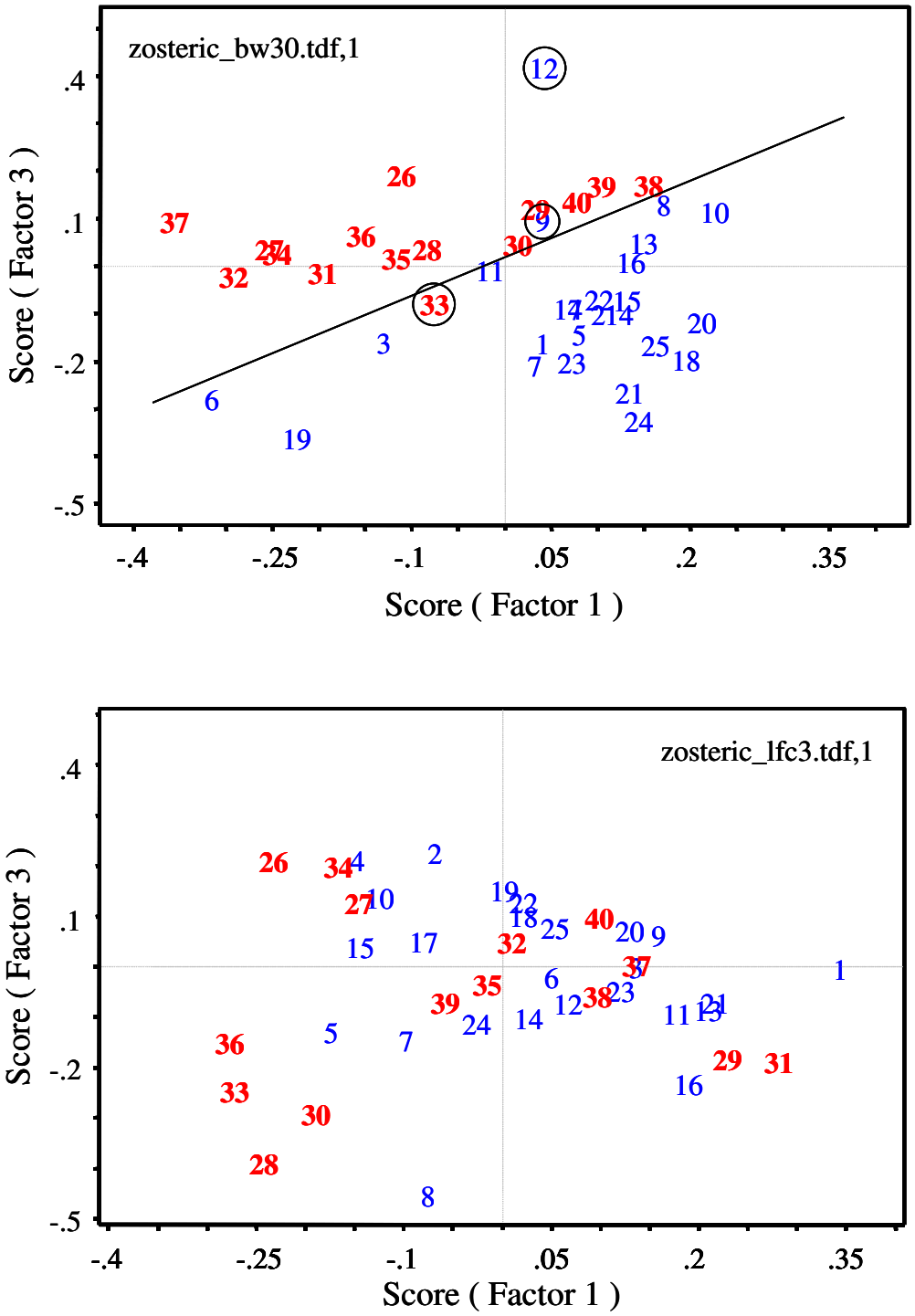

Figure 112. PCA scores plots of the IR spectra of FilmTec BW-30 (top) and Hydranautics LFC3 (bottom) RO membrane exposed to zosteric acid (26-40) and 1,000-ppm NaCl feedwater control (1-25).

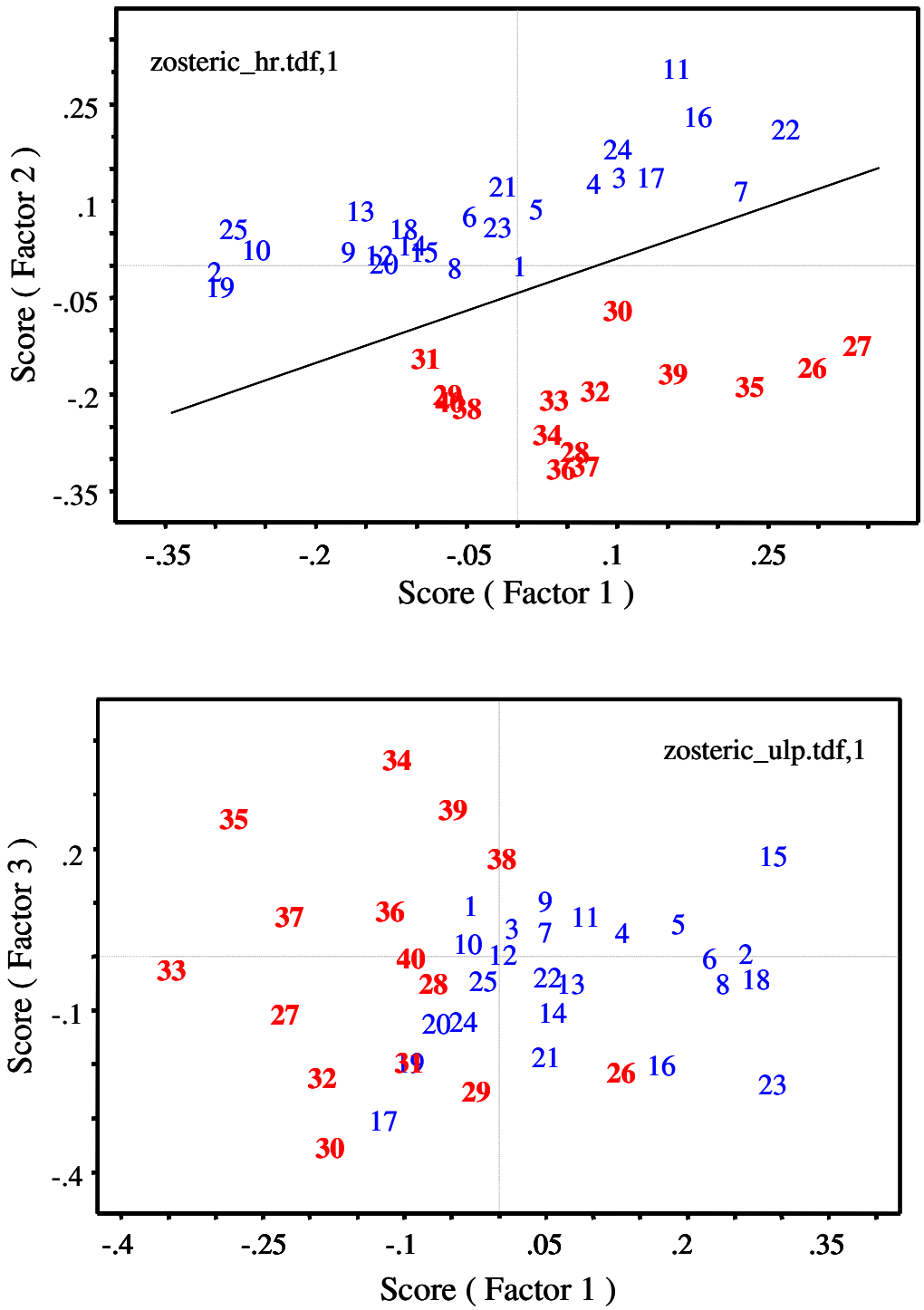

Figure 113. PCA scores plots of the IR spectra of Koch TFC-HR (top) and TFC-ULP (bottom) RO membrane exposed to zosteric acid (26-40) and 1,000-ppm NaCl feedwater control (1-25).

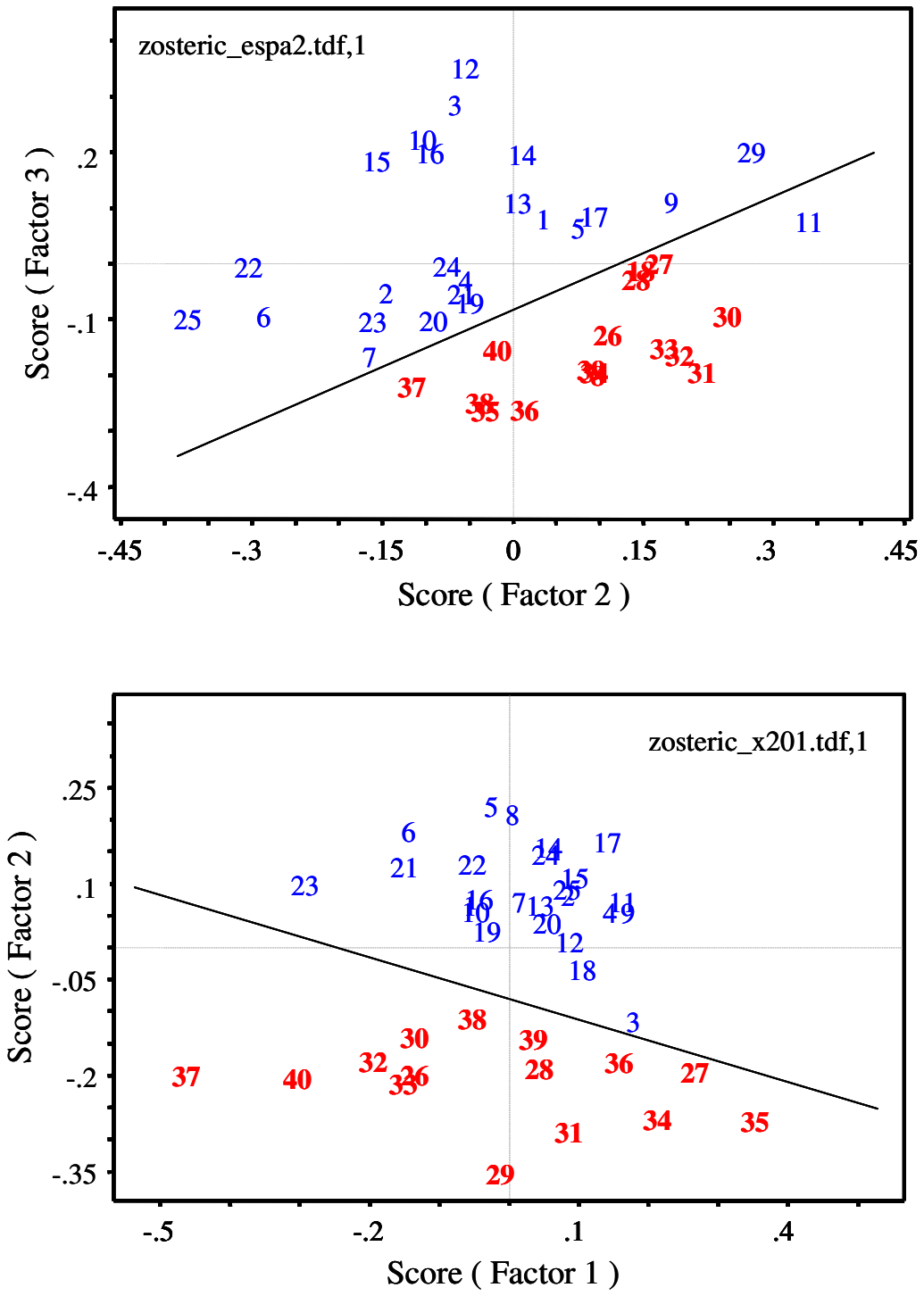

Figure 114. PCA scores plots of the IR spectra of Hydranautics ESPA2 (top) and Trisep X-201 (bottom) RO membrane exposed to zosteric acid (26-40)and 1,000-ppm NaCl feedwater control (1-25).

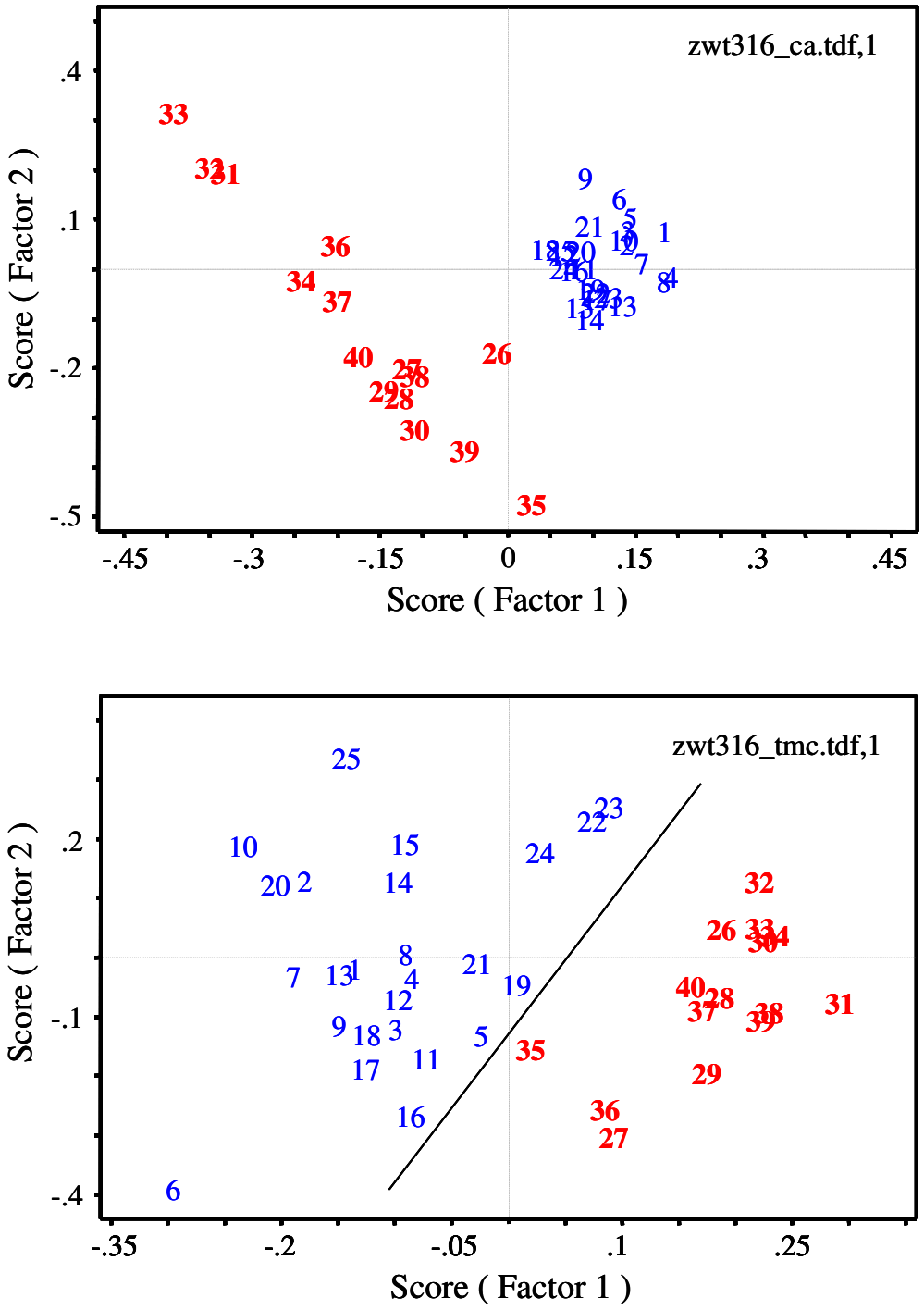

Figure 115. PCA scores plots of the IR spectra of Desal CA and SST TMC/MPD RO membrane exposed to Zwittergent 3-16 (26-40) and 1,000-ppm NaCl feedwater control (1-25).

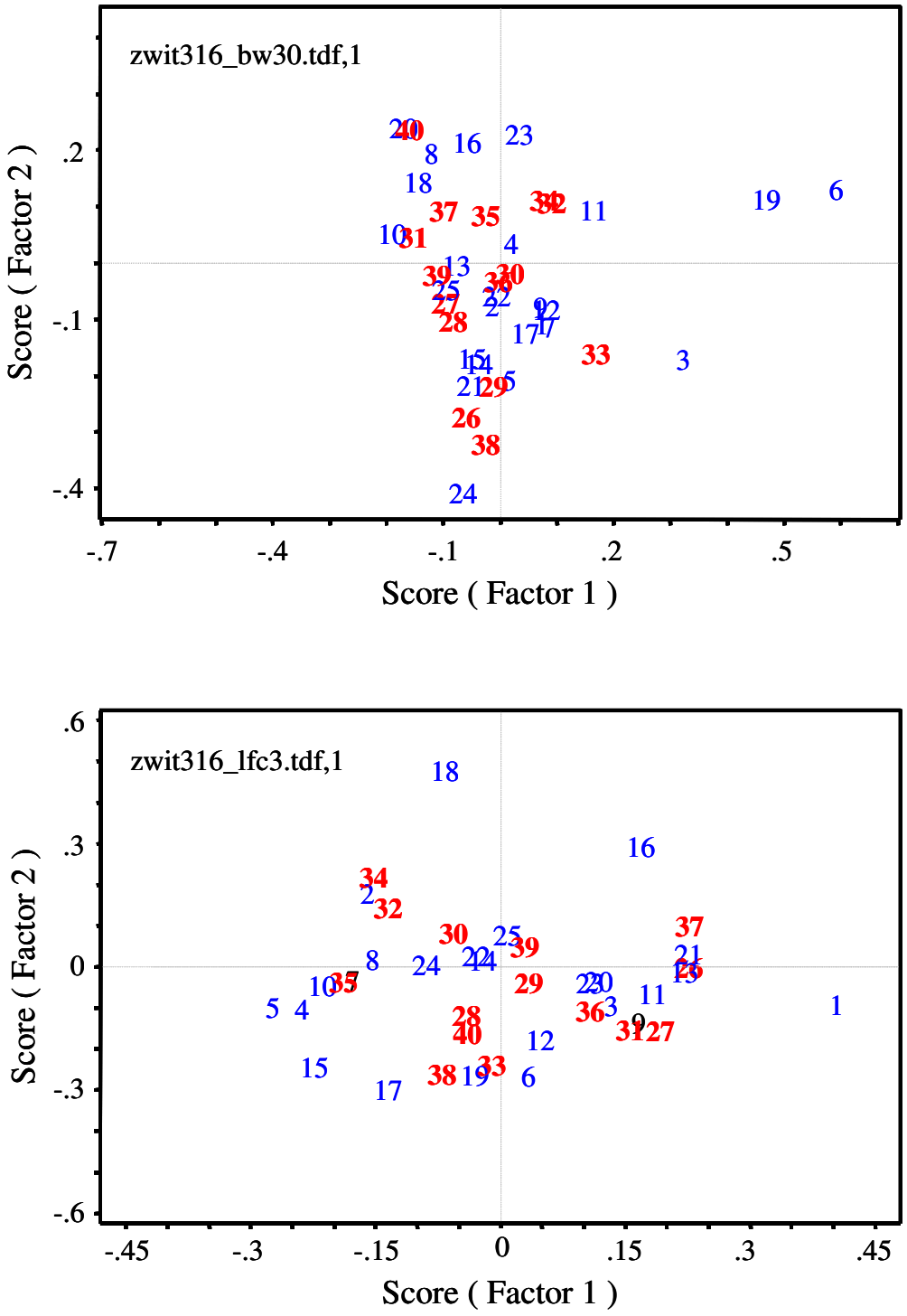

Figure 116. PCA scores plots of the IR spectra of FilmTec BW-30 (top) and Hydranautics LFC3 (bottom) RO membrane exposed to Zwittergent 3-16 (26-40) and 1,000-ppm NaCl feedwater control (1-25).

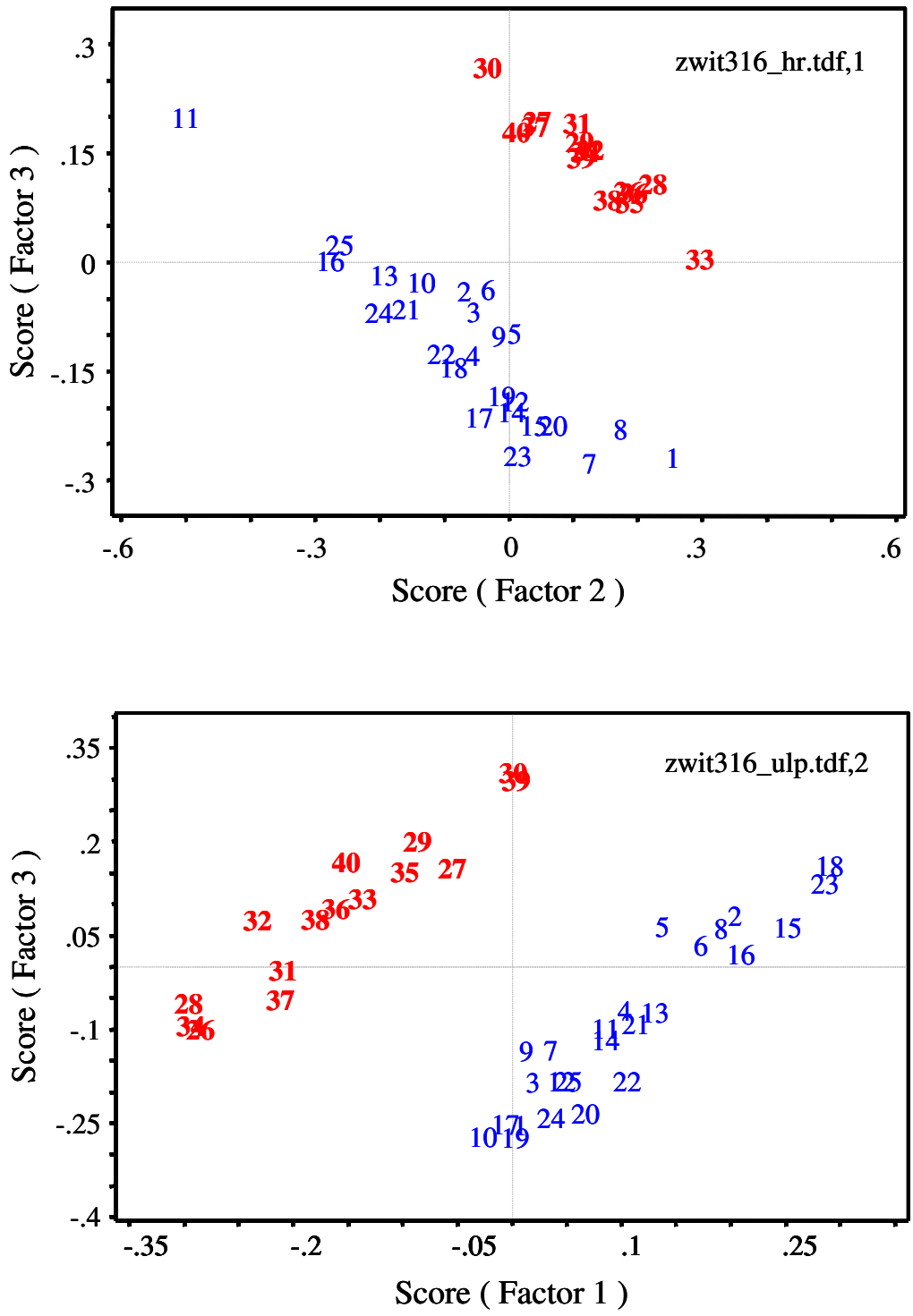

Figure 117. PCA scores plots of the IR spectra of Koch TFC-HR (top) and TFC-ULP (bottom) RO membrane exposed to Zwittergent 3-16 (26-40) and 1,000-ppm NaCl feedwater control (1-25).

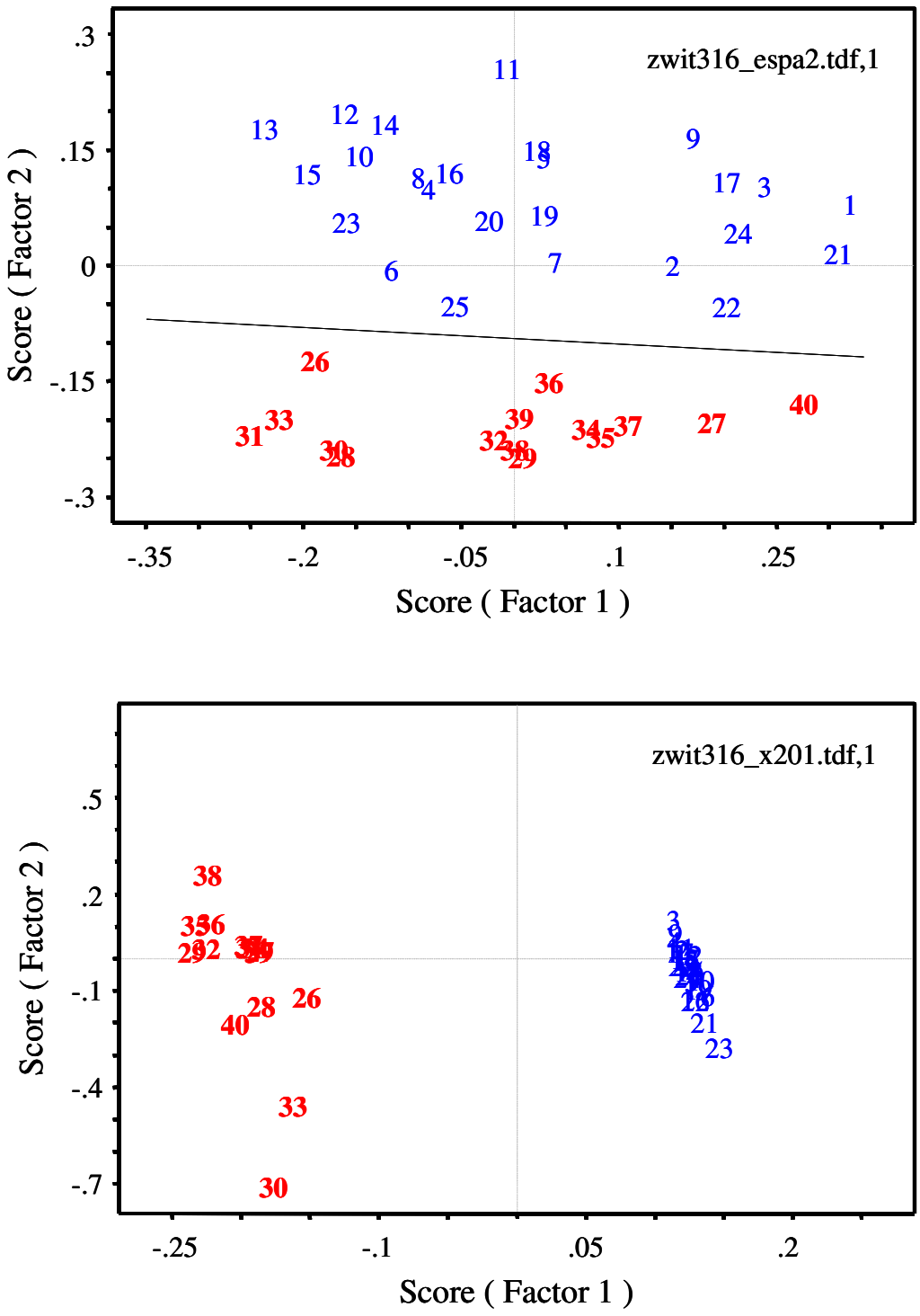

Figure 118. PCA scores plots of the IR spectra of Hydranautics ESPA2 (top) and Trisep X-201 (bottom) RO membrane exposed to Zwittergent 3-16 (26-40) and 1,000-ppm NaCl feedwater control (1-25).

Appendix IV. RO Membrane Performance Following Exposure to Chemical Cleaning Compound

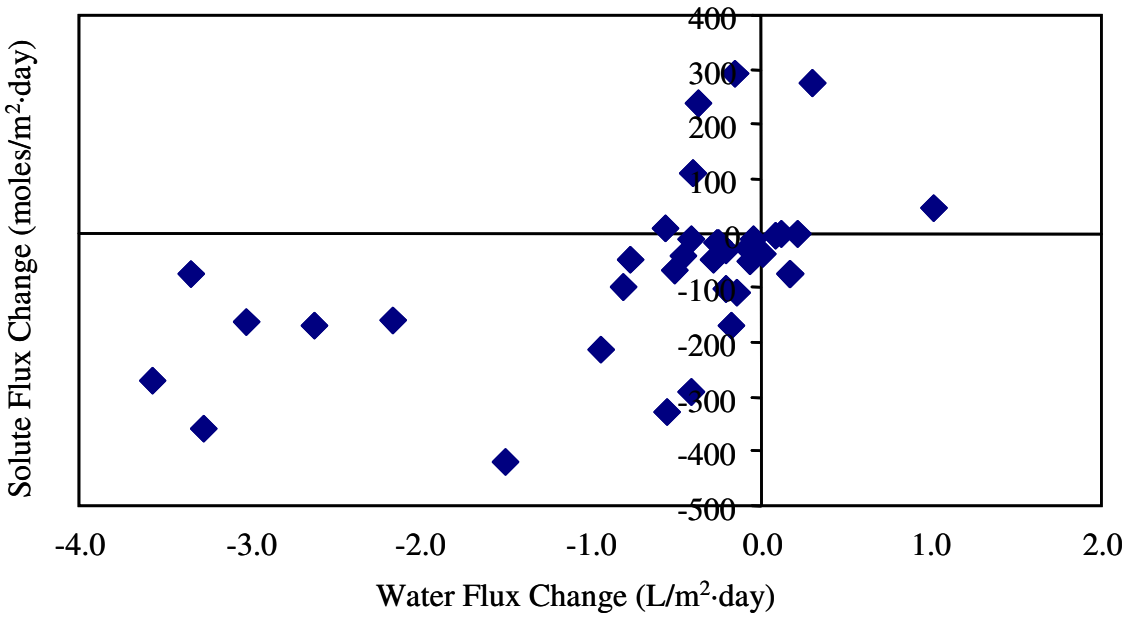

Figure 119. Effect of chemical cleaning agents on FilmTec BW-30 RO membrane performance following 1 hr exposure.

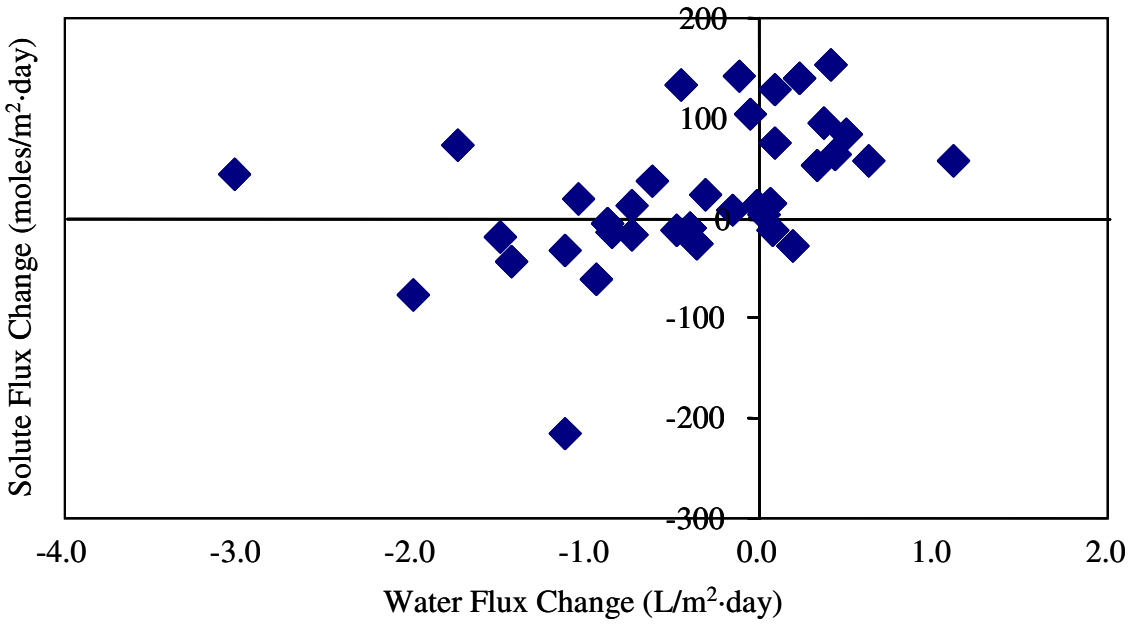

Figure 120. Effect of chemical cleaning agents on Hydranautics LFC3 RO membrane performance following 1 hr exposure.

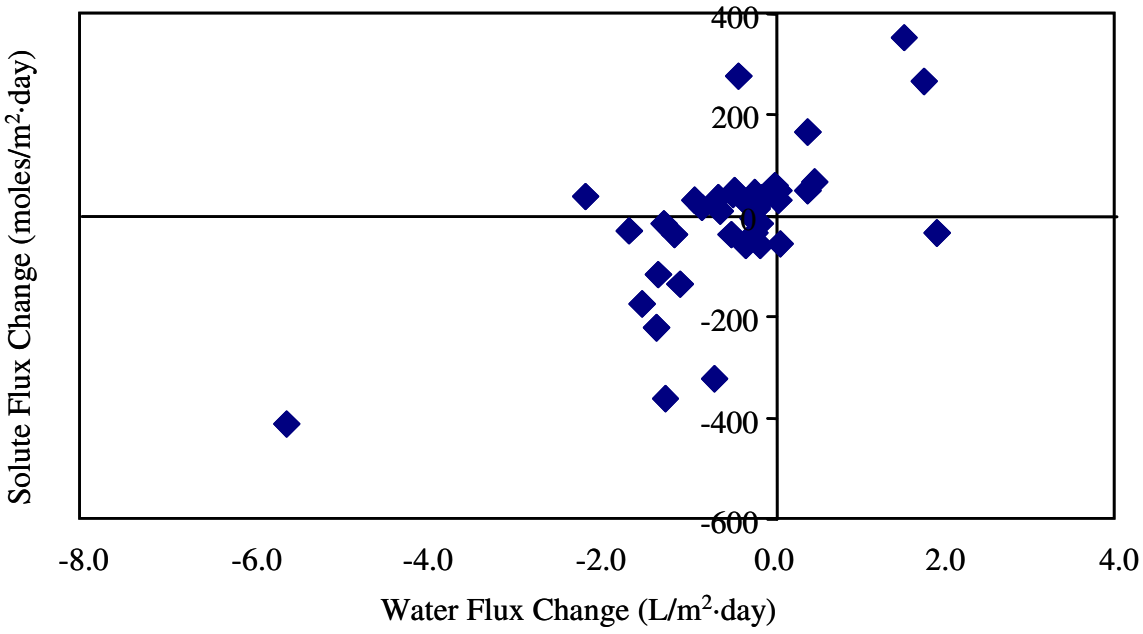

Figure 121. Effect of chemical cleaning agents on Hydranautics ESPA2 RO membrane performance following 1 hr exposure.

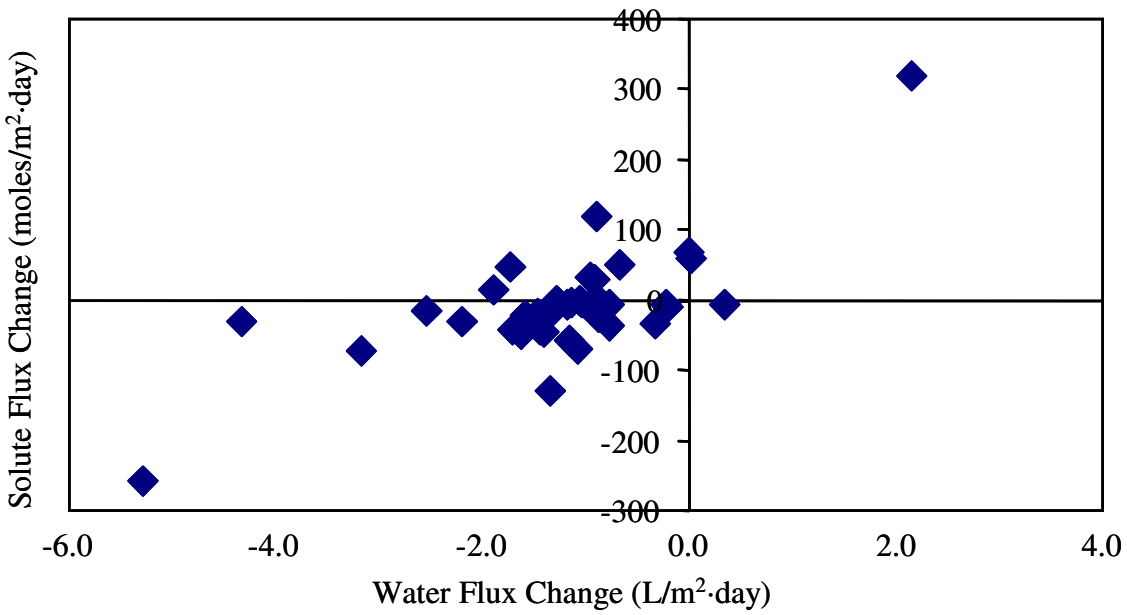

Figure 122. Effect of chemical cleaning agents on Koch TFC-HR RO membrane performance following 1 hr exposure.

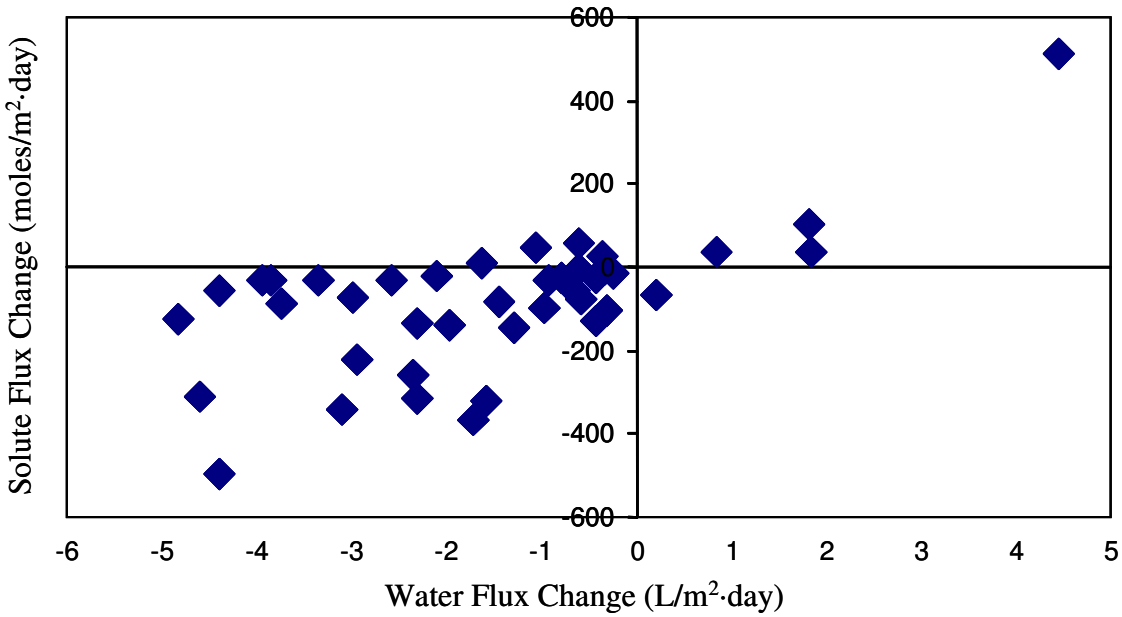

Figure 123. Effect of chemical cleaning agents on Koch TFC-ULP RO membrane performance following 1 hr exposure.

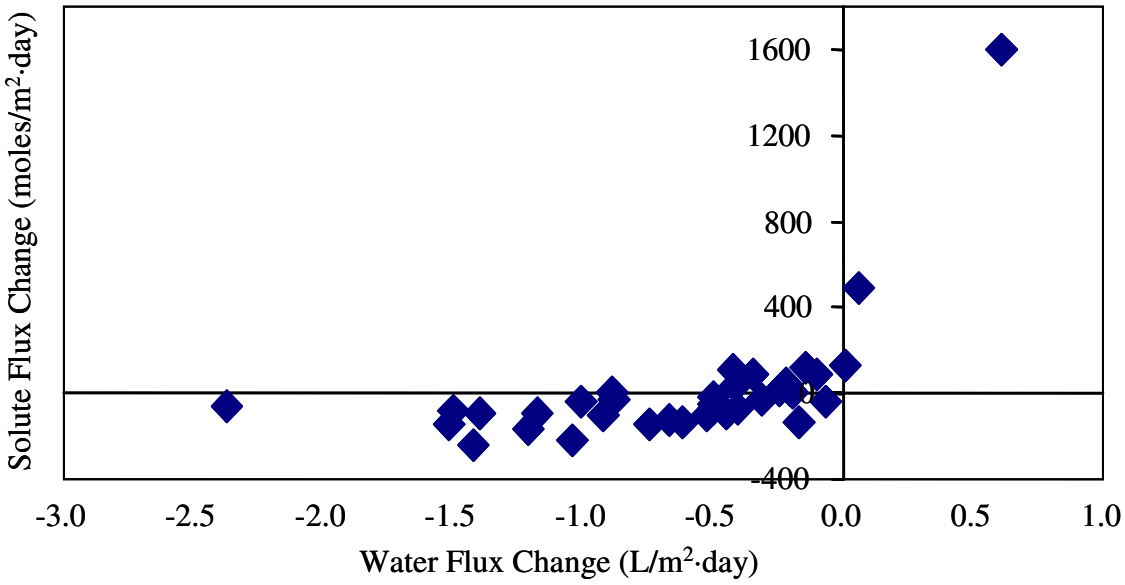

Figure 124. Effect of chemical cleaning agents on Trisep X-201 RO membrane performance following 1 hr exposure

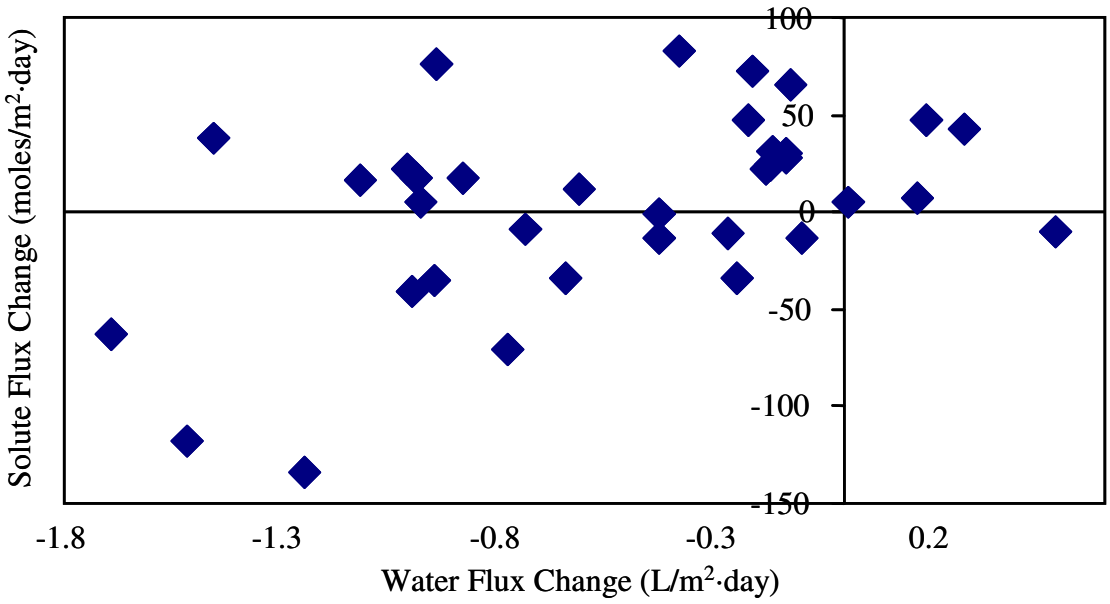

Figure 125. Effect of chemical cleaning agents on SST TMC/MPD RO membrane performance following 1 hr exposure.

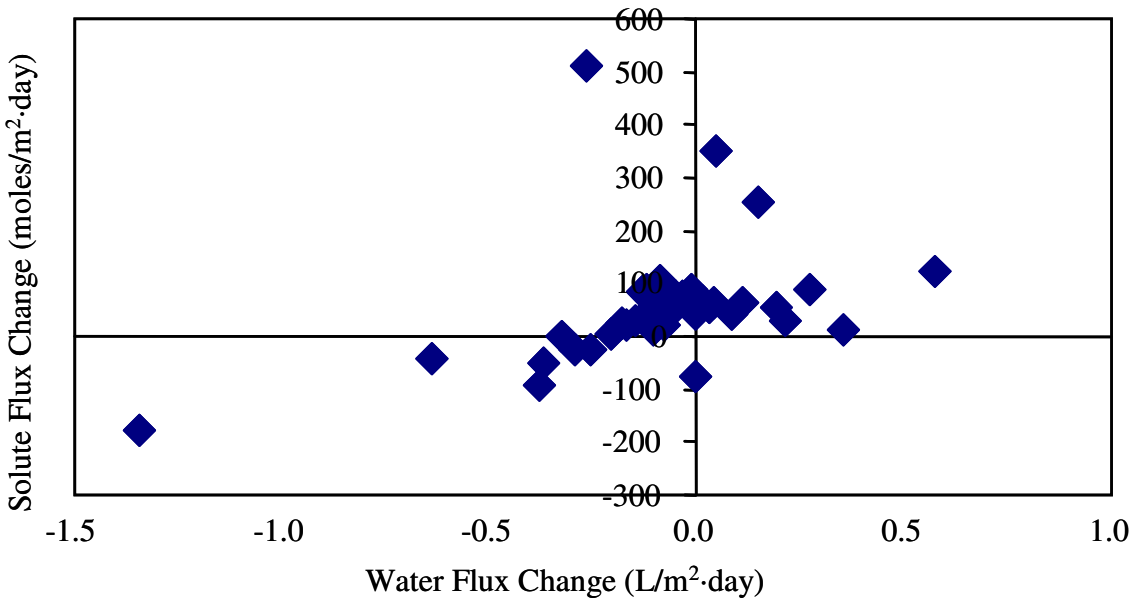

Figure 126. Effect of chemical cleaning agents on Desal CA RO membrane performance following 1 hr exposure.

Appendix V. ANN Models for the Prediction of Water Flux and Solute Rejection for Individual RO Membranes.

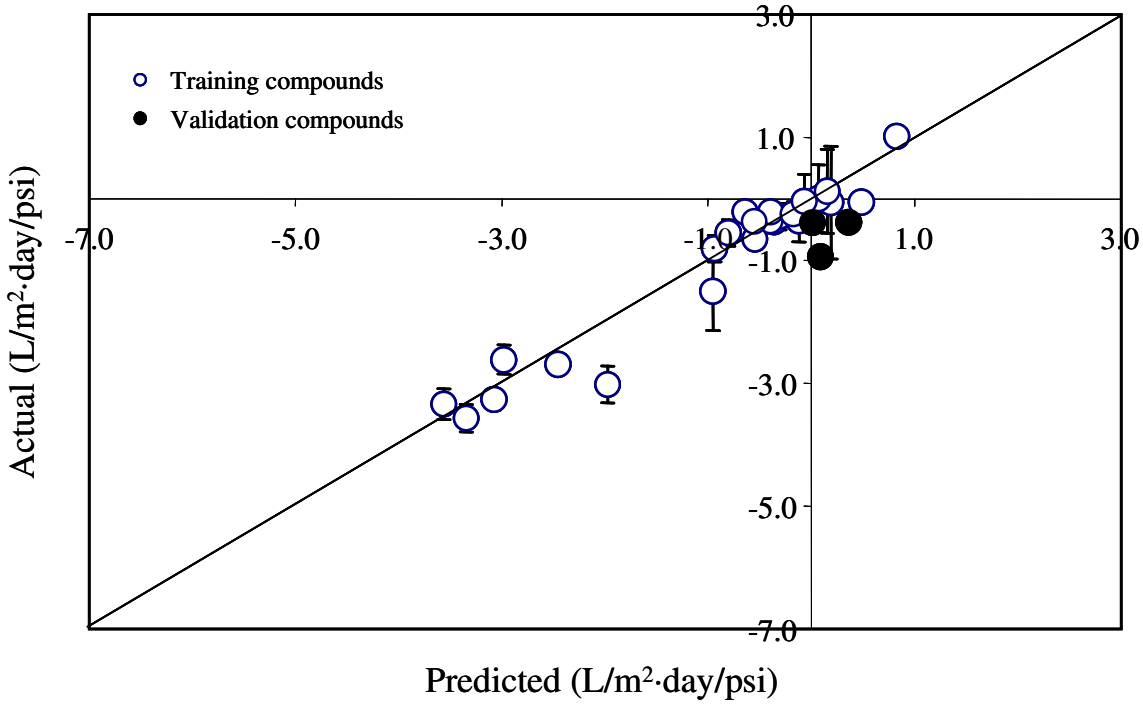

Figure 127. ANN Model results for change in specific water flux for FilmTec BW-30 after treatment with cleaning compounds.

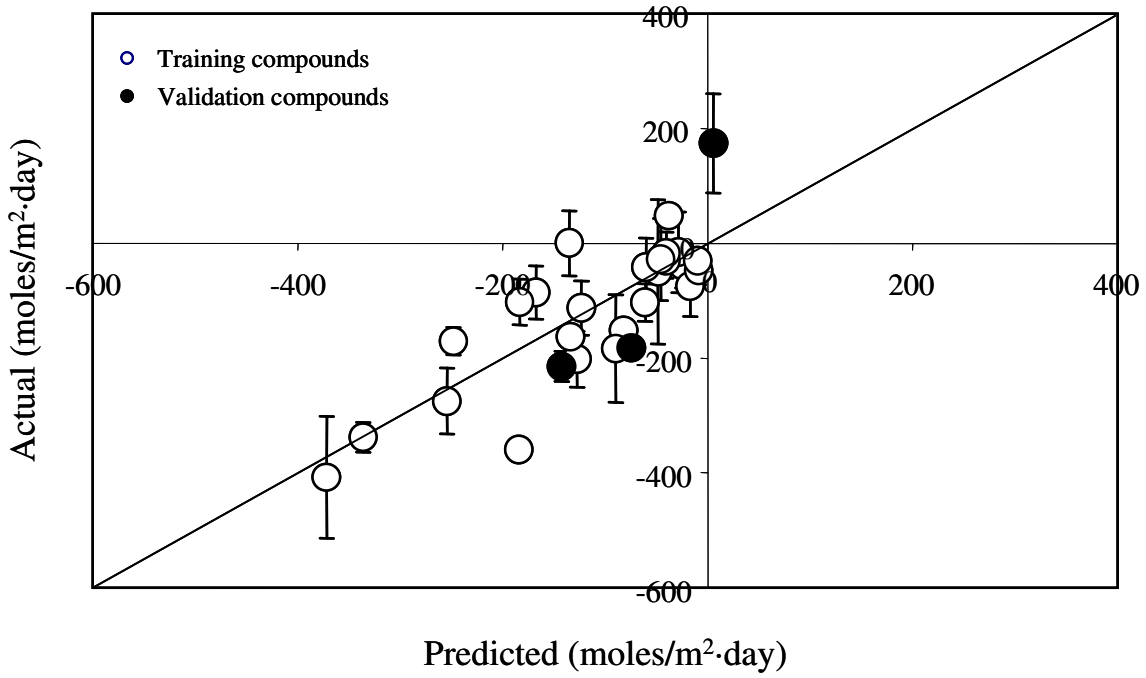

Figure 128. ANN Model results for change in solute flux for FilmTec BW-30 after treatment with cleaning compounds

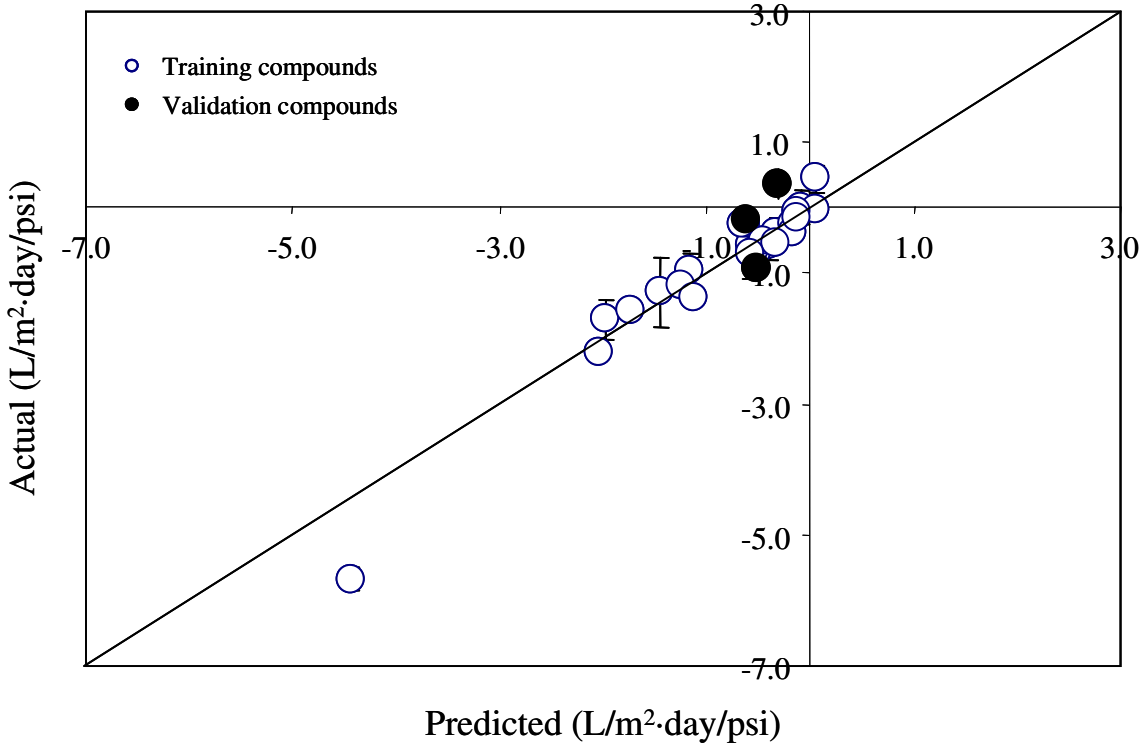

Figure 129. ANN Model results for change in specific water flux for Hydranautics ESPA2 after treatment with cleaning compounds

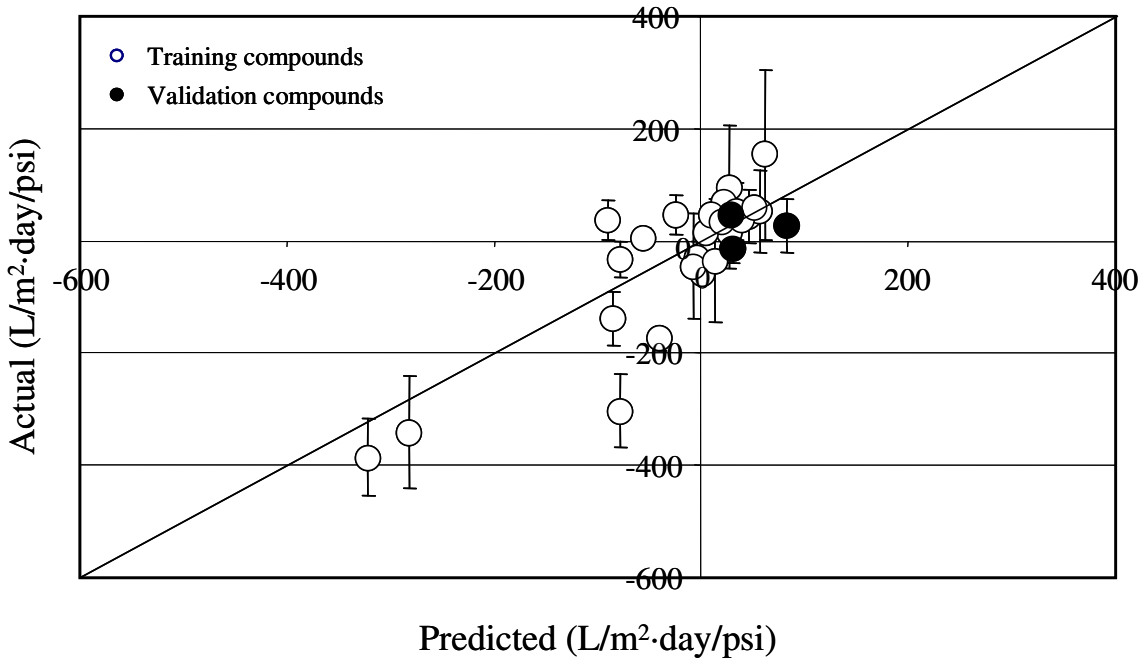

Figure 130. ANN Model results for change in solute flux for Hydranautics ESPA2 after treatment with cleaning compounds

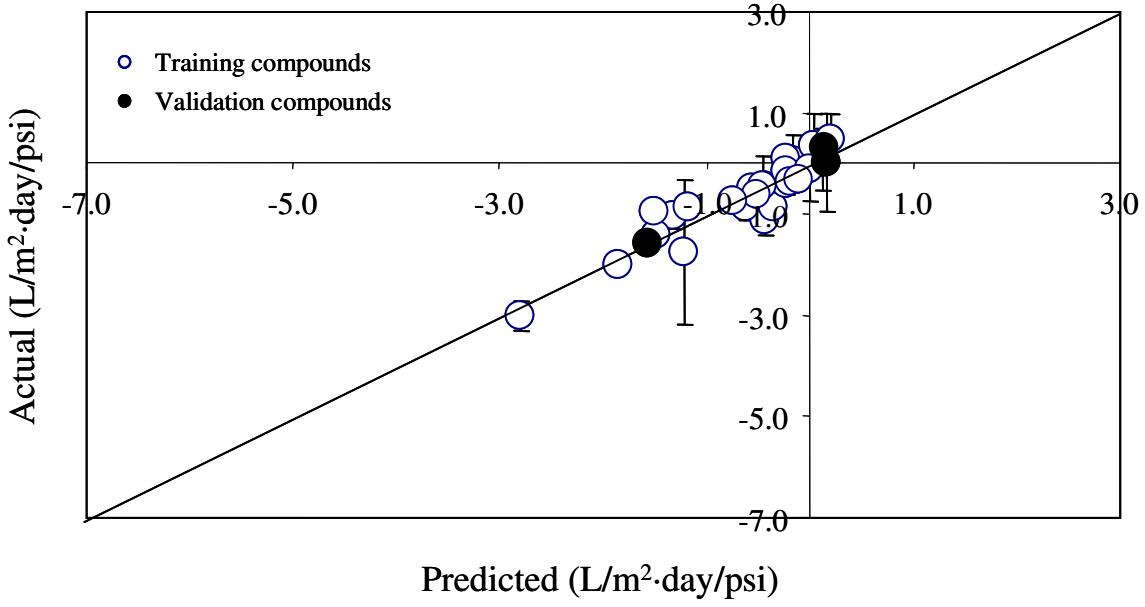

Figure 131. ANN Model results for change in specific water flux for Hydranautics LFC3 after treatment with cleaning compounds.

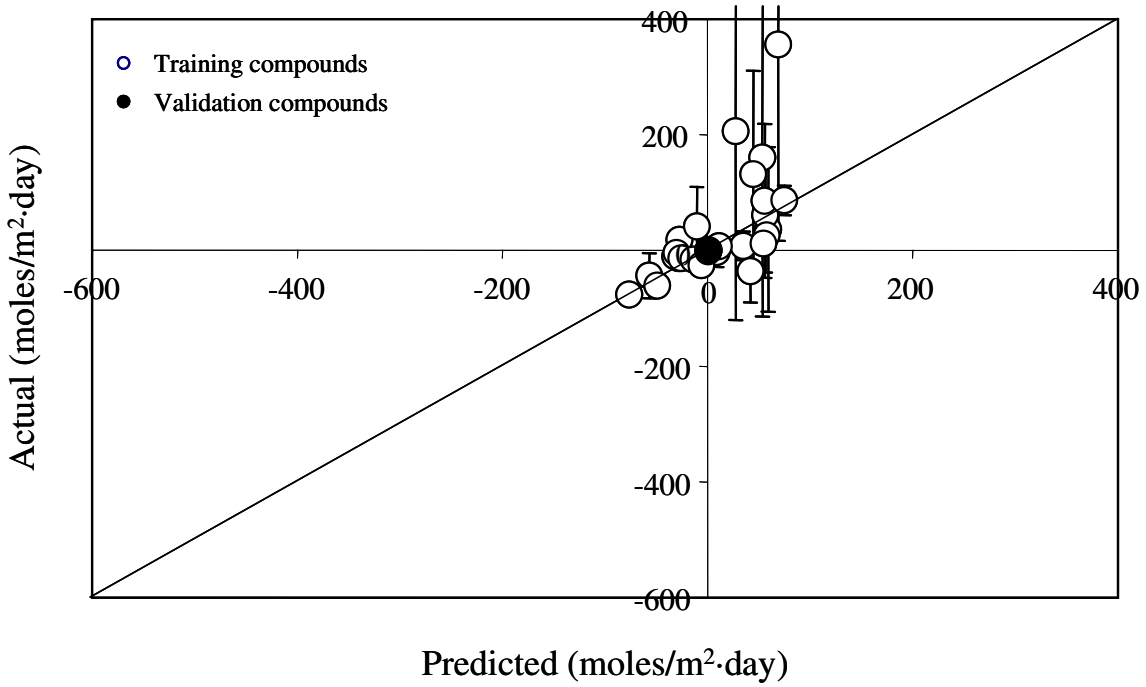

Figure 132. Figure 3.154 ANN Model results for change in solute flux for Hydranautics LFC3 after treatment with cleaning compounds

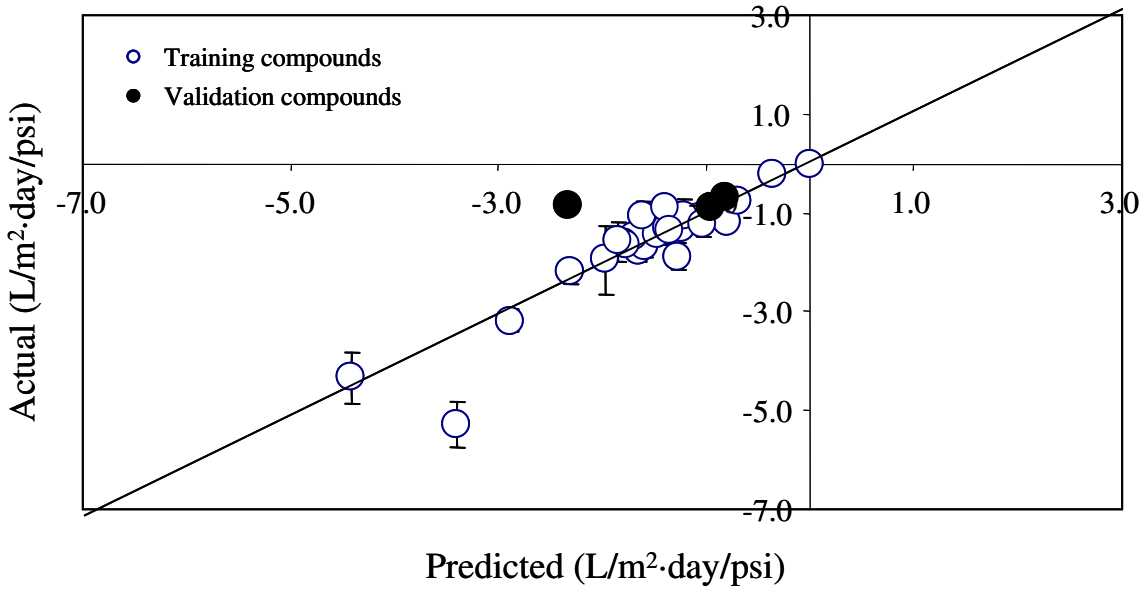

Figure 133. Figure 3.154 ANN Model results for change in specific water flux for Koch TFC-HR after treatment with cleaning compounds

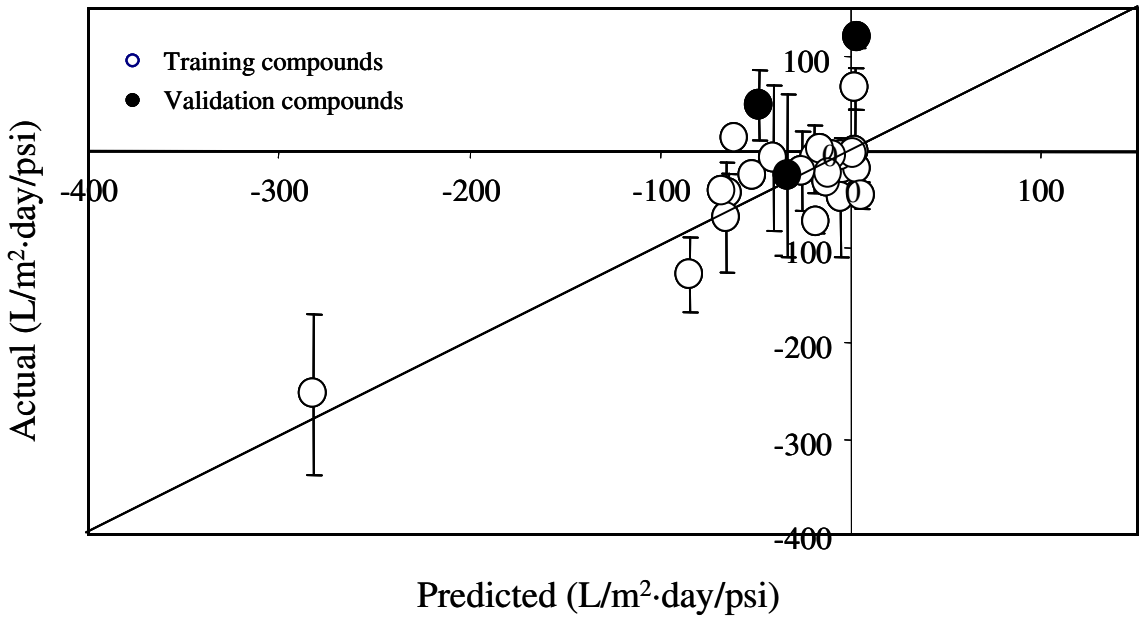

Figure 134. Figure 3.154 ANN Model results for change in solute flux for Koch TFC-HR after treatment with cleaning compounds

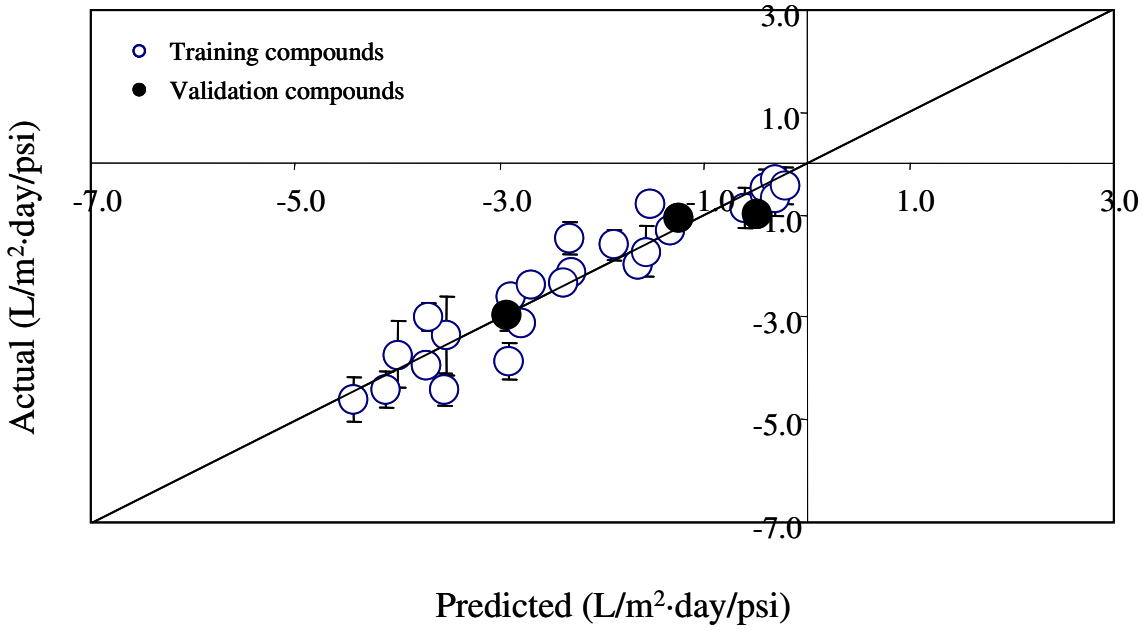

Figure 135. ANN Model results for change in specific water flux for Koch TFC-ULP after treatment with cleaning compounds

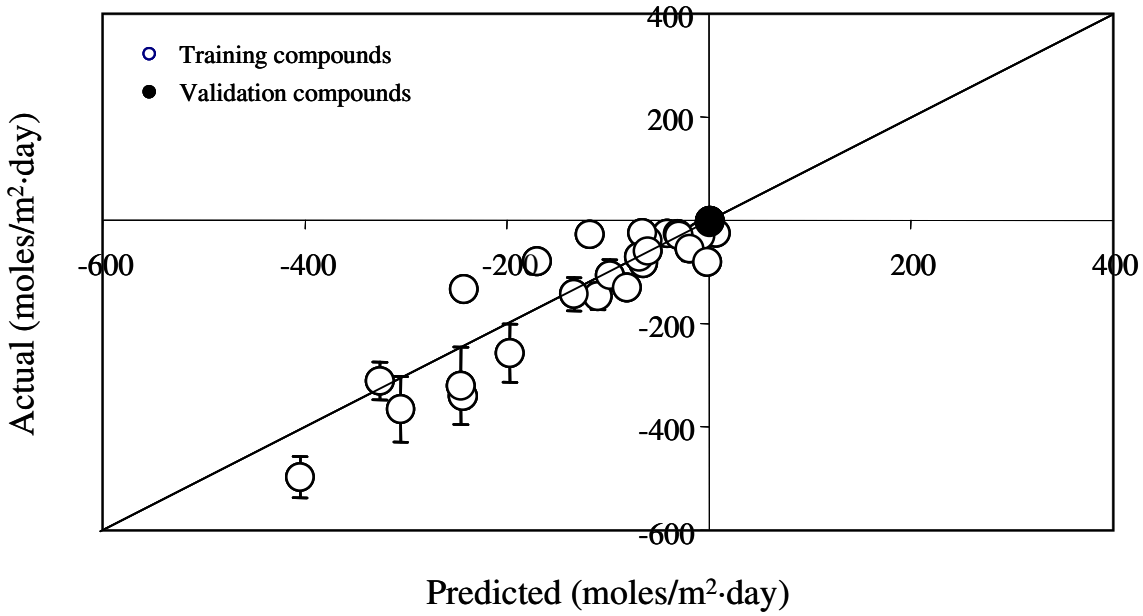

Figure 136. ANN Model results for change in solute flux for Koch TFC-ULP after treatment with cleaning compounds

Appendix VI. Definitions of ANN Model Inputs

1. QSAR Molecular Descriptors used in modeling (* *Indicates inclusion in one or more of the final ANN models*)

General 3D Descriptors: These molecular descriptors describe the 3D properties of the entire molecule.

ABSQ* - The sum of the absolute value of the charges on each atom of a molecule, expressed as electrons.

Dipole - The dipole moment of the molecule expressed in Debyes.

MaxHp - The largest positive charge on a hydrogen atom in the molecule.

MaxNeg* – The largest negative charge over the atoms in the molecule.

MaxQp* – The largest positive charge over the atoms in the molecule.

Ovality* – The ovality of the molecule, expressed as the ratio of the surface of the molecule to that of a perfect sphere (larger values indicate increasingly elongated molecules.

Polarizability – Molecular polarizability calculated on the base of the additive approach. Polarizability is the relative tendency of the electron cloud of the molecule to be distorted from its normal shape by the presence of a nearby external electric field.

Surface* – The surface area of the molecule.

2D Descriptors – These descriptors quantify properties such as bond properties, shape, information content, connectivity topological information and other properties.

Molecular Connectivity Chi Indices – A chi index is a weighted count of values computed for a function of the delta values of the constituent atoms in a given type of subgraph (portion of the molecular skeleton - delta values refer to the count of neighboring atoms bonded to an atom in a hydrogen-suppressed molecule and also corresponds to the count of sigma electrons contributed by that atom to bonded, non-hydrogen atoms). There are two classes of chi indices. *Simple chi indices*, in which all atoms are treated as carbon atoms and *valence chi indices*, in which the value for heteroatoms (non-carbon atoms) are computed differently than for the values of carbon atoms according to their electron characteristics. Chi indices have two attributes, *order* (the number of bonds in the molecule fragment being described) and type (the type of molecular fragment). There are four characteristic types – path (p), cluster (c), pathcluster (pc) and chain (ring) (ch). The molecular connectivity chi indices represent molecular structure by encoding significant features of whole molecules. Five general categories of molecular information are encoded by these indices: *degree of branching* (low order indices 0 – 2), *variable branching patterns* (high order path chi indices 3 – 10), *position and influence of heteroatoms* (valence chi indices), *patterns of adjacency* (chi cluster and path/cluster indices) and *degree of cyclicity* (chi chain indices).

x1 – Simple 1st order chi index – 2 atom simple path index, encodes degree of molecular branching.

xp4 – 4th order path chi index – 5 atom index, encodes variable branching patterns.

xc3 – 3rd order cluster chi index – 4 atom index, encodes patterns of molecular adjacency.

xpc4* – 4th order path/cluster chi index – 5 atom index, encodes patterns of adjacency.

xv1* – 1st order valence chi index – 2 atom index, encodes degree of branching, sensitive to nature of different atom types.
xvp4 – 4th order valence path chi index – 5 atom index, encodes variable branching patterns, sensitive to variations in atom types.
xvp7 – 7th order valence path chi index – 8 atom index, encodes variable branching patterns, sensitive to atom types.
xvp10 – 10th order valence path chi index – 11 atom index, encodes variable branching patterns, sensitive to atom types.
xvc3 – 3rd order valence cluster chi index – 4 atom index, encodes patterns of adjacency, sensitive to atom types.
xvpc4* – 4th order valence path/cluster chi index – 5 atom index, encodes patterns of adjacency, sensitive to atom types.
xvch6 – 6th order valence chain chi index – 7 atom index, encodes degree of cyclicity, sensitive to atom types.

Subgraph count indices – These indices are based on a count of a particular type of molecular feature such as a path, cluster, path/cluster or ring (chain). These descriptors are useful in characterizing the molecular skeleton.
nxp5* – the number of paths in the molecule with 5 edges
nxc3 – the number of 3-way clusters in the molecule
nxch6* – the number of 6-membered rings in the molecule.

3D Descriptors for Comparative Molecular Moment Analysis (CoMMA) – CoMMA descriptors provide a succinct representation of the 3D distribution of molecular mass, shape and charge.
Ix -Principal Moment of Inertia along X-Axis - Measure of the difficulty accelerating the molecule along its X-axis.
Iy* - Principal Moment of Inertia along Y-Axis - Measure of difficulty accellerating molecule along its Y-axis.
Py* - Component of Dipole Moment along Inertial Y-Axis - Magnitude of charge separation along the molecule's Y-axis.
Pz* - Component of Dipole Moment along Inertial Z-Axis - Magnitude of charge separation along the molecule's Z-axis.
P* - Magnitude of Dipole Moment - Magnitude of charge separation across entire molecule.
Q* - Magnitude of Principal Quadripole Moment - High order multipole moment of charge distribution.

Dx - Displacement between Center of Mass and Center of Dipole Moment along X-Axis - Difference between center of mass in the X-axis and point along X-axis where charge is zero.
Dy - Displacement between Center of Mass and Center of Dipole Moment along Y-Axis - Difference between center of mass in the Y-axis and point along Y-axis where charge is zero.
Dz - Displacement between Center of Mass and Center of Dipole Moment along Z-Axis - Difference between center of mass in the Z-axis and point along Z-axis where charge is zero.
Qxx - The xx Component of Second Rank Tensor Translated so Origin Coincides With Center of Dipole.
Qyy - The yy Component of Second Rank Tensor Translated so Origin Coincides With Center of Dipole.

Total Topological Descriptors - These are descriptors related to the geometrical structure of molecules (including the geometry of electron distribution about the molecule).
W - Weiner Index - The number of bonds between all pairs of atoms (based on shortest path around the molecule).
Pf - Platt f Index - Total sum of degrees of edges in the molecular graph; the degree of an edge in the number of adjacent edges.
sumdelI* - Sum of Delta Intrinsic States of atoms - Sum of degree of perturbation of the intrinsic state of all atoms in the molecule caused by the presence of the adjacent atoms.
tets2 - Total Electrotopological Index - Sum of E-States values of all atoms in the molecule. E-State is the sum of the intrinsic state of an atom (group) plus the sum of the perturbations of the intrinsic state caused by all the other atoms in the molecule.
totop - Total Topological Index – The total topological index, based on molecular connectivity formalism.
Wt* - Total Weiner Number - Same as W, but pairs of atoms are counted with respect to all paths in the molecule, not just the shortest path. This makes Wt > W for cyclic molecules.
nclass - # Symmetry Classes in Molecule - Number of classes of topologically similar molecular vertices.

Traditional Kappa Shape Indices – Kappa shape indices represent a method of molecular structure quantification in which attributes of molecular shape are encoded into three indices derived from counts of one, two and three bond fragments.
k0 – Kappa 0 – Encodes the number of vertex symmetry classes in the molecule; the value decreases with increasing molecular symmetry.
k1* - Kappa 1 – Encodes the degree of cyclicity in the molecule; the value decreases as the degree of cyclicity increases. Long, straight chain molecules have the highest value.

k2* - Kappa 2 – Encodes the degree of central branching in the molecule; the value decreases as the degree of central branching increases.

k3* - Kappa 3 – Encodes the degree of separated branching in the molecule. (far it is between branches along the molecular backbone); the index increases as the degree of branch separation increases (as the distance between branch points increases along the molecular backbone).

Other 2D Descriptors

LogP* - The octanol/water partition coefficient. A measure of hydrophobicity, this represents the log of the ratio of the solubility of the molecule in octanol over the solubility in water. The index increases as molecules become more hydrophobic and decreases as they become more hydrophilic.
LD50 - The mouse oral LD50 for the molecule, a measure of toxicity.

Atom Type E-State Descriptors – These descriptors describe the electronic environment (the accessibility of the electrons) of each atom in the molecule that arise due to a combination of the intrinsic properties of the of the atom and the influence of the neighboring atoms in the molecule. These descriptors parameterize such properties as hydrogen bonds, molecular polarity, etc. Atom type and group type E-state descriptors are computed for a number of atoms and functional groups. Large E-state values may indicate the molecule is more apt to participate in intermolecular interactions.
SsCH3* - Describes the sum of the E-state values for all -CH3 groups in the molecule.
SssCH2 - Describes the sum of the E-state values for all –CH2- groups in the molecule.
SaaCH* - Describes the sum of the E-state values for all aromatic carbon-hydride (=CH-) groups in the molecule (the aromatic ring CH).
SdssC* - Describes the sum of the E-state values for all =C< carbon in molecule.
SdO* - Describes the sum of E-state values for all =O oxygen in the molecule.
SsCl – Describes the sum of E-state values for all –Cl chlorine in the molecule.

Hydrogen Atom Type E-State Descriptors – These descriptors describe the sum of the hydrogen E-states (electron accessibility at the hydrogen atoms) for all polar or non-polar hydride groups of a given type in the molecule. These descriptors relate to such molecular properties as hydrogen bonding. As with E-state descriptors, large values indicate an increased ability of the molecule to participate in intermolecular interactions.
SssOH – Sum of the hydrogen E-states for the –OH groups in the molecule.
Shother – Sum of the hydrogen E-states for non-polar hydrogens (CH hydrogen) in the molecule
Hmax – The largest atom hydrogen E-state in the molecule – the largest polarity on a hydrogen atom in the molecule (also correlates with partial charge).
Gmax* - The largest atom E-state in the molecule (the most electronegative atom in the molecule).
Hmin* - The smallest atom hydrogen E-state in the molecule.
Gmin* - The smallest atom E-state in the molecule (also, the most electrophilic atom in the molecule).

Information Indices – These molecular descriptors are related to the information content of the molecule, and are derived from information theory.
si - Shannon Information Index – A measure of molecular complexity accounting for both diversity and concentration of features.
IC - Information Content - Based on the total number of molecular vertices, hydride groups or non-polar hydrogen atoms.
R - Molecular Redundancy – A measure of structural repetition within the molecule (is highest in highly internally symmetrical molecules like benzene and lowest in internally diverse molecules such as tetracycline).
idc - Bonchev-Trinajsti Information Content – Index is based on 2-path counts. Value increases with increasing molecular complexity.
idcbar* - Bonchev-Trinajsti Mean Information Content – Index is based on 2-path counts. Index increases with molecular complexity.

Molecular Properties – These descriptors include some fundamental properties of the entire molecule.
fw* – Formula weight – the molecular weight of the molecule in Daltons.
nelem – Number of elements – The total number of different elements in the molecule.
nrings – Number of rings – The number of rings in the molecule (also known as the cyclomatic number).
ncirc – Number of circuits – The total number of all cycles in the molecule. Includes ring structures as well as path circuits. Example: biphenyl = 2, but naphthalene = 3 because in addition to the aromatic rings, a circuit can be made about the periphery of the naphthalene molecule.
phia - Kappa Flexibility Index (# Bonds in normal graph for alkanes) – Inversely proportional to molecular complexity; increases with homolgation and decreases with increased branching or cyclicity.
knotp - Difference Between Chi cluster-3 and chi path/cluster-4 – Decreases with increasing molecular complexity.
numHBa* – The number of hydrogen bond acceptors in the molecule.
SHHbd – The number of hydrogen bond donors in the molecule.
Qs* – Specific Molecular and Group Polarity Descriptor – This descriptor is inversely proportional to molecular polarity and hydrophibicity.
Qsv* – Average Molecular and Group Polarity Descriptor – This descriptor is inversely proportional to molecular polarity and hydrophibicity.

2. Polyamide (PA) RO membrane properties used as inputs in development of the "Universal" PA model.

Contact Angle (degrees) – The air bubble contact angle of the membrane, measured as the outside angle between the membrane surface and a line tangential to an air bubble trapped against the membrane surface (in 17 MOhm deionized water at 24^{o}C). The contact angle represents a measure of surface hydrophibicity; the smaller the angle, the greater the surface hydrophibicity.

COO^-/Amide I Ratio - A unitless relative index of membrane crosslink frequency derived from attenuated total internal reflection Fourier transform infrared (ATR-FTIR) spectroscopic measurements based on the ratio of the absorption at 1415 cm^{-1} corresponding to the presence of free carboxylate groups and the absorption 1665 cm^{-1} corresponding to the amide I bonds in the membrane. The larger the ration, the less crosslinked the membrane.

COO^-/Amide II Ratio - A unitless relative index of membrane crosslink frequency derived from ATR-FTIR spectroscopic measurements based on the ratio of the absorption at 1415 cm^{-1} corresponding to the presence of free carboxylate groups and the absorption at 1542 cm^{-1} corresponding to the amide II bonds in the membrane. The larger the ration, the less crosslinked the membrane.

OH^-/Amide I Ratio - A unitless relative index of membrane crosslink frequency derived from ATR-FTIR spectroscopic measurements based on the ratio of the absorption at 3400 cm^{-1} corresponding to the presence of hydroxyl groups and the absorption at 1665 cm^{-1} corresponding to the amide I bonds in the membrane. The larger the ratio, the less crosslinked the membrane.

Polyamide Thickness – A unitless relative index derived from ATR-FTIR spectroscopic measurements based on the ratio of the strength of the 1665 cm^{-1} amide I absorption band of the polyamide layer and the 874 cm^{-1} absorption band of the polysulfone membrane support layer. The greater the ratio, the thicker the polyamide layer.

Roughness (nm) – A direct measurement by atomic force microscopy (AFM) of the rugosity of the membrane surface defined as the standard deviation of the height of features on the membrane, expressed in nanometers. The roughness of the membrane may reflect subtle differences in internal physicochemical properties. Interactions of nanoparticles with membrane surfaces are often positively related to surface roughness.

Specific Water Flux (GFD/PSI) – Measurement of the membrane water flux per unit water pressure. Many membrane properties are represented by the specific water flux, including membrane density and intrinsic porosity, hydraulic conductivity, hydrogen bonding, charge interactions and many others.

Zeta Potential (mV, pH 7) – The Zeta potential of the membrane, in millivolts. Zeta , was determined at pH 7.0 at 20^{o}C in 1000 mg/L NaCl using measurement of streaming potential obtained with a streaming potential analyzer (ZetaCAD, CAD Instrumentation, Les Essarts Le Roi, France) and applying the Helmholtz-Smoluchowski equation:

$$\zeta = \frac{\Delta U_s}{\Delta P}\frac{\mu}{\varepsilon\varepsilon_0}\frac{L}{A}\frac{1}{R}$$

where ζ is the zeta potential; U_s is the streaming potential; P is the applied pressure, $\Delta U_s/\Delta P$ is the slope of the streaming potential versus applied pressure curve; μ is the dynamic viscosity of the solution; ε is the permittivity of the test solution; ε_0 is the permittivity of free space; L is the channel length of the membrane test cell; A is the test cell channel cross-sectional area; and R is the test cell channel resistance.

Zeta Potential Slope (pH 5-7) - This is rate of change of the Zeta potential as the pH is shifted from 5 to 7. This index is inversely proportional to the ease with which membrane protons may be introduced or removed as a function of pH; the more negative the index, the more easily the membrane may be protonated or deprotonated.